ALBERTO GÓMEZ BAREA

Modelado de los efectos difusionales en la gasificación de partículas de carbonizado de biomasa

(Modelling of diffusional effects during gasification of biomass char particles in fluidised-bed)

Departamento de Ingeniería Química y Ambiental
Escuela Superior de Ingenieros
Universidad de Sevilla
Sevilla (España)
Mayo 2006

Modelado de los efectos difusionales en la gasificación de partículas de carbonizado de biomasa
ALBERTO GÓMEZ BAREA

Tesis doctoral presentada para optar al título de Doctor por la

Universidad de Sevilla y al titulo de Doctorado Europeo

(Doctoral thesis for the degree of Doctor of Philosophy and European

Doctorate)

Modelado de los efectos difusionales en la gasificación de partículas de carbonizado de biomasa

(Modelling of diffusional effects during gasification of biomass char particles in fluidised bed)

by

Alberto Gómez Barea

Thesis Supervisor: Pedro Ollero de Castro

Chemical and Environmental Engineering Department
Escuela Superior de Ingenieros (University of Seville)
Seville (Spain).
Mayo 2006

Abstract

The gasification rate of char is a key factor for evaluating the reactor volume and gas composition in gasifiers. If diffusional film and intraparticle mass and heat transfer processes in char particles are not rapid enough, the actual gasification rate differs from the intrinsic one evaluated in bulk-gas conditions. Under usual operating conditions in fluidised bed (FB) biomass gasifiers (and often in FB coal gasifiers), the gasification rate usually lies in the transition between the chemically-controlled and pore-diffusion-controlled regions. As a result, the overall gasification rate of a single char particle is determined by combining the intrinsic chemical reaction rate with intraparticle and external diffusional rates. Any char-particle kinetic model to be included as a submodel in an FB biomass gasifier should be capable of capturing diffusional effects. Despite this, it is shown in this work that most FB biomass (and coal) gasifier models in the literature simply disregard transport process limitations inside char particles. The reason seems to be the extreme computational difficulty of introducing a rigorous submodel's code in real FB reactor simulations. The main motivation of the present study is to pave the way towards the development of a more rigorous but simple form to include the gasification of char particles in the modelling of FB gasifiers.

In this work transport effects taking place during the gasification of single char particles were studied theoretically and experimentally. The main contributions of the work are:

1. The development of a method which makes it possible to solve any non-catalytic gas-solid reaction with a single oxidant. The method is applied to the CO_2 gasification of a single char particle. The model needs the intrinsic reactivity as a key input. If the real process is to be carried out in an FB reactor, char reactivity determination in TGA or other lab devices has limitations. Employing a laboratory-scale FB reactor overcomes many of the drawbacks associated with these devices. However kinetic research in an FB is difficult owing to its complex fluid dynamics. This makes it difficult to separate the kinetic information from fluid-dynamic influence. To make this determination possible, transport effects during typical laboratory-scale FB char reactivity tests were studied. This is the second main contribution of this thesis, which is given below.

2. The establishment of a basis for the choice of operating conditions for a laboratory-scale bubbling FB reactor to avoid mass-transport interferences in the determination of char reactivity. When transport effects cannot be fully eliminated, the model developed enables making a correction for the apparent reactivity in order to determine the intrinsic reactivity.

The first objective was achieved by developing an original treatment for obtaining the solution of single isothermal non-catalytic gas-solid reactions. The model was extended to deal with intraparticle heat effects and transport processes within the surrounding gas layer. This simple model facilitates a rapid assessment of non-isothermal intraparticle and external effectiveness factors in single char particles for the whole range of char conversion. Model prediction capabilities were assessed by comparing with a set of TGA char gasification tests with single particles.

The second objective was accomplished by an analysis of transport effects in an FB designed for kinetic determination. This involves the transport of the oxidising agent between bubbles and dense phase, transport within the dense phase and transport with reaction inside the char particles. A modelling approach which combines a kinetic particle model with a simple two-phase flow model was developed. The parameters resulting from the model were expressed in terms of observable quantities, making it possible to evaluate the transport effects in a straightforward way from gas concentration measurements. The model was validated by comparison with a set of FB char reactivity experiments at laboratory scale.

Papers

The thesis is based on a number of papers already published or submitted to journals and international conferences. They are the following:

PAPER 1. Gómez-Barea, A., Ollero, P., 2006. An approximate method for solving non-catalytic gas-solid non-catalytic reactions. Chemical Engineering Science 61, 3725–3735.

PAPER 2. Gómez-Barea, A., Ollero, P., Fernández-Baco, C., 2006. Diffusional effects in CO_2 gasification experiments with single biomass char particles. Part I. Experimental investigation. Energy & Fuels (In press).

PAPER 3. Gómez-Barea, A., Ollero, P., Villanueva, A., 2006. Diffusional effects in CO_2 gasification experiments with single biomass char particles. Part II. Theoretical predictions. Energy & Fuels (In press).

PAPER 4. Gómez-Barea, A., Ollero, P., Fernández-Baco, C., Villanueva, A., Salvador, L., 2006. Evaluation of mass transport effects in a bench-scale BFB gasifier designed for kinetic determination. Proceedings of 19th International Conference on Fluidised Bed Combustion. May 21–24, 2006, Vienna, Austria. Paper 65. (In press).

PAPER 5. Gómez-Barea, A., Ollero, P., Leckner, B., 2006. Transport effects during determination of gas-solid kinetics in fluidised bed. Submitted for publication in Chemical Engineering Science (January 2006).

PAPER 6. Gómez-Barea, A., Leckner, B., Ollero, P., Fernández-Baco, C., Salvador, L., 2006c. Mass transfer effects during char gasification reactivity tests in a laboratory-scale fluidised-bed. Submitted for publication in Industrial & Engineering Chemistry Research (April 2006).

Alberto Gómez Barea is the principal researcher and main author of all the papers. He developed the theory and conducted modelling and simulation tasks, reviewed and interpreted experimental data from TGA and lab-scale FB work, and edited all the papers. Pedro Ollero and Bo Leckner collaborated in the edition of papers 4 to 6. The experiments carried out in TGA (paper 2) were conducted by Sergio Alcantarilla under the supervision of Ricardo Arjona and Pedro Ollero. The experiments in bench-scale fluidised-bed system (papers 4 and 6) were carried out by María Contreras and María Jesús Plumed, supervised by Custodia Fernández, Pedro Ollero and Luís Salvador. All papers were thoroughly discussed by all the co-authors.

The following papers have also been published during the development of this thesis. Their content overlap with the papers 1 to 6, but their aim is beyond the scope of this thesis.

PAPER 7. Gomez-Barea, A., Ollero, P., Arjona, R., 2005. Reaction-diffusion model of TGA gasification experiments for estimating diffusional effects. Fuel 84, 1695–1704.

PAPER 8. Gómez-Barea, A., Arjona, R., Ollero, P., 2005. Pilot plant gasification of olive stone: a technical assessment. Energy & Fuels, 19, 598–605.

PAPER 9. Gómez-Barea, A., Campoy, M., Ollero, P., Fernández-Pereira, C., 2006. Pilot plant experiences with fluidised bed gasification of orujillo and MBM. Proceedings of 19th International Conference on Fluidised Bed Combustion. May 21–24, 2006, Vienna, Austria. Paper 66. (In press).

Content

Acknowledgements

I would like to thank my supervisor, Professor Pedro Ollero, for giving me the opportunity to do this work. His helpful comments inspired many of the ideas included in it. I am greatly indebted to him for supporting me in whatever I needed to achieve my purposes, especially his invaluable support during my stay in Sweden.

I want to express my gratitude to everyone in the Chemical and Environmental Department in the School of Engineering at the University of Seville for their support in so many ways to make this thesis possible. Special thanks to Constantino Fernández, Ricardo Arjona, Manuel Campoy, Ángel Villanueva, Custodia Fernández, Luís Salvador, Luís Vilches, Rosario Villegas, Carlos Leiva, Paco Bueno, Teresa de Manuel, Antonio Vargas and Maruchi.

I should like to express my appreciation to other people from this university. Thanks to Prof. Miguel Pérez-Saborid, Antonio Barrero and José Gordillo of the Fluid Mechanics Group at the University of Seville for their support and teaching contribution during my initiation into fluid dynamics and numerical methods. I also appreciate the support given by Emilio Freire of Applied Mathematics Department at the University of Seville for many discussions on different mathematical aspects. Thanks to the excellent library staff, especially to Marta Suarez and Paco Sánchez, for their great help in searching the literature.

I want to expresses my appreciation to Bo Leckner, Professor at Chalmers University of Technology in Gothenburg, Sweden, for his help and valuable discussions and ideas, especially during my stay in Sweden and while I was writing.

I wish to thank all my colleagues in the Energy Conversion Department at Chalmers University of Technology for an excellent working atmosphere during my stay in Sweden. Special thanks to Henrik Thunman, Srdjan Sasic and Gennadij Palchonok and special recognition to Germán Maldonado and his family and friends for their support and friendship.

I would like to acknowledge the financial support of the University of Seville, the European Commission, the Commission of Science and Technology (CICYT) of Spain and the Junta de Andalucía.

Thanks to Mary Grennan and Martha Hobart-Burela because, without their help, this thesis probably would not have reached so many people.

Family and friends are acknowledged. Special thanks to my five brothers Mamé, Jesu, Miguelito, David and Fernando and my three sisters Pili, Inma and Patri, my lovely girlfriend Bella and my friends Federico, Fleki, Nacho and Pepele. My deepest gratitude is to my parents. I dedicate this thesis to both of them, for their enormous work, love, patience and altruism. I hope, despite the English, my effort can reach them.

Finally, thanks to everybody I have not mentioned who has contributed to the work for this thesis.

"Employ your time improving yourself by other men's writings so that to make important advances in the application you shall come easily to what others have laboured hard for."
(Attributed to Sócrates)

ΑΓΕΩΜΕΤΡΗΤΟΣ ΜΗΔΕΙΣ ΕΙΣΙΤΩ
("Let no one ignorant of Geometry enter here")
(Platón)

"C'est bien plus beau lorsque c'est inutile"
("It is more beautiful because it is not useful")
(From Cyrano de Bergerac)

"The arrival time of a space probe travelling to Saturn can be predicted more accurately than the behaviour of a fluidized bed chemical reactor !"
(Geldart, 1969)

A mis padres

Resumen de la tesis doctoral

1. Introducción

La gasificación de biomasa es un proceso de conversión termoquímica donde un combustible es oxidado parcialmente en un ambiente deficitario de oxígeno para producir un gas combustible, constituido principalmente por CO e H_2, susceptible de ser aprovechado de múltiples formas. Dependiendo del agente gasificante empleado (aire, vapor, oxígeno o mezclas de éstos) y de la forma de aportar calor (directa, mediante la conversión parcial del combustible, o indirecta, mediante aporte externo de calor), la gasificación produce un gas de bajo o medio poder calorífico. Según las condiciones de operación del gasificador (presión y temperatura), del poder calorífico del gas producido y del grado de ensuciamiento del gas, existen tres formas generales de utilización del mismo, aprovechamiento térmico, producción de electricidad y síntesis de combustibles. La gasificación se lleva a cabo en tres grandes tipos de reactores, de lecho fijo, de lecho fluidizado y de lecho de arrastre. Dependiendo de la naturaleza de la biomasa, del uso final del gas, de la escala de producción, y de la economía y logística asociada a cada biomasa, interesará un tipo u otro de gasificación.

A pesar del esfuerzo realizado desde los años ochenta y del gran número de proyectos de demostración llevados a cabo en Europa en la última década, la gasificación de biomasa encuentra todavía serias dificultades para su definitiva implantación a escala comercial. Dejando a un lado barreras de tipo institucional, la tecnología de gasificación de biomasa no ha conseguido aún superar importantes problemas logísticos, técnicos y económicos, como el suministro seguro de la biomasa o la limpieza del gas de forma fiable y suficientemente económica (Maniatis, 2001).

En la gasificación de biomasa, existen en general dos escalas de procesamiento, que con algunas excepciones, se corresponden con los dos tipos de gasificadores de lecho fijo (o móvil) y fluido. El lecho de arrastre, por otro lado, está casi ausente en aplicaciones de biomasa debido al alto coste y dificultad que supone la molienda de la biomasa hasta los tamaños tan pequeños necesarios para procesarlo en este tipo de reactores. Por otro lado, la gasificación en lecho fijo tiene importantes limitaciones, dependiendo de la tipología empleada. Así, mientras los gasificadores de corrientes paralelas (tipo Downdraft) presentan una baja capacidad de procesamiento, los de corrientes cruzadas (tipo Updraft) tienen severas limitaciones de tamaño de partícula y humedad de biomasa a tratar. Además, estos últimos producen un gas con un alto contenido en alquitranes. Otro tipo de gasificadores de lecho fijo, muy utilizados para el tratamiento de cascarilla de arroz en los países del sudeste asiático, son los estratificados. Estos gasificadores sin embargo poseen un deficiente grado de automatización y, en ocasiones, importantes emisiones y vertidos contaminantes. Existen además diseños novedosos que combinan distintos aspectos de las tipologías

mencionadas. Sin embargo, por regla general la escalabilidad de estas instalaciones suele reducirse a 1-2 MW_t.

La tecnología en lecho fluidizado presenta notables ventajas sobre la de lecho fijo, en particular la posibilidad de llevar el proceso a gran escala. Además de ésta, existen otras grandes ventajas como la mejora de la automatización del proceso y la gran versatilidad a diferentes tipos de biomasas y residuos, factores que hacen que los gasificadores de lecho fluidizado sean los únicos técnicamente interesantes por encima de 1-2 MW_t. A pesar de estas ventajas, el estado actual de la tecnología sólo ha alcanzado la escala comercial en aplicaciones de aprovechamiento térmico (Knoef, 2003). Dentro del aprovechamiento térmico, el concepto de co-combustión en calderas de carbón o combustible fósil presenta indudables ventajas, entre las que destacan la sustitución parcial del combustible fósil por otro renovable y la posibilidad de emplear el gas de gasificación como gas de reburning para control de NO_x (Murphy, 2001). Por esta vía el rendimiento de conversión de la biomasa a energía eléctrica es mucho mayor que el que es posible alcanzar en centrales cuyo combustible único fuera la biomasa, al no beneficiarse éstas de la economía de escala. La co-combustión en grandes calderas de combustible fósil presenta la ventaja adicional de no requerir una limpieza exhaustiva del gas, siempre que la biomasa empleada sea la adecuada. Esto quedó demostrado tras el éxito del proyecto llevado a cabo en la ciudad finlandesa de Lahti en 1998 (Kurkela et al., 2004).

Existen vías alternativas a la co-combustión, como el aprovechamiento del gas en motores de combustión interna y la tecnología IGCC (Spliethoff, 2001). El uso del gas en motores tiene un rendimiento teórico aceptable, pero presenta graves inconvenientes derivadas de los altos requerimientos de limpieza exigidos al gas. La tecnología IGCC con biomasa, aunque con un potencial de mercado de mucho interés, no ha tenido implantación industrial por problemas de la logística y acondicionamiento de la biomasa.

Bajo el concepto de gasificación indirecta, la compañía Batelle Columbus desarrolló un genuino concepto de gasificación mediante la separación del reactor de combustión y de pirólisis, y su interconexión a través de un lecho circulante de arena que realiza la función de agente calefactor. La planta de Güssing en Austria también usa este concepto de gasificación indirecta para la generación combinada de calor y electricidad (cogeneración). Otros ejemplos de proyectos donde se ha implementado con relativo éxito la gasificación indirecta con vapor son, el proceso a presión desarrollado por IGT/Carbona (“Renugas Process”) en la central térmica de Tampere (Finlandia) y en la isla de Hawai.

Se han ensayado otros conceptos de gasificación como la combustión indirecta en turbinas de gas, con potencial interesante pero aún en fase de investigación a escala piloto. Otros conceptos novedosos han alcanzado la escala industrial, como el implantado por Corenso en Varkaus con tecnología Foster-Wheeler-VTT. En esta planta se produce la gasificación de tetrabricks con recuperación intermedia de aluminio previa a la combustión del gas en una caldera de especial diseño (Kurkela et al., 2004).

2. Motivación y objetivos de la tesis

Existe un gran número de factores a tener en cuenta al diseñar un gasificador de biomasa. Al ser la gasificación de biomasa una tecnología aún emergente y sin plena implantación comercial, no existe en la actualidad ningún fabricante ni diseño de gasificador firmemente consolidado en el mundo. El diseño y la operación de un gasificador de biomasa, en especial de lecho fluidizado, necesita ser analizado caso por caso, y el criterio de diseño dista mucho de ser universal, necesitando todavía por tanto, de un importante esfuerzo para su correcta puesta a punto.

Entre otras importantes variables, el conocimiento de la reactividad del carbonizado o "char" de biomasa contribuye de forma significativa al correcto diseño de un gasificador. Este carbonizado se produce tras el secado y la volatilización del combustible alimentado a un gasificador. Bajo las condiciones de operación usuales en un gasificador de lecho fluidizado de biomasa, las reacciones heterogéneas entre el carbonizado y el dióxido de carbono y/o el vapor de agua, aún siendo generalmente lentas, contribuyen significativamente a la producción del gas combustible final. Esto tiene un impacto, directo o indirecto, en el diseño del gasificador, especialmente en el volumen de la zona de reacción y en la predicción de la composición del gas obtenido, aspecto este último de carácter decisivo para la aplicación final del gas, y por tanto, para el diseño del tren de depuración de gases necesario.

Durante el análisis o diseño de un gasificador, la simulación del proceso de gasificación así como la predicción del gas de salida, puede ser una herramienta de extrema utilidad (Ranade, 2000). En el modelado de gasificadores, se suele aceptar el modelo de conversión uniforme del carbonizado. Esta hipótesis puede ser razonable en gasificadores operando con carbón de alto rango a temperatura razonablemente baja (850-1000ºC). En la gasificación de biomasa, sin embargo, el carbonizado resultante suele presentar una reactividad de entre diez y mil veces la obtenida con carbones de alto rango. Este hecho, junto con las condiciones de operación típicas de un gasificador en lecho fluidizado de biomasa (tamaño de combustible alimentado de varios centímetros, tiempo de residencia del carbonizado de varios minutos y rango de temperatura de 750-900ºC), hace que gran parte del carbonizado que se está gasificando en un instante dado en la zona de reacción pueda estar en régimen diffusional o de transición. En esta situación, los efectos derivados de la transferencia de materia y calor a través de la partícula de carbonizado pueden ser limitantes, y por tanto, deben ser tenidos en cuenta para la evaluación de la velocidad neta de gasificación del carbonizado.

La simulación de la fluido-dinámica de un reactor de lecho fluidizado representa por si sola un enorme reto, debido a la complejidad del flujo y al gran esfuerzo computacional que requiere pronosticar el mismo de forma rigurosa. La aplicación de un enfoque CFD (Computacional Fluid Dynamics) a este tipo de reactores, permite resolver un gran número de problemas de operación y de diseño (Ranade, 2002). Sin embargo, para simular el proceso es preciso la incorporación de un modelo cinético de partícula, lo que añade mucha complejidad computacional. Un modelo cinético simple, estable y rápido, que pueda ser incorporado como sub-modelo de forma directa, sencilla y fiable, representaría un considerable ahorro de tiempo y permitiría realizar simulaciones realistas en un tiempo razonable.

Esta es la primera motivación de la presente tesis, que consiste en el desarrollo de un modelo de partícula de carbonizado con la capacidad de considerar de forma rigurosa, los fenómenos de difusión y reacción a través de las mismas, en el caso de una reacción heterogénea con un único oxidante. Aunque este modelo cinético de partícula es aplicable en principio a cualquier tipo de reactor (lecho fijo, fluido burbujeante, circulante o de arrastre), encuentra su mayor interés en lechos fluidizados, debido a las condiciones de operación presentes en este tipo de reactores.

La simulación completa de una situación real, necesitaría de la consideración de un gran número de procesos que aquí no se abordan, como la inclusión de otras reacciones heterogéneas , reacciones en fase homogénea dentro y fuera de los poros, el arrastre del carbonizado, elutriación de partículas en el lecho, balances poblacionales, etc. Por ello, el modelo que aquí se plantea constituye solo un primer paso para el desarrollo de un modelo de simulación realista de reactor.

Para la utilización de un modelo como el que se pretende, la reactividad intrínseca de carbonizado es un dato de extraordinaria importancia que debe ser determinada experimentalmente. Por otro lado, la forma de generación del carbonizado tiene un gran impacto sobre la composición y la reactividad del mismo, en particular la velocidad de calentamiento y la temperatura. Para la simulación del proceso de gasificación del carbonizado presente en un reactor de lecho fluidizado, las condiciones de generación del mismo en el laboratorio deben ser similares a las reales. De otra forma, la reactividad obtenida en laboratorio pudiera ser muy diferente de la real. Un procedimiento clásico se basa en el uso de aparatos termogravimétricos (TGA, hornos de mufla, etc.). En estos dispositivos, la velocidad de calentamiento está limitada a unas cuantas decenas de grados por minuto, hecho que contrasta con el caso real de un lecho fluidizado, donde la velocidad de calentamiento puede ser de varios de cientos de grados por segundo. Este hecho hace sospechar que la reactividad del carbonizado pueda ser notablemente diferente de la que se obtendría de un carbonizado generado en una TGA.

Para sortear esta dificultad, la determinación de la reactividad en un lecho fluido de laboratorio se revela idónea. Sin embargo, los efectos fluido-dinámicos de un lecho fluido, junto con los efectos de transferencia de materia y calor en las partículas de carbonizado pueden hacer que la reactividad observada difiera de la intrínseca. Además, el flujo dentro de un reactor de lecho fluido es muy complejo, y un análisis detallado del mismo en aras de evaluar las resistencias al transporte de materia puede ser una tarea muy compleja.

La segunda gran motivación de esta tesis ha sido dar solución a este problema. Para ello, se ha desarrollado una metodología simple, pero suficientemente rigurosa, que permite evaluar los efectos fluido-dinámicos y difusionales durante ensayos realizados en un lecho fluido de laboratorio con el objetivo de obtener la reactividad intrínseca.

3. Contribución de la tesis

En esta tesis se han investigado los efectos difusionales presentes en partículas de carbonizado de biomasa en aras de contribuir al diseño de gasificadores,

especialmente de lecho fluidizado. Los dos grandes objetivos han sido: (1) El desarrollo de una metodología de cálculo que permita evaluar de forma rápida y fiable la velocidad de gasificación de un carbonizado en condiciones de operación dadas, a partir de su cinética intrínseca; y (2) La obtención de la reactividad del carbonizado en lecho fluido de laboratorio libre de efectos difusionales (reactividad intrínseca).

La consecución del primer objetivo se ha concretado en las siguientes contribuciones:

1. El desarrollo de un modelo cinético de partícula, válido para reacciones gas-sólido no catalíticas, cuya resolución es extremadamente rápida y, a la vez, rigurosa.

2. El desarrollo de una metodología para la resolución rápida y rigurosa de un modelo cinético de gasificación de carbonizado con dióxido de carbono.

3. La medida experimental en TGA de la velocidad de gasificación de carbonizado de biomasa con partículas de tamaños similares a las encontradas en gasificadores industriales.

La consecución del segundo objetivo se ha materializado en las siguientes aportaciones:

1. El desarrollo de una metodología para el análisis de los efectos difusionales en experimentos realizados en lecho fluido de laboratorio, para la determinación de la reactividad en una reacción gas-sólido no catalítica en condiciones isotermas.

2. El establecimiento de las condiciones de operación de un gasificador de lecho fluidizado de laboratorio que permitan la obtención de la reactividad intrínseca de un carbonizado, libre de efectos fluido-dinámicos y difusionales.

3. El establecimiento de normas de diseño para la construcción de gasificadores de laboratorio, que aseguren en el mayor grado de lo posible, la obtención de reactividades intrínsecas.

4. El desarrollo de un método para la obtención de un factor de corrección que permita la determinación de la reactividad intrínseca a partir de la reactividad aparente, en situaciones donde no sea posible evitar las interferencias asociadas a los efectos de transporte de materia.

5. La evaluación experimental de los efectos difusionales presentes en experimentos llevados a cabo durante la obtención de la reactividad de gasificación de un carbonizado derivado de orujillo con CO_2 en un lecho fluidizado de laboratorio, utilizando partículas de varios tamaños, incluyendo partículas de tamaño macroscópico similares a las encontradas en gasificadores industriales.

4. Resumen de los capítulos

La primera parte de esta tesis (capítulos 2, 3 y 4) cubre el primer objetivo citado anteriormente. En ella, se desarrolla un método aproximado para la simulación de la gasificación de una partícula de carbonizado con CO_2 en situaciones donde los efectos difusionales puedan estar presentes. El modelo se valida mediante comparación con experimentos llevados a cabo en TGA empleando varios tamaños de partícula, temperaturas y concentraciones de oxidante. En la segunda parte, cubierta en los capítulos 5 y 6, se desarrolla el segundo objetivo de esta tesis, consistente en la puesta a punto de una metodología para evaluar los efectos de transporte presentes en experimentos cinéticos para la determinación de la reactividad de carbonizado en lecho fluidizado. Este método permite operar un lecho fluidizado de laboratorio en condiciones óptimas para evitar la plausible interferencia sobre la reactividad causada por los efectos fluido-dinámicos del lecho y los efectos difusionales dentro y fuera de las partículas de carbonizado. Además, el procedimiento hace posible determinar la reactividad intrínseca por corrección de la observada en experimentos donde no se puedan evitar estas interferencias. Gracias a esta segunda contribución, la reactividad del carbonizado puede ser obtenida en condiciones similares a las de un lecho fluido industrial, permitiendo incorporar al modelo desarrollado en la primera parte, un dato realista de reactividad intrínseca.

A continuación se resume brevemente el contenido de cada capítulo:

En el *capítulo 2* se sientan las bases matemáticas del método aproximado para resolver una reacción gas-sólido no-catalítica y se valida mediante comparación con el modelo matemático exacto, es decir, el representado por el conjunto de ecuaciones diferenciales cuya integración numérica permite predecir la variación temporal y espacial de la concentración del agente gasificante y del reactivo sólido. El método se basa en el desacoplamiento de las ecuaciones de conservación del sólido y del gas, mediante la aplicación de un método numérico recientemente desarrollado, conocido como “Quantize Method”. Mediante este procedimiento, la ecuación de conservación del gas se resuelve en cada instante, como si tratase de un catalizador con una distribución de centros activos variable. Esta distribución se calcula mediante integración de la ecuación de conservación del sólido en el instante anterior. El perfil de concentración del reactivo gaseoso en el instante considerado, se realiza mediante la aplicación del método de perturbaciones regulares y singulares, para valores del modulo de Thiele pequeños y grandes, respectivamente. Conocidos el perfil de concentración del gas en las dos situaciones límites del modulo de Thiele, se construye una solución general para cualquier número de Thiele, mediante la técnica de “matching”. Finalmente la ecuación de conservación del reactivo sólido se integra en el tiempo de forma desacoplada a la del reactivo gaseoso. Con esta metodología el problema de resolver una reacción gas-sólido no-catalítica se reduce a la resolución de dos ecuaciones algebraicas no lineales en cada punto de la partícula. La exactitud del método es sorprendentemente buena, y la reducción del tiempo de computacional respeto de la resolución exacta de hasta tres ordenes de magnitud.

En el *capítulo 3* se desarrolla un programa experimental donde se somete a ensayo en TGA un carbonizado de biomasa generado externamente en un horno. Las condiciones de operación incluyen varios rangos de temperatura, concentración de

CO_2, y tamaño de partícula, desde polvo (menor de 60 micras) hasta varios milímetros. Los efectos difusionales se calculan experimentalmente mediante varios factores de efectividad apropiados según los datos disponibles. El amplio banco de datos generado sirve para establecer las condiciones bajo las cuales las partículas de carbonizado están en régimen difusional, y por tanto, limitada por efectos de transporte de calor y masa. Además, los datos se utilizan para validar el modelo que se desarrolla en el capítulo 4.

El *capítulo 4* extiende el tratamiento del capítulo 2 para incluir efectos térmicos dentro de las partículas, y de transferencia de calor y masa en la película de gas que rodea a las mismas. El modelo predice de forma aceptable los experimentos en TGA presentadas en el capítulo 3, permitiendo identificar los mecanismos limitantes a diferentes grados de conversión. Además, la metodología aplicada resulta útil para ayudar a diseñar y analizar de forma muy simple nuevas experiencias en TGA donde los efectos difusionales pudieran estar presentes.

Como se sabe, cualquier modelo cinético de gasificación de carbonizado requiere como entrada la cinética intrínseca. Como se ha mencionado arriba, la reactividad de un carbonizado generado en TGA puede distar considerablemente del que se produce en un lecho fluido, ya que el proceso de generación del carbonizado condiciona su porosidad, composición y reactividad. Esta última, en consecuencia, debe ser obtenida en condiciones similares a las que se pretenden simular, es decir, en lecho fluidizado. Sin embargo, en un reactor de lecho fluidizado, los procesos fluido-dinámicos en el lecho así como los procesos difusionales dentro y fuera de las partículas, pueden falsificar la reactividad obtenida. Esto hace que un lecho fluidizado sea un tipo de reactor poco indicado para determinaciones cinéticas.

Para solucionar este problema, en el *capítulo 5* se desarrolla una metodología simple para evaluar los efectos difusionales en experimentos cinéticos realizados en un lecho fluido de laboratorio. El método se basa en la obtención de unos parámetros observables, que se calculan directamente a partir de la medida de concentración en el gas de salida. A partir de estos observables, los efectos hidrodinámicos y difusivos a nivel de partícula (intrafásicos e interfásicos), se evalúan de forma rápida y simple. Esta evaluación permite establecer y diseñar condiciones operacionales óptimas para evitar, en la medida de lo posible, que las resistencias al transporte de masa en el reactor sean importantes durante la determinación cinética de una reacción gas-sólido. El método es válido para condiciones isotermas y, por tanto, se puede aplicar a un buen número de situaciones, como la determinación de la reactividad de carbonizado con oxígeno (combustión), con vapor de agua (gasificación con vapor), y a otras reacciones gas-sólido no catalíticas, siempre que sean llevadas a cabo de forma aproximadamente isotérmica.

En el *capítulo 6* se aplica la metodología del capítulo 5 para evaluar los efectos difusionales en una serie de experimentos de gasificación de carbonizado con CO_2, realizados en un reactor de lecho fluidizado de laboratorio de 26 mm de diámetro interno. En él, se pone de manifiesto la validez y utilidad del método, y se verifica que los efectos intraparticulares son el principal motivo de que la reactividad obtenida no sea la intrínseca en los experimentos con partículas de varios milímetros. Se comprueba que la cantidad de carbonizado alimentado al inicio debe estar por debajo

de un máximo, con el fin de garantizar que la conversión en el reactor sea diferencial, y eliminar así la incertidumbre asociada al consumo del CO_2 por reacción química a través del lecho. En todos los experimentos se comprueba que el by-pass causado por las burbujas es pequeño y que los efectos de la fluido-dinámica no causan interferencias apreciables en la medida de la reactividad. En escenarios complejos donde no se puedan evitar los efectos difusionales, la metodología propuesta permite corregir la reactividad aparente y determinar la reactividad intrínseca.

Modelling of diffusional effects during gasification of biomass char particles in fluidised-bed

Chapter 1

Introduction

1. Introduction

Due to growing concern for future energy supplies and for limiting CO_2 emissions, the use of a renewable energy source such as biomass or waste for heat and power production has become an interesting matter. Thermochemical processing of biomass and waste is one of the currently developed alternatives. Biomass- and waste-derived fuels are low-grade fuels, and their economic competitiveness is in many cases low compared to coal-based power production. However, these fuels have definite environmental benefits.

Gasification technology offers an attractive way to use these low-grade fuels with high efficiency, particularly when the product gas is cleaned of impurities and this cleaned gas is burned in a large-scale boiler together with the boiler's main fuel. This integration enables high electricity production efficiency even with biomass or waste fuels due to the utilisation of an efficient large-scale steam cycle. Even more efficient power production can be reached if IGCC technology is applied (Maniatis 2001, 2004). At the beginning of the 1980's several biomass gasification systems were installed. However, most of them were abandoned because of technical, economic and/or institutional problems. The renewed interest in biomass gasification at the beginning of the 1990's was due to discussions of climate change and the commitments of the Kyoto Protocol (Knoef, 2003).

Gasification has considerable benefits over direct combustion because the feedstock is converted to a gaseous fuel, which significantly increases the opportunities for using biomass as an energy source. This process leads to a fuel gas suitable for co-firing in existing boilers and, when sufficiently cleaned, also for feeding efficient gas engines and gas turbines for generating electricity and as a raw gas for the synthesis of liquid fuels or chemicals (Spliethoff, 2001). Gasification also offers potential environmental advantages because the fuel gas produced by gasifiers is lower in both volume and temperature than the fully combusted product from a combustor. These characteristics provide an opportunity to clean and condition the fuel gas prior to use. Combustion of the resulting gaseous fuel can be more accurately controlled than combustion of solid biomass. As a result, the overall emissions from gasification-based power systems, particularly those of NO_x, can be reduced (Stevens, 2001).

Downdraft biomass gasifiers are more specific with respect to fuel quality. This type of gasifiers usually requires fuel with low water content and low amount of ash.

Compared to updraft gasifiers, the producer gas from the downdraft gasifier is hot and only needs a minimum of cleaning. Downdraft gasification is a proven system but calls for fuel preparation. The challenge of the updraft gasifier is, in contrast, the gas cleaning. A number of test plants of the downdraft principle are at the moment either in demonstration or close to demonstration at district heating plants. Fluid bed gasifiers are noted for having high throughput rates, and tend to be used in larger installations. One of their advantages is a wider range of fuel flexibility than fixed bed types.

The gasification of biomass in large-scale applications benefits from being carried out in fluidised-bed (FB) systems because fixed-bed design has strong up-scaling limitations over 1-2 MW. The basic technology exists today but the technical and economic competitiveness of large-scale gasification has to be improved to be comparable with the latest generation of fossil fuel fired power plants. Fluidised-bed gasification of biomass and waste fuels has been successfully demonstrated for a wide variety of feedstocks. A power plant concept consisting of a gasifier connected to a large PC boiler with a high-efficiency steam cycle offers an attractive and efficient way to use local biomass and waste sources and to lower the CO_2 emissions of power production at relatively low cost. The 60-MW gasification plant in Lahti, Finland, has been in reliable operation since early 1998. Another similar gasification concept was recently completed for Electrabel in Belgium. A low-pressure fluidised-bed gasification process has also been developed for high-alkali biofuels (e.g., straw) and contaminated wastes, such as demolition wood, MSW, sewage sludge and autoshredder residues. In these applications, the gas cooler design and gas filtration play the key role. The process has been tested at MW-scale pilot plants with a wide range of fuels. The current phase of gas cleaning R&D for industrial application is the catalytic removal of tars and ammonia (Kurkela et al., 2004).

2. The role of char reactivity in design and operation of FB biomass gasifiers

The design of a FB biomass gasifier commonly consists of two main steps, the first of which is preliminary sizing. This step encompasses the determination of the main flows, reactor dimensions and the distributor plate design, as well as an estimate of other design and operational parameters. A second phase deals with optimisation of the gasifier performance. The approach taken depends on the final application of the gas produced. The main performance parameters are cold and hot gas efficiency, presence of unconverted carbon and tar concentration in the gas and its heating value (van den Enden and Silva, 2004, Souza-Santos, 2005).

There are other important operational factors to consider, such as the tendency of inorganic components to cause bed agglomeration and the entrainment of bed material. These factors must be limited as much as possible in order to achieve proper operation. Other difficulties in the commercial development of biomass technology integrated in advanced cycles are lack of reliability and flow constancy of the fuel-feed system, intensive elutriation in bubbling-bed gasifiers and the lack of viability and efficiency of the hot cleaning technology for tars, particles and alkali metal separation (Silva and Sanchez, 1995).

Char reactivity is a key parameter which usually determines the volume required for the gasifier. It has also a direct impact on the parameters that influence performance, such as dynamic bed height and biomass feeding point position, and indirect in-

fluence on other design and operating parameters like freeboard diameter, insulation, distributor, etc. In addition, nowadays, the design of an FB gasifier may include other objectives apart from the foregoing. For instance, ash quality requirements can take priority over classical parameters like gasification efficiency or high heating value. This is because the improvement of ash quality facilitates its recycling as raw material for other processes. This is a key aspect in biomass gasification because fly ash disposal costs represent a significant share of the overall operating cost of gasification-based energy production (Gasash, 2005). An essential part of the ash quality improvement and ash volume reduction is improvement of carbon conversion. In addition, an increase in carbon conversion results in higher conversion efficiency and this has a direct positive influence on power production efficiency. To optimise the gasification process and develop methods to improve carbon conversion, char reactivity knowledge is essential. The design of a gasifier for this purpose can differ notably from the classical design.

When a biomass particle is fed into an FB gasifier the particle is heated and the moisture and volatile gases are driven off. The final stage is a heterogeneous gas-solid reaction between the char and steam and carbon dioxide, which is usually rate-limiting. At short solid residence time and low temperature, the gas producer is usually of predominately pyrolytic origin (Nilsson, 1990). However, at a high enough temperature and sufficiently long solid residence time, the contribution from gasification of char particles to the final gas composition may be dominant (Bjerle, 1980). In this scenario, the lower rate of char gasification compared to devolatilisation makes the gasification rate of char one of the most important pieces of information for evaluating the whole gasification process. In this case, it mostly determines the required volume of a gasifier (Luo et al, 2001a; 2001b).

3. Modelling of char gasification in FB biomass gasifiers

The gasification rate of char in a gasifier is influenced by a number of process variables, such as particle size, char porosity, mineral content of the char, temperature and partial pressure of the gasifying reactant and products. Many of these variables have a complex impact on the process. In practise a number of simplifications are used to obtain a more tractable model which represents the key factor influencing the gasification of char particles in FBs.

3.1. Intrinsic reactivity

The intrinsic gasification rate, i.e. that determined free of diffusional effects, of char with CO_2 and H_2O is usually represented by n^{th}-order or Langmuir-Hinshelwood kinetic model, the latter when the inhibition effect of the products (CO and H_2) must be taken into account. During the gasification of a char particle, the intrinsic reaction rate varies in a complex manner with residual carbon, because of variation in the internal surface or in pore size distribution. To take this effect into account explicitly, empirical expressions have appeared in the literature for a variety of chars in a given range of operating conditions (Dutta et. al., 1977; Johnson, 1979). However, caution should be exerted in applying the expressions from one char to another (Buekens and Schoeters, 1985). This is true for different coal chars but is especially relevant for char derived from biomass. One of the reasons is that the latter is different from coal

char in two important respects: its ash content is normally low and its porous structure may be highly directional. In addition, alkali element concentration in ash from biomass is high, which has well-know catalytic effects on the char gasification reactions.

3.2. Purely kinetic modelling approach

A general model to represent the gasification of a char particle needs to consider three heterogeneous reactions (H_2–char, CO_2–char and H_2O–char) along with the gas-shift reaction in the gas phase filling the pores of the char. Theoretically, if the intrinsic kinetics for these reactions is known, the rate of gasification of a char particle can be calculated for the case where a smooth field of gas species and temperature prevails within the char particle. To evaluate the reaction rate at any reacting site inside the porous char particle, the species concentration and temperature can be assumed to be those of the bulk gas. If, in addition, the char particle has been reacting in the FB under this kinetically-controlled regime from the initial time of reaction for that particle, the local conversion profile is also smooth within the particle. In this case, the particle model can be lumped to a point so that, a purely kinetic modelling approach is sufficient to analyse the char reaction rate. With these assumptions, the concentration gradient of the gaseous species and the temperature throughout the gasifier can be obtained in the direction of macroscopic flow by considering that the set of reactions is a source or sink point. This sink or source is calculated by using the intrinsic chemical kinetics of the reactions and the available carbon concentration at a given time, the latter being characterised by the overall conversion of the char particle.

3.3. Diffusional effects in a single char particle

If diffusional film and intraparticle mass and heat transfer processes in char particles are not rapid enough, the actual gasification rate differs from the intrinsic one evaluated in bulk-gas conditions. Under these conditions, the overall gasification rate of a single char particle is determined by combining the intrinsic chemical reaction rate with intraparticle and external diffusional rates. Therefore the actual gasification rate may strongly depend on particle size, effective properties of the char (if intraparticle resistance is limiting) and fluid-dynamic conditions (if film resistance is important).

In atmospheric gasifiers methane formation can be disregarded so that only three reactions must be considered. The reaction rate of char gasification with CO_2 is usually slower than with H_2O and at high enough temperature the gas-shift reaction is rapid compared to other reactions so that equilibrium is attained anywhere within the char particle (Bliek et al. 1987). Temperature profiles are nearly uniform under usual conditions, so isothermal conditions can be assumed in most cases (Srinivas and Amundson, 1980). Also, the higher diffusivity of hydrogen compared to other gaseous components leads to nearly uniform concentration throughout the char particle (Bliek et al. 1987; Chang 1988). A typical picture of the situation of a char particle in a biomass FB gasifier is depicted in Fig 1.1.

Mass and heat transfer limitations in char particles have been thoroughly studied under usual conditions in gasifiers (Srinivas and Amundson, 1980; Haynes, 1981; Bliek et al. 1987; Sipilä 1988; Chang, 1988; Weimer and Clough, 1980; Gururajan et

al., 1992; Buekens and Schoeters, 1985). The main effort, however, has been made with coal gasification systems. Due to the variety of chars and operating conditions, different conclusions have been derived from the above studies and it is therefore difficult to establish clear guidelines. In general, coal char particles of 1 mm seem to react according to a uniform conversion model (UM)—that is, negligible diffusional resistance—up to 820 ºC (Agarwal and Sears, 1980). Srinivas and Amundson (1980) analysed the potential impact of char particle sizes in FB coal gasifiers. They found that diffusional effects were significant in the usual range of temperature (1100-1400 K) and char sizes (0.5-5 mm). Taking 1200 K as bulk-gas reference, they found that diffusional effects became acute (effectiveness factor below 0.5) for char particles over 1 mm for Sh=2 and over 4 mm for Sh =200. The Sherwood effect was found to have a strong effect in the range of 2 to 30 and its impact on the gasification rate was negligible above 100. Different authors (Haynes, 1981; Bliek et al. 1987; Chang, 1988) have confirmed similar trends. These findings do not explain the almost universal assumption of disregarding transport process limitations inside char particles in the modelling of FB coal gasifiers.

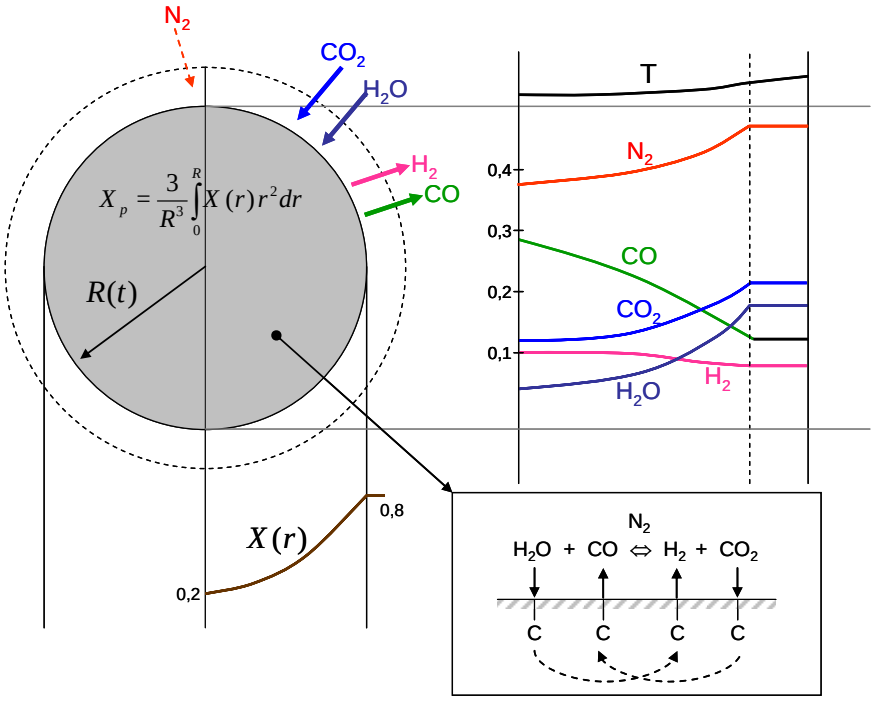

Figure 1.1. Picture of a typical situation inside a char particle in a gasifier

3.4. Modelling of char gasification rate inside an FB gasifier

The calculation of the overall char gasification rate in an FB is quite complex because, in addition to the transport and reaction processes inside the char particles, it is necessary to take into account the fluid-dynamic resistance to the transport of the oxidising agent between bubbles and dense phase and transport within the dense phase. To consider this, it is necessary to solve the gas and solid flow pattern inside the FB gasifier and apply population balances to fuel particles. This involves processes such as drying, devolatilisation as well as others such as attrition, entrainment and elutria-

tion. The gas composition inside the bed is affected by all these processes and influences the actual gasification rate of a char particle in an FB gasifier.

Initial combustion and devolatilisation processes particularly affect the performance of FB gasifiers processing biofuels as compared to coal. The moisture content of the biofuel can be as high as 60 wt%, whereas the char residue may be below 10 wt% of the dry fuel mass. This is in contrast to coal, whose moisture content is lower and for which char combustion accounts for most of the heat release (Thunman, 2002, 2004). Characterisation of the volatile gases from these processes may have a significant impact on gas composition and its distribution inside the reactor and, therefore, on the gasification rate of char particles.

The prediction of fluid dynamics in an FB is a difficult problem. This comprises basically the prediction of gas flow division (gas in emulsion and bubbles), solid and gas mixing in the emulsion and in bubbles, estimation of bubble size and velocity and bed height, just to mention a few. Entrainment and elutriation have a great impact on the proportion and size of char in the bed and on the degree to which particles are affected, on average, by diffusional effects. The reason is that entrainment preferentially removes small particles from the bed, resulting in a larger fraction of coarser char particles in the bed (Kunii and Levenspiel, 1991). Consequently, diffusional effects are likely to be present in these particles because they are less porous, larger, or a combination of both.

As a consequence of all these processes, the rigorous analysis of an FB gasifier is a problem of extreme theoretical and computational difficulty. Therefore, in modelling an FB gasifier, there is a need for relatively simple particle kinetic models to represent the rate of char gasification over the range of normal operating conditions. In practise, simplifications are used to obtain reasonable and tractable models, although most of them do not seem to be appropriate. This is discussed below.

3.5. Char-particle models as submodels in FB gasifiers

The conversion behaviour that best represents the real processes in the gasification of a char particle depends mainly on bed temperature and the fuel particle size fed to reactor. In an FB biomass gasifier these values differ notably from fixed-bed or entrained-bed gasifiers. The size of fuel particles fed into an FB gasifier is typically 0.2-6 mm and the bed temperature 700-900ºC**.** In FB gasifiers external gas-film diffusion is not expected to be rate-limiting at normal operating temperature (Buekens and Schoeters, 1985; Srinivas and Amundson, 1980). In addition, the particle temperature is only slightly higher than that of the bed because of the simultaneous occurrence of exothermal and endothermal reactions (Weimer and Clough, 1980; Srinivas and Amundson, 1980; Bliek et al. 1987; Chang, 1988). As a consequence of these conditions, the overall gasification rate of a char particle in an FB biomass gasifier is likely to be affected by intraparticle mass transport effects. According to Sipilä (1988), the gasification rate in an FB biomass gasifier usually lies in the transition between the chemically-controlled and pore-diffusion-controlled regions.

FB coal gasifiers

Reactor models are abundant for gasification of coal in FB. In contrast, they are not so numerous for the case of biomass. An excellent review of FB coal gasifier models was published by Gururajan et al. (1992), in which they looked at the most important models up to 1992. Table 1.3 in that study includes 21 FB coal models based on their major assumptions. Only one of the 21 includes intraparticle transport effects on char particles—specifically, the model developed by Srinivas and Amudson, 1982. These authors implemented their particle model directly (Srinivas and Amundson, 1980) as a submodel for reactor simulations. In spite of the considerable computational difficulty, they showed that the scenarios with and without intraparticle mass transfer effects were quite different.

To update the perspective given by Gururajan et al. (1992), we reviewed some of the most relevant models for coal published over the last decade (Ciesielczyk and Gawdzik, 1993; Luo et al. 1998; Yan et al.,1997, 1999; Yan and Zhang, 1999; Chejne and Hernandez, 2002; Ross et al., 2001, 2004. Ashman and Mullinger, 2004; Ross et al., 2005). It must be recognised that the new model makers have refined many of the assumptions made by initial researchers. They have been basically concerned with making those assumptions involving fluid dynamics, population balances and intrinsic kinetics real. However, the new studies, almost without exception, still implement a kinetic approach or UM for modelling char-particle gasification. It is noteworthy that that in no model is there a formal explanation about why they disregard these processes. This contrasts strongly with the conclusions of the large number of particle models for single char particles (Arri and and Amundson, 1978; Srinivas and Amundson, 1980; Haynes, 1981; Zygourakis et al. 1982; Reyes and Jensen, 1986a, 1986b; Bliek et al. 1987; Chang 1988; Morell et al. 1990; Wang and Bathia, 2001, Li and Niksa, 2004), where diffusional limitations are often quite significant under usual operating conditions in gasifiers.

FB biomass gasifiers

For the case of biomass gasifiers, Buekens and Schoeters (1985) made an assessment of the models developed up to 1985. Although that review, in principle, deals with biomass gasification, only one model presented was concerned with FB biomass gasification (the rest with coal): the work by Raman et al. (1980). They investigated the gasification of manure using a UM for modelling the gasification of char particles. Hamel (2001) recently reviewed FB gasifier modelling studies on both biomass and coal. However, he concentrated mainly on the fluid-dynamic treatment of the models and did not particularly address the effects of intraparticle resistance in char.

Table 1.1 summarises the main significant FB biomass gasifier models published from the early 1980s to date. As seen in the table, an intrinsic kinetic approach has also been widely used for modelling the gasification of char particles in FB biomass gasifiers. Often, it is not clearly specified (or not justified) the treatment given to the char gasification reactions (Liu and Gibbs, 2003; Corella and Toledo, 2006; Hamel and Krumm, 2001; Fiaschi and Michelini, 2001; Petersen and Werther, 2005a, 2005b). It is typical the use of kinetic reactivity from coal when modelling biomass systems (Petersen and Werther, 2005a; 2006b; Liu and Gibbs, 2003). Petersen and Werther (2005a; 2006b) used the L-H kinetics obtained by Matsui et al. (1985,

1987a, 1987b) for coal chars in order to model the char gasification of sewage sludge in a CFB. This assumption is doubtful because the reactivity of sewage sludge is higher than coal (Scott et al, 2005). Despite this questionable supposition, they clearly specified the use of UM to account for the progress of char conversion.

Table 1.1. Selected FB biomass gasifier models

Reference	Kinetics	Particle model	Biomass	Type of FB	T (K)	Remarks
Raman et al. (1981)	n^{th}	UM	Manure	BFB	700-1200	Pioneer attempt at modelling biomass FBG
Van den Aarsen (1985)	n^{th}	SCM	Wood/Rice husk	BFB	973-1223	Kinetics obtained in lab applied to model pilot-scale FB gasifier
Souza-Santos (1989)	n^{th}	ECM	–	BFB	1000-1100	FB boilers and gasifiers.
Jiang and Vance Morey (1992)	n^{th}	SCM	Corncob	BFB	921-1052	Extend van den Aarsen' model (1985) to freeboard
Bilodeau et al. (1993)	n.a.	UM	Wood, plastic	BFB	973-1181	Simulate FB tests carried out by Czernik et al. (1992)
Jennen et al. (1999)	n.a.	SCM	Wood	CFB	1173-1223	Great influence of char gasification reactions.
Fiaschi and Michelini (2001)	n.a.	n.a.	Various biomasses	BFB	1023-1173	Model elutriation and abrasion
Hamel and Krumm (2001)	n.a.	n.a.	Peat, sawdust	BFB	1100-1200	Atmospheric and pressurized BFB
Sadaka et al. (2002)	EM	EM	Agricultural waste	BFB	1000-1050	BFB divided into three zones
Chen et al. (2003)	n^{th}	UM	Black liquor	BFB	760-820	Three-phase fluid-dynamic model to simulate commercial BFB
de Jong et al. (2003)	n^{th}	UM	Wood Miscanthus	BFB	1036-1160	FB conversion of coal and biomass Fuel sizes between 0.17-1.89 mm
van den Enden and Silva (2004)	n^{th}	UM/SCM / ECM	Sugarcane bagasse	BFB	1273	Use CSFB software
Chen et al. (2004)	n^{th}	GM	Miscanthus	CFB	1026	Model devolatilisation with UM and combustion with SCM
Liu and Gibbs (2003)	LH	empirical	Woody biomass fuel	CFB	1025-1175	Char gasification from coal. Empirical factor in reactivity
Petersen and Werther (2005a; 2005b)	LH	UM	Sewage sludge	CFB	1023-1173	Kinetic from coal (Matsui et al; 1985, 1987a; 1987b)
Corella and Toledo (2006)	n^{th}	UM/SCM	Pine wood	CFB	1073	CO_2-char kinetics from van den Aarsen (1985)

Nomenclature: SCM: shrinking core model. UCM: exposed core model. UM: uniform model. GM: grain model. L-H: Langmuir Hinshelwood. CFB: circulating fluidised bed. BFB: bubbling fluidised bed. FBG: fluidised bed gasifier. n.a.: not available. n^{th} : n^{th} order kinetics;

The same assumption was adopted by Liu and Gibbs (2003). These authors took the char kinetics from that used by Luo et al (1998) for the gasification of coal in

a jetting FB gasifier. However, they introduced an empirical factor (from 1 to 10) to account for the higher reactivity of the biomass derived char compared to coal. In addition, the char gasification kinetics of Luo et al (1998) included an experimentally-determined function to take into account the effects of burn-off in char gasification. This behaviour is difficult to extrapolate from coal to biomass. Moreover, it is not even clear if this experimental function includes the effect of char particle size. Other cases such as Fiaschi and Michelini (2001) do not even report the kinetics of char gasification used in their simulations. This contrasts with the effort made by these authors to model other processes in competition with char reaction like elutriation and attrition.

Some authors, have considered particle models other than the UM (Van den Aarsen, 1985; Jennen et al, 1999; Souza-Santos, 1989; Jaing and Morey, 1992; Chen et al., 2004). For instance, Jaing and Morey (1992) used the shrinking-core model (SCM) for the gasification of corncob and Van den Aarsen (1985) for char derived from wood and rice husk. Models applying shrinking-core behaviour to char particles have usually assumed that the external ash is removed with time, which is called the exposed shrinking-core model (ECM). In it, only external mass transfer and intrinsic kinetics in the external core surface are considered. This is because the severe attrition inside an FB seldom allows the carbonaceous solid particle to retain the ash layer formed as the surface reactions proceed (Souza-Santos, 1989). In general, however, the SCM does not seem reasonable under normal operating conditions of FB biomass gasifiers (Buekens and Schoeters, 1985; Chen et al. 2004). Other researchers have assumed an impervious carbon particle and defined an apparent kinetic constant at the surface, which lumps the diffusion and reaction phenomena inside the particles. Indeed, in this method, the kinetic constant is obtained by referencing the intrinsic gasification rate to the external surface, after accounting for intraparticle diffusion resistance. Therefore, they implicitly account for intraparticle transport effects but often do not report how the effectiveness factor, which is contained in the apparent kinetic constant, is calculated. This could be the case of the model developed by Fiaschi and Michelini (2001), Hamel (2001) and Chen et al. (2003). A noteworthy effort to represent the actual gasification behaviour of single char particles was made by Chen et al. (2004). They developed a model of a CFB biomass gasifier using a grainy pellet model (GM) for the gasification of char. These authors claim that the GM is better suited to gasification processes because it integrates the natures of the SCM and the UM. This model, however, needs the effective diffusivity of gas in the product of the ash layer surrounding the grains and also the original grain size and its progression with time. These are too many parameters, and they are often inaccessible.

From the foregoing considerations we conclude that: (1) A systematic analysis of the relative influence of external and intraparticle transport effects on the behaviour of char particles and their impact on the final off-gas composition does not appear to have been reported. (2) The use of the UM has been almost uniquely used to represent the behaviour of char gasification in FBs processing coal. The case of FB biomass gasifiers is similar, although some other simple models like SCM or GM have also been used. The SCM is not generally applicable to the actual operating conditions in FB biomass gasifiers, whereas the GM, despite being more appropriate, needs parameters difficult to obtain.

Therefore, in the case of biomass and most probably also for coal, any char-particle kinetic model to be included as a submodel in an FB biomass gasifier should be capable of capturing diffusional effects. Simple models are most welcome due to the complexity of the problem. As shown in table 1.1, most FB biomass gasifier models in the literature simply disregard transport process limitations inside char particles. The reason seems to be the complexity of introducing a submodel which involves the simultaneous diffusion of a mixture of CO_2, CO, H_2O, H_2 and N_2 rather than the real need to account for these processes in the problem. In the author's opinion, it is preferable to include an approximate particle model which takes into account intraparticle mass transport effects in a simple manner rather than developing a full-rigorous numerical model. The reason is that, in practise, this type of model is not eventually implemented as the submodel's code in real reactor simulations due to the extreme computational difficulty.

3.6. Strategies used to include char-particle model in FB

From the foregoing discussion, we distinguish three main approaches to include the gasification of char particles in the modelling of FB gasifiers:

1. *Pseudo-empirical approach (PEA)*: The gasification rate of a char particle is calculated using a char reactivity determined previously in the laboratory using single particles with similar properties as those expected to be found in the real-scale process. The effect of burn-off history is considered by including certain empirical expressions as a function of the overall particle conversion. This procedure to determine the rate of gasification is widely used because it avoids the need to solve a particle model for the char particles. If diffusional effects inside char particles are present, however, this method can be questionable. The uncertainty of the FB gasifier models using this approach is high because there are no data about the impact of physical effects on the lab-determined reactivity or on the gasifier conditions.

2. *Rigorous approach (RA)*: The reactivity is obtained free of diffusional effects in the laboratory. In modelling the reactor, the reactivity is used locally at any position inside a char particle. To evaluate the overall gasification rate of the char particle, a kinetic-particle model is formulated together with the overall reactor model. This method is rigorous but is computationally very complicated. However, when diffusional effects are likely to be present, it is, in theory, preferable.

3. *Combined approach (CA)*: In practise a combination of both methods is used in modelling FB coal and biomass gasifiers. Simple particle models like SCM or UM or GM are used. Some models make use of kinetic expressions obtained in the laboratory under doubtful conditions (in many cases obtained by authors other than the model makers). In other cases, the kinetic expressions for the char gasification reactions with CO_2 and H_2O are taken from char from other biomass or coal. Other cases employ the same char but generation takes place by means other than FB (for instance, char prepared in TGA). In general, it is rather difficult to elucidate the acceptance of the model when using this approach.

The ideal methodology which seems to overcome all these difficulties is a *pseudo-rigorous approach (PRA)* consisting of the two following main steps: (1) De-

termining the intrinsic reactivity for the same biomass under analysis and generating the char under conditions similar to the real situation in which the FB gasifier model will be used; (2) Solving a simple particle-kinetic model. Though simple, the model should be capable of taking into account the intrinsic kinetic and diffusional effects inside the char particles. This method combines the benefits of the rigorous and pseudo-empirical approaches.

Table 1.2. Selected FB gasification models adopting the equilibrium approach

Reference	T(K)	Feedstock	Remarks
Bacon (1985)	1000-1060	Wood	BFB. Use degrees of approach to equilibrium
Kovacick et al. (1990)	1173	High-value coal	Use KRW technology
Watkinson et al. (1990)	873-1473	Various coals	Model of various types of coal gasifiers. Predictions poor for FB gasifiers
Kinoshita et al. (1991)	1023-1473	Biomass	BFB. Gasification of biomass for methanol synthesis
Ergudenler (1997)	n.a.	Straw	BFB
Mansaray et al. (1999)	n.a.	Rice husk	BFB
Li et al. (2001)	1023-1153	High-value and Pittsburgh seam coal	CFB. Kinetically-modified equilibrium model is proposed
Schuster et al. (2001)	920-1323	Biomass: beech chips	Dual fluidized-bed gasifier. Steam gasification
Mathieu and Dubuisson (2002)	1053-1323	Wood	BFB. ASPEN PLUS model: Gibbs free energy
Sadaka et al. (2002)	1273-1323	Agricultural waste	BFB. FB divided into three zones: jetting, bubbling and slugging.
Scott et al. (2003)	1073-1573	Sewage sludge subbituminous coal	BFB
Li et al. (2004)	973-1123	Various biomasses	CFB

Another approach for the modelling of FB gasifiers not considered here is to assume equilibrium. Although kinetic models have, in theory, the capability of predicting both the overall gasifier performance and the behaviour inside the gasifier, the many problems involved in making use of kinetic data have been discussed. Probably, due to the inconsistencies discussed above, many authors have chosen this alternative to evaluate gas compositions in FB gasifiers with different degrees of success. Table 1.2 presents some well-known models that have used this approach. In practice, a gasifier may not reach equilibrium. For example, Bacon et al. (1985), Rapanga et al. (1997), Gómez-Barea et al. (2005) reported deviations from equilibrium in three different studies of biomass gasification in a fluidised bed. Despite this limitation, equilibrium models can identify trends and performance limitations and also rationalise results. In any case, the approach is consistent and limitations are known. This can be better than many kinetic models full of contestable assumptions.

4. Determination of char gasification reactivity

From the preceding, it becomes obvious that knowledge of char reactivity is a decisive factor in the design and modelling process. This is supported by many researchers

(Luo et al., 2001a, 2001b; Briedis et al., 2001; Scott et al, 2005; Buekens and Schoeters, 1985; etc) and it is the reason why numerous studies have been performed on char gasification kinetics (Molina et al., 1998; Liliedahl and Sjöström, 1997).

Experiments for determination of char reactivity in the laboratory are usually designed to operate within the kinetic regime, i.e., keeping away from physical effects. However, the particle size used and/or the operating gas composition and temperatures used in experiments often make this assumption doubtful. In this scenario, the actual reaction rate is likely to be affected by mass or heat transfer limitations. As a result, a correction factor should be introduced to correct the apparent kinetics obtained. The diffusional effects are often assessed by introducing an effectiveness factor.

Experimental data for CO_2 and H_2O gasification have been reported using TGA, fixed bed, laminar flow (drop tube), entrained flow and fluidised bed reactors. Although these experiments provide valuable information related to specific aspects of char reactivity, there is a need for further discussion of the range of validity of the determination and extrapolation of reactivity data for biomass fuels. To make it possible to experimentally determine kinetics that are free from diffusion effects, the experiments are usually carried out in typical laboratory apparatus (thermo-balance (TGA), muffle furnaces, etc.) (Rapagna, 1996, Gómez-Barea et al., 2006), where the conditions are under control. However, char reactivity depends greatly on the form of preparation. To simulate high heating rates to meet the requirements of an FB, some researchers use drop-tube reactors (Lee et al., 1996). With this method, however, it is usually the average gasification rate that is measured and it is difficult to give the rate variation as the reaction proceeds. There are also problems like uneven temperature distribution along the length of reactor, uncertainty in reaction temperature, and reaction time (Luo et al., 2001b). Owing to the limitation of the heating rate in a TGA or laboratory furnace, the measured gasification rates in these laboratory devices may deviate from those in commercial equipment, in which fuel particles undergo rapid heating during devolatilisation (Luo et al., 2001a).

Employing an FB reactor to determine the char reactivity seems to overcome many of drawbacks associated with the above devices. The main advantages over them are: (1) It is easy to prepare char in a FB reactor in a nitrogen atmosphere; (2) Fuel can be carbonised under various conditions, including different heating rates (from slow heating to rapid heating) and annealing times; (3) After carbonisation, no cooling of the char is needed and the char can be gasified in situ; (4) Measuring the time variation of outlet gas composition enables determination of the char gasification rate during conversion; (5) Uniform temperatures are maintained in the reaction zone.

However, some handicaps must be taken into account: (1) Combustion of volatiles changes the temperature conditions of devolatilisation and hence the final composition (and therefore reactivity) of the resulting char; (2) Kinetic research in an FB is difficult owing to its complex fluid dynamics. This makes it difficult to separate the kinetic information from mass transfer and/or hydrodynamic influence (Bjerle, 1980). Therefore, it would be desirable to have at one's disposal a simple methodology to evaluate transport effects during char reactivity determination in an FB. This makes it possible to avoid mass-transfer interferences or, when transport effects cannot be

fully eliminated, to make a correction for the observed reactivity in order to determine the intrinsic reactivity. To develop such a methodology is the second objective of this thesis.

5. Scope and outline of the thesis

This thesis describes theoretical and experimental research on transport effects taking place during the gasification of single char particles. The aim is to assist in the design of fixed- and fluidised-bed gasifiers and to aid in establishing operating conditions in a lab-scale FB reactor to avoid mass-transfer interferences during the determination of char gasification reactivity.

The main contributions of this work are:

1. The development of a simple modelling approach for simulating the gasification of a char particle with a single oxidant, which allows for the analysis of diffusional processes occurring in a macroscopic char particle. An original treatment for obtaining the solution of single non-catalytic gas-solid reactions has been developed. In Chapter 2 the model is derived under intraparticle isothermal conditions and large Biot numbers. That model is extended in Chapter 4 for the cases where non-isothermal intraparticle and mass and heat transfer effects in the gas-film layer are important. This simple model facilitates a rapid assessment of non-isothermal intraparticle and external effectiveness factors in single char particles for the whole range of char conversion. Model prediction capabilities are assessed in Chapter 4 by comparison with a set of TGA char gasification tests reported in Chapter 3.

2. The establishment of a basis for the choice of operating conditions for a laboratory-scale bubbling FB reactor to avoid fluid-dynamic and mass-transfer interferences in the determination of char reactivity. A modelling approach which combines a kinetic particle model with a simple two-phase flow model is proposed in Chapter 5. The model developed is validated by comparison with a set of FB char reactivity experiments at laboratory scale given in Chapter 6. When transport effects cannot be fully eliminated, the model developed enables data correction of the apparent reactivity in order to determine the intrinsic reactivity. This is applied to some tests presented in Chapter 6.

A brief description of the content of each chapter is given below.

Chapter 2 presents a simple treatment for obtaining the solution of single isothermal non-catalytic gas-solid reactions. The model is formulated using a local volumetric approach and enables incorporation of non-linear chemical kinetics and changes in porous structure during conversion. The methodology developed is based on the quantize method for decoupling the solid and gas equations and on perturbation and matching techniques for approximating the gas conservation equation. With this strategy, the calculation of gas concentration and solid conversion at any time and position is reduced to the solution of two coupled algebraic equations. The model compares favourably with the numerically calculated solution for a variety of cases.

The procedure provides an effective, general tool for obtaining the solution of gas-solid reactions with minimal calculations.

Chapter 3 is devoted to the analysis of diffusional effects during char gasification reactivity tests carried out in a TGA. Gasification rates of orujillo char measured in a TGA at various particle sizes, CO_2 partial pressures and temperatures of practical interest are presented. Experimental results are compared with the intrinsic reactivities obtained under the same operating conditions but using very fine char. This makes it possible to experimentally identify the limiting phenomena that may take place during WPOS-char gasification experiments with CO_2.

Chapter 4 extends the model developed in Chapter 2 to allow for intraparticle heat effects and transport processes within the surrounding gas layer. It presents a simple methodology to evaluate the experiments given in Chapter 3. The model satisfactorily explains the experiments and points out the importance of the diffusional effects at high temperatures and large particle sizes — i.e., large Thiele modulus. In particular, intraparticle mass limitations have been identified as the main responsible of the strong resistance found at the conditions tested. External heat and mass transfer has also found to play a relevant role. This theoretical treatment also makes it possible to analyse the processes occurring in experiments under different conditions, which sheds light on the different physical aspects involved in a typical char gasification test. The combined theoretical-experimental approach developed in this work has revealed to be of great help in interpreting the experimental results. The model is capable of capturing the major physico-chemical processes with minor computational difficulties.

Chapter 5 establishes the basis for the choice of operating conditions for a laboratory-scale bubbling FB reactor in order to avoid fluid-dynamic and diffusional interferences during solid reactivity determination. The methodology is derived for isothermal conditions, and when only one heterogeneous reaction is involved. This is the case, for instance, in tests of FB CO_2-char gasification reactivity. For other systems these assumptions need to be assessed prior to application of the method presented here. For example, in FB O_2-char reactivity (char combustion) tests, the isothermal assumption may be violated, depending on the char to inert ratio, oxygen concentration, particle size and intrinsic reactivity of the char. In reactivity tests of H_2O-char gasification kinetics, it is necessary to consider a second (independent), homogeneous reaction, for instance, the water-gas shift reaction. These cases are somewhat more complicated. However, the methodology presented here can be readily extended to cover these cases, although the simplicity of the treatment (obtaining analytical solutions) is then lost. It can also be applied to other non-catalytic isothermal systems, where diffusional effects may influence the observed reaction rate and only one reaction occurs. The chapter ends by providing charts for direct and rapid evaluation of transport effects in FB char reactivity experiments. These charts provide valuable information for the correct operation of FB reactivity tests.

In *Chapter 6* the methodology of Chapter 5 is applied to evaluate diffusional effects present during CO_2-char gasification reactivity tests in a bench-scale FB reactor. The char used was wood matter from pressed-oil stone (WPOS), also called orujillo. The experimental programme included the measurements of the gasification rate of

WPOS char at various particle sizes, CO_2 partial pressures, temperatures, and initial mass of char batches. The primary aim was to establish an optimal operating region to carry out lab-scale char reactivity FB gasification free of fluid-dynamics and diffusional effects. Practical difficulties made it impossible to operate completely in a kinetically-controlled regime. Therefore, a second objective was to quantify physical interferences in the measured reactivity in order to make a correction for the resulting apparent reactivity to obtain the intrinsic reactivity.

The thesis ends with *Chapter 7*, which includes the main conclusions of this work. It establishes the significance of the work and gives some recommendations for future research.

Chapter 2

Approximate modelling of gas-solid reactions

1. Introduction

Non-catalytic gas-solid reactions are an important class of heterogeneous reactions. They have received considerable attention and numerous models and techniques for their solution are available in the specialised literature. In a broad sense, these models can be classified into two categories (Groeneveld and van Swaaij, 1980): structural (porous or grain) and volumetric. The structural models explicitly consider the solid structural changes during reaction. This is done by modelling the variation of either the internal solid matrix (grain models: Szekely et al., 1976; Ranade and Harrison, 1979; Heesink et al, 1993) or the internal pore structure (pore development models**:** Bhatia and Perlmutter, 1980, 1981**;** Gavalas, 1980, 1981) during conversion, allowing for changes in the structure as the reaction proceeds. In the volumetric approach, in contrast, the changes in porous structure during conversion can be considered by using experimental correlations. In this approach, effective experimental or estimated properties are introduced into the problem. Ramachandran and Doraiswamy (1982), Doroiswamy and Sharma (1984), reviewed available models up to the eighties, and more recently. Bathia and Gupta (1992) and Sahimi et al. (1990) have updated to 1990s volumetric and structural non-catalytic gas-solid reaction models. More recently Patisson et al. (1998) surveyed advanced numerical models for solving general non-isothermal gas-solid reactions. Most models, whether structural or volumetric, require a numerical solution, as an exact analytical solution cannot be found for most of the rate forms used to describe these systems (Ramachandran, 1983). An extensive literature about the computational aspects of these models can also be found (Xu and Hoffmann, 1989; Patisson et al., 1998; Hindmarsh and Johnson, 1988, 1991**;** Doroiswamy and Sharma, 1984).

There are circumstances where a simpler, more analytical approach seems to be advisable. An analytical or semi-analytical method can provide an ideal approach to solve problems where cumbersome calculations are involved. This chapter presents an original model which allows including any general kinetics, i.e., n^{th}-order, Michaelis-Menten, etc., and any explicitly given solid consumption behaviour with reaction. The main aim is to come up with a model which requires minimum computational effort, while keeping the capability of capturing the major physical features of the problem.

This analytical approach has been extensively developed by a number of investigators and the literature is full of techniques for simplifying the associated mathematical and computational difficulties. The use of cumulative concentration introduced by Del Borghi et al. (1976) and Dudukovic and Lamba (1978) made it possible to reduce the system of equations to a single non-linear diffusion-reaction equation in terms of a new variable — namely, cumulative gas concentration. Ramachandran (1983) defined a new generalised Thiele module, which allowed him to obtain analytical expressions for a variety of cases with non-linear reaction rates with respect to the solid reactant. However, the validity of his solution is limited to first-order kinetics with respect to the gas reactant.

Brem and Brouwers, (1990a) presented an analytical description for the case of reaction rates of a general order with respect to gas concentration and intrinsic reaction surface area and pore diffusion, which change with solid conversion. The complete analytical description of the non-linear conversion process was based on a combination of two asymptotic solutions, for small and large values of the Thiele modulus. Within the intermediate range they adjusted their solution by fitting their approximate solution to the analytical solution for the first-order case. They further extended the model to the non-isothermal case (Brem and Brouwers, 1990b). However, the fitting parameter is, in general, case-dependent and the results are only valid for n^{th}–order kinetics with respect to the gas reactant. Despite these limitations, their formulation represents a pioneer attempt at finding an approximate solution which explicitly includes the combined effects of both non-linear kinetics and a function which takes into account the intrinsic solid surface development.

Other analytical solutions are also available (Marcos et. al., 1991; Doroiswamy and Sharma, 1984; Sahimi et al.,1990) but they are limited for one (or both) of the following reasons: (1) only applicable to first-order with respect to the gas or solid reactant and/or (2) do not explicitly make allowance for structural changes with reaction.

2. A new approach to solving gas-solid reactions

To extend the spectrum of applications of the existing simplified methods, in this chapter another approach is described, based on methods developed in the field of catalysis. This is full of attempts focussed on seeking approximate analytical or semianalytical expressions. Like its non-catalytic counterpart, the catalytic problem tends to be influenced to a great extent by heat and mass transport processes. In non-catalytic reactions, however, it is necessary to describe the evolution of the solid structure (local conversion or solid reactant concentration) as the reaction proceeds. This is because the reaction rate depends on both solid and gas concentration. This is the essential distinctive feature of non-catalytic systems compared to their catalytic counterparts. From the mathematical point of view, this leads to the coupling of gas and solid conservation equations and introduces additional difficulty.

Research carried out by Gottifredi and Gonzo (1996, 2005) provides one of the most general solutions found for the isothermal catalytic steady-state case. Their solution allows for obtaining an easily handled analytical prediction of the effectiveness factor and concentration with general kinetics. To take advantage of Gottifredi's solu-

tion, it is first required to overcome the coupling between the two equations of the model. In other words, it is necessary to transform the non-catalytic problem to its catalytic counterpart. To achieve this, we applied the Quantize Method (QM), a semi-analytical, semi-numerical method originally developed by Jamshidi and Ale-Ebrahim(1996a, 1996b, 1997, 1999). This new strategy for solving coupled partial differential equations (CPDE) considerably reduces the mathematical difficulties normally present in gas-solid problems. These authors illustrated the QM potential by applying it to several gas–solid reaction models, including the grain model (Jamshidi and Ale-Ebrahim, 1996a)**,** half-order model (Jamshidi and Ale-Ebrahim, 1996b)**,** nucleation model (Jamshidi and Ale-Ebrahim, 1997) and modified grain model (Jamshidi and Ale-Ebrahim, 1999). More recently Rafsanjani et al. (2002) applied this method and reported a new mathematical solution for predicting char activation reactions. In their model, they included a term to account for the variation of the activation energy with the progress of the reaction but they assumed a first-order reaction for the gas reactant. This methodology, however, can readily overcome this limitation, as described below.

3. Theoretical development of a volumetric particle model with general kinetics

The general isothermal model for the reaction

$$\mathrm{A(gas)} + b\,\mathrm{B(solid)} \rightarrow c\,\mathrm{C(gas)} + d\,\mathrm{D\ (solid)}, \tag{2.1}$$

can be written as follows:

$$\varepsilon \frac{\partial c_A}{\partial t} = \frac{1}{r^m}\frac{\partial}{\partial r}\left[r^m D_e \cdot \frac{\partial c_A}{\partial r} \right] - (-r_A) \tag{2.2}$$

$$\frac{\partial c_B}{\partial t} = -(-r_B) = -b(-r_A) \tag{2.3}$$

The boundary and initial conditions of the problem are

$$\text{at } r = L: \quad c_A = c_{As} = c_{A0} \quad \therefore \quad \text{at } r = 0: \quad \frac{\partial c_A}{\partial r} = 0 \tag{2.4}$$

$$\text{at } t = 0: \quad c_A = 0 \text{ and } \quad c_B = c_{B0} \tag{2.5}$$

The use of m in (2.2) allows for the treatment of different geometries (m=0: slab, m=1: cylinder and m=2: sphere). This formulation is applicable to the cases where external mass transfer resistance can be neglected (large Biot numbers). The accumulation term in (2.2) is several orders of magnitude smaller than the diffusion

and reaction terms (quasi-steady-state assumption). The reason is that in $c_A / c_B \leq 10^{-3}$ usually holds in gas-solid reactions. In view of that, it will be neglected in what follows.

Also, a continuum description of the porous solid particle has been assumed in the formulation given. This assumption presumes that the largest length scale characteristic of the solid structure is much smaller than the characteristic length associated with concentration gradients. However, at any given position of the particle, the reaction rate per unit of volume can be formulated in structural form by means of a function which represents the available reaction sites at a given time. To incorporate this feature explicitly, the modelling approach followed here assumes that the intrinsic kinetics at any location within the particle is given by the following expression:

$$(-r) = r(c_A) \cdot F(X) \quad (\text{mol/m}^3 \cdot \text{s}) \tag{2.6}$$

In Eq.(2.6), the reaction rate has been split into two factors (Ollero et al. 2002, 2003; Gomez-Barea et al. 2005). The $r(c_A)$ factor takes into account the effect of gas concentration on reaction rate while $F(X)$ embodies the effects of the changes of available reacting surface. Note that the initial concentration of the solid reaction c_{B0} is included in the factor $r(c_A)$. This means that its value is a parameter that does not change with reaction. The change with conversion is fully captured by the function $F(X)$.

In principle, the structure of (2.6) can accommodate any kinetic model, whether structural or continuous, provided it has been obtained free of physical effects. This aspect and the formal derivation of expression (2.6) are presented in Appendix 2.1. For instance, n^{th}-order kinetics with respect to gas reactant and a uniform approach model with respect to solid consumption gives

$$(-r) = k\ c_A^{\,n}\ (1-X) \tag{2.7}$$

where k is the kinetic constant in $(\text{mol/m}^3)^{1-n} \cdot \text{s}^{-1}$. The variation of reaction rate with conversion, i.e., the $F(X)$ function, can be obtained by kinetic experiments provided they have been carried out without diffusional limitations. In TGA experiments, it is a common practise to report this information in the form of a so-called structural profile, which is defined as $f(X) = F(X)/(1-X)$. However, most of these experimental studies provide the structural profiles as a way to compute the reactivity at conversions other than that taken as reference. Thus, they usually include situations where diffusional effects are appreciable and the profiles are global structural profiles and not intrinsic (or local). In this case, they should not be directly used in Eq.(2.6). This has been recently discussed by Gomez-Barea et al. (2005).

Another approach for obtaining $F(X)$ is to use a published kinetic model under a kinetically-controlled regime. Typical non-catalytic models well established in the literature are the grain model (Szekely et al., 1976), the random pore model **(**Bhatia and Perlmutter, 1980, 1981**),** etc. In this approach the $F(X)$ function can be interpreted as the ratio of available solid surface at any conversion to that of a reference

case. The latter can be chosen ad hoc, but it is usual to take the original surface (Bhatia and Perlmutter, 1981). If the surface development can be assumed independent of the operating conditions (temperature and concentration) within a given range, the $F(X)$ function can be taken as intrinsic, and therefore unique for a given solid. Table 2.1 and Figure 2.3 provide some accepted models used for gasification reactions.

Owing to solid consumption or the difference between the volume of the solid reactant (B) and product (D), the void fraction (or local porosity) may change during the reaction. Whatever the case may be, the variation of local porosity (or local conversion) can be modelled by including an experimentally-obtained behaviour of the effective diffusivity. An accepted way to do this is to assume the following expression:

$$D_e = D_{e0}\, g(X) \tag{2.8}$$

where $g(X)$ is a function of local porosity and D_{e0} the initial effective diffusivity. For computational purposes, we will assume the following empirical equation for $g(X)$ (Wen, 1968; Brem and Bouwers, 1990; Gómez-Barea et al. 2006a):

$$g(X) = \left(\frac{\varepsilon}{\varepsilon_0}\right)^{\beta} = \left[1 + \left(\frac{1-\varepsilon_0}{\varepsilon_0}\right) X\right]^{\beta} \tag{2.9}$$

Taking into account Eqs. (2.6) and (2.9), the (2.2)-(2.5) set can be converted into dimensionless form

$$\frac{1}{z^m}\frac{\partial}{\partial z}\left[z^m\, g(X)\,\frac{\partial C}{\partial z}\right] = \phi_s^{\,2}\cdot F(X)\cdot R(C) \tag{2.10}$$

$$\frac{\partial X}{\partial \tau} = F(X)\cdot R(C) \tag{2.11}$$

$$\text{at } z=1:\ C=1 \quad \therefore \quad \text{at } z=0:\ \frac{\partial C}{\partial z} = 0 \tag{2.12}$$

$$\text{at } \tau = 0:\ X = 0 \tag{2.13}$$

where the following dimensionless variables have been used:

$$z = r/L, \quad \tau = t/\tau_{ref}, \quad C = c_A/c_{As} \quad \text{and} \quad X = 1 - c_B/c_{B0} \tag{2.14}$$

where the following time scale and reference reaction rate $r(c_{As})$ are given by

$$\tau_{ref} = c_{B0} / \left(b \cdot r\left(c_{As}\right) \right) \tag{2.15}$$

$$R(C) = r(c_A) / r(c_{As}) \tag{2.16}$$

Table 2.1. Main structural or empirical models applied to gasification kinetics

Name	Abbrev.	$F(X)$	Param.	$\Theta(X)$	Reference
Volumetric model	VM	$(1-X)$	–	$-\ln(1-X)$	Adánez. and de-Diego (1993) Adschiri et al. (1986)
Grain model; or Shrinking core model	GM (SCM)	$(1-X)^{2/3}$	–	$3\cdot(1-(1-X)^{1/3})$	Szekely et al.(1976) van den Aarsen (1985) Wang and Knoshita (1993)
Random Pore Model	RPM	$(1-X)\left(1-\psi_0 \ln(1-X)\right)^{1/2}$	ψ_0	$(2/\psi_0)\cdot$ $\left(1-\psi_0 \ln(1-X)\right)^{1/2}$	Bhatia and Perlmutter (1980)
Struis	MRPM	$(1-X)\left(1-\psi_0 \ln(1-X)\right)^{1/2}$ $f(t)$ (*)	p, α, ψ_0	(**)	Struis et al. (2002)
Simons Model	SM	$(1-X)\left(X+\alpha_0(1-X)\right)^{1/2}$	α_0	$2\cdot\text{atanh}\left((1-\alpha)X+\alpha\right)^{1/2}$	Simons (1980)
Johnson Model	JM	$(1-X)^{2/3}\, e^{\alpha X^2}$	α	NAEF	Johnson (1979)
Dutta Model	DM	$\left[1\pm 100\cdot X^{\gamma\cdot\beta}\exp(-\beta\cdot X)\right]$ $(1-X)$	α, β	NAEF	Dutta et al. (1977)
Gardner Model	GM	$(1-X)\, e^{aX}$	a	NAEF	Gardner et al. (1979)
Chornet Model	CM	$\sqrt{X}\,(1-X)$	–	$2\,\text{atanh}\,(\sqrt{X})$	Chornet et al.(1979)
Modified VM	MVM	$a^{1/b}\, b\cdot(1-X)\left[-\ln(1-X)\right]$	a, b	NAEF	Kasasoka et al. (1985)
Traditional	TM	$(1-X)^{\alpha}$	α	$(\alpha-1)^{-1}\cdot$ $\left[(1-X)^{1-\alpha}-1\right]$	
Polinomial Model	PM	$\sum_{i=1}^{n} a_i X\,(1-X)^i$	a_i	NAEF	Ollero et al. (2003) Gómez-Barea et al. (2005)

Comments:
NASF: Not analytical expression found.
(*) $f(t) = \left[1+(p+1)(\alpha\cdot t)\right]$.
(**) If the time appears in $F(X)$ explicitly it is necessary to integrate the expression (2.26) taking into account this feature. In principle, analytical solution is available for this Model

The ϕ_s parameter, which emerges from Eq. (2.10), is the Thiele modulus evaluated at surface conditions

$$\phi_s^2 = L^2 \frac{r(c_{As})}{D_{e0} c_{As}} \tag{2.17}$$

Once the conversion profile has been obtained, the overall particle conversion, X_p, is computed by

$$X_p(\tau) = (m+1)\int_0^1 X\, z^m dz \tag{2.18}$$

4. Approximate modelling

4.1. Foundations of the approximate method

Solving Eqs. (2.10)-(2.13) is difficult and an analytical solution can be obtained only for some special cases (Doroiswamy and Sharma, 1984). These are very specific cases, however, and their applicability is limited. We have developed a new method to extend the range of application, keeping the capability of determining the solution of general cases. This is based mainly on the two following steps:

- Step 1: The decoupling of solid and gas conservation equations at a given time.

- Step 2: The use of an approximate analytical expression for calculating the gas reactant concentration within an isothermal solid catalyst at pseudo-steady-state at that time. The solid particle is considered a catalyst with an activity distribution. This distribution is determined by the level of local conversion.

Step 1 is accomplished by the application of the Quantize Method (QM). This technique has been demonstrated to provide a powerful approach to solving coupled partial differential equations (CPDE). With this strategy, the equation set of a CPDE problem can be solved approximately by assuming some degree of independence between the independent variables, i.e., time and position. In particular, the application of the QM to (2.10)-(2.11) makes it possible to assume that the variables C and X are related to (z_i, τ_j) but are independent of (z_{i-1}, τ_j) or (z_i, τ_{j-1}). Here, "i" and "j" represent the indexes of a computational grid node; i.e., index "i" defines the position and "j" the time. In other words, at any point of the domain (z_i, τ_j), the variables C, X, τ and z are related to each other, but they are assumed to be explicitly independent of any other surrounding point, such as (z_{i-1}, τ_j) or (z_i, τ_{j-1}). This concept dramatically reduces the computational complexity because it makes it possible to solve the (2.10)-(2.11) set in two sequential stages. In the first stage, the method makes use of $X(z_i, \tau_{j-1})$ in-

stead of $X(z_i, \tau_j)$ in (2.10). This permits the spatial integration of (2.10) taking X as a constant. In the second stage, the use of $C(z_{i-1}, \tau_j)$ instead of $C(z_i, \tau_j)$ in (2.11) allows for the integration with respect to time by assuming C to be constant. Of course, some computational errors are expected with this two-fold simplification, but this error has proven to be small (Jamshidi and Ale-Ebrahim, 1996a, 1996b, 1997, 1999; Rafsanjani et al., 2002).

The second level of approximation, step 2, is achieved by solving the gas conservation equation as a catalytic problem at a given time. This adds, in principle, an additional error to the approximate method, but this error has been reported as small (Gottifredi and Gonzo, 2005). This two-step approximation has been used in some studies found in the literature, but only particular cases were implemented (Rafsanjani et al., 2002; Dutta et al., 1977).

4.2. Development of the approximate model

By taking $X(z_i, \tau_{j-1})$ instead of $X(z_i, \tau_j)$ in (2.10) the equation becomes

$$\frac{1}{z^m}\frac{d}{dz}\left[z^m \frac{\partial C}{\partial z} \right] = M^2(X) \cdot R(C) \tag{2.19}$$

$$\text{at } z = 1: \quad C = 1 \quad \therefore \quad \text{at } z = 0: \quad \frac{\partial C}{\partial z} = 0 \tag{2.20}$$

In the expression above, a new Thiele modulus which depends on conversion is introduced

$$M^2(X) = \phi_s^2 G(X)\,, \tag{2.21}$$

where $G(X)$ is a function of conversion defined as

$$G(X) = \frac{F(X)}{g(X)} \tag{2.22}$$

This formulation coincides with that used by Dutta et al. (1977). However, these authors employed this approach without making a distinction between local and overall particle conversion. In that case, their approximation should only be valid when both values coincide; that is, when no gradient exists within the particle. This is a strong limitation since they developed the model as an attempt to estimate certain diffusional effects detected with some coal chars at high temperatures.

Equations (2.19)-(2.20) have the structure of a reaction-diffusion problem in a solid catalyst. The only difference is that the Thiele modulus is conversion-dependent in Eq. (2.19). This feature, however, does not add any supplementary difficulty since, as explained above, the application of step 1 makes it possible to take X as a parameter. We can approximate Eq.(2.19) as if it were a catalytic problem.

Gottifredi and Gonzo (2005) reported an approximate treatment for the determination of the gas concentration within a catalytic pellet valid for any kinetics. They used perturbation and matching techniques to match the two asymptotic limits, i.e., the Petersen solution (Petersen, 1965), for large Thiele modulus, and the solution previously reported by Gottifredi and Gonzo for small ϕ_s values (Gottifredi et al., 1986). They obtained the following equation for the gas concentration profile:

$$C(z) = C^* + (1 - C^*) \cdot \exp\left[-\frac{\lambda (1 - z^2)}{2 - \dfrac{1 - z\,h(z)}{1 + 2/\lambda}} \right] \tag{2.23}$$

The symbols in Eq. (2.23) are defined below and in notation. Integration of Eq. (2.11) yields

$$\Theta(X) = \tau \cdot R(C) \tag{2.24}$$

where the $\Theta(X)$ function is defined according to

$$\Theta(X) = \int_0^X \frac{d\,X}{F(X)} \tag{2.25}$$

Expressions for $\Theta(X)$ associated with some well-known kinetic models are presented in Table 2.1. Note that in deriving Eq. (2.24) it has been assumed that $F(X)$ is not explicitly a function of τ. This is the usual situation (see Table 2.1). However, when τ is explicitly included, as in the case of $F = F(X, \tau)$, the procedure above must take it into account. This is, for instance, the case of the function given by Struis et al. (2002) for CO_2 char gasification (also covered in Table 2.1). These authors extended the original random pore model given by Bhatia and Perlmutter (1980), to take into account the catalytic and additional structural effects that they observed at high conversions.

Finally, by mathematically rearranging Eq. (2.24), the conversion profile within the particle can be obtained as

$$X(z) = \Theta^{-1}\left(\tau \cdot R(C(z))\right) \tag{2.26}$$

where Θ^{-1} is the inverse transform of the Θ function. The parameters appearing in Eq. (2.23) are defined as (Gottifredi and Gonzo, 1996, 2005):

$$M^* = \frac{M}{\sqrt{2 \cdot IR} \cdot (m+1)}\,,\quad a = 1 - 4\frac{(m+1)}{(m+3)} \cdot IR \cdot R'\,,\quad h(z) = \frac{1 - \exp(-\lambda\, z)}{1 - \exp(-\lambda)}$$

$$\lambda = \frac{M^2 \eta_{GOT}}{(m+1)(1-C^*)},\ R' = (dR/dC)_{C=1},\ IR = \int_0^1 R(C)\cdot dC \qquad (2.27)$$

$$\eta_{GOT} = \left[M^{*2} + \exp(-a \cdot M^{*2}) \right]^{-1/2}$$

where C^* is the root of the $R(C)$ function, which is zero for most kinetic expressions. The solution of the set given by Eqs. (2.23) and (2.26) provides C and X for a given position in the particle and time. This procedure is repeated for all points of the particle to give profiles of concentration and conversion, i.e., $C(z)$ and $X(z)$. Once these profiles are available for a given instant, the overall particle conversion is readily computed with Eq. (2.18).

It is worth noting that it is possible to obtain particle conversion without integrating from the initial time. This means a saving in the time needed to solve the ordinary differential equation (2.36) with respect to time. By way of example, if the time interval is split into 100 divisions for the numerical integration of the full problem (Eqs. (2.10)-(2.13)), the computational time is reduced roughly by the same factor. In addition, this is not the only advantage of the present method. It should be kept in mind that it is also very stable. This could be not the case of the full numerical solution where propagation errors during time integration could lead to stability problems. Finally, note that the only requirements for solving the problem are: (1) the specification of the reaction rate, that is, $R(C)$ and $F(X)$, and (2) the specification of D_{e0} and $g(X)$ (i.e. ε_0 and β if (2.9) is assumed).

5. Computational aspects

The approximate model given by Eqs. (2.23)-(2.26) was solved by dividing the spatial coordinate, z, into N + 1 points [$z_i = (i - 1)\ \Delta z$, i = 1: N + 1, $\Delta z = 1/(N - 1)$]. The solution (C_i, X_i) was found by solving (N+1) systems of two non-linear equations. This was done by applying the Newton-Raphson method. In most of the cases calculated in this work, a value of N=10 (typically 2 or 3 for small Thiele modulus values and 10 for large values of Thiele modulus) turned out to be enough for obtaining acceptable values of X_p (close agreement with the full numerical solution given by Eqs. (2.10)-(2.13)).

The numerical integration of Eqs. (2.10)-(2.13) was done by applying an explicit line method. The discretisation of Eq. (2.10) into N + 1 points along the spatial direction [$z_i = (i - 1)\ \Delta z$, i = 1: N + 1, $\Delta z = 1/(N - 1)$] allowed efficient integration of them. Using second-order central differences, a system of N non-linear equations was obtained and numerically solved with a Newton-Raphson method. Once the concentration profile was obtained for a given time**,** the local conversion at each point was found by integrating in the τ-direction Eq. (2.11) together with the initial condition given by Eq. (2.13). This was done by using a variable-step-size fourth-order Runge-Kutta method. For calculation, the number of lines, N = 20, was enough to successfully solve the problem even for large values of Thiele modulus. Results were insensitive up to the fifth digit for N > 20. Our procedure made it possible to control auto-

matically the error during downstream integration along the lines (τ-direction) by using an adaptive step size Runge-Kutta; the relative error tolerance given to the Runge-Kutta solver was 10^{-5}. The use of this method of lines avoided the expensive non-linear iteration required by finite difference methods.

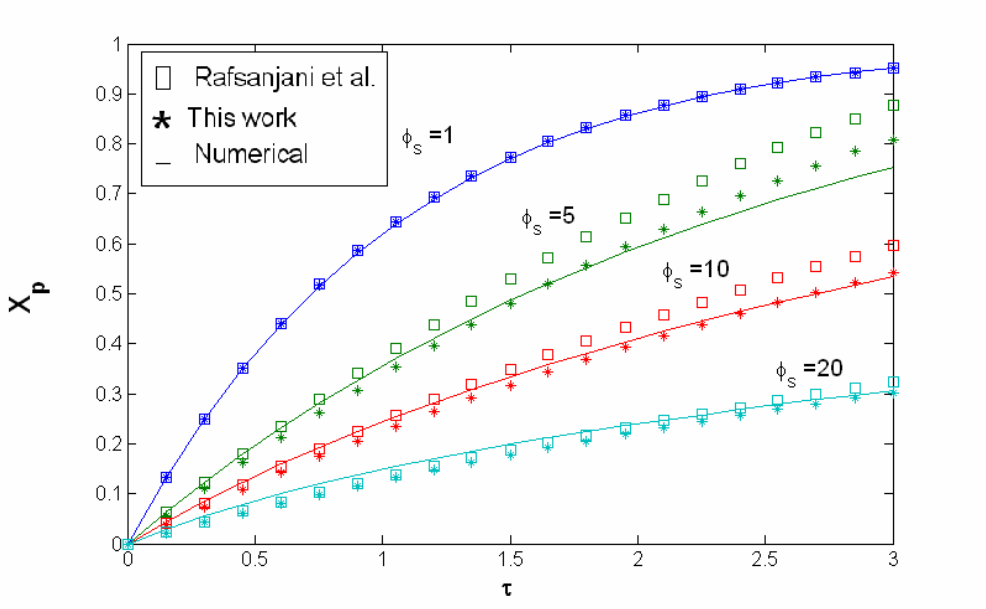

Figure 2.1. Overall conversion (X_p) vs. dimensionless time (τ) for the approximate solutions (Rafsanjani and this work) and the numerical solution for the $R(C) = C$ and $F(X) = (1 - X)$ case.

6. Model Validation

In this section the results of the approximate method given by Eqs. (2.23)-(2.26) are compared with the exact solution given by Eqs. (2.10)-(2.13). The model validation is basically done by comparing the overall particle conversion vs. time for the whole range of Thiele modules. When possible, i.e., first-order kinetics with respect to the gas reactant, the results are compared with the approximate method developed by Rafsanjani et. al. (2002). The comparison with the solution given by Rafsanjani et al. makes it possible to assess the error associated with step 2, i.e., gas concentration estimation. All the cases simulated correspond to spherical geometry (*m*=2). with the following values for the $\beta = 1.5$ and $\varepsilon_0 = 0.6$ parameters.

6.1. First-order kinetics with volumetric structural model

For first-order kinetics with respect to the gas reactant, $R(C) = C$, an analytical solution can be found for any structural profile by applying the QM (Rafsanjani et. al., 2002)

$$C(z) = \frac{\sinh(M\,z)}{z\sinh(M)} \tag{2.28}$$

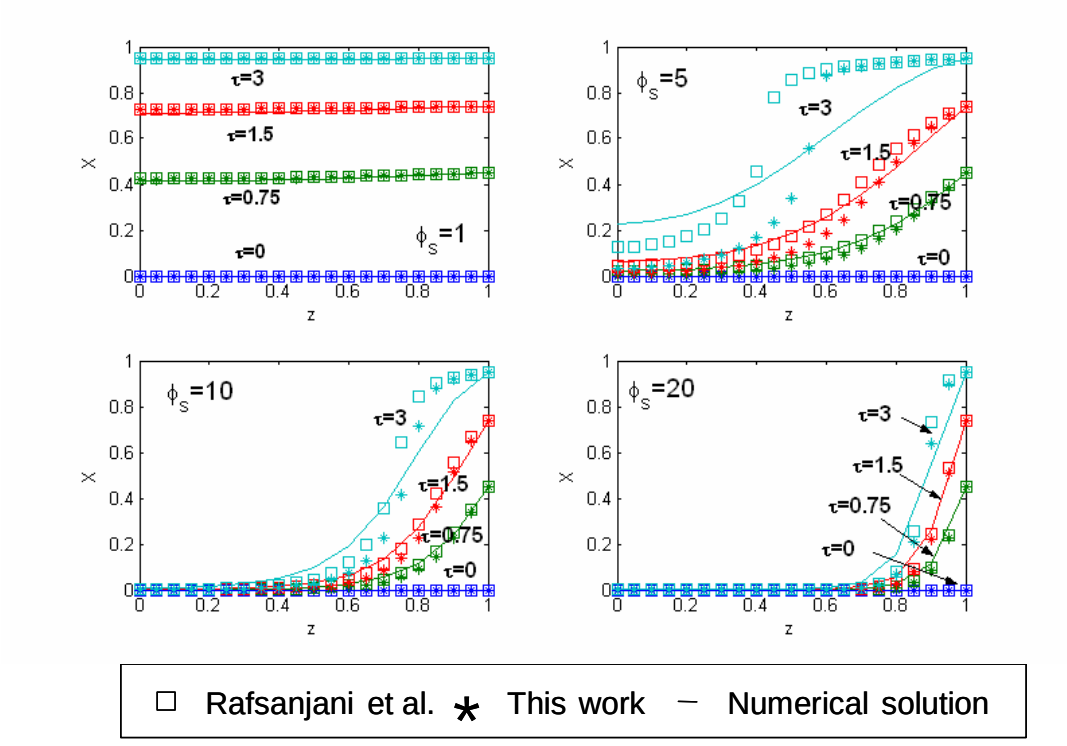

Figure 2.2. Particle conversion profiles within the particle for the approximate and numerical solutions for the $R(C) = C$ and $F(X) = (1 - X)$ case.

In principle, Eq. (2.28) is more exact than Eq. (2.23) because step 2 does not contribute to the overall error. However, both methods approximate the exact solution with similar agreement, as shown in Fig. 2.1. The differences between the two approximate methods are very small. In Fig. 2.1 the structural profile chosen for solving the model is the simplest one given in Eq. (2.7). For this case, $f(X) = 1$, or $F(X) = (1 - X)$ (see Table 2.1). The use of this profile presumes that the reacting sites are uniformly distributed. This kinetic model has been widely used in the specialised literature (Adánez and de Diego, 1993; Adschiri et al., 1986). For this case $\Theta(X) = -\ln(1 - X)$ and $X(z) = \exp\left(-\tau \cdot C(z)\right)$. As seen, the approximation developed in this work is excellent and it does not introduce a significant error as far as overall conversion vs. time curves are concerned.

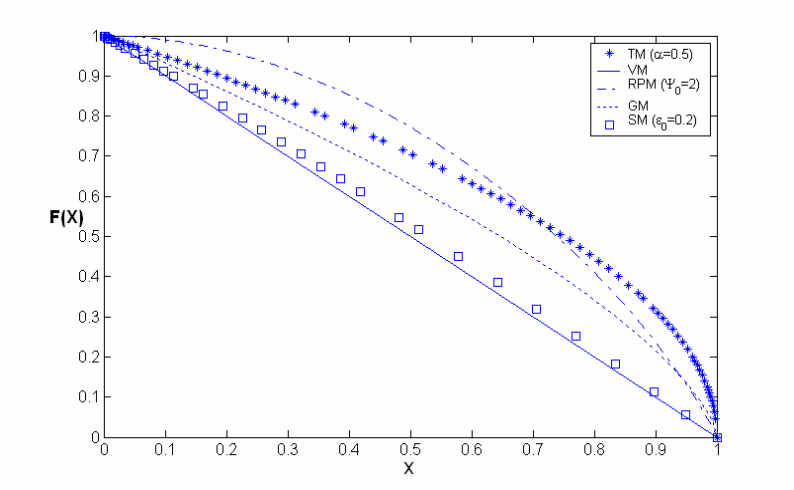

Figure 2.3. $F(X)$ vs. X for various kinetic models taken from Table 2.1.

Profiles of local solid conversion are displayed in Fig. 2.2. We note that the error is more appreciable at high conversions (for instance, see curves $\tau = 3$). The discrepancy is especially notable for the intermediate range of Thiele modules. This is consistent with the analysis made by (Gottifredi and Gonzo, 2005), who found higher discrepancies in the middle range of Thiele modules. Figs. 1 and 2 show that the solution given by Rafsanjani et. al. is in worse agreement than the solution developed here. The disagreement also increases with time and within the intermediate range of Thiele modules. This is a surprising result since it would have been more reasonable to find closer agreements with the solution described by Rafsanjani et al. This leads us to speculate that the error must be a consequence of the sum of both step 1 and step 2, and in some cases the individual errors may balance each other out, leading to lower overall error.

6.2. First-order kinetics with general solid structural model

Despite the initial agreement found, the discrepancies may be greater when using more complicated $F(X)$. This is, of course, structural-profile dependent and it must be confirmed by comparing different kinetic models. Fig. 2.3 displays various $F(X)$ associated with some selected kinetic models from Table 2.1. Fig. 2.4 compares the results of the three methods — i.e., exact, Rafsanjani et al., and the one developed here. In this figure the computations are done with different kinetic models, including the random pore model (RPM), the Simons model (SM), the traditional model (TM) and the grain model (GM). The analysis of the curves displayed in Fig. 2.4 again shows good agreement between the approximate methods and the exact solution. This is true for the four kinetic models considered and for the whole range of Thiele modulus.

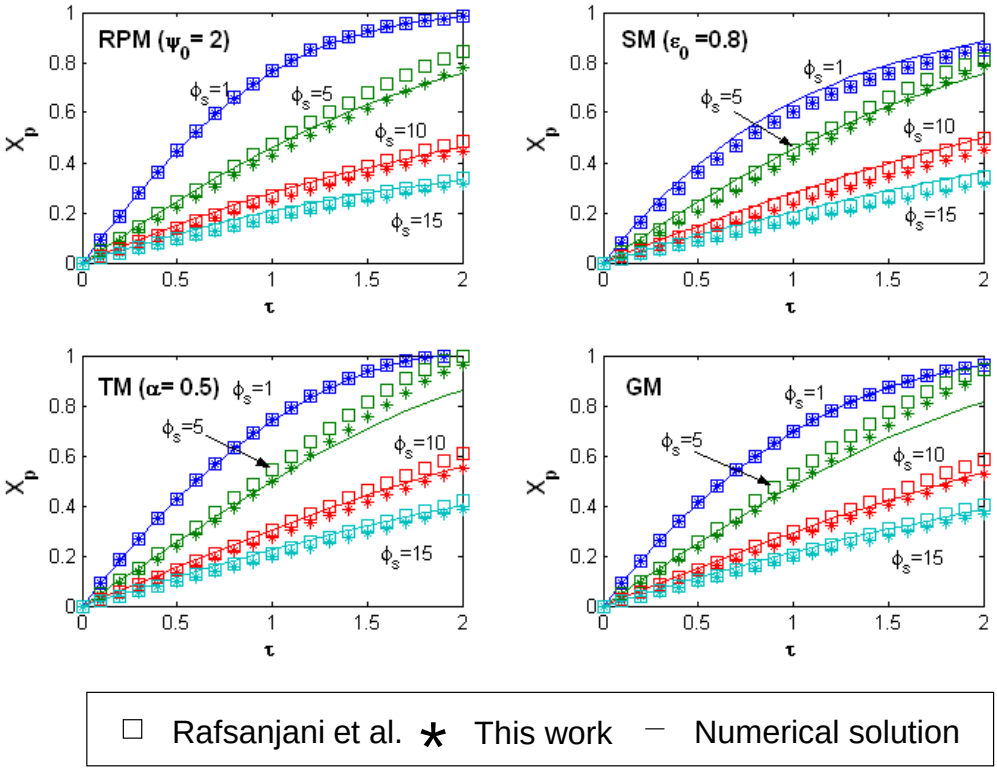

Figure 2.4. Comparison of the approximate and numerical solutions for the kinetic models ($F(X)$) presented in **Fig. 2.3.**

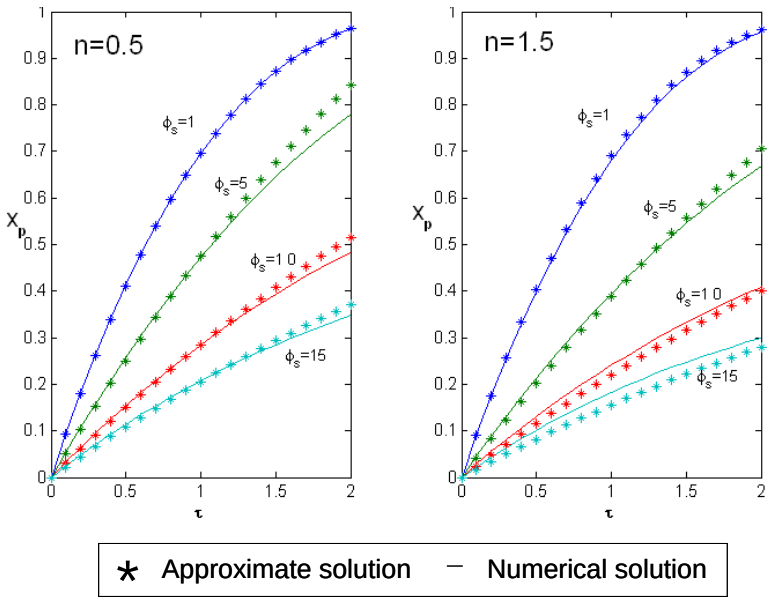

Figure 2.5: Comparison of the proposed approximate method with the numerical solution for the $R(C) = C^n$ (n =0.5 and n =1.5) and $F(X) = (1-X)^{2/3}$ cases.

6.3. General kinetics with general solid structural model

Analytical solutions for the gas reactant conservation equation are not possible for general non-linear kinetics. The Rafsanjani et al. solution does not apply anymore, while the method developed here makes it possible to incorporate any non-linear kinetics. The curves of overall particle conversion versus time for more general kinetics are shown in Figs. 5 and 6. In particular, Fig. 2.5 illustrates the agreement between the numerical and this approximate method. The computations are made for n^{th}-order kinetics, $R(C) = C^n$, by using the grain model (GM), i.e., $F(X) = (1-X)^{2/3}$. More specifically, Fig. 2.5 displays the n=0.5 (left-hand side) and n=1.5 (right-hand side) cases. Again, the approximate solution is close to the numerical one. In this figure, however, the agreement is not so good for large values of Thiele modulus.

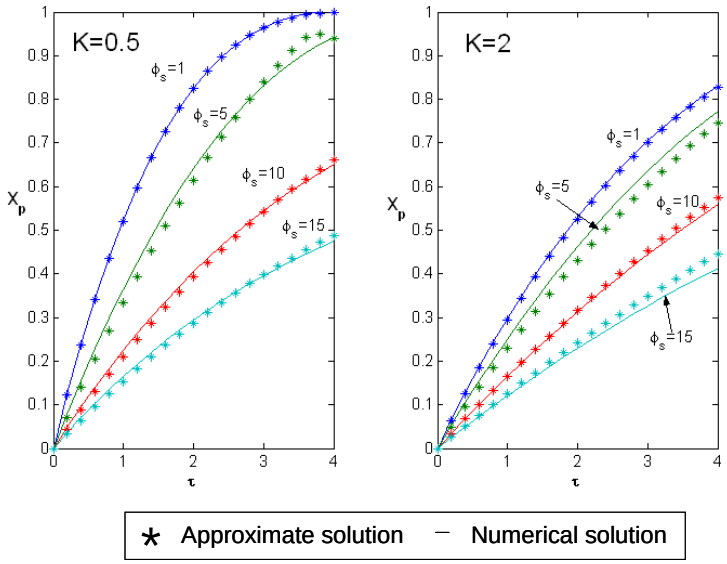

Figure 2.6: Comparison of the proposed approximate method with the numerical solution for the $R(C) = 1/(1+K\cdot C)$ (K =2 and K =2) and $F(X) = (1-X)^{2/3}$ cases.

Finally, the approximate method is further validated (Fig. 2.6) for Michaelis-Menten kinetics, $R(C) = C/(1+K\cdot C)$. In each graph of this figure the particle conversion evolution is displayed for two values of the K parameter: 0.5 and 2. The kinetic model used is again the grain model. The results obtained with the approximate method show similar agreement to the case of n^{th}-order kinetics.

7. Conclusions

The simple method of solution developed in this chapter can be applied to any isothermal non-catalytic gas-solid reactions. It makes it possible to incorporate a non-linear chemical reaction rate and the changes in porous structure during conversion. The application of this simplified treatment can be a valuable tool in situations where rapid calculations are advantageous. In these cases this treatment has been shown to have the potential of providing extremely high computational savings in performing

the calculations. The model described in this chapter is extended and applied to char gasification TGA experiments in Chapters 3 and 4.

Appendix 2.1. Relations applied in the kinetically-controlled regime–Case of gasification reactions

The evolution of available carbon sites during char conversion has been studied by several authors and numerous models have been proposed to take into account the differences in reactivity due to changes in the char structure (Liliedahl and Sjöström, 1997; Molina and Mondragón, 1998). This is normally based on the calculation of the gasification rate, defined as $r_{ch} = dw/dt$ or, in order to avoid the influence of the sample mass, on char reactivity, R in s^{-1}, defined as

$$R(X_p) = \frac{r_{ch}}{w} = \frac{dX_p/dt}{1-X_p} \tag{2.29}$$

where $X_p = (w_0 - w)/w_0$ is the char particle conversion, and w and w_0 are, respectively, the mass of char at any instant and at initial conditions, both free of ash. The conversion rate for the solid reactant (B) in the general reaction given in Eq. (2.1) is

$$(-r_B) = c_{B0}\frac{dX}{dt} = b(-R) \quad (\text{mol/m}^3\cdot\text{s}) \tag{2.30}$$

where the stoichiometry of the reaction $(-r_B) = b(-R)$ has been used. According to this work, the reaction rate at any point inside a particle has been defined in Eq. (2.6) as

$$(-r) = r(c_A)\cdot F(X) \quad (\text{mol/m}^3\cdot\text{s}) \tag{2.6}$$

When experiments are carefully designed to operate in the kinetic regime the following expressions hold:

$$c_A \approx c_{As} \;; \quad X_p \approx X \text{ for any } z; \quad (-R) \approx (-r) \tag{2.31}$$

Under some operating conditions (Ollero et al., 2002**;** Liliedahl and Sjöström, 1997) it is possible to separate the effects influencing the reactivity as follows,

$$R(X) = f(X)\cdot R_{ref} \tag{2.32}$$

where $f(X)$ is invariant over the relevant temperature and partial pressure ranges tested in the experiments. By taking into account Eqs. (2.29)-(2.32), the following expression is obtained

$$f(X)\cdot R_{ref}\cdot(1-X) = \frac{b\,r(c_{As})}{c_{B0}}\cdot F(X) \quad (\text{s}^{-1}) \tag{2.33}$$

From Eq. (2.33), the following relations can be identified:

$$R_{ref} = \frac{b\, r(c_{As})}{c_{B0}} \quad (s^{-1}) \text{ and } F(X) = f(X)\cdot(1-X) \tag{2.34}$$

Now, if we use the dimensionless time proportional to that defined in Eq. (2.15) with a constant of proportionality, k', equation Eq. (2.30) gives

$$\frac{d\,X}{d\,\tau} = k'\,F(X) \tag{2.35}$$

or taking a τ' in the form, $\tau' = \tau \cdot k'$, Eq. (2.35) is converted to

$$\frac{d\,X}{d\,\tau'} = F(X) \tag{2.36}$$

Equation (2.36) is the one commonly found in the specialised literature for representing the effect of conversion in gas-solid reaction kinetic models. τ' is often defined as $\tau' = 1$ for X=0.5, but other possibilities exist (Liliedahl and Sjöström, 1997). This is formally done by selecting the appropriate value of the k' constant.

Chapter 3

Diffusional effects in TGA gasification experiments with single biomass char particles

1. Introduction

The literature on gasification kinetics is extensive. However, kinetic studies dealing with single macro-sized char particles are not so abundant. Literature on single-particle studies and diffusional effects occurring in char gasification kinetic experiments was critically surveyed. We found neither general criteria for a kinetic model to be selected nor quantitative consensus about the impact of variables such as particle size on the diffusional interferences. In addition, many of studies on macroscopic-sized particles, i.e., using 0.5-5 millimetres char particles, reveal that biomass-derived char particles inside industrial gasifiers may be limited by diffusional effects. Therefore, suitable kinetic-particle models that capture plausible physical limitations should be used when simulating such gasifiers.

In this chapter the importance of the diffusional effects as Thiele modulus increases is experimentally analysed. To do that, a kinetic study is carried out to elucidate the effects of diffusional limitations at particle scale during TGA char reactivity tests. The main objective was to identify the limiting phenomena that may take place during biomass char gasification experiments with CO_2. The char used was wood-matter from pressed-oil stone (WPOS), also called *orujillo*. The gasification rates of WPOS were measured at four different particle sizes (0.06, 0.9, 1.2 and 2.1 mm), three CO_2 partial pressures (0.20, 0.35 and 0.50 bar) and four temperatures (800, 850, 900 and 950ºC).

2. Literature survey

2.1. Single-particle studies

Ergun (1956) showed that particle effects were of minor importance during the fluidised-bed gasification of active carbon and graphite 0.08-1.8 mm in size. De Groot and Shafizadeh (1984) gasified 0.4-0.85 mm particles of Douglas fir and cottonwood charcoal in CO_2. They correlated their experiments with an overall expression in terms of the initial particle size. A reaction order of 0.7 was observed. Groeneveld and van Swaaij (1980) investigated carbon particle profiles in 40x20x20 mm parti-

cles. Neither a shrinking core model (SCM) nor a uniform conversion model (UCM) predicted their experiments satisfactorily. A local volumetric model enabled them to explain conversion profiles found experimentally. The overall reaction order observed was 0.7. Standish and Tanjung (1988) analysed the effects of temperature, CO_2 gas composition and particle size in 10-34 mm-sized wood charcoal gasification. They correlated their observations with an apparent n^{th}-order kinetic expression having a reaction order of 0.71. The initial particle size effect was also included in the expression raised to -0.81. Although the resulting kinetics was apparent (and not intrinsic), they claimed that the correlation developed served for comparison with other charcoal gasification data as long as similar rate control conditions applied. This is, however, a considerable restriction because most kinetic studies do not provide a formal analysis of diffusional effects (Gómez-Barea et al., 2005).

The work by Standish and Tanjung was further analysed by Dasappa et al. (1994), who developed a non-isothermal computational model for explaining some "open" aspects of the Standish and Tanjung work. They succeeded in explaining some of Standish and Tanjung's findings. In addition, they computationally verified conclusions already given by Ergun (1956). Hawley et al. (1983) analysed intraparticle mass resistance with a simple catalytic model of 1-2 mm wood char particles. They concluded that, up to 5 mm, the particle size did not alter the resulting kinetic expression. Van den Aarsen (1985) analysed heat and mass transfer effects in wood and rice-husk particles. For 1 mm particles he estimated Thiele modules under 0.3 and maximum temperature difference below 3ºC. Dutta et al. (1977) estimated diffusional effects detected during TGA gasification tests with coal chars run at high temperature. More recently, Mermoud et al. (2004) presented experimental results of 10-30 mm wood-char particle gasification in a "macro-TG" reactor. They analysed the influence of the particle size and heating rates on the observed gasification rate at various steam concentrations and temperatures. Golfier et al. (2004) used the experimental findings of Mermoud et al. to develop a model for the simulation of fixed-bed gasifiers. Other investigators have used different approaches to analyse physical limitations during char reactivity tests (Reyes and Jensen, 1986a, 1986b; Bathia and Perlmutter, 1980, 1981; Liu et al., 2003; Struis et al. 2002).

2.2. Kinetic models in kinetic studies

We looked at findings discussed in the literature on systems where diffusional effects may have been present — i.e., diffusional regime or intermediate regime. In the kinetically-controlled regime, a number of kinetic models have been proposed to describe the gasification of char particles. The simplest of these are the "homogeneous or uniform-conversion" (UCM) and "shrinking-core" (SCM) models (Froment and Bischoff, 1991). Bhat et al. (2001) recently surveyed studies using both UCM and SCM for coal-derived and biomass-derived chars. In their own kinetic research on rice-husk char powders, they concluded that, up to 800ºC, the SCM fits their experimental data better. However, at temperatures higher than 850ºC the gasification rate is influenced by diffusional resistances. The SCM is better suited for high-temperature predictions. Yasyerli et al. (1996) stated that the uniform model with a constant specific reaction rate is considered inadequate to describe char gasification. They employed a deactivation model for the prediction of gasification rates of a variety of lignites. Their kinetic data correlated well with a single generalised relation.

They further emphasised the incapacity of both SCM and UCM to explain their experiments acceptably.

Other researchers have used more advanced treatments for fitting their experiments with different degrees of success, and their arguments are often inconsistent with each other. Most of them were surveyed by Doraiswamy and Sharma (1983) for general gasification reactions. More recently, Liliedahl and Sjöstrom (1997) and Molina and Mondragón (1998) surveyed gasification-kinetics models for biomass-derived chars and coal-derived chars. A general approach to extend these models to the region of diffusional control is contained in (Gómez-Barea and Ollero, 2006).

2.3. Conclusion of kinetic study review

From this review we conclude that for char gasification systems: (1) there is a lack of consensus with regard to the type of kinetic model to be used for fitting experimental kinetic data, even within the kinetically-controlled regime. (2) The diffusional resistance limitations vary widely. In systems with similar characteristics — i.e., type of char, size, and operating conditions, — different control regimes have been proposed. (3) Kinetic experiments are often carried out without a rigorous assessment of plausible physical interactions. (4) Criteria for quantifying the impact of conversion on the magnitude of the diffusional effects have not been formally established in the literature. In spite of this, many investigators use different degrees of conversion (even averages within a given range) for expressing the experimental kinetic data.

3. Intrinsic gasification char reactivity

The reactivity R (s^{-1}) was defined in Chapter 2, Eq.(2. 29) as

$$R(X_p) = -\frac{1}{w}\frac{d\,w}{d\,t} = \frac{1}{1-X_p}\frac{d\,X_p}{d\,t} \tag{3.1}$$

As discussed in Chapter 2, the reactivity depends on the char conversion as well as on temperature and gas composition. For most coal, lignite and peat chars, reactivity decreases with increasing conversion, whereas for most biomass chars it increases. It can also exhibit a maximum or a minimum. So if a representative reactivity or a unique set of representative kinetics is reported, it should be referred to a specific conversion value. Different values of conversion such as 5% (Bandyopadhyay, 1991) and 50% (Rathmann, 1995; Risnes, 2000) have been used. Moreover, other authors use the average reactivity between two degrees of conversion as a representative value of reactivity (DeGroot and Shafizadeh, 1984; Chen et al., 1997). In our study the reactivity at 50% char conversion, R_{50} , is taken as representative.

If the kinetic experiments are carried out with very fine char well exposed to the gas, Eq. (2.31) of Chapter 2 holds and then, both the structural profile and the reference reactivity, R_{50} (see Eq. (3.3)), should be intrinsic. Under some operating conditions (Ollero et al. 2003; Sørensen, 1994) it is possible to separate these effects as follows:

$$R(X) = f(X) \cdot R_{50} \tag{3.2}$$

where $f(X)$, the so-called structural profile, takes into account the changes in the number of active sites during conversion, which is usually assumed to be "invariant" over the relevant *T-P* domain (DeGroot and Shafizadeh, 1984; Ollero et al., 2003; Rathmann, 1995). In the absence of CO, which has a well-known inhibition effect, n^{th}-order kinetics are often used to express the temperature and CO_2 pressure-dependence of the representative reactivity (DeGroot and Shafizadeh, 1984; Groeneveld, M.; van Swaaij, 1985; Standish and Tanjung, 1988). Furthermore, by assuming Arrhenius-type kinetics for the kinetic constant, the reactivity results in

$$R_{50} = K p_{CO_2}^n \qquad K = A \cdot \exp(-E / R_g T) \tag{3.3}$$

In this work we determined the reactivity by measuring the weight loss of a small sample of char particles. We used both powdery char particles and macroscopic char particles. For the experiments using powdery char, the intrinsic reactivity is obtained directly by applying the relations presented above. However, when particles are of macroscopic size, diffusional effects may limit the provision of heat and reactant to the active sites. In this case the conversion obtained is the overall conversion and may differ significantly from the local conversion, especially near the centre of the particle. This is because, due to the existence of gradients in particles, the concentration and temperature differ from those in the bulk. To compute these variables, in principle, it is necessary to solve the gas mass and energy conservation equations at any degree of conversion. This is modelled and discussed in Chapter 4. In this chapter the diffusional effects are obtained experimentally, by assuming that the differences found between the measured reactivity for powdery and macroscopic char are due to diffusional limitations (Gómez-Barea et al., 2005a, Ollero et al., 2002).

However, if particle size increases, the CO concentration could become high inside the particle. In this scenario, the inhibition effect caused by CO is likely to be significant. Therefore, more complex kinetics, such as Langmuir-Hinshelwood, should be used in order to adequately separate the inhibition effect of CO (chemical limitation) from purely diffusional effects (physical limitation). Otherwise, i.e., by using n^{th}-order kinetics, these two different effects would be lumped into only one. This would lead to misunderstanding the real effects of diffusional limitations.

4. Experimental

4.1. Apparatus

The kinetic experiments were performed in a Mettler Toledo thermogravimetric analyser. This experimental rig has been described in detail in previously published articles (Ollero et al. 2002, 2003). In TGA the weight-loss of a small fuel sample can be measured as the fuel reacts under controlled gas composition, pressure and temperature.

4.2. Sample preparation

The WPOS is a granular solid made up of irregular and heterogeneous agglomerates of small particles of pit and pulp. The material received from an olive-oil extracting plant was air-dried at 35-40ºC and sieved to a size between 1.41 and 2.83 mm. These particles were pyrolysed in a PTF700 (LECO) furnace under a flowing nitrogen atmosphere. The pyrolysis temperature reached 900ºC at a heating rate of 30ºC/min. The samples were kept at 900ºC for 7 minutes to complete the pyrolysis. The nitrogen flow was maintained until the sample had cooled down to below 100ºC to ensure that no reaction with air would occur. Table 3.1 shows the proximate and ultimate analysis of the char used in this study.

The char samples were ground in a mortar into four different sizes: (1) below 150 μm, (2) from 800 to 1000 μm, (c) from 1000 to 1410 μm, and (4) from 1410 to 2830 μm. Mean values associated with each particle size cuts were 0.060, 0.9, 1.2 and 2.1 mm, respectively. Finally, the char was gasified with the reactive gas mixture at the test temperature until it reached constant weight.

A total of 190 particles were counted in a batch of 0.5 g of 2.1 mm char, which means an average of 2.63 mg per particle. The particles appeared to be nearly spherical. Assuming a mean diameter equal to the average size cut, the calculated apparent density was 543 kg/m^3. The true density of the char was measured by liquid (water and alcohol mixtures) displacement using a commercial pycnometer gave an average value of 1522 kg/m^3. The porosity was calculated from the apparent and true densities (1- 543/1522=0.65).

4.3. Test procedure

The experimental tests were carried out using char samples with an initial mass of approximately 10 mg for the tests using 0.060 and 0.9 mm char. For the tests carried out with 1.2 and 2.1 mm char, initial masses were 20 and 28 mg, respectively.

Table 3.1. Char characterisation

Orujillo Char- Proximate analysis		
	Wet	Dry
Moisture %	5.53	-
Volatile Matter %	7.75	8.21
Ashes %	13.51	14.30
Fixed Carbon %	73.20	77.49
Orujillo Char. Ultimate analysis		
Carbon %		79.54
Sulphur %		<0.05
Nitrogen %		1.14
Hydrogen %		1.73
Oxygen %		17.54

Ash Analysis (wt%)	
Si as SiO_2	18.2
Al as Al_2O_3	2.5
Fe as Fe_2O_3	2.3
Ca as CaO	11.9
Mg as MgO	7.3
Na as Na_2O	0.4
K as K_2O	36.6
Mn as MnO_2	0.1
P_2O_5	4.7
Others	16.0

The cylindrical crucible (10 mm inside diameter, 7 mm high) was filled with

alumina up to 1 mm from the crucible mouth, allowing good exposure of the single particle layer to the gas. System control and data acquisition were performed on a personal computer. The procedure used for each experiment in the TGA was as follows:

1. In an inert atmosphere of pure N_2, heating from ambient temperature to 105ºC at a constant rate of 30ºC/min.

2. To dry out the sample completely, the temperature was maintained at 105ºC for 5 minutes.

3. Heating from 105ºC to 1000ºC at a constant rate of 30ºC/min in an inert atmosphere of pure N_2.

4. To pyrolyse the sample completely, the temperature was maintained at 1000ºC for 10 minutes.

5. Cooling from 1000ºC to the established test temperature (800-950ºC) at a constant rate of 25ºC/min in an inert atmosphere of pure N_2.

6. Gasification of the char with the reactive gas mixture at the test temperature until a constant weight was reached.

4.4. Experimental programme

To evaluate the external and internal mass and heat transfer effects, the following set of experiments was carried out: four temperatures (800, 850, 900 and 950ºC), three CO_2 partial pressures (0.2, 0.35 and 0.5 bar) and four particle sizes 0.060, 0.90, 1.2 and 2.1 mm (average diameters). All these tests were repeated to assess the reproducibility of the results, making a total of 48x2 tests.

4.5. Method of data analysis

In each TGA test the instantaneous weight value of the sample and the time were saved. The data processing for a given test involved the following steps: (1) Calculation of the conversion degree, X_i, at each time. (2) Calculation of the experimental reactivity, R_i, at each time. (3) Interpolation between the recorded data to obtain a first estimate of R_{50}. (4) Calculation of f_i at each time, $f_i = R_i / R_{50}$. (5) Fitting the f_i - X_i data to a 5th-order polynomial function led to $f(X)$. (6) A representative reactivity value, R_{50}, for each test was determined from the weighted mean value,

$$R_{50} = \frac{\sum_i \omega_i R_i / f(X)}{\sum_i \omega_i} \tag{3.4}$$

calculated for the conversion range of 20-80%. The statistical weight was set to $\omega_i = R_i(1-X_i)$ to ensure that the experimental values were equally weighted with respect to

X (Rathmann et al., 1995). Some authors (Ollero et al., 2003; Risnes et al., 2000; Barrio et al., 2000) use the same structural profile for all tests. An accepted practise to obtain such a reference profile is to normalise all reactivity profiles according to $R_n(X) = R(X)/R(0.2)$ and then select a reference profile to set $f(X)$, the one that shows average behaviour. In this work R_{50} for each test was calculated by means of the last equation but using its own structural profile. However, it was verified that there were no significant differences between these two options with respect to $f(X)$.

5. Assessment of diffusional resistances during kinetics tests using powdery char

A single-layer bed of very fine char particles (d_p = 0,060 mm) located at the mouth of the crucible was used in the experiments. In principle, these experiments can be limited by internal and external heat and mass transfer resistances. Some authors (Rathmann et al., 1995; Ollero et al., 2003), feel that, in tests carried out with such a fine char spread out in a single layer in contact with the reactive gas, the only resistances that need to be accounted for are external mass and heat transfer. We are not sure, however, if intraparticle pore diffusional resistance plays a relevant role in the kinetic determination, and we therefore quantify both plausible contributions by means of estimations.

5.1. External effects

The radiative heat transfer from the hot walls of the TGA furnace to the layer of char ensures a minimal temperature difference between the gas and the sample. The convective mass transfer mechanism, however, may not be so effective and the associated effect on the gasification rate must be checked in each test. In order to quantify this effect, a diffusion limitation index (Rathmann et al., 1995; Ollero et al., 2003), is calculated for each experiment as,

$$\text{DLI} = \frac{\text{Observed gasification rate (mol/s) at } X_p = 50\%}{\text{Maximum molecular diffusion rate (mol/s)}} = \frac{r_{obs}}{r_{D,e}}$$

This is an observable quantity for any gasification test. The observed gasification rate is calculated as,

$$r_{obs} = \frac{R_{50} \cdot w}{M_c} \quad \text{(mol/s)} \tag{3.5}$$

The external maximum diffusion rate is estimated assuming that the transfer of the reactant to the sample takes place by Fick molecular diffusion and that the length of the diffusion path is half the radius of the hemisphere surrounding the sample tray (Rathmann et al., 1995). In the test carried out in a 10 mm-diameter cylindrical crucible, the maximum diffusion rate according to this approach may be expressed as,

$$r_{D,e} = c_0 D_m \pi d_t \quad \text{(mol/s)} \tag{3.6}$$

Values of the diffusion index up to 0.1 can be considered acceptable as the induced uncertainty in R_{50} would be 10% and presumably somewhat less (Rathmann et al., 1995). The DLI values calculated for the complete set of 0.06 mm experiments ranged between 0.02 and 0.17. As expected, the former corresponds to conditions of (800ºC, p_{CO2}=0.50 bar) while the latter were computed for (950ºC, p_{CO2}=0.20 bar). The tests carried out at 950ºC with the other two partial pressures (0.20 and 0.35 bar) also exceeded the DLI limit (0.1). Because the R_{50} values at 950ºC may be rather uncertain, this set of reactivity values was not used to estimate the intrinsic kinetic parameters.

5.2. Intraparticle effects

Once external resistance has been verified as low, the concentration of CO_2 at the char particle surface can be assumed to be that of the bulk gas. The internal mass transfer resistance can be estimated by means of the Weisz-Prater modulus as

$$c_w = \frac{r_{obs}}{r_{D,i}}$$

where $r_{D,i}$ is the internal maximum diffusion rate per unit volume of char particle. This is calculated according to the following expression

$$r_{D,i}^V = c_0 \frac{D_e}{(d_p/6)^2} \quad (\text{mol/s/m}^3) \tag{3.7}$$

where $d_p/6$ is taken as the characteristic diffusion length. The maximum internal diffusional rate in mol/s, is calculated by multiplying $r_{D,i}^V$ by a factor that takes into account the total volume of char particles exposed to gas (w/ρ_c). Thus,

$$r_{D,i} = \frac{w c_0 D_e}{\rho_c (d_p/6)^2} \quad (\text{mol/s}) \tag{3.8}$$

In principle, two diffusion mechanisms occur inside the porous particles: bulk (molecular/continuum) and Knudsen diffusion. Thus, for the calculation of D_e, both contribution mechanisms must be taken into account. In a simplified approach, we computed D_e using the Bosanquet formula

$$D_e = \frac{1}{1/D_b + 1/D_{Kn}} \tag{3.9}$$

where D_b is calculated according to,

$$D_b = \frac{\varepsilon}{\tau_t} D_m \tag{3.10}$$

where τ_t and ε represent tortuosity and porosity, respectively. The values of D_m and D_{k_n} were calculated with the following expressions:

$$D_m = 1.4 \cdot 10^{-5} \left(\frac{T}{273} \right)^{1.8} \qquad D_{Kn} = \frac{2}{3} \sqrt{\frac{8 R_g T}{\pi M_g}} r_p \qquad (\mathrm{m^2/s}) \tag{3.11}$$

where r_p is the porous radio, estimated as $r_p = 4\varepsilon / S_c$. The values of the different parameters involved in (3.10), (3.9) and (3.11) were taken from our experimental results, literature correlations (Groeneveld and van Swaaij, 1985; Gómez-Barea et al., 2005; Golfier et al. 2004; Scott et al. 2005; Sørensen , 1994; Ollero et al., 2002; Kuijk et al., 200; Dassappa et al. 1993, 1998; Hastaoglu and Karmann, 1987; Thunmann 2001,2003; Palchonok, 1998) and references therein. The values of the effective diffusion coefficient ranged between $5 \cdot 10^{-5}$ and $7 \cdot 10^{-5}$ m^2/s. The Weisz-Prater was calculated as

$$c_w = \frac{\rho_c \, R_{50} \, d_p^{\,2}}{36 \;\; c_0 \, D_e \, M_c} \tag{3.12}$$

For the tests with d_p = 0.060 mm, the Weisz-Prater values for the most unfavourable scenario (950ºC, p_{CO2}=0.20 bar) were less than 0.001. Thus, internal porous resistance to diffusion can be neglected with confidence.

Table 3.2. Summary of kinetic parameters available in the literature

Char	E (kJ/mol)	n	Ln(k_0 *)
WPOS (Ollero et al.,2003)	118.6	0.40	12.45
Birch (Barrio and Hustad, 2000)	215	0.38	19.04
Wheat straw (Ollero et al., 2002)	205.6	0.59	19.67
Spruce (Ollero et al., 2002)	219.9	0.36	20.96
Longyear coke (Ollero et al., 2002)	235.1	0.51	18.66
Coal (Ollero et al., 2002)	212.9	0.89	16.45
Cotton wood (DeGroot and Shafizadeh, 1984)	196	0.6	20.0
Douglas fir (DeGroot and Shafizadeh, 1984)	220	0.6	21.4

- k_0 units: $min^{-1}bar^{-n}$

6. Experimental results

6.1. Intrinsic kinetics

As already stated, a single-layer bed of very fine char particles (0.060 mm) located at the mouth of the crucible was used in the experiments. The reactivities determined with this particle size were considered intrinsic in this study as was proven in section 5. The reactivity obtained from the rest of the tests, performed with other sizes different from powdery char, is likely to be affected by physical processes.

Using the n^{th} model to fit the data we estimated the kinetic parameters by taking the reactivity values from the tests using the smallest char particle size (0.06 mm). The values at 950ºC were rather uncertain with regard to some diffusional limitations. This was decided in order to be consistent with the criteria developed in the Appendix. A multivariate linear regression analysis was used to calculate k_0, E and n. It was based on an Arrhenius plot, where a linear equation between the independent variables 1/T and $\ln(p_{CO2})$ and the dependent variable $\ln(R_{50})$ was obtained. The reaction order obtained according to this method was 0.40, similar to that calculated by other authors for different biomass chars (Barrio, 2000). The activation energy, however, was rather low: 118.6 KJ/mol compared to data from others (Table 3.2). This low value, as well as the relatively high reactivity of the char, could be due to its high potassium content (see ash analysis in Table 3.1). The resulting kinetic model is given by

$$R_{50} = 1993\exp(-14260/T)\,p_{CO_2}^{0.4} \quad (s^{-1}) \tag{3.13}$$

Table 3.3: Experimental reactivities R_{50} (x10^3) (g/g/s)

x_{CO_2}	d_p (mm)	T_0 = 800 ºC	T_0 = 850 ºC	T_0 = 900 ºC	T_0 = 950 ºC
0.20	0.060	1.81	3.34	5.82	7.85
	0.9	1.21	1.72	3.52	5.48
	1.2	0.81	1.53	2.51	3.16
	2.1	0.63	1.21	1.97	2.05
0.35	0.060	1.98	3.99	7.42	10.43
	0.9	1.40	2.70	5.37	6.57
	1.2	1.07	2.33	3.68	4.29
	2.1	0.65	1.31	2.93	3.18
0.50	0.060	2.31	4.69	9.18	12.52
	0.9	1.41	2.84	5.67	6.58
	1.2	1.14	2.50	3.71	5.87
	2.1	0.91	1.71	2.87	3.81

The reaction order obtained according to this method was 0.40, which compares quite well with those calculated by other authors for different biomass chars (Table 3.2). The comparison of activation energies shows, however, that the value obtained is rather low, though similar to those calculated in some studies, as can be seen in Table 3.2. This low value, as well as the high reactivity of the olive waste char relative to other biomass chars at the same operating conditions, could be due to its high po-

tassium content (Table 3.1). The measured values of R_{50} for the four particle sizes for the whole range of temperatures and CO_2 molar fractions are presented in Table 3.3.

6.2. Effects of temperature

Figure 3.1 displays the X_p vs. t curves obtained at all the temperatures studied (800, 850, 900 and 950ºC) with a CO_2 molar fraction x_{CO_2}=0.35 and particle size d_p=2.1 mm. The sensitivity of the reaction rate to temperature was very high in the lower part of the temperature range (800-900ºC), while this influence decreased at higher temperatures (900-950ºC). This trend was also observed for the other two particle sizes and it agrees with the results reported by other authors (Groeneveld and van Swaaij,1980; Standish and Tanjung, 1987). We note that the reaction was very slow at 800ºC. In fact, complete conversion at 800ºC was achieved after 2 hours while the time necessary at the highest temperature, 950ºC, was about 120 seconds. This is better understood by observing the results in Fig. 3.2, where the logarithm of time needed to achieve 50% carbon conversion, t_{50}, is presented vs. the inverse of the absolute temperature. It is clear that the effect of temperature was again very relevant. In addition, a linear relation can be derived for all the particle sizes tested.

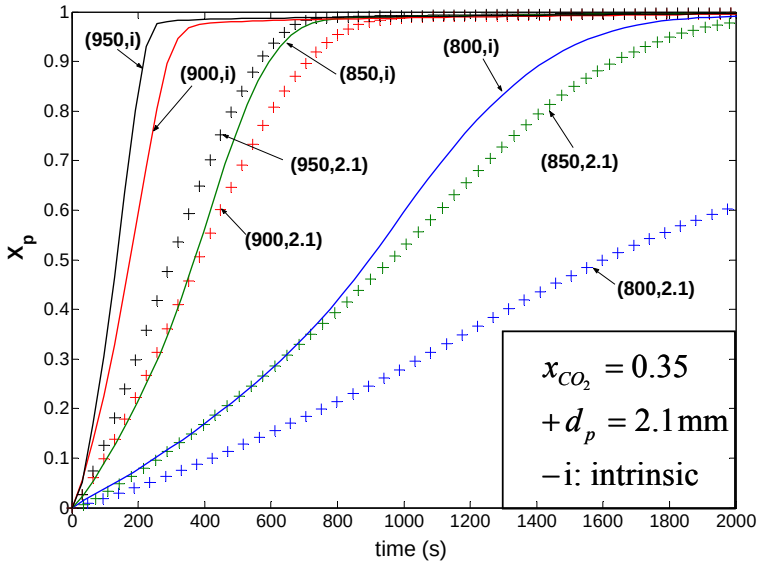

Figure 3.1. Experimental X_p vs. t for various temperatures at x_{CO2}=0.35. Particle sizes: d_p=2.1 mm (cross line) and intrinsic: d_p=0.06 mm (solid line). [Nomenclature: (T_0, d_p): represents the gas temperature and particle size of a test]

It is also noteworthy that there was a dramatic increase in the size range from 0.9 mm to 1.2 mm. This is because the differences in t_{50} at constant temperature were similar between the sizes of 0.06 and 0.9 mm and 1.2 and 2.1 mm, while the differences between 0.9 and 1.2 mm were surprisingly great. This could suggest a change in the control regime. We can see in Fig. 3.2 that this was true for the whole

range of temperatures tested. These results confirm that the temperature is the parameter with the greatest influence on gasification kinetics.

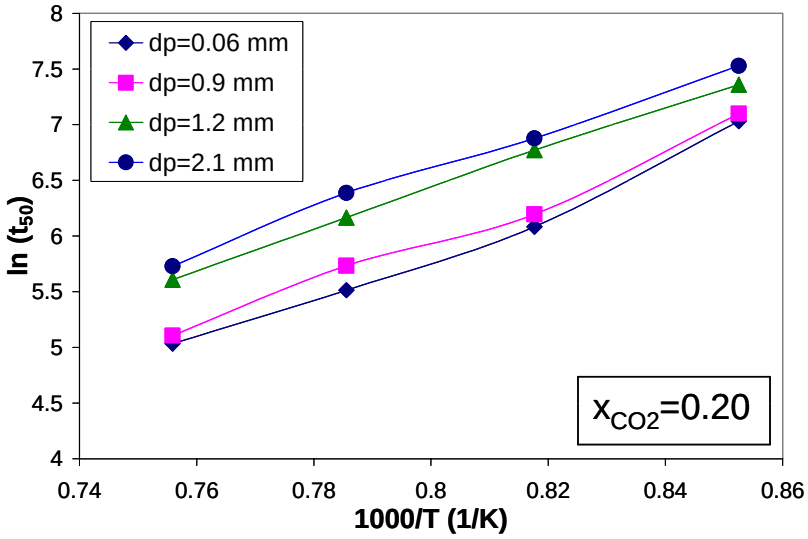

Figure 3.2. ln t_{50} as a function of $1/T$

In addition to the curves corresponding to d_p=2.1 mm, Fig. 3.1 shows the curves for the experiments with the same temperatures and CO_2 molar fraction but with very fine powder (d_p=0.060 mm). These curves are shown in the figure as a solid line. As noted above, the curves represent the intrinsic behaviour of the char because they were obtained without diffusional limitations (see section 5). Again, we conclude that diffusional effects are very significant for the whole range of temperature. As expected, the diffusional resistance increases with temperature. The effects of the CO_2 partial pressure and particle size also affect the magnitude of resistance. These effects are also visible in Fig. 3.3 and Fig. 3.5.

6.3. Effect of CO_2 concentration

Figure 3.3 gives X_p - t curves at fixed temperatures for various CO_2 molar fractions. The curves for the kinetically controlled regime (d_p=0.060 mm) and the curves for d_p=1.2 mm are displayed in the figure. As expected, the reactivity increases with CO_2 concentration and temperature and decreases as particle size increases. It is plain to see that the effect of CO_2 concentration on char conversion progress is not as great as temperature. It is noteworthy that there is a slight difference between the experiments carried out at CO_2 molar fraction of 0.35 and 0.50. Indeed, the effect of CO_2 concentration on reactivity does not follow the expected trend since the increase is much greater in the range of 0.20 to 0.35 as compared to the range of 0.35 to 0.50. This is in agreement with the analysis of CO inhibition found in other studies (Barrio et al., 2000, Ollero et al., 2002, 2003; Dassapa et al. 1994). In effect, although the tests were carried out in the absence of CO, the increase in particle size makes the CO concentration inside the particles higher than in tests using 0.060 mm. The CO concentration in the internal pores can be appreciable and, consequently, the inhibition

effect could play a significant role. This explains why the observed reaction rate is lower than expected.

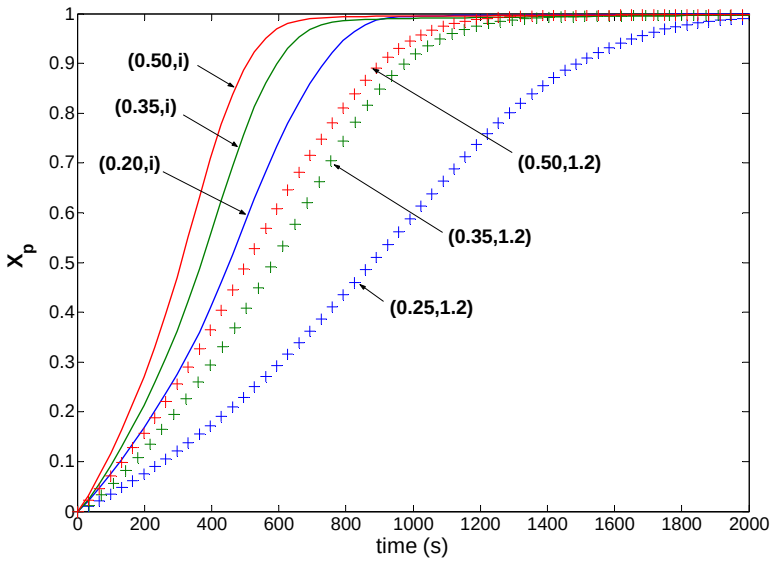

Figure 3.3. Experimental X_p vs. t for various CO_2 molar fractions at T=900ºC. Particle sizes: d_p=1.2 mm (cross line) and d_p=0.06 mm (solid line). [Nomenclature: (T_0, d_p): represents the gas temperature and particle size of a test].

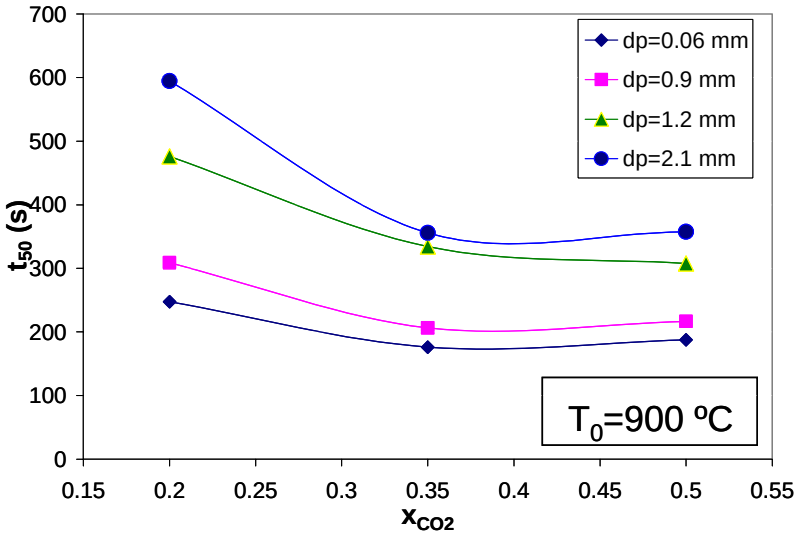

Figure 3.4. t_{50} as a function of x_{CO2}

To describe these observations the inhibition effect caused by CO would need to be modelled using another kinetic expression capable of capturing CO partial pressure effects. In an n^{th}-order kinetic expression, both the diffusional effect and the CO inhibition are lumped into only one. As already discussed, this would lead to misunderstanding the real effects of diffusional limitations. Therefore, more complex kinet-

ics, such as Langmuir-Hinshelwood, should be used in order to adequately separate the inhibition effect of CO (chemical limitation) from purely diffusional effects (physical limitation).

This observation was already underlined by Ollero et al. (2002, 2003) when using their n^{th}-order model (Eq.(3.13)) to fit the experimental results obtained with powdery char at temperatures higher than T≥850ºC. To explain this, they conducted a set of experiments at 0.20 bar CO partial pressure (Ollero et al. 2003), which enabled them to determine the Langmuir-Hinshelwood expression. They concluded that, at high temperatures, it is necessary to account for the CO inhibition effect due to the build-up of CO inside the char bed (Ollero et al., 2002).

The trend of Fig. 3.3 is confirmed in Fig. 3.4, where t_{50} is presented as a function of CO_2 molar fraction at a temperature of 900ºC. This behaviour can be extrapolated to other temperatures by examining Table 3.2. As seen in this table, the difference between the measured reactivities at 50% conversion is quite small for the CO_2 molar fraction ranging from 0.35 to 0.50.

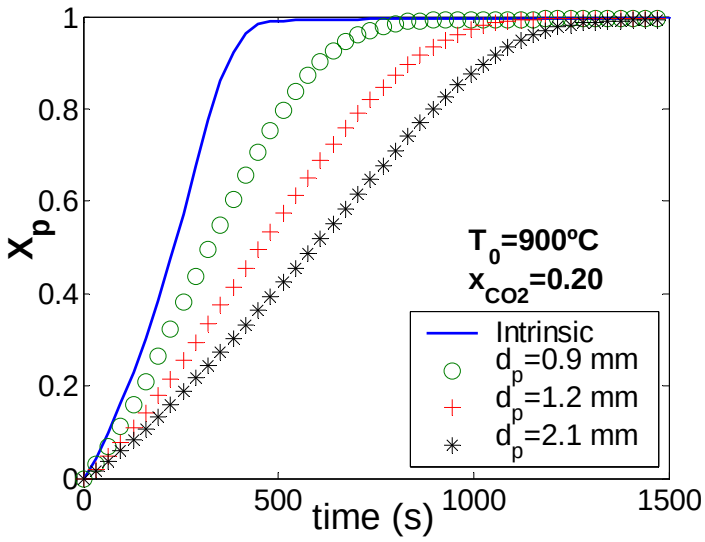

Figure 3.5. Experimental X_p vs. t for various particle sizes at T=900ºC and x_{CO2}=0.2.

6.4. Effect of particle size

The gasification rate was found to be largely influenced by particle size. As usual, the measured reactivity decreases as particle size increases. Fig. 3.5 shows this effect more explicitly. This figure gives the conversion curves at 900ºC and x_{CO_2}=0.2, clearly showing that intraparticle diffusional effects are rate-controlling. We note that the influence of particle size on the time to reach 50% conversion, t_{50}, is not proportional to the initial sizes. In fact, within the size range of 0.9-1.2 mm the value of t_{50} is dramatically affected by physical effects. This supports what was observed in Fig.

3.1 and Fig. 3.2. This behaviour, nevertheless, does not agree with the correlation proposed by Standish and Tanjung (1987) for wood-charcoal particles. As discussed in the survey, they related the initial gasification rate to the initial particle size. In addition, if char particle size is large enough, the CO concentration inside the particle becomes higher. This effect is enhanced at higher temperature because CO production is greater.

6.5. Effectiveness factors

A useful effectiveness factor is defined as the ratio of the actual conversion, X_p, at any instant to the conversion that would be observed if there were neither external nor intraparticle gradients, X_p^{int}:

$$\eta_R(t) = \frac{X_p^k(t)}{X_p^{\text{int}}(t)} \tag{3.14}$$

where the subscripts "k" and "int" represent experiments carried out with diffusional effects and without ("intrinsic"), respectively. To the best of our knowledge, this effectiveness factor was originally introduced by Ramachandran (1980), and it is especially useful for directly discerning diffusional effects from experimental X_p vs. t curves. We calculated this effectiveness factor based on the conversion-time curves obtained in our experiments. The typical results are shown in Fig. 3.6, where the effectiveness factor is plotted vs. temperature at a constant CO_2 molar fraction of 0.2. This figure clearly shows how the effects of physical effects become remarkably prominent at high temperatures and large particle sizes. Of course, to take into account all the effects at once, it would be necessary to plot the effectiveness factor against the Thiele modulus. This is done in a Chapter 4, where further details shown in these experiments are analysed and explained in the light of a simple model.

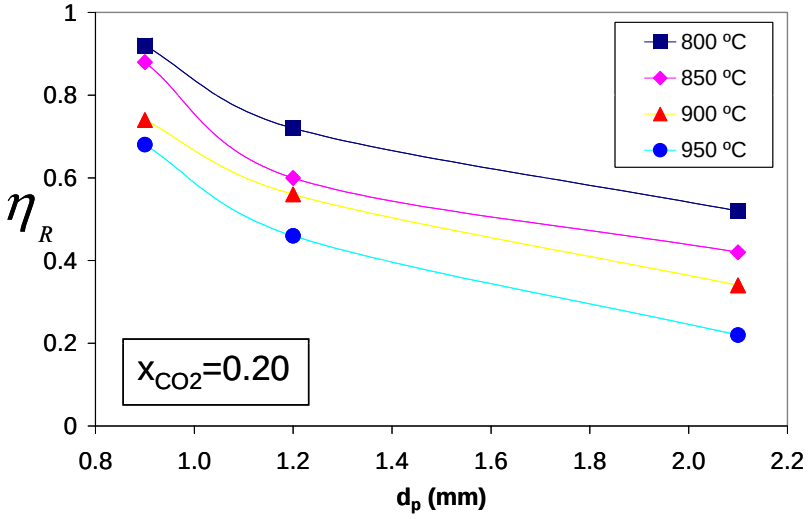

Figure 3.6. Effectiveness factor η_R vs. d_p for various temperatures at x_{CO2}=0.20.

A general trend becomes evident if it is studied the results as a function of the Thiele modulus (based on bulk conditions), ϕ_0. This is defined as

$$\phi_0^{\,2} = L_e^{\,2} \frac{r(c_0, T_0)}{D_{e0} c_0} \tag{3.15}$$

The effectiveness factors defined above were computed and compared with experiments. The typical results are shown in Chapter 4 (Figs. 8 and 9) where the model developed is compared with the experimental results obtained in this chapter.

7. Conclusions

Kinetics studies were carried out to experimentally study the role of diffusional effects found in single char particles. Gasification rates of WPOS were measured in a TGA at various particle sizes, CO_2 partial pressures and temperatures of practical interest (800-950ºC). Experimental results were compared with the intrinsic reactivities obtained under the same operating conditions but using very fine char. Diffusional effects were found to be quite significant for the whole range of "macroscopic size" (different from powder — i.e., 0.060 mm) analysed in this work. They are noteworthy even at the smallest Thiele modulus — d_p =0.9 mm, T=800ºC, p_{CO2}=0.50 bar. At the largest Thiele modulus (T= 950ºC, d_p =2.1 mm, p_{CO2}=0.20 bar), an effectiveness factor as low as 0.22 was experimentally obtained. These results indicate the presence of considerable diffusional resistances in the gasification of "relatively-small" single char particles at practical temperatures. Although the actual situation in a real gasifier is more complex, the conclusions from this study are a first step toward estimating reactivities and the diffusional effects present in char particles inside fluidised bed gasifiers. These physical effects are especially relevant when gasifying highly reactive chars, such as biomass-derived chars. The overall rate of gasification can be affected by chemical kinetics but also by mass and heat transfer processes. Consequently, an appropriate kinetic-particle model that captures plausible physical limitations should be used when simulating fluidised-bed biomass gasifiers. In Chapter 4, a simple particle model is developed and tested with the results described in this chapter.

Chapter 4

Modelling of diffusional effects in TGA gasification experiments with single biomass char particles

1. Introduction

The experimental study carried out in Chapter 3 is analysed theoretically in this chapter. The objective is to evaluate the diffusional effects in the gasification of a single char particle under different operating conditions. A kinetic particle model which takes into account the diffusion-reaction processes within a finite-size particle is formulated, based on the method developed in Chapter 2. It is further extended to allow for intraparticle heat effects and heat and mass transfer phenomena occurring in the external gas layer. The model has the essential advantage of requiring minor computations while still reproducing the major physico-chemical processes that may affect the observed reaction rate.

2. Literature on modelling of char gasification in single particles

Char gasification has been widely simulated and numerous models are available, either structural (Bathia and Perlmutter, 1980, 1981; Zygourakis et al., 1982, Szekely et al., 1976) or volumetric (Groeneveld and van Swaaij, 1980). A structural model allows for explicitly including changes in the internal structure with conversion. An inherent problem of these models is the need for extensive experimental input data (Standish and Tanjung, 1988). In the volumetric approach, however, this problem is overcome by using experimental correlations and effective properties. Several volumetric models have analysed CO_2–char gasification with a computational approach (Groeneveld and van Swaaij, 1980; Bliek et al. 1986; Chen and Gunkel, 1987; Dassapa et al., 1994; Hastaoglu and Karmann, 1987; Haynes, 1981; Srinivas and Amundson, 1980; Turkdogan and Vinters, 1970; Bandyopadhyay et al., 1988, 1991). Some of them have analysed the diffusional effects of single particles, predicting major limitations under some operating conditions.

Bliek et al. (1986) presented a model under conditions in which intraparticle mass transfer was rate-controlling and intraparticle heat transfer was negligible. The main controlling parameters during the gasification of single particles were found to be gasification temperature, particle size and diffusive permeability of the particle. Chen and Gunkel (1987) formulated a non-isothermal model for gasification of single

char particles in an environment of a gas mixture commonly occurring in moving-bed reactors. They found significant intraparticle gradients of gas concentrations, temperature and carbon-conversion profiles at the largest particle size and highest temperature tested. Bandyopadhyay et al. (1988, 1991) derived a modified version of the formulation developed by Turkdogan and Vinters (1970) to explain the intraparticle heat effects experimentally observed. Dasappa et al. (1994) developed a rigorous non-isothermal computational model to explain Ergun's experiments (Ergun, 1956), finding that the observed gasification rate using particle sizes under 1.8 mm was not affected by diffusional resistances.

A simple approach to estimate physical effect limitations in wood char particle experiments was developed by Hawley et al. (1983). They used a simple catalytic isothermal model and found no physical interference for particle sizes over 5 mm. The model is, nevertheless, too simple and does not make it possible to discern the mechanism responsible for the limitation or take into account the effect on the magnitude of these limitations as the reaction progresses. Moreover, the gas kinetics is first-order. In general, simple modelling approaches are usually limited for one (or both) of the following reasons: (1) only applicable to first-order kinetics with respect to gas or solid reactant and/or (2) do not explicitly make allowance for structural changes with reaction. Rafsanjani et al. (2002) applied a new simple mathematical method for solving gas-solid non-catalytic reactions to predict char activation processes. In their model, they included a term to take into account the variation in the activation energy as the reaction proceeds, but they assumed a first-order reaction for the gas reactant.

Most models, whether structural or volumetric, require an intense numerical treatment since analytical or semi-analytical solutions cannot be found for most of the rate forms used to describe gasification systems. In situations when particle-size distribution must be taken into account, together with non-linear kinetics and hydrodynamic effects, the computational effort can be considerable. In this scenario an analytical or semi-analytical approach is advisable for simulating the diffusional and kinetic effects at particle level in order to simplify the overall calculations. The analytical or semi-analytical approach has also been extensively developed by a number of researchers (Ramachandran, 1983; Brem and Brouwers, 1990a, 1990b; Brem 1990; Doraiswamy and Sharma, 1984).

In Chapter 2 the spectrum of applications for existing simplified methods has been extended, using an approximate methodology which can accommodate any general kinetics and any explicitly given intrinsic behaviour of the solid structure variation with reaction. This methodology has been shown to be potentially capable of providing major computational savings while giving very close agreement with the exact (numerical) solution. In the following, the model described in Chapter 2 is expanded to incorporate external mass and heat transfer effects and intraparticle heat effects, both in a very simple manner.

3. Theoretical modeling

3.1. Volumetric local reaction rate

The intrinsic reactivity at any degree of local char conversion was expressed as (**see** Eqs (3.1)-(3.3)),

$$R(X) = f(X) \cdot R_{50} \tag{4.1}$$

$$R_{50} = K p_{CO_2}^n \qquad K = A\exp(-E / R_g T) \tag{4.2}$$

As discussed in Chapters 2 and 3, if the kinetic experiments are carried out with very fine char well exposed to the reacting gas, both the structural profile and the reference reactivity, R_{50}, can be considered intrinsic. In that case, a volumetric reaction rate at any point in a particle can be defined as follows (see Eq. (2.6)):

$$(-r) = r(c,T) \cdot F(X) \qquad (\text{mol/m}^3 \cdot \text{s}) \tag{4.3}$$

where $r(c,T)$ and $F(X)$ are defined as

$$r(c,T) = R_{50} \cdot \rho_{c0} / M_c \quad \text{and} \quad F(X) = f(X) \cdot (1 - X) \tag{4.4}$$

The $r(c,T)$ function is the part of the reaction rate which depends on gas composition and temperature (The non-isothermal counterpart of $r(c_A)$ defined in Chapter 2). In what follows the subscript A is dropped. $F(X)$ was defined in Chapter 2 as the function that treats the change in accessible reacting surface at any conversion level. The usefulness of Eq. (4.3) is seen if it is further postulated that the particle is made up of small particles or grains where diffusional effects are absent. The latter is a reasonable hypothesis because these grains have very small particle sizes. At this local scale intrinsic kinetics should be applicable. Note that the complex problem of surface pore enlargement and development in each of the grains is not explicitly considered but it is implicitly taken into account by the $F(X)$ function. Moreover, the actual size and/or shape of the micro-particles or grains are not relevant in our treatment. We only assume that they are small enough. This assumption ensures that diffusional effects are not present within the grains and thus intrinsic reactivity can be applied at this local level.

In Chapter 2 was also discussed the forms of obtaining the function $F(X)$: (1) by performing kinetic experiments in a kinetic regime and (2) By using expressions given by published kinetic models (also in a kinetically-controlled regime). Normally, for the experimental determination of $F(X)$ it is necessary to assume certain functional forms. In other words, this function must be determined by fitting one or various parameters that best reproduce the experimental variation of reactivity with conversion. Many researchers make the fit by using an arbitrary polynomial of *X*. Nevertheless, in principle, nothing is "banned" a priori; there are some forms which have

been derived on the basis of physico-chemical arguments that describe the evolution of the solid matter. These provide an "ideal" initial guess for the determination of the $F(X)$ function. Examples of this are the random pore model (Bathia and Perlmutter, 1980, 1981), Simons model (Simons, 1980), etc., in a kinetically-controlled regime. These models have free parameters and, therefore, the actual values of the parameters can be evaluated for a given char based on the experimental data by applying the least-square procedure. However, other models like the grain model (Szekely et al., 1976) or the uniform model (Adánez and De Diego, 1993; Adschiri et al., 1986) do not have free parameters. For instance, n^{th}-order kinetics with respect to gas reactant and a uniform model with respect to solid consumption gives

$$(-r) = k\, c^n \cdot (1 - X) \tag{4.5}$$

where k is the kinetic constant expressed in $(\text{mol/m}^3)^{1\text{-}n}\cdot\text{s}^{-1}$. Some examples of functions $F(X)$ for kinetic models under kinetic regime can be found in Table 4.1, Chapter 2 (Gómez-Barea and Ollero, 2006). To sum up, for estimating diffusional effects, it is possible to use Eq. (4.3) with experimentally-determined $F(X)$ and $r(c,T)$ functions. The former depends mainly on the nature of the char and the conditions in which it was generated — i.e., the heating rate and the pyrolysis temperature — while the latter depends on the actual conditions at the internal reaction sites within the porous char particle — i.e., operating conditions and particle size.

3.2. Modelling a diffusion-reaction process a char particle

We modelled the process of a reaction with diffusion within an isothermal particle on the basis of the model developed in Chapter 2 (Gómez-Barea and Ollero, 2006). This model makes it possible to incorporate a non-linear chemical reaction rate given by $R(C)$, and the changes in porous structure during conversion by the specification of $F(X)$. It also allows for changes in the effective diffusivity with reaction through the input of $g(X)$. For a given time, τ, and position in the particle, z ,we can obtain the concentration profiles within the particle with the method by solving the following two-dimensional set of equations displayed in Table 4.1. In the table the values of the parameters are given for spherical geometry and n^{th}-order kinetics. For this case, C^* is null. Table 4.1 includes further details on how to solve the problem with this method.

As discussed in Chapter 2, the model applies to isothermal particles when external mass and heat transfer are not rate-limiting (large Biot heat and mass numbers). These assumptions are probably violated in the TGA experiments like the one described in this study. Therefore, the model needs to be expanded to include intraparticle heat effects, as well as external heat and mass transfer effects. The extension of the model is developed below.

Table 4.1. Model of Chapter 2 for and spherical particle with n^{th}-order kinetics

Equations

$$C(z) = C^* + (1-C^*)\cdot\exp\left[-\frac{\lambda(1-z^2)}{2-\frac{1-z\,h(z)}{1+2/\lambda}}\right] \qquad X(z) = \Theta^{-1}\left(\tau\cdot R(C(z))\right)$$

Parameters

$$\phi_s^{\,2} = R^2\frac{k\,c_{As}^{\;n-1}}{D_{e0}}; \qquad M^2(X) = \phi_s^{\,2}G(X); \qquad G(X) = \frac{F(X)}{g(X)};$$

$$\Theta(X) = \int_0^X \frac{d\,X}{F(X)}; \qquad M^* = \frac{M}{3}\sqrt{\frac{n+1}{2}}; \qquad a = 1-\frac{12}{5}\cdot\frac{n}{n+1};$$

$$h(z) = \frac{1-\exp(-\lambda\,z)}{1-\exp(-\lambda)}; \qquad \lambda = \frac{M^2}{3}\eta_{GOT}; \qquad \eta_{GOT} = \left[\,M^{*2} + \exp(-a\cdot M^{*2})\,\right]^{-1/2},$$

Dimensionless variables

$$z = r/R; \quad \tau = t\cdot\left(k\,c_s^{\;n}\right)/c_{B0}; \quad C = c/c_s; \quad X = 1-c_B/c_{B0}; \quad R(C) = C^n$$

Method of solution: Given τ: for i=1 to N solve → $C(z_i)$ and $X(z_i)$

Input	***Output***
(1) Reaction rate: $R(C)$ and $F(X)$	$C(z,\tau)$ and $X(z,\tau)$ → $X_p(\tau)$, $\eta_i(\tau)$, $\eta_R(\tau)$
(2) Diffusivity: D_{e0} and $g(X)$	

3.3. Modelling intraparticle heat effects

In principle, the temperature field within the particle can be readily estimated by applying the method given in Chapter 2, summarised in section 3.2 and Table 4.1. The following expression is obtained (Gotifredi and Gonzo, 1996):

$$T' = 1 + \mathrm{B}(X)\cdot(1-C) \tag{4.6}$$

in which the following dimensionless parameters and variables are used

$$T' = T/T_s; \qquad \mathrm{B}(X) = \beta_i\cdot p(X); \qquad \beta_i = \frac{\left(-\Delta H_r\right)D_{e0}c_s}{k_{e0}T_s} \tag{4.7}$$

where T' is the dimensionless temperature (based on the surface temperature), β_i and $\mathrm{B}(X)$, are the classical and modified Prater numbers, respectively, and $p(X)$ is a certain function of conversion. The last item is discussed in the Appendix. We can see that the modified Prater number is conversion-dependent. This feature, however, does not add any supplementary difficulty since, as explained in (Gómez-Barea and Ollero, 2006; Rafsanjani et al., 2002), the application of the quantize method allows us to take X as a parameter when integrating the concentration within the particle. Now, taking into account Eq. (4.6), the $R(C)$ function must be modified in the non-isothermal case as follows:

$$R(C)= r(c,T)/r(c_s,T_s) \tag{4.8}$$

For n[th]-order kinetics this leads to

$$R(C)= k(T)/k(T_s)\cdot C^n \tag{4.9}$$

The ratio between the two kinetic constants can be expressed as (Doraiswamy and Sharma, 1984)

$$\frac{k(T)}{k(T_s)} = \exp\left[B(X)\cdot\gamma_s\cdot\frac{1-C}{1+B(X)\cdot(1-C)}\right] \tag{4.10}$$

where γ_s is the classical Arrhenius number defined as $\gamma_s = E/RT_s$. If $B(X)\cdot(1-C)$ is assumed to be small enough, the so-called two-parameter model (Satterfield, 1991) is obtained and the dimensionless reaction rate, $R(C)$, can be expressed as

$$R(C)= C^n\cdot\exp\left[\varsigma(X)\cdot(1-C)\right] \tag{4.11}$$

where $\varsigma(X)=\gamma_s\cdot\mathrm{B}(X)$. The non-isothermal problem can now be solved with the method of Table 4.1, by using Eq. (4.11) instead of its isothermal counterpart $R(C)= C^n$. For the region of significant diffusional limitation and for small values of $\varsigma(X)$, typically $\varsigma(X)<1$, the relative error introduced by assuming isothermal operation for n^{th}-order kinetics and any geometry may be estimated from the following expression (Satterfield, 1991):

$$\delta_t(X)=1-\frac{\varsigma(X)}{2(n+2)} \tag{4.12}$$

For an endothermal reaction, the non-isothermal effectiveness factor can be calculated by means of the following expression (Satterfield, 1991):

$$\eta_i(\tau) = \eta_i^{iso}(\tau) \cdot \delta_t(\tau) \tag{4.13}$$

in which $\eta_i^{iso}(\tau)$ is the intraparticle effectiveness factor calculated according to the model presented in Table 4.1.

3.4. Modelling external mass and heat transfer

Under pseudo-steady-state conditions, the equations that govern the non-isothermal mass and heat transfer problem for general n^{th}-order kinetics are

$$(-R) = k_G / L_e \left(c_0 - c_s\right) = k_a \, c_s^n \tag{4.14}$$

$$(-R)(-\Delta H_R) = h / L_e \left(T_0 - T_s\right) \tag{4.15}$$

The apparent kinetic constant, k_a, lumps the intraparticle diffusion-reaction problem, that is, $k_a = \eta_i \cdot k(T_s)$, in which η_i is the intraparticle effectiveness factor, defined as the ratio of the observed total reaction rate to the total reaction rate when the concentration of the reactant is equal to that at the surface. Mathematically, this is expressed as

$$\eta_i = \frac{(-R)}{k(T_s)\, c_s^n} \tag{4.16}$$

Similarly, the global effectiveness factor η_G is the ratio of the observed reaction rate and the reaction rate when the concentration of the reactant is equal to that in the bulk gas,

$$\eta_G = \frac{(-R)}{k(T_0)\, c_0^n} \tag{4.17}$$

The external effectiveness factor, η_e, is defined as the ratio between the intrinsic reaction rates evaluated at the surface and in bulk-gas conditions

$$\eta_e = \frac{k(T_s)\, c_s^n}{k(T_0)\, c_0^n} = \frac{(-R)}{\eta_i \, k(T_0)\, c_0^n} \tag{4.18}$$

Eqs (4.17) and (4.18) readily give

$$\eta_G = \eta_e \cdot \eta_i \tag{4.19}$$

Detailed derivation of relations presented above can be found in Chapter 5 of this work. For the isothermal case, an approximate explicit solution for η_e can be derived (Förtsch et al, 2001; , Frank-Kamenetskii, 1955; Froment and Bischoff, 1991)

$$\eta_e = \frac{1}{\left[\left\{(1-n)\,\mathrm{Da_p}\right\}^{1/n}+1\right]^n + n\,\mathrm{Da_p}} \qquad 0<n<1 \qquad (4.20)$$

where $\mathrm{Da_p}$ is the Damköhler number of a particle, which represents the ratio of the maximum diffusional rate ($c_s \approx c_0$) to the diffusion-controlled reaction rate ($c_s \approx 0$), which is

$$\mathrm{Da_p} = \frac{k(T_0)}{k_G / L_e}\, c_0^{\,n-1} \qquad (4.21)$$

By considering the definition given for the Damköhler number in Eq. (4.21) and Eqs. (4.21) and (4.19), we can transform Eqs. (4.20), (4.14) and (4.15) into the following dimensionless equation set (Carberry and Kulkarni, 1973):

$$\eta_e = (1-\mathrm{Da_p}\,\eta_i\,\eta_e)^n \cdot \exp\left[-\gamma_0\left(\frac{1}{1+\beta_e\,\mathrm{Da_p}\;\eta_i\,\eta_e}-1\right)\right] \qquad (4.22)$$

$$T_s' = 1+\beta_e\,\mathrm{Da_p}\;\eta_i\,\eta_e \qquad (4.23)$$

$$C_s = 1-\mathrm{Da_p}\;\eta_i\,\eta_e \qquad (4.24)$$

where the β_e parameter is defined as

$$\beta_e = \frac{(-\Delta H_R)\,c_0}{(1+\xi)\,\rho c_p T_0}\,\mathrm{Le}^{-2/3} \qquad (4.25)$$

To derive equations (4.22) and (4.23) the heat and mass transport analogy, $j_D = j_h$, was invoked, where j_D and j_h are the Chilton-Colburn j-factors for mass and heat transfer, respectively. However, the coefficient *h* in equation (4.15) should take into account the radiant contribution of the heat transfer as computationally verified in (Gomez-Barea et al., 2005). Thus, the coefficient ξ in Eq. (4.25) was introduced in order to make an approximate correction to include the radiation effects. This factor is defined as the ratio between the convective and "radiative" film coefficients

$$\xi = \frac{h_{rd}}{h_{cv}} \qquad (4.26)$$

where the radiative film coefficient is defined according to the following approximation

$$h_{rd} = 4\varepsilon_c \sigma T_0^{\,3} \tag{4.27}$$

This estimate is assessed in Fig. 4.1, where ξ is displayed as a function of T_0, taking $\Delta T / T_0$ as a parameter, being ΔT the temperature drop between bulk gas and char surface. The solid lines are the "exact" solution resulting from calculating the radiative flux by its formal expression, which is

$$\xi^{exact} = \frac{\varepsilon_c \sigma (T_0^4 - T_s^4)}{h_{cv}(T_0 - T_s)} \tag{4.28}$$

while the asterisk-marked curve is calculated by considering the approximation given by Eq.(4.27).The value of ΔT is estimated as between 20 and 40ºC for drawing the figure. This hypothesis is verified in the section on results. As seen in Figure 4.1, the approximation is very good for the whole range of bulk-gas temperatures. Moreover, a linear relation can be derived between ξ and T_0 as follows:

$$\xi = 0.66 + 0.0016 \cdot \left(T_0(\mathrm{K}) - 1073\right) \tag{4.29}$$

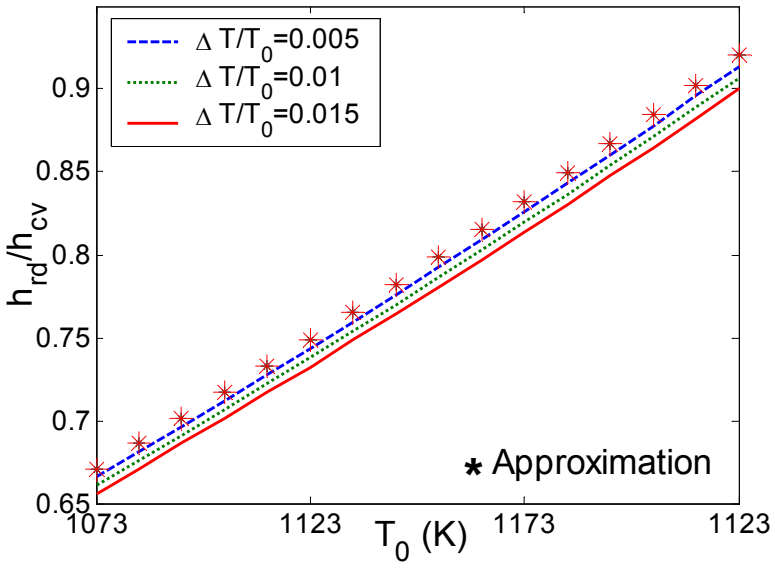

Figure 4.1. Analysis of the radiant approximation

This approximation avoids making the correction factor dependent on the surface temperature and allows for the direct estimation of the radiative effects under different bulk-gas conditions. With regard to char emissivity, experimental measurements of carbonaceous ash have shown values as low as 0.4, as well as a marked variation with temperature (Elliot, 1981). However, the absorptivity of a carbonaceous porous surface has been shown to be very high and, consequently, its emissivity should be

close to 1. In the course of an actual test, the surface of a char particle is made up of ash and carbonaceous material and the proportion between both materials changes as the reaction progresses. Thus, the uncertainty about this parameter is very high. In the absence of further information, we used a value of 0.5.

3.5. Model Inputs

3.5.1. Rate law

We use the char reactivity at 50% conversion determined in Chapter 3 for the experiments carried out with 0.060 mm particles (Eq. (3.13)):

$$R_{50} = \left[1993 \cdot \exp(-14260/T)\right] \cdot p_{CO_2}^{0.4} \quad \text{(g/g/s)} \tag{4.30}$$

This expression can be transformed in terms of the model's needs as

$$r(c,T) = k \cdot c^n \quad \text{(mol/m}^3\text{)} \cdot \text{s}^{-1} \tag{4.31}$$

with $n = 0.4$ and a rate constant given by

$$k = \left[c_{B0} \cdot (R_g T)^n \cdot 1993 \cdot \exp(-14260/T) \right] \quad \text{(mol/m}^3\text{)}^{1-n} \cdot \text{s}^{-1} \tag{4.32}$$

3.5.2. Structural profile

Rigorously, the structural profile depends on the reaction temperature and the gas composition. However, for the sake of simplicity, this model uses an average structural profile derived from the set of experiments carried out without diffusional limitations (see Ollero et al., 2003 for details). The structural profile used is

$$f(X) = 66X^5 - 140X^4 + 110X^3 - 37X^2 + 6.3X - 0.09 \tag{4.33}$$

For this 5th-order polynomial no analytical solution can be found for $\Theta(X)$. In order to avoid numerical integration in every run we used the best-fit (in the sense of the least-square) 5th-order polynomial of the numerical integration of $\Theta(X)$. The result is the following polynomial:

$$\Theta(X) = -18.9X^5 + 53X^4 - 51X^3 + 18.9X^2 + 0.61X - 0.06 \tag{4.34}$$

which can be used for all the computations since, as already noted, we assume the same structural profile for the full range of operating conditions. In the present case, Eq. (4.34) turns out to be almost a straight line, and we can therefore choose a simpler polynomial. This point is further discussed in the section on results.

3.6. Model Outputs

The model developed is used for the computation of particle conversion as well as the internal and external effectiveness factors and, therefore, the overall effectiveness factor. The particle conversion is calculated with

$$X_p(t) = 3\int_0^1 X\, z^2\, dz \tag{4.35}$$

The intraparticle effectiveness is defined as the ratio between the actual (observed) total reaction rate at any instant and the total reaction rate at that instant if the concentrations of the reactants were equal to those at the surface, that is:

$$\eta_i(t) = \frac{\int_0^1 \left[R(C)\cdot F(X)\cdot z^2 \right]\cdot dz}{\int_0^1 \left[F(X)\cdot z^2 \right]\cdot dz} \tag{4.36}$$

The second effectiveness factor is defined as the ratio of the actual conversion, X_p, at any instant to the conversion that would be observed if there were no intraparticle gradients

$$\eta_R(t) = \frac{X_p^k(t)}{X_p^{\text{int}}(t)} \tag{4.37}$$

where the subscripts "k" and "int" represent experiments carried out with diffusional effects and without ("intrinsic"), respectively. The first effectiveness factor defined, η_i, is the classical definition as used by Wen (1968) and is merely a direct translation from catalytic systems. The effectiveness factor, η_R, originally introduced by Ramachandran (1983), is especially useful for directly discerning diffusional effects in experimental X_p vs. t curves. Finally, the global effectiveness factor is computed according to Eq. (4.19).

3.7. Method of solution and numerical treatment

1. Assume an internal effectiveness factor, η_i.

2. With η_i given in step (1) and from bulk-gas data, calculate the external effectiveness factor, η_e, with Eq. (4.22), and thus T_s' and C_s, with Eqs. (4.23) and (4.24), respectively. An ideal first guess for the solution of Eq. (4.22) is the one calculated according to the isothermal case, given in Eq. (4.20).

3. Given T_s' and C_s from step (2), solve the the intraparticle problem (Table 4.1) to calculate the internal effectiveness factor, η_i. To achieve this, the reaction rate must be firstly expressed in the form given in Eq. (4.3), with the non-isothermal version of $R(C)$ presented in Eq. (4.11). The remaining inputs are defined in section 3.5. In a simpler approach, it is possible to estimate the isothermal effectiveness factor and make the correction given in Eq. (4.13). Both procedures give similar results for the experiments simulated in this work. However, the first method is more general and, since it is very simple to implement, it is recommended for other situations.

4. Check to determine whether the difference between the intraparticle effectiveness factor η_i, assumed in step (1) and the one calculated in step (3) is small enough. If so, go to (5). If not, go to step (2) and repeat the procedure in steps (2)-(4) with a new value of η_i. The selection of a new candidate can be implemented with a Newton-Raphson algorithm.

5. Generate outputs (particle conversion and effectiveness factors).

The system of Table 4.1 is solved by dividing the radial coordinate, z, into N + 1 points [$z_i = (i - 1)\,\Delta z$, i = 1: N + 1, $\Delta z = 1/(N - 1)$] (see Chapter 2, Section 5, for details). The solution (C_i, X_i) is found by solving (N+1) systems of two non-linear equations, which is done by applying the Newton-Raphson method. A value of N=5 was chosen for all the calculations in this work. Normally no more than three iterations were necessary to achieve an absolute error less than 0.02 (2% relative error). However, the relative error is always under 5% with only one correction, which should be enough for the approach developed here. Finally, note that the above procedure must be applied for a given *t*. The reason is that the external effectiveness factor varies with conversion and must be calculated for a given degree of conversion. This procedure may seem to be cumbersome because the internal problem requires considerable effort. However, the model used for solving the intraparticle problem is highly suitable for this situation, since it directly solves the problem for a given t, and it is therefore not necessary to integrate the problem from the start. This was discussed in Chapter 2.

4. Results and discussion

4.1. Intrinsic kinetics

The experimental data include the measurements of gasification rate at three CO_2 molar fractions (0.20, 0.35 and 0.50), four temperatures (800, 850, 900 and 950ºC) and four different particle sizes (0.06, 0.9, 1.2 and 2.2 mm). As discussed in Chapter 3, the reactivity found in the experiments using 0.06 mm can be considered intrinsic, at least up to 900ºC. Tests carried out at 950ºC are somewhat doubtful according to the criteria used in Chapter 3 (see Section 5). Experiments using char sizes other than 0.06 mm are likely to be affected by physical processes.

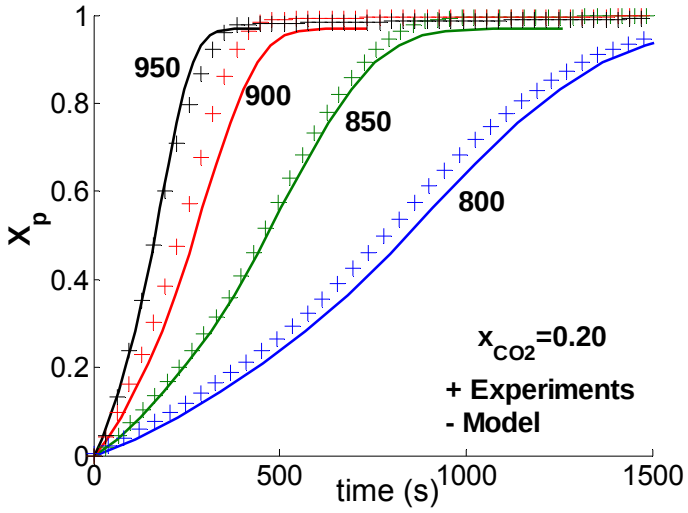

Figure 4.2. Experimental (symbols +) and theoretical predictions (solid line) of intrinsic X_p vs. t curves. Case of x_{CO_2}=0.20

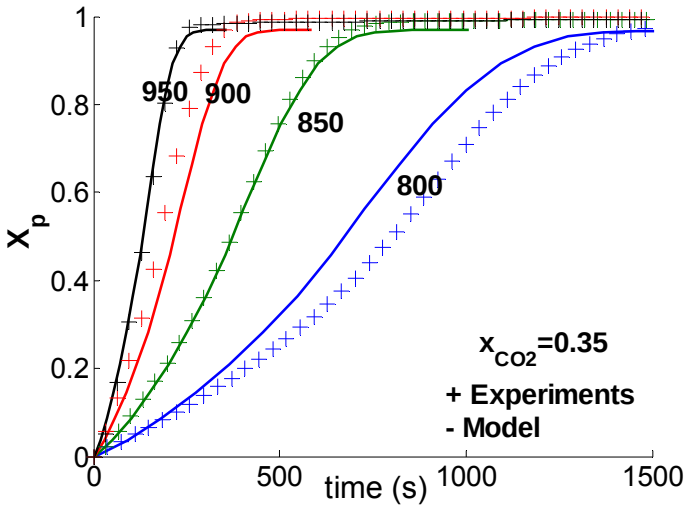

Figure 4.3. Experimental (symbols +) and theoretical predictions (solid line) of intrinsic X_p vs. t curves. Case of x_{CO_2}=0.35

For the particular case of intrinsic experiments, the model can be used for simulating the X_p vs. t curves. This is illustrated in Figs. 4.2-4, which displays the X_p vs. t curves for the whole range of experimental operating conditions analysed in Chapter 3. We note that the agreement is quite good. Obviously, this result is just a confirmation that the kinetic expression, Eqs. (4.31)-(4.32), the structural profile, Eq. (4.33), and the approximate function given by Eq. (4.34) are suitable for describing the system under kinetic regime, apart from the method itself. This is, however, highly relevant since the use of the classical shrinking core (SCM) and uniform con-

version (UCM) models in the kinetically-controlled regime, did not reproduce the actual behaviour of the char analysed in this work. As discussed in the literature survey sections of this and the previous chapter, this approach has been widely used in the specialised literature for explaining the X_p vs. t curves for char gasification experiments, with controversial results (Groeneveld and van Swaaij, 1980; Standish and Tanjung, 1988; Hastaoglu and Karmann, 1987).

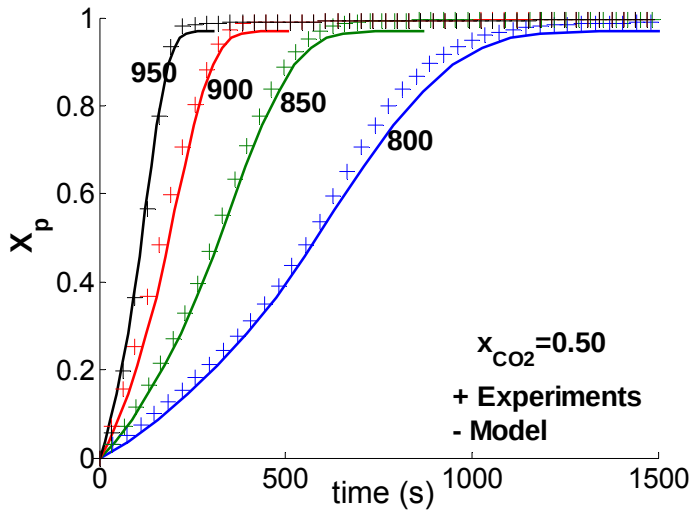

Figure 4.4. Experimental (symbols +) and theoretical predictions (solid line) of intrinsic X_p vs. t. Case of x_{CO_2}=0.50

4.2. Diffusional effects in the experiments

The experimentally obtained X_p vs. t curves in the diffusional or intermediate regime are also in close agreement with the model results up to 900ºC. This is seen in Fig.4.5 where the X_p vs. t curves for (d_p=2.1 mm, x_{CO_2}=0.35) are plotted for various gas temperatures. The curves in the graph are for char conversions ranging form 0.1 to 0.9. Outside this range the model disagrees considerably with the experimental data. This may be due to the structural profile used, which was optimised for a range of 0.2-0.8 (Ollero et al, 2003).

As discussed in Chapter 3, the Ramachandran effectiveness factor (Eq. (4.37)) can be used for assessing the diffusional effects at any time from experimental X_p vs. t curves. Fig. 4.6 (see graphs (a) and (b)) illustrates the procedure and defines the nomenclature used in this work. The example given in the figure is (T_0=850ºC, x_{CO_2}=0.35). The dotted curve in graph (a) is the X_p vs. t curve for d_p=1.2 mm ($X_p^k(t)$), while the solid line represents its intrinsic counterpart, d_p=0.06 mm ($X_p^{int}(t)$). Here, superscript "k" means any experiment carried out by using a particle size different from 0.06 mm while superscript "int" refers to the intrinsic curve. Graph (b) was constructed by using the curves from graph (a): At any time t, η_R is

obtained by the ratio of X_p^k / X_p^{int}. In the horixonatal axis of graph (a) two times, t_{50}^{int}, and t_{50}^k, are indicated. These are, respectively, the time to reach 50% conversion in the intrinsic experiment and in the test "k".

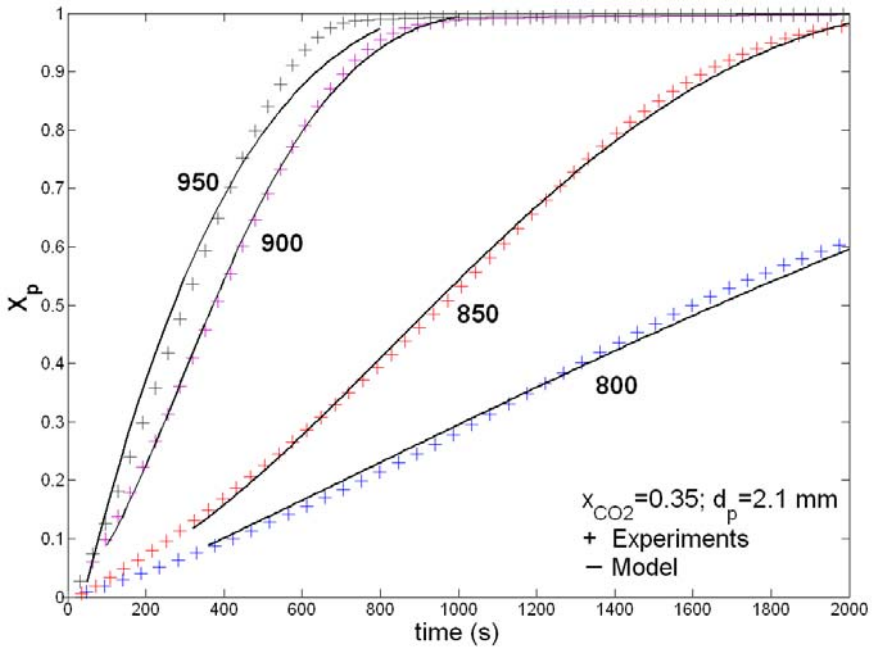

Figure 4.5. Experimental (symbols +) and theoretical predictions (solid line) of X_p vs. t curves for various temperatures. Case of d_p=2,1 mm and x_{CO_2}=0.35.

Figure 4.6 further illustrates the reactivity vs. conversion curves (graph (c)), and the way to compute the overall effectiveness factor experimentally (graph (d)). Graph (d) was constructed by using the curves from graph (c): At any particle conversion $X_p = \text{j}$, η_G is obtained by the ratio of R_j^k / R_j^{int}. By way of example, Figure 4.6 (c) and (d) illustrates the values of η_G computed at 50% (j=0.5) and 75% (j=0.75) char conversion. In graph (d) these are respectively, $\eta_G^k(X_p{=}0.5) = R_{50}^k / R_{50}^{\text{int}}$ and $\eta_G^k(X_p{=}0.75) = R_{75}^k / R_{75}^{\text{int}}$. We can see that the curves in graph (d) are quite irregular and vary significantly in the initial range of char conversion. Furthermore, there is strange behaviour with a relative maximum and minimum in the middle of the conversion range. This strange behaviour is the result of the curves depicted in graph (c). Although it is not obvious in the graph (c) in the figure, little changes in the reactivity curves make great differences in the experimentally calculated η_G. This behaviour has direct consequences, as we will discuss below.

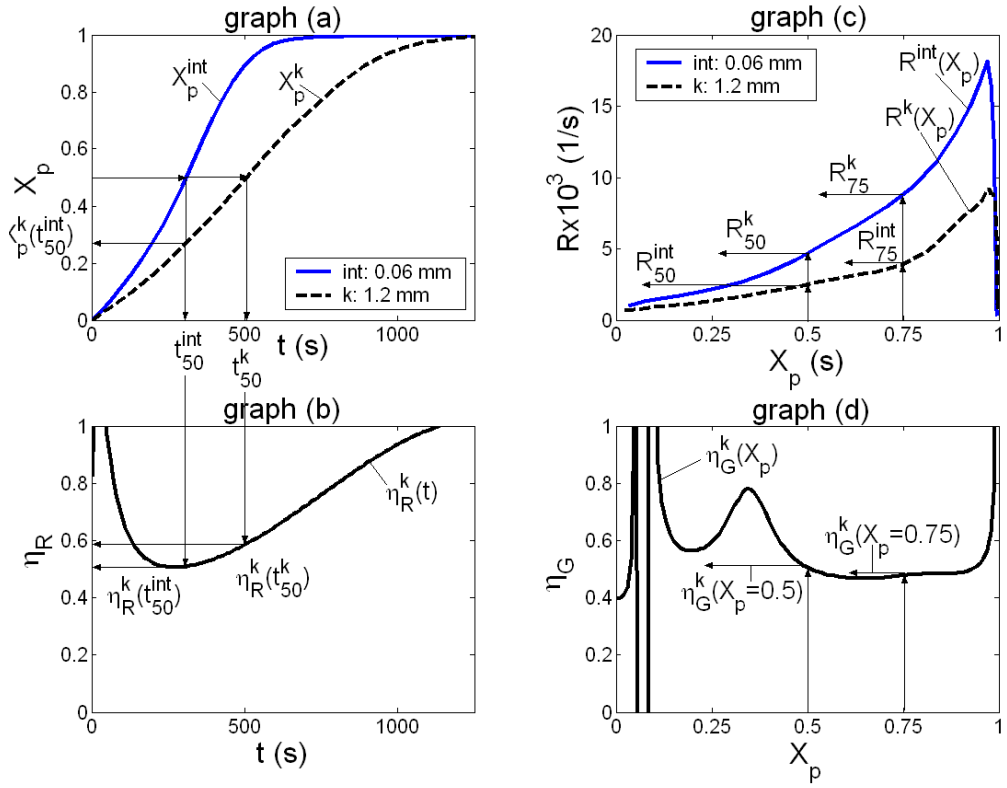

Figure 4.6. Methodology for determining experimental values of η_R and η_G. (Example case of T_0=850ºC, x_{CO_2}=0.50, d_p=1.2 mm).

Figure 4.7 gives the η_R^k curves for various experiments carried out at T=900ºC, clearly showing the impact of size on η_R. Solid lines represent the model predictions while the dotted lines are the corresponding experimental η_R. As we can see, the model prediction is quite good for the char conversion plotted. In addition, we include a test using the largest particle size and changing the gas-phase CO_2 molar fraction, x_{CO2}. We note that the curves are quite similar in shape, but the curve representing the higher CO_2 molar fraction (0.20) is slightly under the curve using 0.35.

A general trend becomes evident if we study the results as a function of the Thiele modulus (based on bulk conditions), ϕ_0. This is defined as

$$\phi_0^{\,2} = L_e^{\,2}\,\frac{r(c_0,T_0)}{D_{e0}\,c_0} \tag{4.38}$$

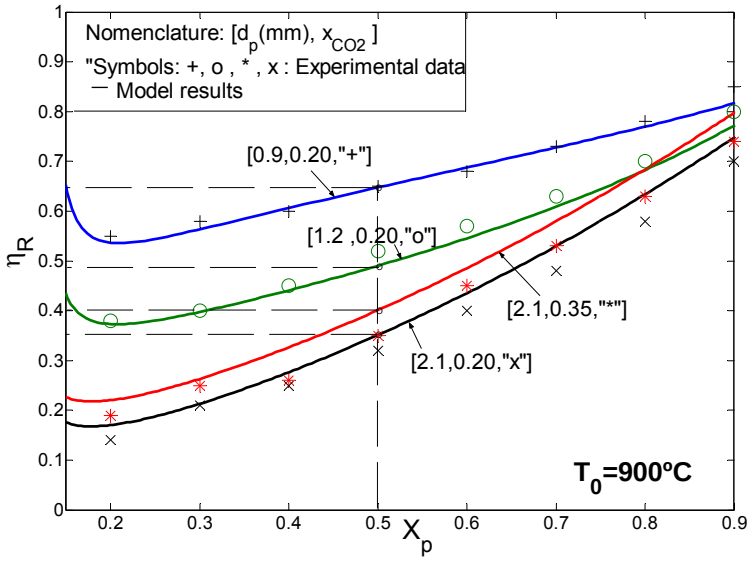

Figure 4.7. Experimental and theoretical predictions of curves η_R vs. X_p for various particle sizes (d_p =0.9, 1.2, 2.1 mm) and CO_2 molar fractions (x_{CO_2} =0.20, 0.35). Case of T_0 =900ºC.

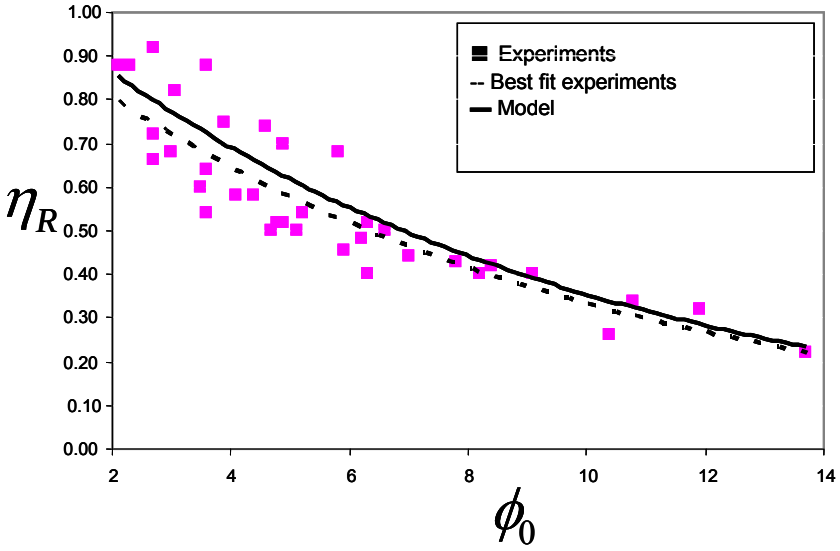

Figure 4.8. Ramachandran effectiveness factor (η_R) at 50% conversion vs. Thiele modulus (ϕ_0).

The two effectiveness factors defined above were computed and compared with experiments from Chapter 3. The results are shown in Figs. 4.8 and 4.9 where the effectiveness factors, $X_p^k(t_{50}^{\text{int}})$ and $\eta_G^k(X_p=0.5)$, respectively, are displayed against ϕ_0.

Figures 4.5 and 4.6 clearly showed how the impact of physical effects is prominent at high temperatures and large particle sizes — i.e., large Thiele modulus. The Ramachandran effectiveness factor, η_R, is seen to be more suitable than the classical effectiveness factor, η_G. This is evident in Fig. 4.8, where the experimental data are less scattered than in Fig. 4.9. Although the experiments are the same, the way to determine the value of these two effectiveness factors is quite different, as was discussed during the anlysis of Fig. 4.6. The overall effectiveness factor is too sensitive to small changes in the reactivity slopes. Therefore, these experimental values cannot be confidently calculated with the procedure described in this research and in other works (Ollero et al., 2003; Gómez-Barea et al., 2005a).

As shown in Fig. 4.8, the general trend of the experiments is captured effectively by the model. This is confirmed by comparing the model results (solid line) to the dotted line in Fig. 4.8. The dotted line represents the best-fit curve (in the sense of least squares) of the experimental data (displayed as single squares in the figure). We note that the two curves are in close agreement, whereas a similar analysis of Fig. 4.9 reveals greater disagreement. Despite this, the general trend is reasonably well captured. In addition, the scattering of the data displayed in Figs. 4.8 and 4.9 leads us to think that more than two experiments would be necessary to minimise the experimental error associated with the effectiveness factor determination.

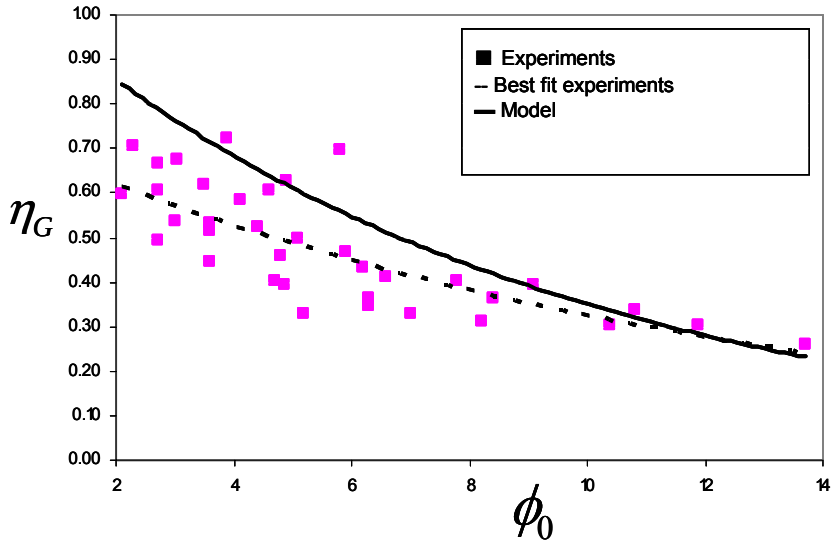

Figure 4.9. Overall effectiveness factor (η_G) at 50% conversion vs. Thiele modulus (ϕ_0)

4.3. Relative contribution of different effects

The experimental results described in Chapter 3 of this study illustrate the strong diffusional effects present in the experiments carried out. In Section 4.1 and 4.2 the model's capabilities were validated for the intrinsic tests (powdery char) and for the experiments where the diffusional effects were appreciable (larger char particle

sizes). The model can also be useful for assessing the actual contribution of different mechanisms involved in a typical char reactivity test. Table 4.2 shows some model results at 50% char conversion. From left to right, each cell shows the Thiele modulus at bulk-phase conditions, ϕ_0, the external effectiveness factor, η_e, the intraparticle effectiveness factor, η_i and the overall effectiveness factor, η_G. As expected, the diffusional resistance rises (effectiveness factor decreases) as temperature increases. This is not true for the case of T_0=950ºC, d_p=2.1 mm, x_{CO2}=0.20 (ϕ_0=13.70). In this test the external effectiveness factor increases as compared to T_0=900ºC. This result is explained by observing that, although η_e is lower for T_0=950ºC, the drop in η_i, is much higher for the latter. Therefore, the overall effectiveness factor, η_G, is lower for T=950ºC (η_G=0.24) as compared to T_0=900ºC (η_G=0.34). This clarifies the situation: The particle as a whole is more diffusion-limited for the test at 950ºC. However, the distribution of the diffusional resistances changes from one situation to another. This behaviour is well documented in the analysis of catalytic systems (Doraiswamy, and Sharma, 1984). For the conditions reported in Table 4.2 the values computed for δ_N and δ_t are also close to unity and fall within a narrow range. Hence, the non-equimolar and intraparticle non-isothermal effects are not relevant. At high temperature and large particle size the major contribution to the observed diffusional resistance is almost entirely attributed to intraparticle mass-diffusional effects. Furthermore, as observed in the table, external effects are important for all the cases.

Table 4.2: Analysis of model results: Contribution of different effects

T (ºC)	ϕ_0	η_e	η_i	η_G
	d_p=2.1 mm			
800	6.22	0.82	0.72	0.59
850	8.42	0.78	0.61	0.47
900	10.90	0.76	0.45	0.34
950	13.70	0.81	0.29	0.24
	d_p=1.2 mm			
800	3.60	0.90	0.86	0.78
850	4.80	0.87	0.80	0.70
900	6.19	0.83	0.74	0.61
950	7.80	0.80	0.65	0.52
	d_p=0.9 mm			
800	2.70	0.93	0.91	0.85
850	3.60	0.90	0.86	0.78
900	4.65	0.87	0.81	0.71
950	5.80	0.84	0.74	0.63

Case x_{CO2}=0.20: δt between 0.98 and 0.99. δN between 0.96-0.98

4.4. Further discussion

As we proceeded, we simplified the model considerably. Details about the impact of the most noteworthy simplifications are discussed below, and the range of the model's applicability is also examined.

4.4.1. Intraparticle thermal effect

In order to check the capability of Eqs. (4.12) and (4.13) to predict the thermal gradient within the particle, we calculated the value of the intraparticle non-isothermal effect by numerically solving the differential energy equation. For the experimental conditions tested, the approximate approach derived in this work was found to be excellent. No significant changes in the values of the four effectiveness factors were observed. For example, for the worst-case scenario, at T_0=950ºC and d_p=2.1 mm, the difference between the numerical solution and our simplified approach was within 1%. However, we must recognise that the intraparticle thermal gradients that emerged from the tests analysed in this study were rather low. In a situation where thermal gradients within the particle were expected to play a major role, the deviation could be considerable. In such a situation, most likely the condition expressed as $\varsigma(X)<1$ would not be fulfilled. Therefore, the approximation given in Eqs. (4.12) and (4.13) could deviate from the exact (numerical) solution. In such situation, the problem should be solved by incorporating Eq. (4.11) into the method described in Table 4.1. In any case, this does not introduce much additional difficulty.

4.4.2. Equimolarity

When a volume change accompanies a reaction, a correction should be applied to the effectiveness factor given by Eq. (4.13) (Satterfield, 1991). That correction, however, proves to be small in our case. In the case of a gasification reaction (two moles of gaseous product per mole of gaseous reactant, i.e., ε_v =1), the correction factor is less than one. As demonstrated in (Ollero et al., 2002), this is quite small. For instance for ε_v = 1, x_{co_2} =0.2 and ϕ_0=1, the correction factor yields 0.97. In conclusion, Eq. (4.13) provides a very simple way to rapidly estimate the role played by heat effects in gasification experiments.

4.4.3. External heat transfer

As shown in Table 4.2, external effects are important for all cases. Moreover, although not explicitly shown in Table 4.2, the external effectiveness must be computed taking into account energy Eq. (4.15). This is because the value of the thermal gradient in the external gas layer depends mainly on β_e, as Eq. (4.23) expresses. For the isothermal case, the value of η_e is computed with $\eta_e=(1-\mathrm{Da}\,\eta_e)^n$ and the thermal drop between bulk and surface is calculated by $T_0-T_s=\beta_e\,\mathrm{Da}\,\eta_e$. We recomputed all the tests assuming isothermal conditions in the external gas layer. The values of the global effectiveness factor found by these computations were well above the non-isothermal ones. Deviations over 60% were calculated for the effec-

tiveness factor. As a result, a model that does not consider thermal effects will not reproduce the observed diffusional effects.

4.4.4. Radiant heat transfer

Radiant heat effects were found to be quite important, even at the lowest temperature (800ºC). We introduced this effect by two-staged approximations: (1) the use of (4.29) in the β_e parameter (Eq. (4.25)) for the inclusion of radiant effects in the purely convective formulation (Eqs. (4.22)-(4.25)), and (2) the approximation devised by using ξ given in Eq. (4.26) instead of ξ^{exact} given in Eq. (4.28). Assumption (1) was shown to be valid because the computed values of ΔT ranged between 5 and 35ºC. So the analysis in Fig. 4.1 is correct. Assumption (2) was assessed by recalculating all the tests without considering radiant effect — i.e., ξ=0 in Eq. (4.25). All computations had very low given values for the external effectiveness factor, especially the tests at higher temperatures. This was expected since radiative heat transfer is enhanced at high temperature. The heat and mass transport analogy used in deriving Eqs. (4.22) and (4.23) made coefficient *h* in Eq. (4.15) much smaller than those calculated by incorporating radiant effects. The deviations were found to be significant at high temperature, at which the ξ factor was around 0.66 (at 800ºC) to 0.9 (at 950ºC).

4.4.5. Conversion-dependent profiles

Function $f(X)$. Char particles are composed of pure char (solid carbon) and ash. It is assumed that char is the only reactive matter during particle conversion. It is also assumed that the amount of ash and its bulk density remain constant during the conversion of the char particle (see Appendix 4.1). However, it is likely that phenomena such as the catalytic effects of the growing alkali concentration or other physical effects such as a phase change — namely, a change in the solid solution — might affect the results, especially at high temperature and conversion using coarse particles. As already discussed, we did not explicitly take into account the possible catalytic effects of ashes. However, we took it into account implicitly through the use of an average structural profile obtained experimentally in (Ollero et al., 2002; 2003). Less agreement found experimentally at higher temperatures and conversion was consistent with what was expected in advance by simply comparing the discrepancies between the individual structural profiles with the average (universal) one (especially at high temperatures). This has been thoroughly analysed in studies already published (Gómez-Barea et al., 2005a; Ollero et al., 2003). In addition**,** the situation in diffusion-limited tests is even more complicated because of the non-uniform conversion of the particles during reaction. In this case, for a given overall conversion, the external part of the particle reaches higher local conversion than internal parts. Therefore, the local catalytic effects are enhanced in this part of the particle, which introduces additional discrepancies with respect to the test carried out with powdery char, where uniform conversion makes overall and local conversion the same (see Appendix 2.1). Nonetheless, the model results give quite good agreement. Caution must be taken when extrapolating the model for other operating conditions different from those in which the structural profile was obtained.

Function $\Theta(X)$. Expressing the $\Theta(X)$ function by means of a 5th-order polynomial (Eq. (4.34)) seems to overcomplicate things. Actually, a simpler function (even a linear function) could have been used for the situation described in this article. However, as discussed in the present and the foregoing chapters, the reactivity for most coal, lignite and peat chars decreases with increasing conversion, whereas it increases for most biomass chars. Furthermore, it can also exhibit a maximum or a minimum, which means that changes in reactivity with conversion vary widely from one char to another. Therefore, due to the variety of potential cases, a general treatment such as the one given here by using a general nth-order polynomial could be more appropriate.

5. Conclusions

The simple model developed in this chapter provides a quick way to estimate the diffusional effects in single particles. The prediction of diffusional effects from the model developed in this chapter are in reasonable agreement with the experimental results from the set of TGA char gasification tests using single particles given in Chapter 3. The model satisfactorily explains the very low measured effectiveness factor found at high temperatures and large particle sizes — i.e., large Thiele modulus. The model also makes it possible to identify the contribution of the different effects that generate physical interaction in the determination of char gasification reactivity tests. This makes it possible to quantitatively estimate the different effects taking place within the char particle and in the boundary layer. In particular, intraparticle mass limitations were identified as the main factor responsible for the high resistance found under the test conditions. External heat and mass transfer were also found to play a relevant role. The combined theoretical-experimental approach developed in Chapters 3 and in this chapter has revealed itself to be of great help in interpreting experimental results.

Appendix 4.1.: Expressions for the effective properties

Two diffusion mechanisms occur inside porous particles: bulk and Knudsen diffusion. The corresponding coefficients can be estimated as indicated in Section 5 of Chapter 3. In that chapter, the Bosanquet formula was used to take both diffusional contributions into account explicitly. Knudsen diffusion was found to be non-limiting. Consequently, a simpler, more empirical approach to model effective properties with conversion in order to simplify the calculations is used in this model. The expressions used for diffusivity and thermal conductivity variation are the following (Srinivas and Amundson, 1980; Gómez-Barea et al., 2005a)

$$D_e = \frac{\varepsilon}{\tau_t} D_m \tag{4.39}$$

$$k_e = (1-\varepsilon)^{\beta} k_m \tag{4.40}$$

The exponent of Eq. (4.40) usually ranges between 1 and 2. In our computations, for simplicity, we estimated an initial value of ε_o, D_{e0} and k_{e0}, and we assumed the following empirical expressions (Doraiswamy and Sharma, 1983; Sahimi et al., 1980; Hastaoglu; Srinivas and Amundson, 1980; Haynes, 1981; Bandyopadhyay et al., 1988, 1991; Dassapa et al., 1994):

$$D_e = (\varepsilon/\varepsilon_o)^{\beta} D_{e0} \tag{4.41}$$

$$k_e = \left[(1-\varepsilon)/(1-\varepsilon_o)\right]^{\beta} k_{e0} \tag{4.42}$$

We further assumed that a linear relation holds between local porosity and conversion — that is $\varepsilon = 1-(1-\varepsilon_0)\left[1-X\right]$ — and that the bulk-ash density remains constant during particle conversion. With these assumptions it is possible to derive the following expressions:

$$g(X) = \left(\frac{\varepsilon}{\varepsilon_0}\right)^{\beta} = \left[1 + \frac{(1-\varepsilon_0)}{\varepsilon_0} X\right]^{\beta} \tag{4.43}$$

$$q(X) = \left[(1-\varepsilon)/(1-\varepsilon_o)\right]^{\beta} = \left[\frac{1-(1-\varepsilon_0)\cdot X}{1-\varepsilon_0}\right]^{\beta} \tag{4.44}$$

Finally, note that the ratio between the two above equations is the $p(X)$ function of Eq. (4.7), which is defined by this expression:

$$p(X) = \frac{g(X)}{q(X)} = \left[\frac{1-\varepsilon_0(1-X)}{X+\varepsilon_0(1-X)}\right]^{\beta} \tag{4.45}$$

Chapter 5

Mass transport effects during determination of gas-solid reaction kinetics in fluidised bed

1. Introduction

Many gas-solid reaction processes benefit from being carried out in a fluidised bed (FB). Examples of these can be found in the petrochemical industry (cracking of hydrocarbons, polymerisation of oleofines, etc), in the metallurgical processes (limestone calciner, roasting of sulfides, etc.), and in thermochemical conversion processes (combustion of coal, gasification of coal and biomass, waste incineration, etc). Design, optimisation and scale-up of these processes often need an accurate understanding of the intrinsic kinetics of a heterogeneous reaction between a reactant gas and a solid.

Gas-solid reactions tend to be influenced to a great extent by heat and mass transport processes. Thus, in determining the intrinsic reactivity in laboratory studies, diffusion processes may seriously affect the observed reaction rate and must be considered when interpreting results. To remove diffusional effects from the experimental determination of solid reactivity, the experiments are usually carried out in typical laboratory apparatus (thermo-balance (TGA), muffle furnaces, etc), where the conditions can be well kept under control. In this situation the overall reaction is to be kinetically controlled. There are, however, circumstances where kinetic studies benefit from being conducted in FB (see for instance the example of char reactivity in Chapter 6).

2. Literature survey on diffusional effects in FBKE.

The experimental strategy in studying solid reactivity in an FB involves measuring the extent of conversion of gas passing in steady flow through a batch of char. Any flow model can be used, as long as the flow pattern selected is known. The gas flow-pattern in an FB is, however, difficult to predict. In practise, a fluidised bed influences kinetic data mainly in three ways (Bjerle et al., 1980) (1) back-mixing of the gas phase, (2) mass transfer resistance between the bubble and emulsion phases and (3) segregation of char particles within the emulsion phase. Firstly, back-mixing of the gas phase with deviation from plug flow introduces an uncertainty about the partial pressures of the gas components at different points in the bed. Secondly, the gas in the

bubble phase could be in poor contact with the solids, and for very fast chemical reactions the mass transfer resistance between the bubble and emulsion phases may become important. Some authors have used shallow beds in order to obtain very low conversion of the gas phase, in most cases below l0% (Luo et al., 2001a; Scott et al., 2005). In this way, the bed can be looked upon almost as a differential reactor, and the influence of gas back-mixing is negligible. Other authors design the experiments with particle sizes that make the minimum fluidization velocity differ from the fluidising velocities by a factor of 1.5 to 2 (Adánez et al., 1985). This means that a considerable amount of the gas flow will pass through the emulsion phase, fast bubbles are avoided, and so, bypassing of the reactant within the bubbles is more or less eliminated.

There is published work especially devoted to determine non-catalytic kinetics in FB (Corella, 1980; Doraiswamy et al., 1959). These publications are generally restricted to the assumption of ideal reactor flow-pattern for the gas (plug flow and perfect mixing) and non-porous particles. When the solid are nonporous the method described by Doraiswamy et al. (1959) and Corella (1980) are appropriate. They adjusted the superficial velocity very close to that of minimum fluidisation. Most of the gas passes through the dense phase and assumption of plug flow for the gas phase and complete mixing for the solid phase is quite valid. Here the conversion of the gas will vary with time and position, whereas the solid conversion varies with time alone. Moreover, when the products of reaction are gaseous, the progress of the reaction can be easily followed by the analysis of the product gas. Examples of such reactions are selective chlorination of ilmenite (Doraiswamy et al., 1959) and fluorination of uranium tetrafluoride (Corella, 1980). However, when the particle are porous (or becomes porous during the experiment) the change in reacting surface area with reaction must be considered. Typical examples of these are char gasification (Luo et al., 2001) and char combustion (Dennis et al., 2005).

The assumption of plug flow for the gas through the dense phase is not often, valid under usual FB kinetic experiment (FBKE) conditions. Extreme precautions must be taken to make the FB operate under the conditions assumed. For instance, to apply the method developed by Corella (1980), the superficial gas velocity must be adjusted to be close to the minimum fluidising velocity in order to fulfil the hypothesis made in deriving the method, so that the gas is in plug-flow. Otherwise, the method cannot be applied. Moreover, most of the FBKE use superficial velocities well above that of minimum fluidisation Luo et al., 2001; Dennis et al., 2005; Scott et al., 2005; Bjerle et al., 1980; Schmal 1982; Goring et al., 1952; Sipilä, 1988; van den Aarsen, 1985; Mleczko and Wurzel, 1997; Brunello et al., 1996; Wurzel et al. 2000; Khraisha, 2004, etc.). This greatly limits the method developed by Doraiswamy et al., 1959 and Corella, 1980. The reason to keep the superficial velocity low is often in opposition to other conditions required (for instance, to attain good solid mixing, to avoid segregation, etc.). The flow pattern of the solids in an FB also may have an impact on the final conversion. The usual assumption of perfect mixing may not be true for char due to segregation with respect to the inert solids. Fluidisation of mixtures of solids with different densities and sizes, and segregation that appears when fluidising these mixtures, have been thoroughly investigated (Aznar et al., 1992). To reduce the influence of mutual interaction among biomass char particles, relatively high gas flow rates and low biomass/char masses have been adopted in many experimental laboratory and pilot scale FBs (Luo et al., 2001; Scott et al., 2005). Also, a careful selection

of densities and particle sizes has a strong impact on the segregation in a bed (Yates, 1983). In a FB operated with a superficial velocity above that of minimum fluidisation the flow pattern can be complex and can interfere with kinetics, making it often difficult to separate the kinetic information from mass transfer influence (Rapagna and Latif, 1997). This reason makes an FB to be not well suited equipment for accomplishing kinetic investigations.

A typical solid (for instance char) reactivity test in an FB is performed in batchwise mode as follows. The reactant gas concentration and volumetric gas-flow in the inlet gas stream are given. The bed is kept at fixed temperature. The measurement of the concentration of the key outlet gas-component with time is registered (i.e. CO in CO_2-char gasification, CO_2 in char combustion). The mass of the batch is adjusted according to the temperature range in order to keep the measured outlet gas-concentration low enough. This guarantees that the reactant consumption is small, as well as the thermal effects, and that the change of volume due to reaction (if non-equimolar, i.e., gasification) remains low enough to be ignored. In this scenario, bed temperature, inlet reactant concentration and gas flow-rate can be assumed uniform along the bed and can be taken directly as an input in the estimations of the intrinsic kinetic parameters.

During the course of a real reactivity test, however, the concentration of the reactant can drop considerably due to the consumption caused by the chemical reaction, as well as by physical resistances from diffusional effects (Howard, 1989). As the gas agent (a gas mixture of the reactant and some inert component) is introduced into the reactor, it passes through the bed as bubbles and also as gas flowing in the emulsion. For the reaction to take place on the internal surface of the particles, the reactant has to overcome various resistances on its travel from the bubbles to the reacting sites. This reduction in reactant concentration affects the reaction rate because the concentration at the reacting sites differs from that of the inlet gas stream. Thus, during determination of the intrinsic char or solid reactivity, these considerations are of considerable concern. Obviously, the complete suppression of these interferences would be the best solution. When not possible, however, the grade of interaction should be assessed. In both cases, therefore, estimation of diffusional effects is of major importance.

Catalytic and non-catalytic gas-solid kinetic experiments in FB (FBKE) can be considered to be equivalent with regard to transport effects. However, in non-catalytic reactions, it is necessary to describe the evolution of the solid structure (local conversion or solid reactant concentration) as reaction proceeds. This is because the reaction rate depends on both solid and gas concentration, and thus, it changes in the course of reaction. This fact is the essential distinctive feature of the non-catalytic systems compared to the catalytic counterpart. From a mathematical point of view, this aspect leads to a coupling between the gas and the solid conservation equation and introduces an additional difficulty. Therefore, in this chapter we focus mainly on non-catalytic systems, since the catalytic counterpart can be considered as a particular, simpler case (Gómez-Barea and Ollero, 2006).

The objective of this work is to establish a basis for the choice of operating conditions for a laboratory-scale bubbling FB reactor in order to avoid fluid-dynamic and mass-transfer interferences in the determination of solid reactivity. The methodology

is derived for isothermal conditions, and only one heterogeneous reaction is involved. This is the case, for instance, in tests of FB CO_2-char gasification reactivity. For other systems these assumptions need to be assessed prior to application of the method presented here. For example, in FB O_2-char reactivity (char combustion) tests, the isothermal assumption can be violated, depending on the char to inert ratio, oxygen concentration, particle size and intrinsic reactivity of the char. In reactivity tests of H_2O-char gasification kinetics, it is necessary to consider a second (independent), homogeneous reaction, for instance, the water-gas shift reaction. These cases are somewhat more complicated. However, the methodology presented can be readily extended to cover these cases, although the simplicity of the treatment (obtaining of an analytical solution) is then lost. It can also be applied in other non-catalytic isothermal systems, where diffusion effects may influence the observed reaction rate and only one reaction occurs.

It is possible to sort published works on FBKE into five classes, depending on the way the diffusion effects are reported (to simplify, we refer to work developed for determination of char reactivity and particularly gasification in laboratory-scale FB): (1) discussion about transport effects is totally absent in the published work (Briedis et al., 2002) (2) discussion about fluid-dynamic interaction and /or physical effects (film and internal diffusion) is only qualitative or not explicitly included (Bjerle et al., 1980; Schmal 1982) (3) quantitative discussion about the hydrodynamic interaction is reported, but nothing is said about physical effects at particle scale (Goring et al., 1952; Sipilä, 1988), (4) Physical limitations are tested, but fluid-dynamics are assumed not to be limiting (Avedesian and Davidson, 1973; van den Aarsen, 1985; Scott et al., 2005; Adánez et al., 1985) (5) A thorough study was made of both physical and fluid-dynamic effects (Luo et al., 2001a; Brem, 1990; Corella, 1980; Mleczko and Wurzel, 1997; Brunello et al., 1996; Wurzel et al. 2000; Khraisha, 2004). Often, there is not a clear distinction between (4) and (5). The works included in Items (4) and (5) are the best documented ones with regard the analysis of transport effects in FBKE.

To sum up, existing FBKE work shows that transport effects are often present. Most of catalytic FBKE studies make great efforts in analysing plausible fluid-dynamic and diffusional resistances (Mleczko and Wurzel, 1997; Wurzel et al., 2000). The same is not true for non-catalytic FBKE work. In fact, the analyses of transport effects in these systems vary widely. Some cases are particularly well documented, such as the study of Corella (1980). Char combustion studies are thoroughly analysed in most cases (Avedesian and Davidson, 1973; Brem, 1990; Brunello et al., 1996; Khraisha 2005). One of the reasons is that char combustion kinetics often are not rate-limiting due to the high reactivity of the char with oxygen for the conditions of practical importance. Brem (1990) formulated a "map of combustion regimes" of char combustion based on experiments and mathematical modelling made up to 1990 in fluidised beds. The scenario of char gasification with CO_2 and with H_2O is, however, rather different. Transport effects are often disregarded and FBKE is carried out assuming that the bed is under the kinetically-diffusional regime. This is mainly due to the slow kinetics of these reactions under practical operating conditions. An exception of this can be found in entrained flow coal gasifiers (Luo et al, 2001a). Thus, the validity of the given reactivity is, in many cases, doubtful. Most work reported deals with the analysis of diffusional effects in a qualitative way. Exceptions to this are

found in the works of van der Aarsen (1985), Adánez et al. (1985), Scott et al. (2005) and Luo et al. (2001a).

3. Modelling mass transport effects during FBKEs

3.1. Overall strategy for evaluation of diffusion effects

Without loss of generality, throughout what follows we shall illustrate the problem under consideration by taking CO_2 gasification as an example. The data treatment necessary for evaluating the gas conversion in a typical FB char-CO_2 test of gasification reactivity is covered in Chapter 6.

Figure 5.1 illustrates the problem dealt with. The gasifying agent (a mixture of CO_2 and N_2) is introduced into the reactor with a CO_2 concentration of c_{in}. It passes through the bed as bubbles in plug flow with a concentration c_b, and through the well mixed emulsion phase, where the char particles are found most of the time with concentration c_e. For reaction to take place on the internal surface of the char particles, the CO_2 has to overcome various resistances on its travel from the bubbles to the reacting sites. These resistances are shown in Fig. 5.1. They are: (1) fluid-dynamic resistance against transfer from bubble to emulsion phase, (2) external particle film resistance around the char particle (boundary layer) and (3) internal porous resistance inside the particle (intraparticle resistance). The resistance within the dense emulsion phase is ignored and the gas composition is treated as being the same in the particles as in the local interstitial gas. This assumption is valid unless the particles are large or the reaction very rapid (Grace, 1986). Other assumptions of the fluid dynamic model are summarised in Section 3.2.1. The CO_2 concentration in the bubble phase falls with height in the bed, while CO_2 is removed for reaction. This affects the reaction rate, as the concentration available in the reacting sites differs from that of the inlet gas stream.

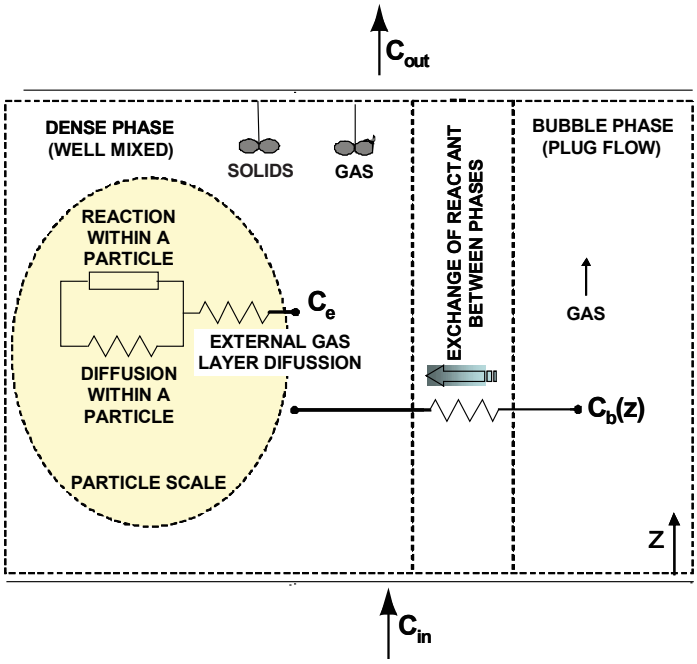

Figure 5.1: Model description

To evaluate the differences between the actual conversion $(-R)$ and the conversion that would have been obtained if the concentration in the internal reacting sites of the porous char had been equal to the concentration at the entrance $(-r)_{in}$, the following global effectiveness factor is defined:

$$\eta_G = \frac{(-R)}{(-r)_{in}} \tag{5.1}$$

where the rates have the units of mol/m^3/s. Throughout what follows we shall assume nth-order kinetics, $(-r)_{in} = k\, c_{in}^n$. The actual value of η_G depends on the resistances encountered along the CO_2 path. If the times of physical transport processes are much smaller than the chemical reaction time, measurements directly yield the char conversion kinetics, provided that the average CO_2 concentration along the FB reactor is known. However, if diffusion effects are noticeable, the intrinsic kinetics cannot be directly obtained. An assessment of the diffusion effects should then be done. In what follows, the resistances between phases in the bed and at a particle scale (external film and pore-diffusion resistances) are modelled to quantify these in FBKE.

3.2. Evaluation of fluid-dynamic effects

3.2.1. Two-phase fluidised-bed model

We apply a two-phase fluidisation approach to estimate the drop in CO_2 concentration between the inlet gas c_{in} and the emulsion c_e. The main assumptions of the two-phase model are (see Fig. 5.1): (1) plug flow of gas in the bubble phase, (2) perfect mixing between gas and solids in the emulsion phase, (3) perfect mixing of solids in the emulsion phase, (4) the gas-solid reaction takes place only in the emulsion; the bubbles are assumed to be free of solids, (5) the emulsion is at minimum fluidisation ($\varepsilon_p = \varepsilon_{mf}$), (6) the particular behaviour of the region close to the gas distributor is neglected, and (7) thermal effects are assumed to be small. By applying these assumptions, a molar balance for the gas in the bubble and emulsion phases (expressed per unit cross-section area of the reactor) leads to

$$\beta\, u_0\, dc_b = k_b\, \varepsilon_b \left(c_e - c_b\right) dz \tag{5.2}$$

$$(1-\beta)\, u_0 \left(c_{in} - c_e\right) = \int_0^{L_f} k_b\, \varepsilon_b \left(c_e - c_b\right)\, dz + \varepsilon_c \left(\eta_p k\, c_e^n\right) L_f \tag{5.3}$$

where η_p is the effectiveness factor of a char particle, defined in Eq. (5.39) and β is a parameter which measures the deviation from minimum fluidisation conditions, defined in (5.23). The boundary condition at the inlet to the bubble phase is

$$z = 0 \quad c_b = c_{in} \tag{5.4}$$

The CO_2 concentration of the outlet stream (at $z = L_f$) is the result of the contribution of both bubble and emulsion gas concentrations,

$$c_{out} = \beta c_b + (1-\beta) c_e \tag{5.5}$$

The gas conversion X_g is computed from the exit concentration as

$$X_g = 1 - \frac{c_{out}}{c_{in}} \tag{5.6}$$

The interphasic effectiveness factor η_{ph} is defined as the ratio of the intrinsic reaction rates under emulsion conditions and under inlet gas conditions. For isothermal conditions this definition yields

$$\eta_{ph} = \frac{c_e^n}{c_{in}^n} \tag{5.7}$$

By defining the following dimensionless variables

$$C = \frac{c_{in} - c}{c_{in}} \quad \text{and} \quad y = \frac{z}{L_f} \tag{5.8}$$

Equations (5.2) and (5.3) are expressed in dimensionless form as

$$\frac{dC_b}{dy} = \left[\frac{1}{\beta} \frac{k_b \varepsilon_b}{u_0 / L_f} \right] \left(C_e - C_b \right) \tag{5.9}$$

$$(1-\beta) C_e = \int_0^1 \frac{k_b \varepsilon_b}{u_o / L_f} \left(C_b - C_e \right) dy + \mathrm{Da_R} \left(1 - C_e \right)^n \tag{5.10}$$

By integrating Eq. (5.9) from 0 to *y* the solution is

$$C_b = C_e \left[1 - \exp\left[-\frac{\mathrm{NTU}}{\beta} y \right] \right] \tag{5.11}$$

where NTU and Da_R are defined, respectively by Eqs. (5.22) and (5.19). At the exit, *y*=1 and Eq. (5.11) becomes

$$C_b\big|_{y=1} = C_e \left[1 - \exp\left[-\frac{\mathrm{NTU}}{\beta} \right] \right] \tag{5.12}$$

By substituting Eq. (5.11) in Eq. (5.10) and integrating, an algebraic equation for the dimensionless concentration, C_e, is obtained

$$1-\beta\cdot\exp\left(-\frac{\mathrm{NTU}}{\beta}\right)=\mathrm{Da_R}\,\frac{\left(1-C_e\right)^n}{C_e} \tag{5.13}$$

Taking into account the definition of $\mathrm{N_a}$ (Eq. (5.20)), Eq. (5.13) can be expressed as

$$\frac{\mathrm{N_a}}{\mathrm{Da_R}}=\frac{\left(1-C_e\right)^n}{C_e} \tag{5.14}$$

Gas conversion, X_g Eq. (5.6) and the interphasic effectiveness factor, η_{ph}, Eq.(5.7) can also be converted to dimensionless form and then Eq. (5.14) is

$$X_g=C_e\cdot\mathrm{N_a} \tag{5.15}$$

$$\eta_{ph}=\left(1-C_e\right)^n \tag{5.16}$$

3.2.2. Governing parameters

By combining Eqs (5.2) to (5.7), X_g as function of $\mathrm{N_a}$ and $\mathrm{Da_R}$ are written as

$$\frac{(1-X_g/\mathrm{N_a})^n}{X_g/\mathrm{N_a}}=\frac{\mathrm{N_a}}{\mathrm{Da_R}} \tag{5.17}$$

and with Eqs (5.15) and (5.16) η_{ph} as function of $\mathrm{N_a}$ and $\mathrm{Da_R}$ are written as

$$\frac{\eta_{ph}}{(1-\eta_{ph}^{\,1/n})}=\frac{\mathrm{N_a}}{\mathrm{Da_R}} \tag{5.18}$$

Two dimensionless parameters $\mathrm{Da_R}$ and $\mathrm{N_a}$ have been defined

$$\mathrm{Da_R}=\frac{K_v}{u_0/L_f} \tag{5.19}$$

$$\mathrm{N_a}=1-\beta\exp\left(\frac{-\mathrm{NTU}}{\beta}\right) \tag{5.20}$$

The first parameter, $\mathrm{Da_R}$ is the Damköhler number at reactor scale. It expresses the relative importance of the gas residence time L_f/u_0 and the reaction time K_v^{-1}. The latter is defined as

$$K_v = \varepsilon_c \, \eta_p k_e \, c_e^{n-1} \tag{5.21}$$

The second dimensionless group, $\mathrm{N_a}$, is related to two other parameters: the number of transfer units, NTU and β,

$$\mathrm{NTU} = \frac{k_b \, \varepsilon_b}{u_o / L_f} \tag{5.22}$$

$$\beta = \frac{u_o - u_{mf}}{u_o} \tag{5.23}$$

where k_b ($\mathrm{s^{-1}}$) is the bubble to emulsion mass transfer coefficient. In Eq. (5.21), ε_c is the char hold-up in the bed, given by

$$\varepsilon_c = (1-\varepsilon_{mf})(1-\varepsilon_b)\, v_c \tag{5.24}$$

where v_c is the char hold-up of the solid phase,

$$v_c = \left[1+\left(w_s /(w_c \, x_c)\right)\cdot\left(\rho_c / \rho_s\right)\right]^{-1} \tag{5.25}$$

Thus, v_c depends on the mass of solids in the bed and their density ratios. In addition, in order to avoid bed segregation (v_c is uniform throughout the bed) the superficial velocity should be chosen well above the minimum fluidising velocity. Another measure to avoid segregation is to perform the experiments with low enough char content in the bed, v_c. The expressions necessary to evaluate the parameters given above depend on the rig geometry and operating conditions. Table 5.1 includes typical expressions valid for FB operated in the bubbling regime. Similar expressions can be found in other FB kinetics studies (Gómez-Barea et al., 2006a, 2006b; Luo et al., 2001).

3.2.3. Physical significance of parameters

The parameter NTU measures the relative importance between the bubble residence time and the gas residence time in the bed, while β expresses the quantity of gas travelling through the bubbles in relation to the total gas flow through the bed. $\beta \sim 1$ means fast bubbles and indicates that the bed is likely to be affected by bypassing of gas. NTU and β indicate the state of fluidisation of the bed, but only their combination is expressed in Eq. (5.20), i.e. $\mathrm{N_a}$ is a result of the combined effect of bypassing and exchange of gas between the phases. The actual form of Eq. (5.20) is the consequence of assuming that the bubbles pass the bed in piston flow. The parameter $\mathrm{N_a}$ is to some extent an average of the ratio of the gas residence time and the time of transfer between the phases. In section 3.2.1, a physical interpretation of $\mathrm{N_a}$ in terms of

differences of concentration was given (see Fig. 5.2). N_a establishes the extent to which fluid-dynamics interact with kinetics. Limiting values of N_a are 0 and 1: full and no fluid-dynamic interference, respectively. In practise, the effectiveness factor for transport between the phases, η_{ph} needs to be estimated. Determination of η_{ph} in terms of observables is given in the following.

Beside the expression given in Eq.(5.20), the parameter, N_a can be expressed in terms of concentrations as

$$N_a = \frac{c_{in} - c_{out}}{c_{in} - c_e} \tag{5.26}$$

Thus, the physical interpretation of parameter N_a is the "concentration efficiency of the bed". Eqs. (5.26) and (5.20) are similar than expressions found in heat exchangers for the effectiveness. This is readily visualised through the diagram presented in Fig. 5.2.

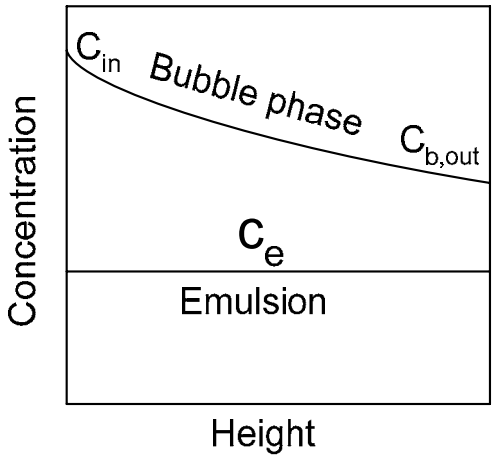

Fig. 5.2. Diagram for the definition of N_a

3.2.4. Observables at reactor scale

In FBKE the parameter Da_R cannot be readily determined because the intrinsic kinetics is not a priori known. Consequently, Eq. (5.18) cannot be directly used for the calculation of the interphase effectiveness factor. Nevertheless, by combining Eqs. (5.17) and (5.18) the following expression is obtained

$$\eta_{ph} = \left[1\text{-}X_g/N_a\right]^n \tag{5.27}$$

Equation (5.27) directly gives the effectiveness from gas conversion and N_a. Moreover, once this interphase effectiveness has been found, the Damköhler number is computed from

$$Da_R = X_g / \eta_{ph} \tag{5.28}$$

The group X_g/N_a is an observable, because it does not require previous knowledge of the intrinsic kinetic constant. X_g/N_a is directly calculated from a gas concentration measurement at the exit and an estimation of N_a. The latter is calculated from fluid-dynamic information in Table 5.1. Furthermore, the relation between X_g/N_a and Da_R can be expressed as (Eq.(5.17))

$$N_a / Da_R = \frac{\left(1-X_g/N_a\right)^n}{X_g/N_a} \tag{5.29}$$

The group N_a / Da_R can also be interpreted as an observable quantity. This group expresses the ratio of the chemical time and the residence time of the gas in the bed. The solution of Eq. (5.29) for X_g/N_a is

$$X_g/N_a = \frac{1}{1+N_a / Da_R} \tag{5.30}$$

which is useful when analysing a reactor, once the kinetics have been obtained. In particular, Eq. (5.30) gives the conversion as function of the parameter N_a / Da_R. In this case, the practical expression for calculation of η_{ph} (Eq.(5.27)) is

$$\eta_{ph} = \left[\frac{N_a / Da_R}{1+ N_a / Da_R} \right]^n \tag{5.31}$$

In the limiting case when $N_a / Da_R >> 1$, the interphasic effectiveness factor is close to unity, i.e. $\eta_{ph} \sim 1$, and the heterogeneous flow pattern associated with the different phases in the bed (the global heterogeneity or heterogeneity at reactor scale) loses importance for the reaction (but the heterogeneity at particle scale, remains to be analysed, as will be shown below). Conversely, if the conditions in the bed lead to $N_a / Da_R << 1$ ($\eta_{ph} \sim 0$), the fluid-dynamic effects are rate-limiting. Kinetic experiments should not be carried out under such conditions.

In summary, Eqs. (5.27) and (5.29) are the same as Eqs. (5.30) and (5.31). Both represent the solution of the two-phase model given by Eqs. (5.2)-(5.7). Eqs. (5.27) and (5.29) are useful in a FBKE, because they are in 'design-form'. On the other hand, Eqs (5.30) and (5.31) represent the 'analysis-form'. They are helpful for estimating the expected conversion when the intrinsic kinetics of the char is known.

Table 5.1. Formula and correlation used in fluid-dynamic calculations

Symbol	Correlation	Unit	Reference
u_{br}	$u_{br} = 0.711 \cdot \left(g \cdot d_b \right)^{1/2}$	m·s^{-1}	Davidson and Harrison (1963)
u_b	$u_b = 1.6 \cdot \left[(u_0 - u_{mf}) + 1.13 \cdot d_{b,av}^{1.35} \right] \cdot D_t^{1.35} + u_{br}$	m·s^{-1}	Werther (1983)
d_b	$d_b = d_{bm} - (d_{bm} - d_{b0}) \cdot e^{-0.3 L_f z / D_t}$	m	Mori and Wen (1975)
d_{b0}	$d_{b0} = 0.082 / g^{0.2} [(u_0 - u_{mf}) / N_t]^{0.4}$ for $d_{b0} \le l_{or}$ $d_{b0} = 0.0278 / g \cdot (u_0 - u_{mf})^2$ for $d_{b0} > l_{or}$	m	Mori and Wen (1975) Kunii and Levenspiel (1991)
d_{bm}	$d_{bm} = \mathrm{Min} \left\{ 163.77 \cdot \left[\pi D_t^4 / 4 \cdot (u_0 - u_{mf}) \right]^{0.4}, D_t \right\}$	m	Mori and Wen (1975)
ε_b	$\varepsilon_b = (u_0 - u_{mf}) / (u_b - u_{mf})$ (*)	m	Kunii and Levenspiel (1991)
Sh	$\mathrm{Sh} = 2 \varepsilon_{mf} + 0.69 (\mathrm{Re}_p / \varepsilon_{mf})^{1/2} Sc^{1/3}$	–	Kunii and Levenspiel (1991)
k_b	$k_b = 2 u_{mf} / d_b + 5.7 \left(D_g \varepsilon_{mf} \right)^{0.5} g^{1/4} / d_b^{1.25}$	s^{-1}	Grace (1986)
u_{mf}	$\frac{1.75}{(\varepsilon_{mf}^3 \cdot \phi_s) \mathrm{Re}_{p,mf}^2} + \frac{150(1-\varepsilon_{mf})}{(\varepsilon_{mf}^3 \cdot \phi_s^2) \mathrm{Re}_{p,mf}} = \mathrm{Ar}$	m·s^{-1}	Fogler (1992)
ε_{mf}	$\varepsilon_{mf} = 0.586 \phi_s^{-0.7} \frac{\mu^2}{(\rho_g g (\rho_p - \rho_g) d_p^3)} \left(\rho_g / \rho_s \right)^{0.021}$	–	Kunii and Levenspiel (1991)
L_{mf}	$L_{mf} = (w_s + w_c) / (\rho_p (1 - \varepsilon_{mf}) \pi D_t^4 / 4)$	m	Fogler (1992)
$d_{b,av}$	$d_{b,av} = 1 / L_f \int_0^{L_f} d_b \, dz$	m	Luo et al. (2001)
L_f	$L_f = L_{mf} / (1 - \varepsilon_b)$	m	Kunii and Levenspiel (1991)

3.3. Evaluation of diffusion effects at particle scale

3.3.1. Modelling of the observed volumetric reaction rate

Up to now the diameter of the char particles has not been explicitly considered. This is because the inert bed material is dominant in the bed, and the fluid-dynamics are well established by taking into account only the properties of the inert material. In the calculation of the diffusional effects at particle scale, however, the char particle size should be considered.

The reaction rate is defined as

$$(-R) = \frac{1}{V_p}\int_0^{V_p}(-r)\,d\Omega = -\frac{1}{V_p\,\mathrm{M_c}}\frac{d\,w_c}{d\,t} \tag{5.32}$$

We measure the rate of char conversion dx_c/dt and therefore we need to find the link between this quantity and $(-R)$. As gasification proceeds, there is a progressive change of mass of carbon. This leads to a decrease of the particle size and/or density. The following simple models can be assumed for these two quantities (Oka, 2004),

$$d_c(x_c) = d_{c0}\cdot(1-x_c)^{\alpha} \tag{5.33}$$

$$\rho_c(x_c) = \rho_{c0}\cdot(1-x_c)^{\delta} \tag{5.34}$$

By substituting Eqs. (5.33) and (5.34) in (5.32), the following expression is obtained

$$(-R) = \rho_{c0}(1-x_c)^{\delta-1}\cdot\frac{d\,x_c}{d\,t} \tag{5.35}$$

At any instant, by definition, the relationship $w_c/w_{c0} = (1-x_c)$ holds. This leads to the following relationships between the two coefficients: $1 = 3\alpha + \delta$. If, in a given situation, a shrinking-core behaviour is assumed, $\alpha \sim 1/3$ and $\delta \sim 0$, and then the reaction rate would be $(-R) = \rho_{c0}(1-x_c)^{-1}dx_c/dt$. When uniform conversion is more appropriate, the consistent values of the coefficients should be $\alpha \sim 0$ and $\delta \sim 1$, and the rate would be $(-R) = \rho_{c0}dx_c/dt$. In between these two limiting cases, the more general progressive conversion model with changes in size and density should be used. For instance, to obtain kinetic data under gasification conditions, an experiment should be conducted in the kinetically controlled regime. In this case, it is expected to be closer to the uniform reaction model than to the shrinking-core model. In such a case, $\alpha \sim 0$ and $\delta \sim 1$.

3.3.2. External mass transfer effects

Under pseudo-steady-state conditions, the isothermal mass transfer problem for n^{th}-order kinetics is described by

$$(-R) = k_G / L_e \left(c_0 - c_s\right) = k_a \, c_s^n \tag{5.36}$$

where the external mass transfer coefficient is estimated as

$$k_G = \frac{\mathrm{Sh}\, D_g}{d_c} \tag{5.37}$$

Sherwood's number can be obtained by correlations, like the one in Table 5.1. The apparent kinetic reaction constant k_a includes the intraparticle diffusion-reaction problem, that is $k_a = \eta_i \cdot k$, where η_i is the intraparticle effectiveness factor, defined as the ratio of the observed total reaction rate to the total reaction rate when the concentration of the reactant is equal to that at the surface. Mathematically, this is expressed as

$$\eta_i = \frac{(-R)}{k c_s^n} \tag{5.38}$$

Similarly, the particle effectiveness factor η_p is the ratio of the observed reaction rate and the reaction rate when the concentration of the reactant is equal to that in the emulsion,

$$\eta_p = \frac{(-R)}{k \, c_e^n} \tag{5.39}$$

The external effectiveness factor η_e is the ratio of the intrinsic reaction rates evaluated for the surface and for emulsion conditions. For nth-order kinetics and an isothermal case, this factor represents the drop in concentration between the emulsion and the surface, raised to the order of the reaction,

$$\eta_e = \left(\frac{c_s}{c_e} \right)^n \tag{5.40}$$

Eqs (5.38) and (5.40) readily give $\eta_e = \eta_p / \eta_i$. A second Damköhler number, $\mathrm{Da_p}$, which represents the ratio of the maximum diffusion rate ($c_s \approx c_e$) to the diffusion-controlled reaction rate ($c_s \approx 0$), is defined as

$$\mathrm{Da_p} = \frac{k}{k_G / L_e} \, c_e^{\,n-1} \tag{5.41}$$

$\mathrm{Da_p}$ is a measure of the processes occurring at a particle scale, whereas $\mathrm{Da_R}$ involves calculations on the reactor scale, i.e. residence time. The product of particle-Damköhler number and particle effectiveness factor is an observable, because the expression

$$\mathrm{Da_p}\eta_p = \frac{(-R)}{k_G / L_e c_e}, \tag{5.42}$$

can be computed from bulk conditions and the measured reaction rate. Luo et al. (2001a) have called this observable "fraction of mass transfer resistance". In terms of this observable, the external effectiveness factor can be directly obtained by combining Eqs (5.36), (5.40) and (5.42)

$$\eta_e = (1 - \mathrm{Da_p}\eta_p)^n \tag{5.43}$$

Eq. (5.43) enables computation of the external effectiveness factor from the second observable quantity, $\mathrm{Da_p}\eta_p$.

3.3.3. Intraparticle mass transfer effects

The apparent kinetic constant of Eq. (5.36) is estimated by the expression

$$k_a = k\,\eta_i = \frac{(-R)}{\eta_{ph}\,\eta_e\,c_{in}^n} \tag{5.44}$$

derived from Eqs (7), (28) and (30). Eq. (5.44) enables the estimation of k_a , provided that $\eta_{ph}\,\eta_e$ has been determined. In order to separate the effects of intraparticle pore diffusion η_i and chemical kinetics k , a kinetic particle model has to be solved. This is a difficult task for a general n$^{\text{th}}$-reaction rate, but the treatment can be simplified. First, the following parameter is defined similar to the Weisz-Prater modulus used in catalysis theory (Carberry, 1976)

$$\omega = \frac{(-R)}{D_e\,c / L_e^{\,2}} \tag{5.45}$$

This parameter, in principle, can be obtained under three conditions, depending on the location where the gas concentration c is evaluated: surface ω_s , emulsion ω_e , or gas inlet ω_{in} . The known concentration of the inlet gas c_{in}, makes ω_{in} an observable, because it can be computed from the observed reaction rate $(-R)$ and from known particle (solid reactant) properties: effective diffusivity D_e and equivalent length L_e . Furthermore, the Weisz-Prater module for surface conditions, ω_s can be evaluated from the observable ω_{in} , once η_{ph} and η_e have been estimated. In effect, by express-

ing the drop of gas concentration, c_s / c_e in terms of η_{ph} and η_e by using Eq. (5.7) and (5.40), the following expression for ω_s is obtained

$$\omega_s = \omega_{in} /(\eta_{ph}\,\eta_e)^{1/n} \tag{5.46}$$

Following a similar treatment by Dutta et al. (1977), η_i is estimated as

$$\eta_i = \omega_s / M_s^2 \tag{5.47}$$

where the parameter M_s was found by solving the following non-linear equation

$$M_s\left(\frac{1}{\tanh(3M_s)} - \frac{1}{3M_s}\right) = \omega_s \tag{5.48}$$

Equation (5.48) has been derived by taking into account Eq. (5.47) and by using the solution for the effectiveness factor for an nth order reaction in a catalyst (Dutta et al., 1977)

$$\eta_i = \frac{1}{M_s}\left(\frac{1}{\tanh(3M_s)} - \frac{1}{3M_s}\right) \tag{5.49}$$

By taking Eqs. (5.46), (5.40) and (5.7) into account, the parameters ω_s and M_s^2 appearing in Eq. (5.47), can be related to inlet gas conditions as

$$\eta_i = \frac{\omega_{in}}{M_{in}^2}\cdot(\eta_{ph}\,\eta_e)^{(1-2n)/n} \tag{5.50}$$

which emphasizes the relationship between ω_{in} and M_{in}^2 for a given $\eta_{ph}\,\eta_e$ and reaction order. From a physical point of view, M_s can be seen as a conversion dependent version of the classical Thiele module ϕ_s. In particular, M_s is defined as follows:

$$M_s = \phi_s\left[(1-x_c)\frac{f(x_c)}{g(x_c)}\right] = \phi_s\, G(x_c) \tag{5.51}$$

where $f(x_c)$ is a structural profile, which depends of the intrinsic behaviour of the char (Gómez-Barea and Ollero, 2006). The function $g(x_c)$ is, in general, an experimental correlation, which captures the change in effective diffusivity with conversion (Dutta et al., 1977; Gómez-Barea and Ollero, 2006). The parameter ϕ_s is the Thiele module, evaluated at surface conditions. When $G(x_c)$=1 becomes

$$\phi_s = L_e \left[\frac{n+1}{2} \frac{k\, c_s^{n-1}}{D_{e0}} \right]^{1/2} \tag{5.52}$$

Despite the fact that M_s and ϕ_s are defined by Eqs. (5.51) and (5.52), respectively, they are not explicitly used in the computation below. Only Eq. (5.48) has to be solved for the solution of the particle kinetic model.

3.4. Algorithm of calculation

Figure 5.3 displays the algorithm for estimating diffusional effects in the gas conversion. Gas conversion is calculated from the measured CO_2 concentration in the exit gas. Input hydrodynamic data are obtained from operation and design data and from correlations (see Table 5.1). After this and by providing the reaction order and the coefficient δ, the three observables (1) interphasic X_g/N_a, (2) external $Da_p\eta_p$ and (3) intraparticle or internal ω_{in}, are sequentially obtained. In parallel, the three effectiveness factors η_{ph}, η_e and η_i are calculated. Typical design and operation data for FBKE are included in Table 5.2.

The variables have been listed in five groups according to their potentiality of adjustment during a typical FBKE. Group 1 represents variables that can be adjusted (within a small range) in an experiment in order to avoid hydrodynamic interferences: gas flow-rate, amount of char, and bed material. Group 2 includes properties of the inert particles, which can, in principle, be changed from one test to another. Group 3 to 5 represent variables that cannot usually be modified. Group 3 and 4 are fixed by the constraints of the determination of the kinetics, whereas Group 5 contains geometrical properties of the rig.

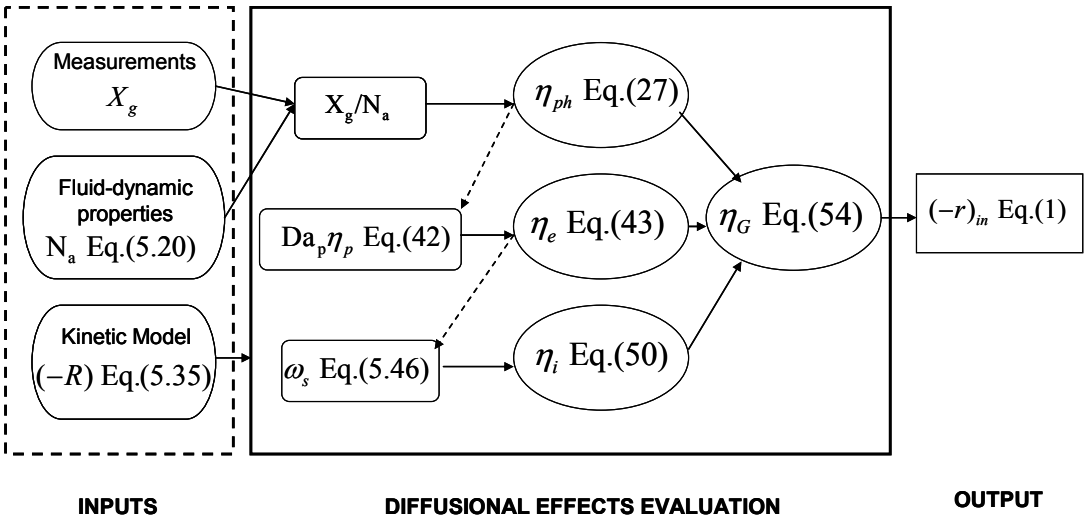

Figure 5.3: Evaluation of diffusional effects in FBKE

3.5. Model limitations

3.5.1. Fluid dynamic limitations.

It was assumed that the bed is operated in the bubbling regime. Moreover, the gas flow in the emulsion was assumed perfectly mixed. This assumption is often reasonable due to the vigorous stirring action of bubbles when the superficial velocity is considerably in excess of the minimum fluidising velocity and when the bed diameter is large. However, these two conditions may be violated on the laboratory scale, where the slugging regime is often near to occur, mainly due to the small diameter usually employed in these rigs. The correlations used in Table 5.1, as well as the flow pattern assumed in the two-phase model, could be affected by this. The treatment given can be readily extended to include plug flow of the gas in the emulsion instead of perfect mixing, but slugging could change conditions more radically. Stewart and Davidson (1967) presented a simple criterion to test whether slug flow is likely to occur; an upper limit for the superficial velocity in FBKE. According to this criterion, most of the FBKE works mentioned in the above literature survey would have been running in a slugging regime if the beds had been high enough. The critical height at which complete slugging starts, however, is usually well above the actual bed height in the experiments. For instance, Luo et al. (2001) found a critical height of 70 cm according to Baeyens and Geldart's equation (Kunii and Levenspiel, 1991) compared to 5-50 cm in most reactors. Thus, they assumed that no slugging would occur and the above mentioned potential problem does not seem to be relevant in the present context.

3.5.2. Thermal effect limitations

Isothermicity is usually assumed in CO_2 and H_2O char gasification due to low reaction rates (van den Aarsen, 1985; Scott et al., 2005; Adánez et al., 1985; Luo et al. 2001a). However, large particle size or char derived from biomass (with higher reactivity than char derived from coal) could result in a thermal gradient between the phases and at the particle scale. Van den Aarsen (1985) estimated the maximum between the emulsion and the particles from a heat balance over a reacting particle by assuming that the Biot modulus (the ratio of film heat transfer to conduction heat transfer within the solid) was very small. The maximum decrease in temperature was estimated to be 3 K. Bliek et al. (1985) formulated a model to describe the gasification of coal-derived chars, reflecting the situation of most practical gasification systems, although they ignored the intraparticle heat transfer effects. This assumption was validated by estimating the maximum intraparticle differences from the Prater criterion for strongly diffusion- controlled reactions. They found a typical temperature drop of 4 K. From more exact numerical calculations they showed that this value was 7 K as a maximum so that the previous rough estimation (4 K) was rather good.

On the other hand, during FB char-combustion tests temperature gradients within char and in the boundary layer have been observed in FBKE (Oka, 2004, Avedesian and Davidson, 1973). These experimental observations have lead to the conclusion that under the conditions of full-scale FB combustors (700-900 ºC, 1-10 mm), the char-oxidation process is controlled by pore diffusion and diffusion in the boundary layer around the char particles. However, FBKE works often try to adjust the test

conditions to guarantee the isothermal conditions (Brem, 1990; Brunello et al., 1996; Khraisha, 2005). This is also usually the case in catalytic systems, such as the experimental investigations by Mleczko and Wurzel (1997) and Wurzel et al. (2000) on catalytic partial oxidation of methane and CO_2 reforming of methane, respectively. As a result, the present treatment is also applicable in these cases. However, in general, char combustion and other non-catalytic and catalytic system FBKE are more susceptible to be thermally limited than char gasification FBKE. Hence, to be applied in such cases, the model developed here should be extended to account for the thermal effects.

Table 5.2. Common values of design parameters and operating conditions in char FBKE

Group Nr.	Group name	Symbol	Range of values	Unit	Remarks
1	**Operating variables**	u_0 w_{c0} w_s	0.1-1.2 0.1-20·10^{-3} 10-50·10^{-3}	m/s kg kg	Variable, which can be adjusted (within a small range) in an experiment to avoid fluid-dynamic interferences
2	**Sand properties**	ρ_s d_s	2000-3500 0.1-1.0·10^{-3}	kg/m^3 m	Particle properties, which can be selected in each test
3	**Char properties**	ρ_{c0} d_{c0}	300-1000 0.1 - 5·10^{-3}	kg/m^3 m	Non modifiable Modifiable (feeding problems can constraint) Depends of the others
4	**"kinetic" conditions**	T_{in} p_{in}	800-1500 0-1	K bar.	Variables that are imposed by the experimental programme. They vary from one experiment to another.
5	**Design variables**	D_t N_t d_{or} H	0.015-0.1 0.1–1·10^{-3} 0.1 – 1·10^{-2} 0.05-0.5	m m^{-2} m m	Non-modifiable variable, once the rig has been built-up. In a design-phase modifications are possible.

4. Model results and discussion

4.1. Parameter evaluation

Figure 5.4 displays Eq. (5.27). More specifically, η_{ph} is presented as a function of the global observables of the reactor, X_g/N_a (in %) for various reaction orders, n. The interphasic effectiveness is above 0.9 for low values of X_g/N_a, (typically below 10%) and reaction orders up to 1. The larger X_g/N_a, the smaller is η_{ph}, and so, the greater is the fluid-dynamic interaction. At a given gas conversion, the parameter N_a is the key

for the assessment of the transport limitation. N_a depends on β and NTU in the form given by Eq. (5.20) as displayed by Fig. 5.5. As seen, NTU higher than unity approximately yields $N_a > 0.95$ for $\beta < 0.5$ ($u_0 < u_{mf} < 2u_0$).

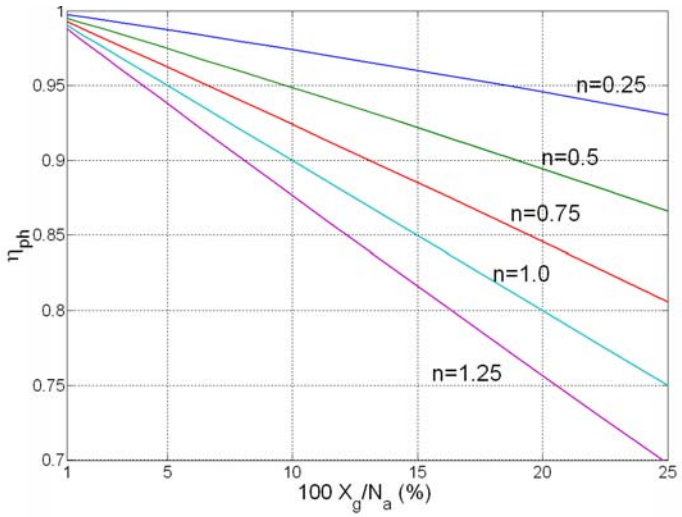

Figure 5.4: η_{ph} vs. X_g/N_a for various n

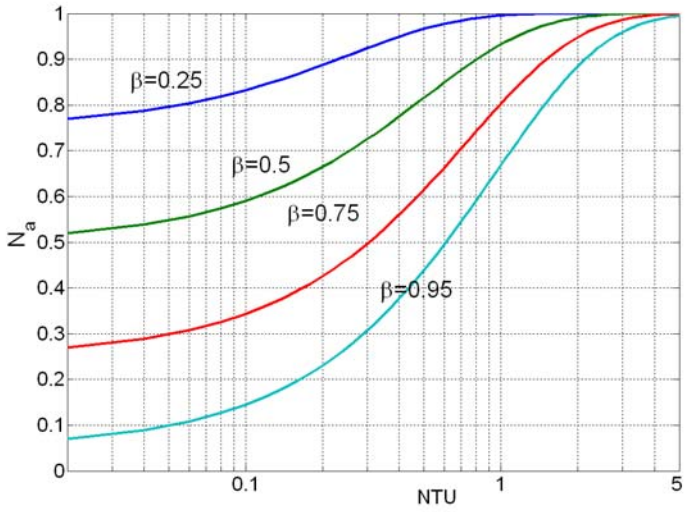

Figure 5.5: N_a vs. NTU for various β

Typical FBKE reported in literature have been carried out at u_0/u_{mf} ~2-6 m/s (Goring et al, 1952; Jensen, 1975; Schmal et al., 1983; Adánez et al., 1985; Adschiri et al., 1986; Luo et al., 2001, Briedis et al., 2002, Bjerle et al., 1980; Sipilä, 1988; Scott et al., 2005; Mleczko and Wurzel,1997; Wurzel et al., 2000). In these studies common sand was used as bed material with a minimum fluidising velocity between ~0.08-0.2 m/s. These ratios lead to β ranging from 0.5 to 0.85 (taken u_0 ~0.2-1.2 m/s)**.** For these two limiting cases, NTU should be higher than 2 to 3 to guarantee values of N_a above 0.95.

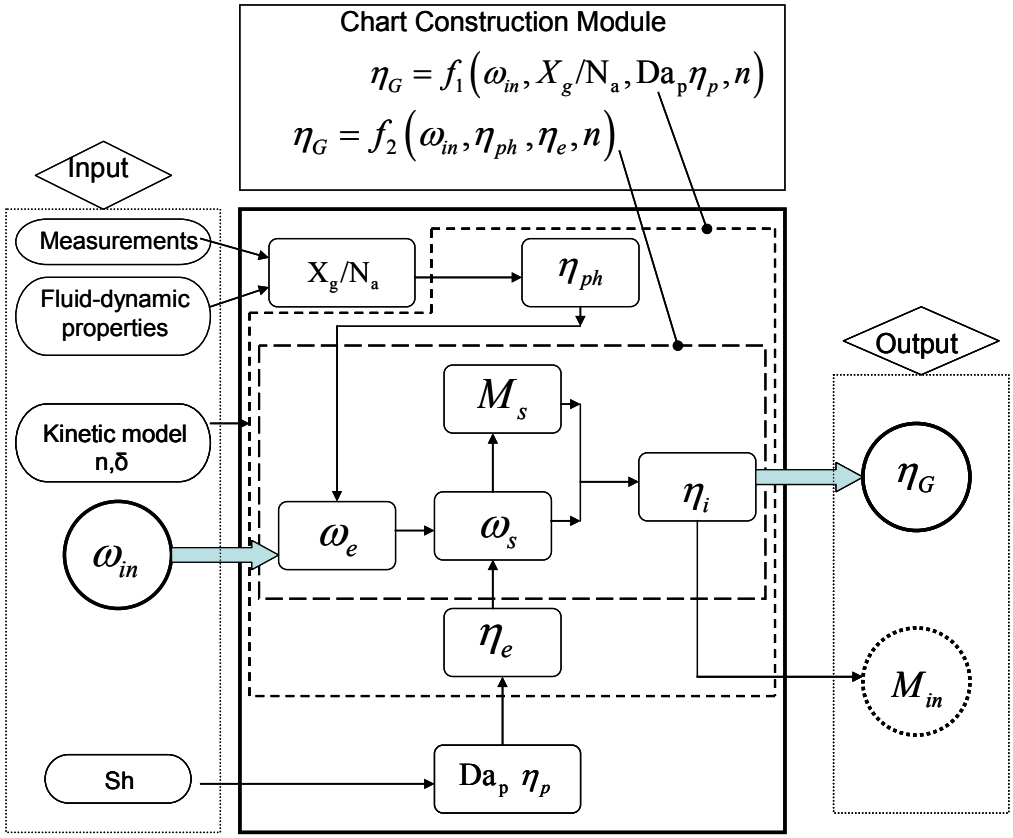

Figure 5.6: Strategy for overall effectiveness factor evaluation and algorithm for construction of charts $\eta_G = f_1\left(\omega_{in}, X_g/\mathrm{N_a}, \mathrm{Da_p}\eta_p, n\right)$ and $\eta_G = f_2\left(\omega_{in}, \eta_{ph}, \eta_e, n\right)$

4.2. Criteria for avoiding fluid-dynamic interferences

When the bypass of gaseous reactant caused by bubbles can be neglected, i.e. at $\mathrm{N_a} \sim 1$, the degree of gas conversion dictates whether the interphasic effectiveness factor is low or, conversely, closes to one. In other words: as far as $\mathrm{N_a} \sim 1$, for FBKE the value of X_g should be kept low enough. Quantitative estimation of X_g can be obtained from Fig. 5.4, for various *n*. For instance, for *n*=1 and a gas conversion of 20%, the typical effectiveness factor is around 0.8. To remedy this situation, a reasonable measure could be to decrease the amount of char relative to inert solids in the reactor. This could lead to lower gas conversion, and the fluidised bed could be looked upon as a differential reactor. For instance, if the batch of particle is reduced, so that $\mathrm{X_g}$ is set below 5 %, the resulting effectiveness factor is above 95%. Eq. (5.31) makes this aspect clear. If $\mathrm{N_a}$ is close to unity, but the reaction rate is high, the interphasic effectiveness would be lower than unity. Only if the combined group $\mathrm{N_a}/\mathrm{Da_R}$ becomes low enough, the effectiveness would tend to unity, and the transport effects associated with FB fluid-dynamics would lose importance.

From these considerations a simple criterion for a rough estimation of the maximum conversion can be derived. By establishing a minimum threshold η^* of the in-

terphase effectiveness the gas conversion that would guarantee an effectiveness equal to or higher than η^* should fulfil the following criterion

$$X_g \le \mathrm{N_a} \cdot \left[1-(\eta^*)^{1/n}\right] \tag{5.53}$$

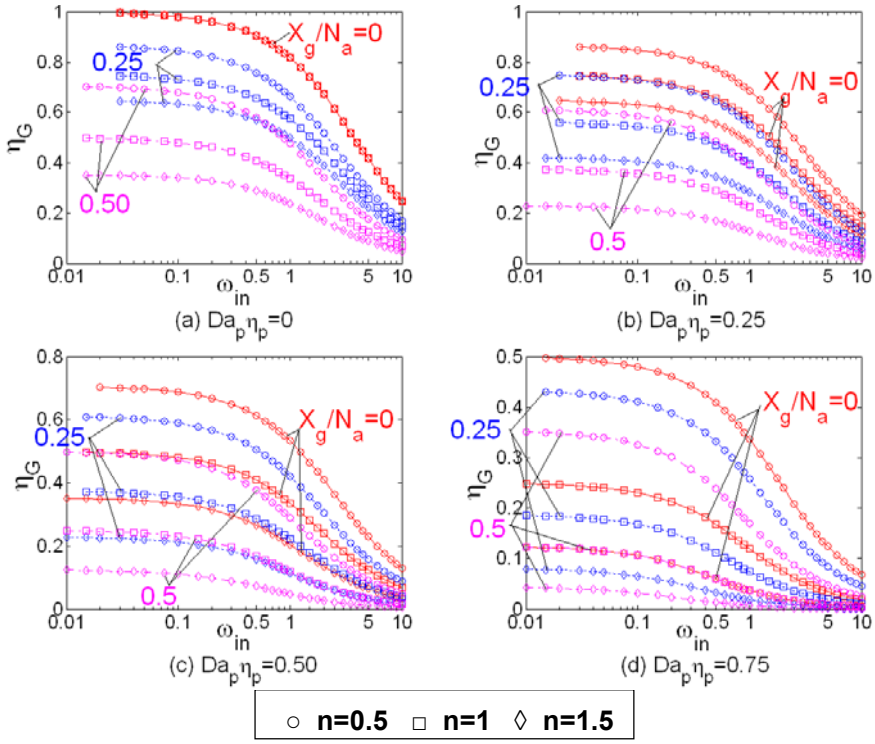

Figure 5.7: Chart $\eta_G = f_1\left(\omega_{in}, X_g/\mathrm{N_a}, \mathrm{Da_p}\eta_p, n\right)$

4.3. Charts for evaluation of the diffusion effects

Equations (5.1) and (5.44) give the global effectiveness factor as

$$\eta_G = \eta_{ph} \cdot \eta_e \cdot \eta_i \tag{5.54}$$

By substituting the values of the effectiveness factor, given by Eqs. (5.27) (5.43) and (5.50) into Eq. (5.54) an expression can be found, which explicitly includes the three observables, $X_g/\mathrm{N_a}$, $\mathrm{Da_p}\eta_p$ and ω_{in},

$$\eta_G = f_2\left(\omega_{in}, X_g/\mathrm{N_a}, \mathrm{Da_p}\eta_p, n\right) \tag{5.55}$$

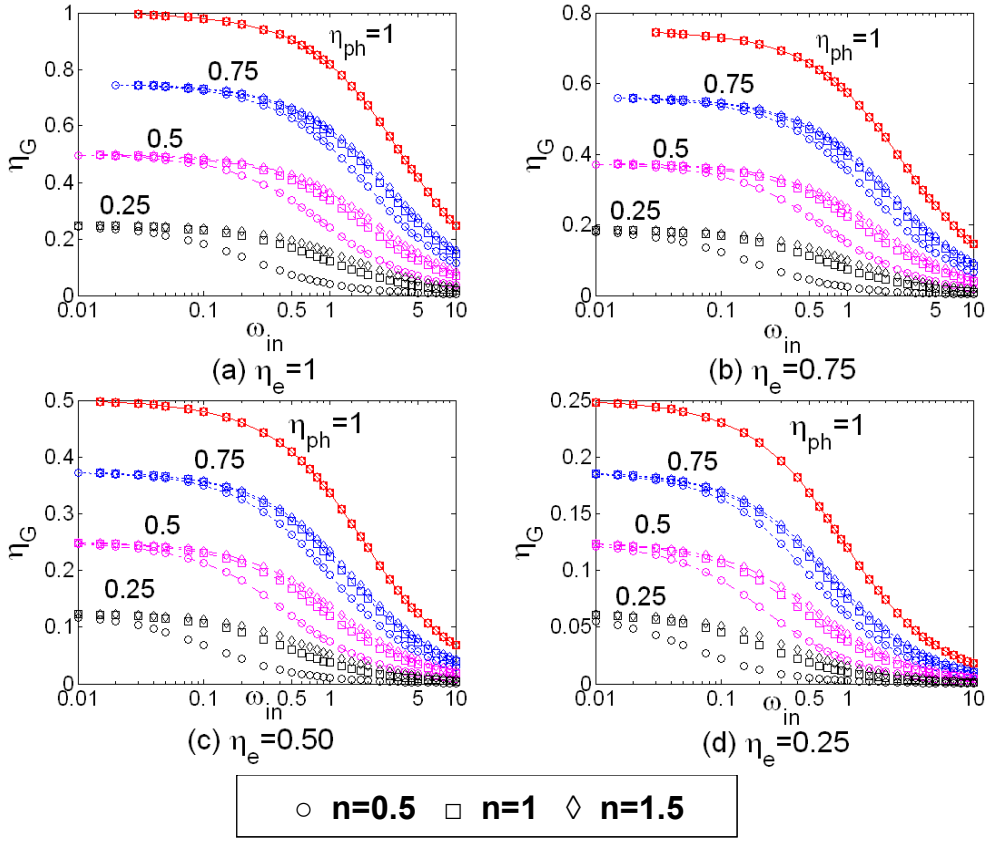

Figure 5.8: Chart $\eta_G = f_2\left(\omega_{in}, \eta_{ph}, \eta_e, n\right)$

Figure 5.6 exemplifies the procedure for obtaining Eq. (5.55) in practise. There is no analytical solution, because the calculation involves Eq. (5.48), which cannot be solved analytically. However, the procedure is straightforward, as Fig. 5.6 illustrates. The solution procedure of Fig. 5.6 yields Fig. 5.7 that displays Eq. (5.55). The closer the parameters $X_g/\mathrm{N_a}$ and $\mathrm{Da_p}\eta_p$ are to zero, the closer is the global effectiveness factor to unity, and consequently, the smaller are the interferences of the transport effects. A clear establishment of the influence of various parameters, illustrated in Fig. 5.7, is, however, difficult to visualise. This is mainly due to the strong influence of n at fixed values of $X_g/\mathrm{N_a}$ and $\mathrm{Da_p}\eta_p$. This dependency is easily depicted, taking into account Eqs. (5.43), (5.46), (5.47), and (5.48) into (5.55)

$$\eta_G = f_1\left(\omega_{in}, \eta_{ph}, \eta_e, n\right) \tag{5.56}$$

The solution procedure of Fig. 5.6 yields Fig. 5.8 that displays Eq. (5.56). Qualitatively, the impact of η_{ph} and η_e on η_G in Fig. 5.8, is similar to that in Fig. 5.7 for $X_g/\mathrm{N_a}$ and $\mathrm{Da_p}\eta_p$, but the trends in Fig. 5.8 are clearer. The following observations are worth noting in Fig. 5.8: (1) In the case η_{ph} ~1, η_G is not affected by the reaction order n. For this case, one graph (one of the four in Fig.5.8) should be enough. This is because for n=1 the parameter η_{ph} could be extended to $\eta_{ph} \cdot \eta_e$, there is no

need to separate them. For other n-values; the lower the value of η_{ph} , the greater the influence of n . (2) The shape of the curves for different η_e -values is similar, as seen by a comparison between the graphs (a)-(d) in Fig. 5.8. This contrasts with Fig. 5.7, where the behaviour of η_G vs. ω_{in} at constant $X_g/\mathrm{N_a}$ and $\mathrm{Da_p}\eta_p$ is quite different. (3) The ordinate of all the curves at $\omega_{in} \to 0$ is $\eta_G \to \eta_{ph} \cdot \eta_e$.

Finally, Fig. 5.8 makes it possible to isolate the individual effects of the intraparticle resistance from those of the surrounding bed η_{ph} , η_e . In addition, M_{in} can be obtained from Eqs. (5.50) and (5.54). At any point (ω_{in} , η_G , η_{ph} , η_e) of the map displayed in Fig. 5.8 the following relation holds

$$M_{in} = \left(\omega_{in} / (\eta_G \cdot \eta_{ph} \cdot \eta_e)\right)^{1/2} \tag{5.57}$$

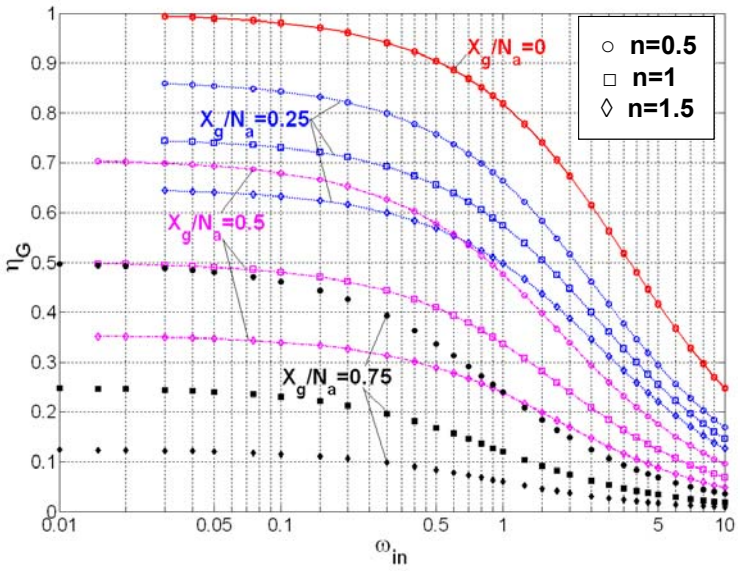

Figure 5.9: η_G vs. ω_{in} for various $X_g/\mathrm{N_a}$ and n for η_e =1 (chart $\eta_G = f_1\left(\omega_{in}, X_g/\mathrm{N_a}\, n; \mathrm{Da_p}\eta_p = 0\right)$

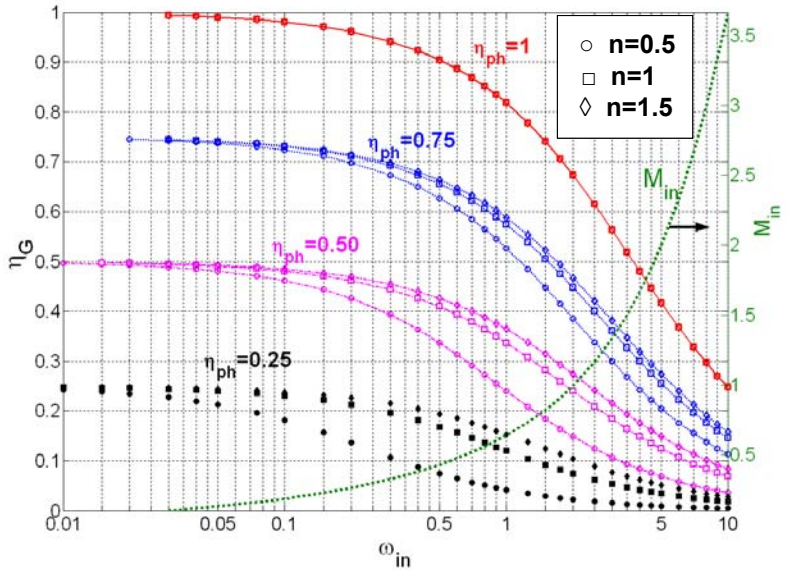

Figure 5.10: η_G vs. ω_{in} for various η_{ph} and n, for the case $\mathrm{Da_p}\eta_p$ =0 (chart

$$\eta_G = f_2\left(\omega_{in}, \eta_{ph}, n; \eta_e = 1\right)$$

An external effectiveness factor close to unity is a common feature in many situations such as in char gasification test. In effect, this is true if FBKEs are carried out within a range of temperature of 750 to 950 ºC and with relatively small particle size (below 1 mm). In addition, if the fluid-dynamic effects are relatively small, the parameter $X_g/\mathrm{N_a}$ should be close to unity. Thus, for FBKE, the most useful graphs from Figs. 5.7 and 5.8 are the ones situated at the upper-left corner. These graphs are expanded in Figs. 5.9 and 5.10. In Fig. 5.10 also M_{in} as a function of ω_{in} has been included for the case of η_{ph} =1. For other cases, the evaluation of M_{in} is readily carried out by applying Eq. (5.57).

5. Conclusions

This chapter deals with the assessment of mass transport effects in solid reactivity tests carried out in batch-operated, laboratory-scale, bubbling FB reactors. The main aim of the work is to isolate the intrinsic kinetics from the fluid-dynamic and diffusional interferences. The interphasic effectiveness is expressed as function of a dimensionless fluid-dynamic observable, which can be directly evaluated from gas concentration measurements. The effectiveness factor on a particle scale, which assesses the diffusion effects in a particle, is also expressed in terms of two observables. These are the well known Weisz-Prater module and the product of Damköhler number at a particle scale and the particle effectiveness factor. With a well-posed algorithm, the transport effects can be evaluated in a straightforward way from the three observables mentioned. A criterion has been developed to determine the maximum permitted gas conversion in a given test to keep the interphasic effectiveness factor above a critical value. Moreover, charts for rapid estimation of diffusion effects in a given typical FBKE have been presented. The treatment developed is rather simple and reduces the

practical difficulties found in the interpretation of experimental reactivity data, obtained from FB devices. This kind of analysis can be used to select optimum operating conditions for tests, aiming at the determination of solid reactivity in FB. Moreover, it can represent a good support for dimensioning new rigs for determination of kinetics. This study has been primarily developed for the assessment of mass transport effects in isothermal systems, where only one heterogeneous reaction occurs, i.e. CO_2-char gasification reactivity tests in FB. However, the methodology derived can be applied in other catalytic and non-catalytic systems, where diffusion effects may influence the observed reaction rate as far as those two assumptions are fulfilled. In cases that one (or both) of the assumptions are violated, the extension is readily done, but analytical solutions cannot be found. The application of the methodology developed in this chapter is applied in the Chapter 6 to estimate the diffusional effects present in CO_2–char reactivity test carried out in a bench-scale FB reactor.

Chapter 6

Mass transfer effects in char gasification reactivity tests in a lab-scale fluidised bed

1. Introduction

To make it possible to experimentally determine a char reactivity that is free from diffusional effects, kinetic experiments are usually carried out in typical laboratory apparatus (thermo-balance (TGA), muffle furnaces, etc) (Rapagna et al., 1996), where the conditions are under control. The reactivity of char depends greatly on the form of its preparation. To simulate high heating rates, like those taking place in an FB, some researchers utilized drop tube reactors (Lee et al., 1996). With this method, however, an average rate is measured, and it is difficult to obtain the variation of the rate with evolution of reaction. There are also some problems, such as uneven temperature distribution along the length of the reactor, uncertainty in reaction temperature of a particle and in reaction time (Luo et al., 2001b).

Employing an FB reactor many of the drawbacks associated with the abovementioned devices seem to be overcome (Gómez-Barea et al., 2006c). The main advantages of FB are: (1) Preparation of char in a fluidised bed in a nitrogen atmosphere is easy; (2) It enables the fuel to be carbonized under a variety of conditions, including different heating rates (from slow heating to rapid heating), different annealing times; (3) After carbonization, no cooling of the char is needed, and in-situ gasification of char can be conducted; (4) The time variation of gas composition during gasification and the variation of reaction rate with evolution of reaction of the char can be measured; (5) Uniform temperature is maintained in the reaction zone. However, some handicaps must be taken into account: (1) Combustion of volatiles changes the temperature conditions of devolatilisation and, hence, the final composition (and so the reactivity) of the resulting char; (2) It is difficult to accomplish kinetic investigations in an FB owing to the complex fluid-dynamics. This makes it difficult to separate the kinetic information from mass transfer and/or hydrodynamic influence (Bjerle, 1980). These considerations must be kept in mind when analysing the reactivity of a char resulting from any solid fuel.

This chapter analyses the transport effects in a set of char gasification experiments carried out in a 26 mm ID bench-scale FB reactor. The char used was woodmatter from pressed oil-stone (WPOS), also called orujillo. In this work the char was prepared under externally controlled conditions in order to minimise uncertainties about the char fed into the FB reactor. The gasification rates of WPOS were meas-

ured at two particle sizes (0.75 and 2.2 mm), three CO_2 partial pressures (0.20, 0.35 and 0.45 bar) and three temperatures (850, 900 and 925 ºC) using several initial char batches (from 0.5,1 and 2 g). In this chapter the methodology developed in Chapter 5 is applied. The method presented enables to separately assess the contribution of fluid-dynamic effects, external film as well as porous diffusional resistances in a typical FB char gasification test. Global effectiveness factors are computed to correct the observed gasification rate in order to obtain the intrinsic char reactivity.

The investigation presented in this chapter is part of a wider work where a general comparison between CO_2 and H_2O char gasification reactivity in TGA and FB is made. The overall work aims at analysing the impact on heating rate, gas composition, particle size and temperature on char reactivity of different coals and biomasses. Works on TGA and diffusional effects present in these systems have already been published (Ollero et al., 2002, 2003; Gómez-Barea et al. 2005; Gómez-Barea et al. 2006a, 2006b). In a second phase, determination of FB char reactivity will be dealt with. Determination of the intrinsic kinetics obtained from reaction with CO_2 and H_2O and a comparison between TGA and FB with char produced in situ or under various given external conditions are beyond the scope of this thesis. They will be dealt with in subsequent work.

2. Literature survey on TE during FBCRE in FB

Existing work on diffusion effects in char gasification reactivity tests in FB can be sorted into five classes, depending on the way that diffusion effects are reported: (1) Discussion about transport effects (TEs) is totally absent in the published work **(**Briedis, 2002) (2) Discussion about hydrodynamic interaction and /or physical effects (film and internal diffusion) is only qualitative or not explicitly included (Goring et al. 1953; Sipilä, 1988; Katta and Keairns, 1981) (3) Quantitative discussion about the hydrodynamic interaction is reported, but nothing is said about physical effects at particle scale (Bjerle, 1980; Schmal 1983) (4) Physical limitations are tested, but hydrodynamics are assumed not to be limiting (van den Aarsen 1985; Scott et al., 2005; Adánez et al., 1985) (5) A thorough study was made of both physical and hydrodynamic effects by Luo et al. (2001a). Actually, there is not a clear distinction between (4) and (5). The four works included in Items 4 and 5 are the best documented ones with regard the analysis of transport effects (TEs) in fluidised bed char reactivity experiments (FBCRE), especially the work of Luo et al. (2001a). These experimental findings are further explained in the following. All work mentioned concerns gasification in laboratory-scale FB.

Class 2: Goring et al (1952) carried out experiments on CO_2 and steam gasification. They determined indirectly the intrinsic carbon gasification rates from the experimentally measured rates by extrapolation to zero bed mass of carbon in a plot of observed gasification rate versus mass of carbon. Sipilä (1988) conducted experiments on various chars derived form peat, lignite and willow. The operation conditions were: bed temperature 750-850 ºC, superficial velocity 1.5 m/s, char size 2-5 mm and gas composition (10 % CO_2, 30 % H_2O and 60 % N_2). The author concluded that the observed char reactivity depends on the chemical rate and on the rate of mass and heat transfer. However, the authors did not quantify the relative importance of these processes.

Class 3: Bjerle et al. (1980) reported atmospheric gasification trials with Swedish oil-shale. They recognised that the high ash content of shale could introduce an internal mass transfer resistance. Therefore, they investigated the influence of pore diffusion in two ways. Firstly, they carried out steam gasification tests at 800 ºC in a fixed bed differential reactor with two particle-size fractions: one between 1.4 and 2 mm and one below 0.1 mm. They found a maximum difference of 2% in the observed reaction rates in the two cases. Secondly, char from an FB, gasified in steam at 800 ºC and 1 h residence time, was fractionated and analyzed with respect to carbon. No significant difference from the first set of results was found. They further stated that the lack of influence of pore diffusion in CO_2 gasification was justified in the experiments, because the chemical reaction is slower than for the steam-carbon system in the temperature interval investigated. Schmal et al. (1982) carried out experiments to determine whether high ash-content (>40 %) Brazilian coal could be gasified with steam in a dense fluidised bed. Previous fluidisation tests showed that, in order to provide an excess of vapour, good fluidisation was needed, and to avoid segregation, mixtures of coal and ash of different mass ratios and of different particle sizes were used. They found that the shrinking core model for chemical reaction control fitted well the experimental data of gasification at different temperatures and pressures. Although the authors qualitatively discussed fluid-dynamic issues, they did not mention plausible external or pore-diffusion limitations in their experiments.

Class 4: Van den Aarsen (1985) investigated gasification of wood and rice husk. He checked the resistance of the interface between the bubble and the emulsion phases by carrying out tests at different superficial velocities in a bench-scale reactor for fixed and fluidised conditions. He observed no clear increase in reaction rate with gas velocity and concluded that the resistance between phases was small. For evaluation of diffusional effects at the particle-scale, he estimated that the external and internal mass transfer resistances were of the same order. The comparison of pore diffusion with the observed rate was made through the Thiele modulus. His computations revealed that the upper limit of this module was 0.3 for the operating conditions tested. Consequently, he neglected the influences of mass transfer. Adánez et al. (1985) carried out FBCRE of lignite char in the temperature range of 800–1000 ºC. Their FB system was operated with a superficial velocity, twice the minimum fluidisation velocity. They investigated the impact of the mass of the initial char batch and char particle size on the observed reaction rate. They carried out experiments by using batches of 8, 10 or 15 g and particle sizes ranging from 100 to 630 μm. In each run the composition of the gas mixture and the temperature were predetermined. It was observed that internal diffusion began to influence the total rate only at sizes above 500 μm. They determined the conditions, under which physical effects had no influence on total reaction rate, and the experimental kinetic programme was designed to work within this region to assure the determination of intrinsic kinetics. Scott et al. (2005) investigated CO_2-char gasification in a temperature range of 800 to 1050 ºC. The chars were derived from dried sewage sludge, car tyres and a bituminous coal with particle sizes ranging from 500 to 710 μm. They used the measured initial rate as a reference. Fluidising velocities of 4 to 8 times the minimum fluidising velocity were employed. The observed gasification rate was largely determined by chemical kinetics under almost all operating conditions. The mass of the char-batch was adjusted between 0.02 and 0.1 g in order to avoid gas conversion in excess to 1 mol%, and so to maintain the FB as a differential reactor. The effect of mass transfer

was assessed for the worst case scenario (1000 ºC, 100 % CO_2 molar fraction, assuming a Sherwood number of 2, and using the most reactive material, i.e. sewage sludge char). In this case, the reaction rate was 12 times slower than would be expected if controlled by external mass transfer. By experimental estimation of the effective diffusivity, they computed values of the internal effectiveness factor of around 0.85 for the sewage sludge char at 1000ºC.

Class 5: Luo et al. (2001a) developed a FB reactor for measurement of char reactivity at elevated temperatures to simulate the conditions of existing entrained flow reactors. They thoroughly analysed the transport effects caused by the fluidising velocity, mass of bed, char particle size and temperature on the gasification rate in a set of coal-derived CO_2 char experiments. They analysed the measurements by a global model incorporated in a simple two-phase model of the bed. The results indicate that, as long as the operating conditions were properly selected, the influence of the external mass transfer resistance was limited, so that reasonable measurements could be conducted. On the other hand, the intraparticle mass transfer resistance was significant at high temperatures, and they concluded that the use of small particles was preferable in that range. To the best of our knowledge, the work carried out by Luo et al. (2001a) represents the most advanced and detailed effort for the assessment of diffusion effects in FB gasification.

From the foregoing analysis, a clear picture of transport effects in FBCRE is obtained: Design of a lab-scale FB reactor, as well as the choice of its operating conditions, such as the selection of bed material, mass of inventory, superficial velocity, etc should be analysed to avoid diffusion interferences. Existing FBCRE work shows that transport effects are often present but the TEs are analysed in a qualitative way. Consequently, the validity of the reactivity obtained is, in many cases, doubtful. Exceptions to this are the works of Adánez et al. (1985), Scott et al. (2005) and Luo et al. (2001a) where TEs are analysed in detail.

3. Theoretical

Char gasification with CO_2 is described by the Boudouard reaction

$$\mathrm{C\,(s) + CO_2\,(g) \;\rightarrow\; 2CO\,(g)} \tag{6.1}$$

To evaluate intraparticle diffusional effects a volume-based intrinsic reaction rate is defined as

$$(-r) = k(X(r),T)\; c_{CO_2}{}^{n} \qquad (\mathrm{mol \cdot m^{-3} \cdot s^{-1}}) \tag{6.2}$$

where $k = k(X(r),T)$ is an n^{th}-order kinetic constant, which depends on local conversion $X(r)$ and temperature. Isothermal conditions are assumed here. In a FBCRE, in which intraparticle mass transfer is limiting, the local conversion is not known, but it is related to the global conversion x_c as

$$x_c = \frac{24}{d_p^3} \int_0^{d_p/2} X(r)\, r^2\, dr \tag{6.3}$$

The more important the intraparticle effects are, the greater is the difference between the global and local conversion due to gradients within the particle. On the other hand, when the Thiele modulus is small, intraparticle effects are also small and global and local conversions can be assumed equal. In this case the kinetic constant and the structural profile obtained experimentally are intrinsic (see Chapter 2).

The experimental strategy for char gasification in FB usually involves measurement of the conversion of gas passing in steady-flow through a batch of char. To derive the kinetic parameters from outlet gas measurements, the gas and solid flow patterns must be known. The flow pattern in an FB is, however, difficult to predict. There are published works on the determination of non-catalytic FB kinetics (Szekelly et al., 1986, Corella, 1980) but they are generally restricted to the assumption of ideal reactor flow patterns. In this work the approach developed by Gomez-Barea and Ollero (2006) is followed, enabling to account for the heterogeneous nature of a fluidised bed in a simple way.

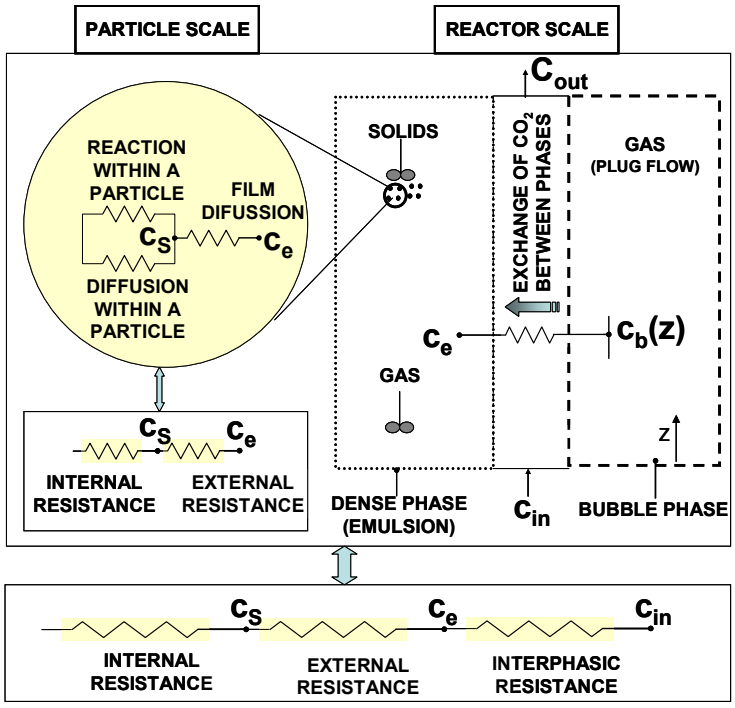

Figure 6.1: Problem description.

A typical CO_2-char reactivity test in an FB is performed in batchwise mode (Luo et al. 2001a, Scott et al. 2005; Adánez et al. 1985; Gómez-Barea et al., 2006a, 2006b, 2006c). In such a test the CO_2 concentration and gas-flow rate in the inlet are given. The bed is kept at a fixed temperature. The concentration of CO is registered. The mass of the batch is kept small to maintain the CO_2 consumption, the thermal effects,

and the change of volume small enough to be ignored. Under such conditions, bed temperature, inlet reactant concentration, and gas flow-rate can be assumed uniform along the bed, and they can be taken directly as input to the estimation of the intrinsic kinetic parameters. In the course of a real gasification test, however, the CO_2 concentration can drop considerably owing to the chemical reaction, as well as to physical resistances caused by diffusional effects. The gasifying agent (a gas mixture of CO_2 and N_2), introduced into the reactor, passes through the bed as bubbles and also through the emulsion. Before the reaction takes place on the internal surface of the particles, CO_2 has to overcome various resistances on its travel from the bubbles to the reacting sites. Figure 6.1 illustrates this problem. The related decrease in CO_2 concentration affects the reaction rate if the concentration at the reacting sites differs from that of the inlet gas stream. Thus, for the capture of intrinsic char reactivity, these resistances are of concern. If complete suppression of these interferences is not possible the degree of interaction should be assessed: estimation of the diffusion effects is always of major importance.

To evaluate the differences between the observed global conversion *(-R)* and the conversion if the concentration in the internal reacting sites of the porous char were equal to that at the entrance c_{in}, the following effectiveness factor is defined:

$$\eta_G = \frac{(-R)}{k_{ps}\, c_{in}^n} \tag{6.4}$$

where k_{ps} is a "pseudo-intrinsic" kinetic constant. The reason to introduce a "pseudo-intrinsic" constant is that k_{ps} is a function of the global conversion x_c. This kinetic constant represents the reactions taking place in a char particle, as can be expressed by Eq.(6.2), yielding the relation between the observed and the intrinsic local reaction rate

$$(-R) = \frac{24}{d_p^3} \int_0^{d_p/2} \left[k(r) c^n(r) \right] r^2\, dr \tag{6.5}$$

By combining Eqs. (6.4) and (6.5), an expression for k_{ps} is obtained

$$k_{ps} = \frac{24}{\eta_G\, c_{in}^n\, d_p^3} \int_0^{d_p/2} \left[k(r) c^n(r) \right] r^2\, dr \tag{6.6}$$

which clearly shows that k_{ps} depends on particle size and consequently, strictly speaking, is not intrinsic. For a small char particle, Eq. (6.6) is simply $k_{ps}(x_c) \sim k(x_c)$ (recall that $x_c \sim X$ in this case), and the kinetic constant determined experimentally can be considered intrinsic. From Eq. (6.5), an apparent kinetic constant k_{ap} can be defined as

$$k_{ap} = \frac{(-R)}{c_{in}^{n}} \tag{6.7}$$

The relation between the apparent and the pseudo-intrinsic kinetic constants is obtained by Eqs. (6.6) and (6.7):

$$k_{ps} = \frac{k_{ap}}{\eta_G} \tag{6.8}$$

To avoid the intraparticle diffusional effects, small char particle size is preferred. However, feeding powdery solid reactant in laboratory-scale FB is not attractive due to entrainment of char, especially in FBCRE operated batchwise with feeding at the top. This type of arrangement makes it sometimes necessary to select larger char particle size to minimise the entrainment, especially during operation at high superficial velocity. Under such circumstances, the char size is not small enough to assure that particles are gasified in the kinetically controlled regime. However, intraparticle effects are not expected to be prominent. Typically, the effectiveness factor in FBCRE can reach values as low as 0.5-0.6 (Luo et al., 2001a; Scott et al, 2005). In addition, the contribution of intraparticle mass limitation to the global effectiveness strongly depends on particle size and operating conditions. In this situation, the solid and gas concentration profiles in the particle are expected to be flat enough so that the kinetic constant k_{ps} calculated by means of Eq. (6.8) could be assumed intrinsic, at least, as a first approximation. Moreover, even in cases where the global effectiveness factor is smaller than 0.5-0.6 (say 0.3, 0.4), the above is reasonable, providing that the intraparticle effects are not limiting. This is, however, not usually the case in FBCRE. In general, the smaller the contribution of intraparticle diffusional resistance to the global resistance, the closer is x_c to X.

η_G depends on the resistances involved on the CO_2 path. Therefore, this value should be estimated. Figure 6.1 illustrates a simplified model of this physical situation where the resistances considered are: (1) Interphasic resistance, (2) External particle film resistance (boundary layer) and (3) Internal porous resistance (intraphasic). With the procedure of Chapter 5 these resistances can be easily evaluated from gas measurements in the off-gas stream. Once the global effectiveness factor is estimated at any conversion, the kinetic constant can be evaluated as

$$k_{x_c}(x_c) = \frac{1}{\eta_G}\frac{(-R)}{c_{in}^{n}} \tag{6.9}$$

where $(-R)$ is computed from the measured gas concentration n_{CO}, as

$$(-R) = \frac{1}{V_c}\frac{1}{2}\frac{dn_{CO}}{dt}(t) \tag{6.10}$$

The volume of the char particles at any degree of conversion, $V_c(x_c)$ needs to be modelled for use in Eq. (6.10). As gasification proceeds there is a change of the mass of carbon. This leads to a decrease of particle size and/or density. The reduction of the char volume V_c can be expressed (Oka, 2004; Gómez-Barea et al., 2006b),

$$V_c(x_c) = V_{c0} \cdot (1 - x_c)^{\delta - 1} \tag{6.11}$$

For shrinking-core behaviour δ should be close to 0. In a case of uniform conversion, the value should approach 1. Further discussion about this coefficient is included in Section 7**.**

4. Experimental

4.1. Char preparation and characterisation

The char preparation method is the same as that in Chapter 3 for TGA tests. The WPOS is air-dried at 35-40 ºC and sieved to a size between 1.41 and 2.83 mm. These particles were pyrolysed in a PTF700 (LECO) furnace in an atmosphere of flowing nitrogen. The pyrolysis temperature reached 900 ºC at a heating rate of 30 ºC/min. The samples were kept at 900 ºC for 7 minutes to complete the pyrolysis. The nitrogen flow was maintained until the sample had cooled down to below 100 ºC to ensure that no reaction with air would occur. Table 3.1 in Chapter 3 shows the proximate and ultimate analysis of the char used in this study.

Table 6.1. Chemical characterisation of the ofite

Ofite. Major analysis (%)			
Si as SiO_2	53.93	Na as Na_2O	3.49
Al as Al_2O_3	13.61	K as K_2O	0.48
Fe as Fe_2O_3	9.15	Sulphates as SO_3	-
Ca as CaO	11.15	Moisture at 105 ºC	0.47
Mg as MgO	7.90	Weight loss at 750 ºC	0.64

The char samples were ground in a mortar into two different sizes: (1) from 500 to 1000 μm, and (2) from 1410 to 2.830 μm. Mean values associated with each particle-size range were, 0.75, and 2.1 mm. A total of 190 particles were counted in a batch of 0.5 g of 2.1 mm char, which means an average of 2.63 mg per particle. The particles appeared to be nearly spherical. Assuming a mean diameter equal to the average size cut, the calculated apparent density was 543 kg/m^3. The true density of the char was measured by liquid (water and alcohol mixtures) displacement using a pycnometer gave an average value of 1522 kg/m^3. The porosity was calculated from the apparent and true densities as 1- 543/1522=0.65.

4.2. Inert material

Ofite, a subvolcanic rock, has been used as inert material for the bed. Ofite is a silicate with formula $(Ca{\cdot}Mg{\cdot}Fe{\cdot}Ti{\cdot}Al)_2{\cdot}(Si{\cdot}Al)_2O_6$. It has an average particle size of 750 μm and a particle density of 2620 kg/m^3. The chemical characterisation of ofite is given in Table 6.1.

4.3. Apparatus

The FB apparatus as well as the rest of the equipment used for the present investigation are shown in Fig. 6.2. The bubbling FB gasifier consists of three parts, a preheating section, a reaction (bed) part, and the freeboard. The preheating part is a fixed bed of sand which is heated up at the beginning of each test. During steady state operation this section preheats the fluidising agent before entering the fluidised bed. The main body of the reactor, the fluidized bed, is a refractory-lined stainless steel reactor AISI ·316 (26.64 mm ID), and 3 mm thickness. The distributor plate is drilled with 27 holes with 1 mm internal diameter. It has a total height of 375 mm and two sections, the bed zone of 26.64 mm ID and the freeboard of 52 mm ID. Fig. 6.2 illustrates further details of the reactor design.

Bed and freeboard are surrounded by an electrical 6 kW_{th} furnace, controlled to obtain the desired reaction temperature (800-950 ºC). The gasifier is equipped with two thermocouple probes (K-type). One pressure tap is located along the side of the reactor (PT) to monitor the fluidisation conditions of the bed. A steam generator is located prior to reactor to produce the desired steam for the steam tests. The results with steam are not reported in this work.

The gas is fed up through the bed and leaves from the freeboard section. It passes through a thimble filter that collects entrained particles. The gas sampling point is located downstream of the cyclones. A stream of the fuel gas is taken out by an Inconel probe supplied with a filter to remove particles. The sampling line is electrically heated to avoid condensation of organic compounds within the probe. The composition of the gas produced is measured continuously (CO, CO_2, CH_4, H_2 and O_2) by a Siemens analyser. This device uses a non dispersed infrared method for CO, CO_2 and CH_4 measurements and thermal conductivity and paramagnetic methods for H_2 and O_2 measurements, respectively. The flow rate of the outlet gas is measured by a rotameter. The reactor temperature is controlled by a PID, which manipulates the power input to the electrical furnace. The signals from the analyser are transmitted to the computerised data acquisition system, where they are monitored and registered with a sampling period of 4 s.

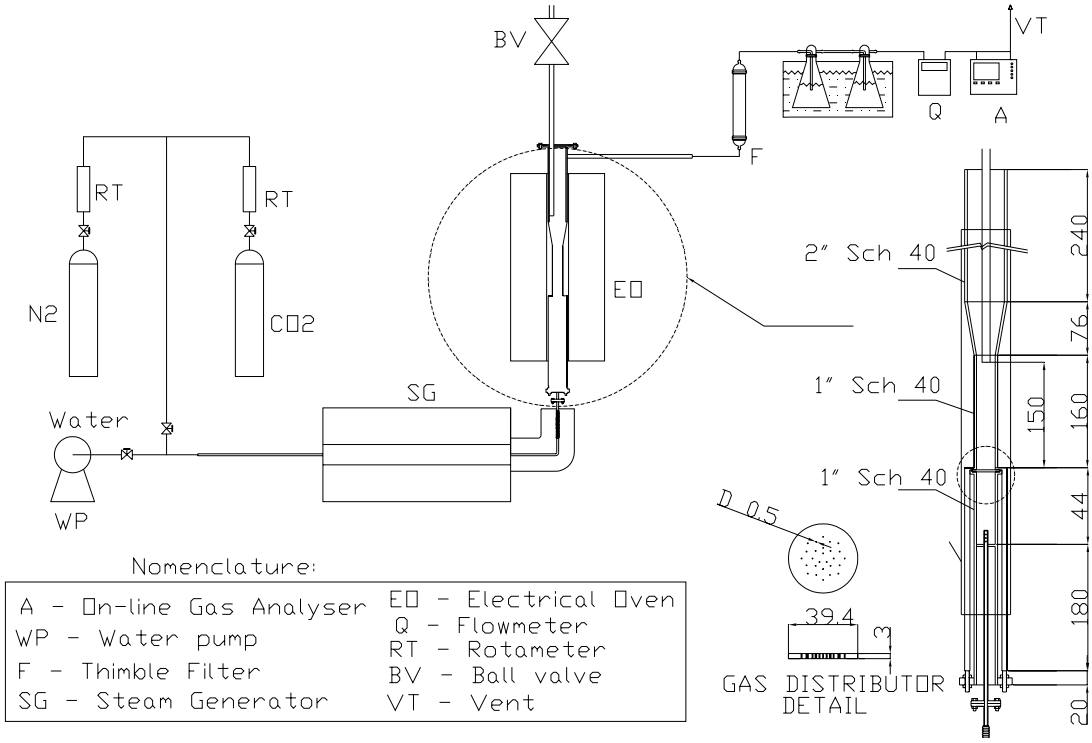

Figure 6.2: Flow sheet of the laboratory-scale bubbling FB gasifier used in the reactivity tests

4.4. Test procedure

The procedure used for each experiment was as follows:

1. The FB reactor is heated by the electrical furnace to the desired test temperature. The reactor is kept at this temperature for 5 minutes.

2. The reactor is fluidised using pure N_2. The volumetric flow of nitrogen is adjusted to establish the desired fluidising velocity. The nitrogen stream is preheated in a fixed bed of ofite particles situated under the distributor. The stream temperature is controlled so that the inlet temperature was the same as the reactor temperature. The system is kept under these conditions for 5 minutes.

3. A batch of char is injected to the bed by two ball valves. Char particles are fed 150 mm above the distributor.

4. The char is maintained in this inert atmosphere until no CO, H_2, CO_2 or CH_4 were detected (approximately 2-3 minutes). Fig. 6.3 illustrates experimental curves obtained in a typical test in this phase. As seen, the reactor is kept under these conditions for roughly 10 minutes before the gasifying reactant is fed (Step 5).

5. The gasification reactant is established. Gasification of the char continues under these conditions until no CO was detected in the outlet stream.

6. Air is fed into reactor to burn the remaining char. The beginning of this phase is also illustrated in Fig. 6.3 where the time is indicated on the horizontal axis when the new stream composition is detected by the analyser.

7. Cooling from the established test temperature to ambient conditions.

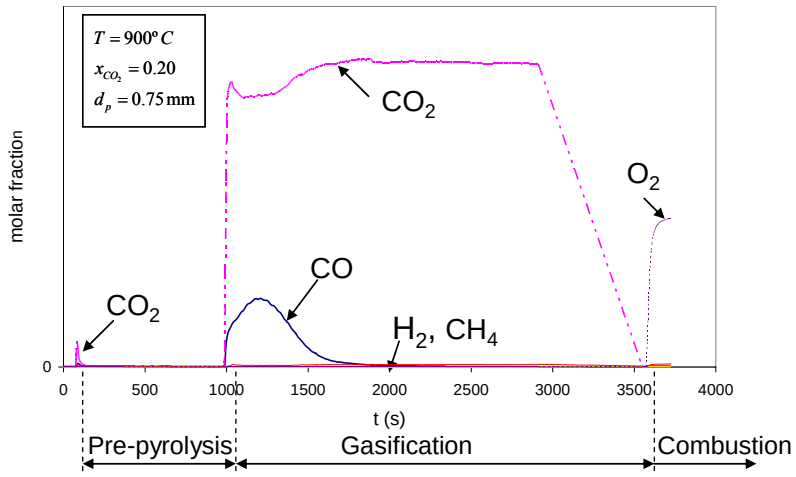

Figure 6.3: Phases in a typical char reactivity test

Typical results of reactivity measurements are illustrated in Fig. 6.3. The phases of pre-pyrolysis and gasification of char are shown. The concentrations of volatile components (CO, H_2 and CH_4) are very small when only N_2 is injected into the reactor and when switching from N_2 to CO_2 diluted in N_2. The initial char available for gasification was calculated by considering the weight loss of the char during this pre-pyrolysis step.

4.5. Experimental conditions

The experimental conditions included two particle sizes (0.75 and 2.2 mm), three CO_2 partial pressures (0.20, 0.35 and 0.45 bar), three temperatures (850, 900 and 925 ºC) using three char batches (from 0.5, 1 and 2 g).The volumetric flow of nitrogen was adjusted in all tests to establish a fluidising velocity of around 0.80 m/s.

The experimental conditions have been detailed in Table 6.2. The different variables have been listed in five groups. Group 1 represents variables which can be adjusted (within a small range) in an experiment in order to avoid fluid-dynamic interferences. They are gas flow rate, amount of char and ofite (inert) inventory. The mass of the char-batch is usually adjusted to avoid gas conversion in excess to a specified threshold. This guarantees the operation of the FB as a differential reactor.

Group 2 lists the main properties of the inert particles, which can, in principle, be selected in each test. Group 3 to 5 represent variables that can not be modified. Group 3

and 4 are fixed by constraints related to the determination of kinetics, whereas Group 5 includes the most relevant geometrical properties of the rig.

Table 6.2. Operation conditions and design parameters in the experimental rig for FBCRE

Group Nr.	Group name	Symbol	Range of values	Unit	Remarks
1	Operating variables	u_0 w_{c0} w_s	0.7-1.0 $0.5\text{-}4\cdot10^{-3}$ $30\cdot10^{-3}$	m/s kg kg	Variable, which can be adjusted (within a small range) in an experiment to avoid fluid-dynamic interferences and to guarantee differential conversion
2	Inert properties	ρ_s d_s	2600 $0.75\cdot10^{-3}$	kg/m^3 m	Inert properties, which can be selected in each test
3	Char properties	ρ_{c0} d_p	500-600 $0.75 - 2.1\cdot10^{-3}$	kg/m^3 m	Non modifiable Modifiable (feeding problems can constraint) Depends of the others
4	"kinetic" conditions	T_{in} $x_{CO2,in}$ **(*)** p	1073-1198 0.20-0.45 1	K bar bar	Variables that are imposed by the experimental programme. They vary from one experiment to another.
5	Design variables	D_t N_t d_{or} H	$2.66\cdot10^{-2}$ 4.84^{-4} $1\cdot10^{-6}$ 0.165	m m^{-2} m m	Non-modifiable variables, once the rig has been built-up. In a design-phase modifications are possible.

(*) $p_{CO_2} = p\,x_{CO_2}$. Throughout what follows we will use: x_{CO_2} and T stead of $x_{CO2,in}$ and T_{in}

4.6. Treatment of data

From the stoichiometry of the Boudouard reaction, Eq. (6.1), the measured outlet gas flow rate, $Q(t)$, and the analysis of the gas composition, $x_{CO}(t)$ and $x_{CO_2,in}$, the gas conversion is calculated by

$$X_g(t) = K(t)\cdot\frac{x_{CO}(t)}{2\cdot x_{CO2,in}} \tag{6.12}$$

The constant $K(t)$ lumps thermal effects and change of volume due to reaction. For all the tests, $K(t)$ has been very close to unity and, thus, it is assumed equal to unity in

what follows. The instantaneous overall rate of conversion, dx_c / dt is calculated by equalling the rate of disappearance of solid carbon in the char with the rate of generation of CO. This leads to the following expression

$$\frac{d\,x_c}{d\,t} = \frac{12 \cdot x_{CO2,in}}{22.4 \cdot w_{c0}} \cdot Q_g(t) \cdot X_g(t) \tag{6.13}$$

w_{c0} being the initial mass of carbon in the char sample. The carbon conversion is obtained by integrating Eq.(6.13).

$$x_c(t) = \int_0^t \frac{d\,x_c}{d\,t}(t')\,dt' \tag{6.14}$$

Additionally, a quantity λ, which represents the difference between the initial carbon content of the char and the carbon detected by measuring the CO concentration in the outlet stream, was computed for each test

$$\lambda = 1 - x_c(t_\infty) \tag{6.15}$$

The experiments included in the present work have provided values of λ over 0.90.

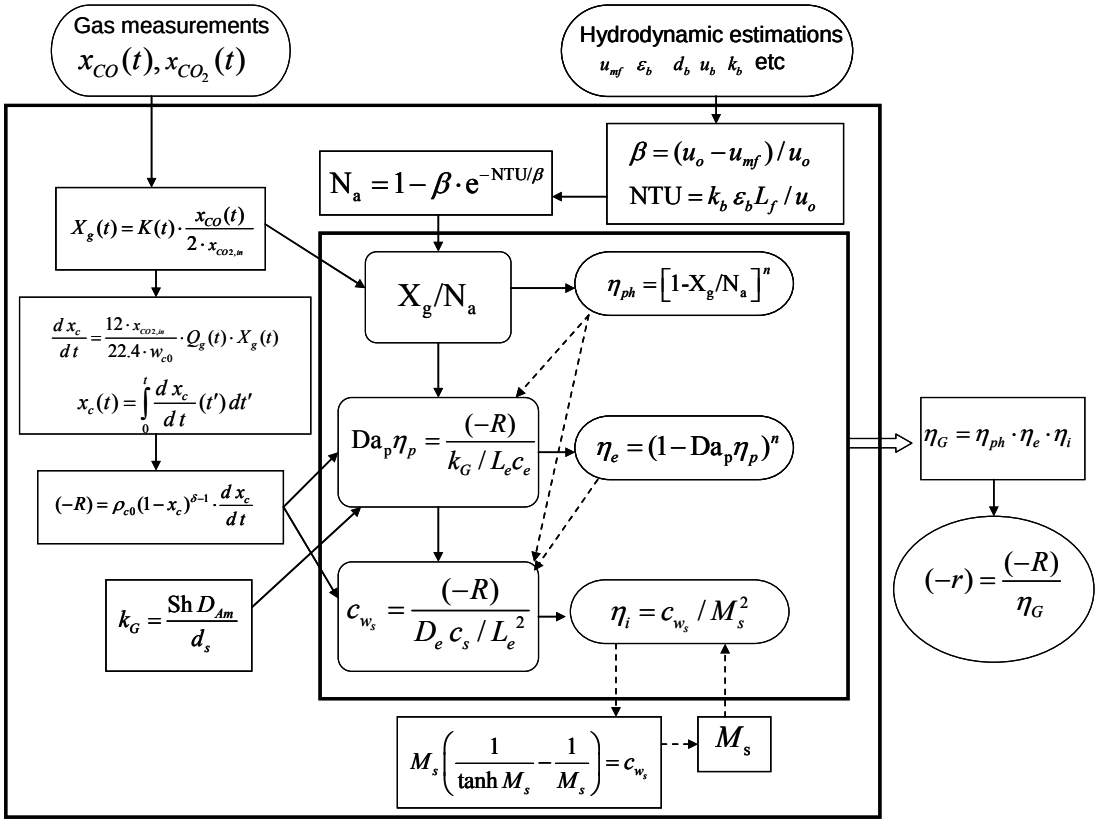

Figure 6.4: Algorithm for evaluation of diffusional effects

5. Evaluation of transport effects

For the evaluation of transport processes the treatment developed in Chapter 5 is followed. Fig. 6.4 summaries the method and presents the equations needed for carrying out the procedure of Chapter 5.

6. Results and discussion

6.1. Effects of delay time and back-mixing of apparatus

Delay time and back-mixing of gases were studied by carrying out a blank test in the system. Fig. 6.5 presents the information acquired from the blank test. On the horizontal axis the time is indicated, at which the valve is switched on. The step is displayed by the dotted line. The dashed line represents the response to the CO_2 concentration step in the inlet of the reactor. The curve fitted to the points in Graph (a) represents the theoretically calculated CO_2 molar fraction given by a dynamic model adjusted to the experimental data. The analytical expression of the transfer function G(s) is also included in the graph, from which it is seen that first order dynamics were assumed. From G(s) it is seen that the delay time for refreshment of gas when the supply line is switched from N_2 to CO_2-N_2 is roughly 40 s and the time constant 6.57 s. Graph (b) includes the curves C(t) and E(t) obtained from the experimental outlet of Graph (a). The definitions of these two curves (see Levenspiel (2003)) are also given on the graph. The dimensionless dispersion coefficient calculated from Curve E(t) of Graph (b) was quite small (D/uL = 0.0097). This indicates that back-mixing in the system is limited. From the preceding analysis it can be concluded that correction of the experimental concentration curves from the char reactivity tests is not needed.

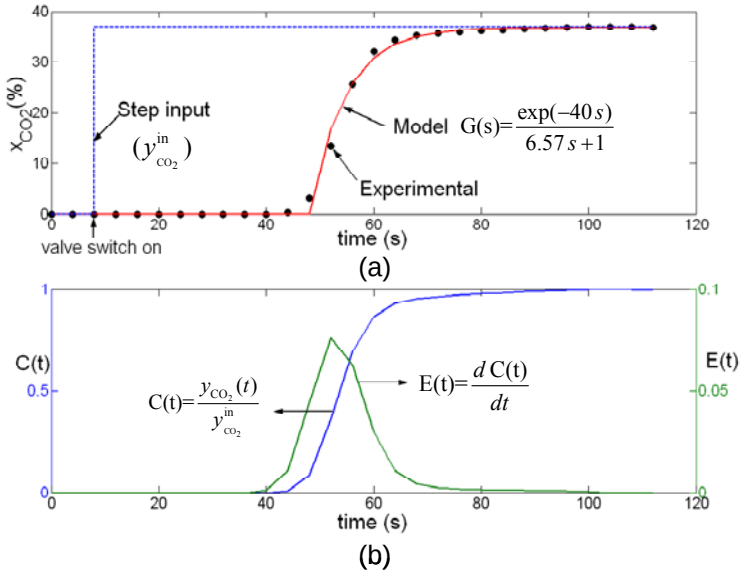

Figure 6.5: Blank test output

6.2. Effect of fluid-dynamics

The superficial velocity is the main operation variable responsible for different flow patterns in a FB. This affects mass transfer in two ways: (1) it can increase the bubble to emulsion mass transfer resistance, leading to bypass of gasification agent in the bubbles and (2) it can affect the magnitude of particle film diffusion resistance (external effectiveness).

In this work, the effect of superficial velocity was studied theoretically and experimentally. For the experimental conditions of the rig (see Table 6.2) NTU ranged between 7 and 11. This means that the time for bubbles to flush out the CO_2 during their passage through the bed is small (~0.015 s) compared with the residence time (~0.14 s). The reason is probably the presence of small bubbles (typically from 5 to 9 mm). Bubble velocities were computed to be in the range of 0.7-0.8 m/s. Therefore, effect (1) was shown to be reasonably far from fluid-dynamic limitations (N_a is very close to unity). Effect (2), the calculated film diffusion resistance, was also found to be small. This is experimentally verified in the following section (Section 6.8) for all tests. This result is in agreement with various relevant works on FBCRE, such as those of Scott et al. (2005), Adánez et al. (1985) and Luo et al. (2001a).

In conclusion, fluid-dynamic limitations seems to be absent in our rig. The superficial velocity was fixed for all gasification tests to 0.80 m/s. This velocity corresponds approximately to $u_0 \approx 5u_{mf}$. The FB was operated in the range of $u_0 \approx 3-7u_{mf}$ without significant changes in the observed reactivity.

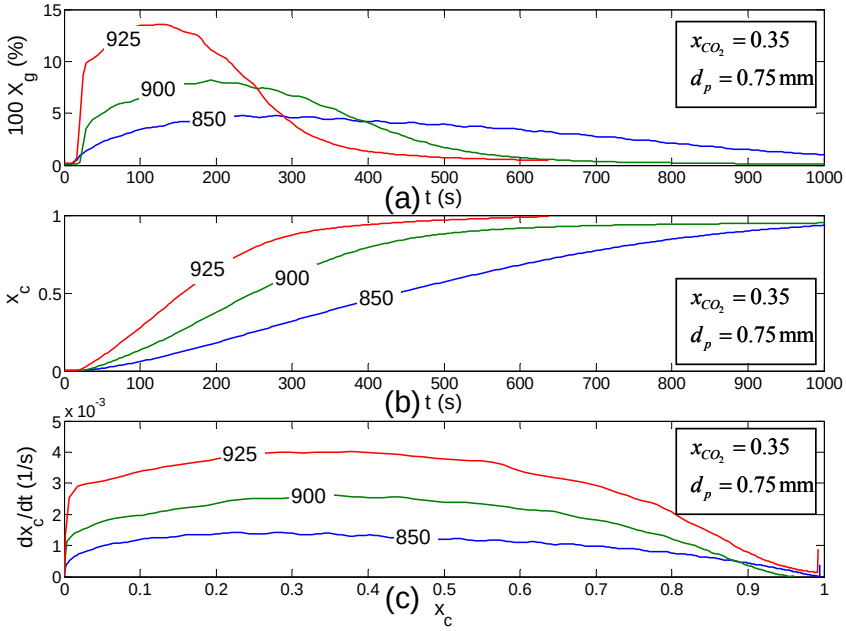

Figure 6.6: Influence of temperature (a) Gas conversion vs. time. (b) Solid conversion vs. time. (c) Conversion rate vs. conversion. (w_0=1 g)

6.3. Effect of temperature

Figures 6.6 displays the curves for a test carried out with 0.75 mm initial char size. The mass of the batches used was 1 g and the CO_2 molar fraction was $x_{CO_2} = 0.35$. All tests were performed with the same fluid-dynamic conditions by adjusting the superficial velocity to 0.8 m/s (for the inlet gas condition). As mentioned, the parameter N_a is around unity in all the tests. Graph (a) presents gas conversion vs. time, while Graph (b) and (c) present respectively, char conversion vs. time and rate of conversion vs. conversion. As expected, the higher the temperature, the higher the rate of conversion. Graph (a) shows that tests carried out at higher temperature also had higher gas conversion. The shape of the curves for higher temperatures also shows smaller dispersion. It can be seen in Graph (b) and (c) that that the sensitivity of the reaction rate to temperature is very high in the range of temperature tested (850-925 ºC).

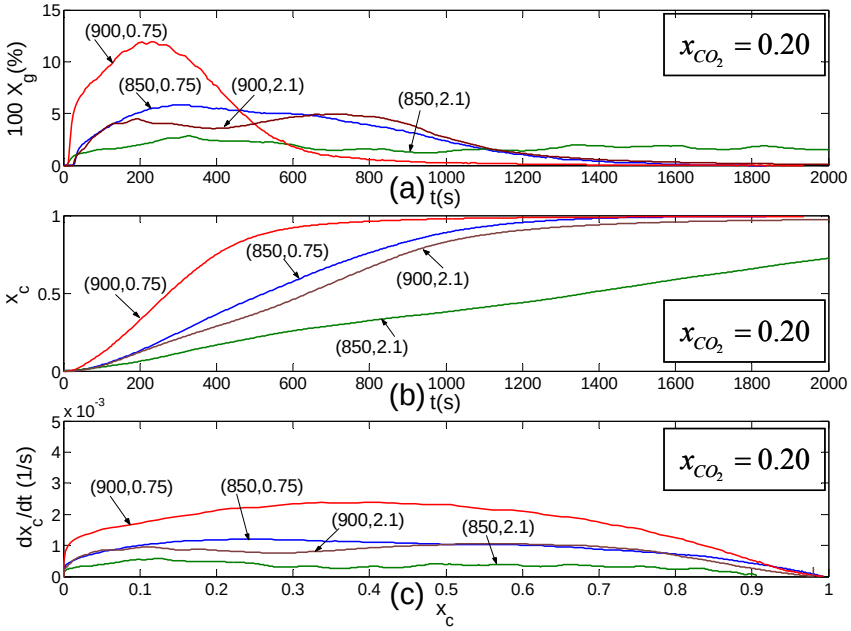

Figure 6.7: Influence of temperature and particle size. (a) Gas conversion vs. time. (b) Solid conversion vs. time. (c) Conversion rate vs. conversion. (w_0=1 g)

6.4. Effect of particle size

Figure 6.7 presents the curves corresponding to four tests carried out at a given CO_2 molar fraction ($x_{CO_2} = 0.20$) with two sizes of char particles (0.75 and 2.1 mm) and two temperatures (850ºC and 900ºC). As seen, the effect of particle size affects greatly the observed reaction rate (gas conversion, char conversion and conversion rate are presented in the figure). Diffusional limitations are remarkable in the curves corresponding to tests using d_p=2.1 mm. In fact, the curve of the test under conditions d_p=0.75 mm and T=850ºC is quite similar than that using d_p=2.1 mm at T=900ºC. This points out that, in the range under study, both particle size and temperature have

strong impact on the observed reactivity. This remarkable effect of char size illustrates the important role of diffusional limitations when using 2.1 mm char size.

It is worth observing that the curves representing tests carried out with an initial char particle size of 0.75 mm appear well-defined with a peak at short times, as well as a long tail at long times. In contrast, the curves corresponding to the larger char size (2.1 mm) show rather different, noisier, shapes. The curves are not sharp and remain flat during a longer period of time.

6.5. Effect of CO_2 partial pressure

The effect of CO_2 partial pressure is analysed in Fig. 6.8, which displays the same information as Figs. 6.6 and 6.7, but this time the curves correspond to tests at given temperature using several CO_2 partial pressures (0.20, 0.35 and 0.45 bars). On the one hand, Fig.6.8 illustrates that the gasification is enhanced by higher CO_2 partial pressures, because the reactivity increases with CO_2 concentration. We observe that the effect of CO_2 concentration on the progress of char conversion is not as great as that of temperature. On the other hand, two major conclusions can be drawn from Fig. 6.8: (1) The impact of the CO_2 partial pressure on the gas and char conversion (Graph (a) and (b)) and the rate of conversion (Graph (c)) differs considerably when the size of char particles are 0.75 mm and 2.1 mm. As seen in the figure, the three tests shown for char size of 0.75 mm are very close, while the curves corresponding to the larger char particle size are quite separate from each other. (2) At the smaller particle size, where the effect of intraparticle diffusion is expected to be limited (this is confirmed below), the effect of CO_2 partial pressure is not as important as those of particle size and temperature.

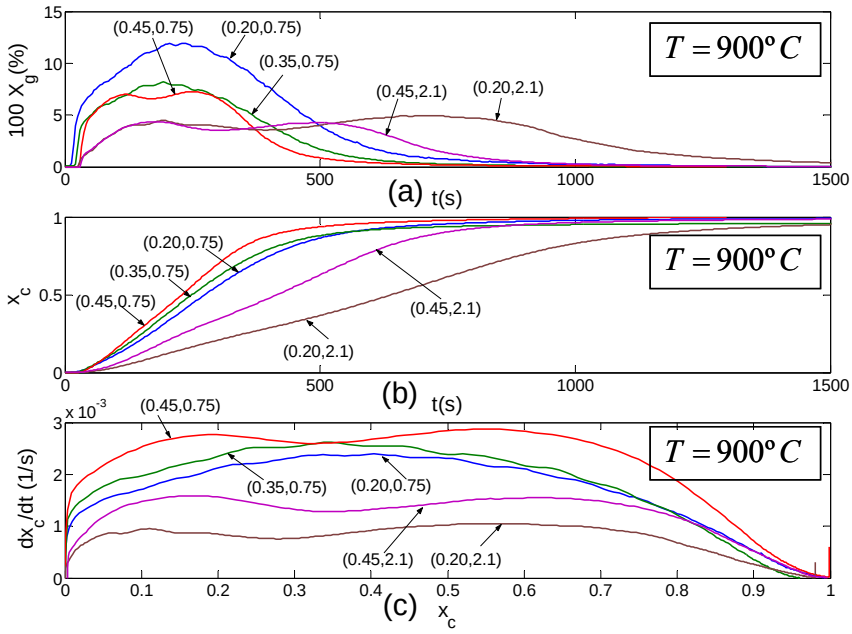

Figure 6.8: Influence CO_2-partial pressure and particle size. (a) Gas conversion vs. time. (b) Solid conversion vs. time. (c) Conversion rate vs. conversion. (w_0=1 g)

Finding (2) just mentioned is worth further discussion. The effect of particle size on the relative increment of reactivity with CO_2 concentration does not follow the expected trend because the relative increase is much greater with 2.1 mm particle size as compared to the 0.75 mm size. The reason is that the diffusional interferences invalidate a purely chemical kinetics analysis of the situation. As particle size increases, so does the difference between the CO_2 concentration in the emulsion and on the sites within the particle where the reaction takes place. The relative drop of CO_2 concentration decreases as CO_2 concentration in the inlet stream increases. Therefore, the impact from variation of the CO_2 concentration in the inlet gas stream is higher with larger particle size. This is clearly illustrated in Fig. 6.8 where the diffusional effects are clearer in the test carried out at $x_{CO_2} = 0.20$ than in that at $x_{CO_2} = 0.45$.

This explanation is not, however, entirely satisfactory because the effect of CO inhibition can play a relevant role also as particle size increases. The CO inhibition has been discussed in various studies (Ollero et al., 2002; Barrio et al., 2000; Gómez-Barea et al., 2006d, 2006e). Although the tests were carried out in the absence of CO in the inlet stream, the increase in particle size above 0.75 mm could make the CO concentration inside the particles higher than in tests using 0.75 mm. The CO concentration in the internal pores can be appreciable and, consequently, the inhibition effect could play a significant role. This could also explain that the observed reaction rate is lower than expected. To describe these observations, the inhibition effect caused by CO needs to be modelled by another kinetic expression capable of capturing CO concentration effects. In an n^{th}-order kinetic expression, both the diffusional effect and the CO inhibition are lumped together. This could lead to a misunderstanding of the real effects of diffusional limitations. Therefore, more complex kinetics, such as Langmuir-Hinshelwood, should be used in order to adequately separate the inhibition effect of CO (chemical limitation) from purely diffusional effects (physical limitation). This aspect, however, is far beyond the scope of this work.

6.6. Effect of mass of char batch

The mass of the batch was adjusted in this work to keep the measured CO concentration below an acceptable value in order to avoid that the CO_2 concentration changed too much to ensure differential conversion. However, feeding small amounts of char in our laboratory-scale FB was difficult. The reason is that feeding small size char at the top leads to severe entrainment of char.

To establish a reference guess of the initial char batch, a comparison was made with work carried out in similar rigs, such as by Scott et al. (2005), Adánez et al. (1985) and Luo et al. (2001a). Scott et al. (2005) used batches between 0.02 and 0.01 g, for activated carbon, tyre char, and sewage sludge char, whereas for Rietspruit char they used 0.10 g. They adjusted the mass of char in order to get a CO concentration in the off-gas that was always less than 1 mol %. Adánez et al. (1985) used different batches of 8, 10 and 15 g and obtained the true reactivity by extrapolation of the rates determined at different batch contents down to zero-batch mass. Luo et al. (2001a) used batches of 180 and 350 mg to determine the reactivity of coal char at very high temperature (1450 K), but differences in the measured reactivities of the two batches were found very small (below 5% in the worst scenario). In our tests the batch sizes were in between the ones of Scott et al. (2005) and Adánez et al. (1985). However,

the char analysed by Adánez et al. (1985) had much lower reactivity than ours. Chars and the operating conditions of Scott et al. (2005) were more similar to our experiments. Therefore, the impact of batch size was carefully studied in this work, using different initial batches from 0.5 to 4 grams.

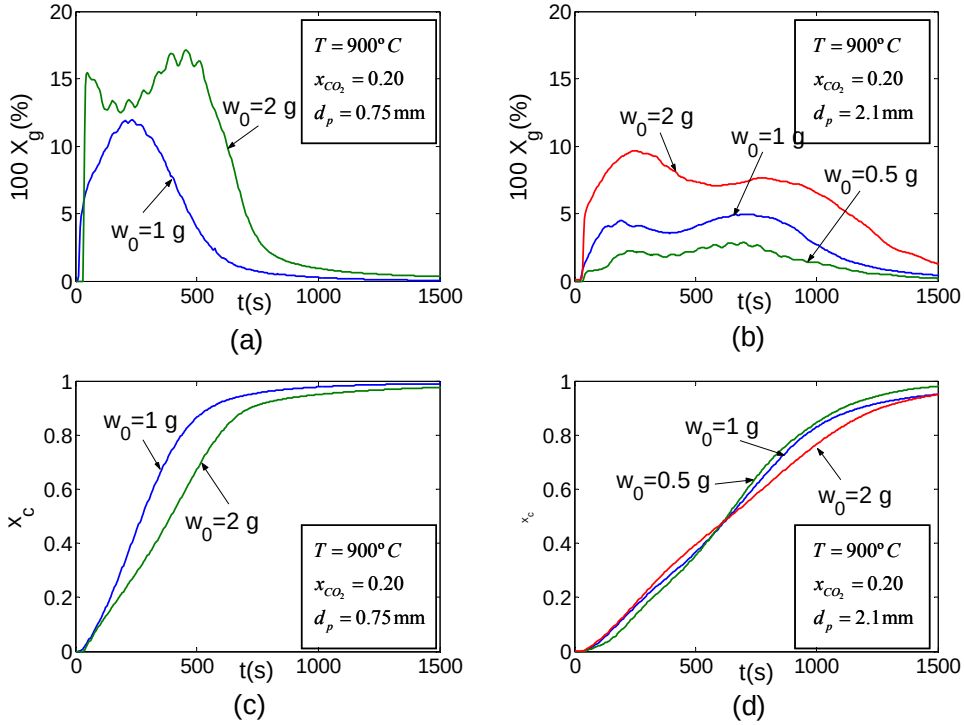

Figure 6.9: Influence of mass of char batch. Graphs (a) and (c): Evolution of gas and char conversion for d_p=0.75 mm. Graphs (c) and (d): Evolution of gas and char conversion for d_p=2.1 mm.

The effect of the mass of a batch in the experiments is illustrated in Fig. 6.9. This figure displays gas and char conversion curves vs. time for two particle sizes (0.75 and 2.1 mm). The effect of batch size is rather different, depending on the char size used. The effect is small for 2.1 mm char, whereas it is considerably greater at smaller char particle size. Once again, this finding illustrates that diffusional effects are limiting in the tests with larger particle size. In effect, in the tests with char size of 0.75 mm, intraparticle effects are not rate-limiting, and, thus, gas conversion has a considerable effect on the measured gasification rate. In this situation, increasing the batch size leads to a reduction of the interphasic effectiveness, because the gas conversion is high (the differential conversion condition is violated). The situation in the 2.1 mm test, however, is different. The rate-limiting mechanism is now intraparticle diffusion, and, thus, the measured gasification rate is almost not affected by the batch size (gas conversion). This is because at larger particle size the contribution of the interphasic effectiveness to the global effectiveness is limited. To sum up, the char size is not important at 2.1 mm particle size within batches of 0.5 – 2 g, whereas the impact is severe for 0.75 mm particles. In our experiments the results were similar using 0.5 and 1 g, and so we deduced that batch sizes within this range were acceptable.

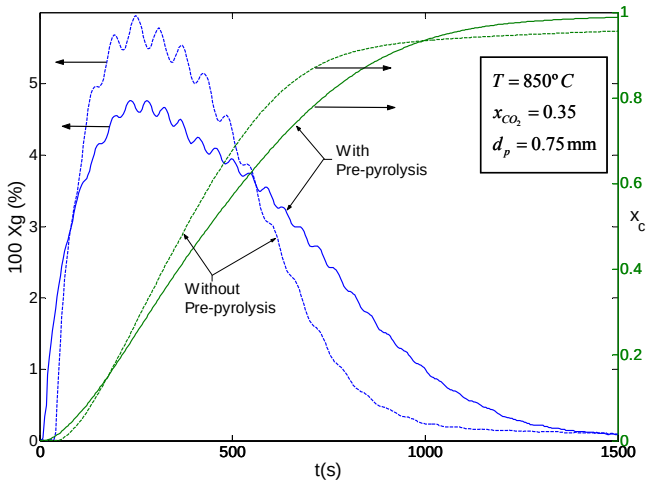

Figure 6.10: Influence of pre-pyrolysis on char reactivity

6.7. Effect of char pre-pyrolysis

As indicated in the experimental section, the char was prepared in an external oven at relatively slow heating rate (30 ºC/min until 900 ºC in N_2 atmosphere). This is one of the most critical factors, which defines the final reactivity and composition of the char. However, as already indicated, this point is not analysed in this work. We analysed here the way of operation once the char is fed into the reactor. We operated our FB in two forms. The first one is as described in Section 4.4, that is, by introducing the char into the reactor, where an atmosphere of pure N_2 prevails. This atmosphere is kept until no CO, CO_2, etc. were detected in the analyser (see Fig. 6.3). This step was called pre-pyrolysis, because it eliminates the remaining volatiles still present in the char after the production phase in the external oven (7.75 %, see Table 6.1). An optional form to initialise the char gasification is undertaken by directly feeding the char into a gas stream with the N_2-CO_2 composition already established. A comparison between the two forms was made as seen in Fig. 6.10 (in Fig. 6.10 the latter case is called "without pre-pyrolysis"). Despite the similarity of the two trends there are some slight differences. The reason of this slightly different behaviour is that the char formed without pre-pyrolysis has a small initial phase where combustion of residual volatiles modified the temperature conditions of the char. This probably slightly alters the final porosity and reactivity of the resulting char. All the results presented in this work correspond to test with pre-pyrolysis.

6.8. Theoretical evaluation of transport effects

Fig. 6.11 displays results from a typical char reactivity test. In particular, the four effectiveness factors defined in Chapter 5 are shown as a function of char conversion. The input data are measurements of the concentration of CO_2 from gasification of char derived from biomass in a test at 20 % CO_2 partial pressure and 925 ºC with a char particle size of 0.75 mm. It is clear that the progress of reaction strongly affects the effectiveness factor. The external effectiveness factor is close to unity for the entire char conversion range, whereas the interphasic and internal factors (and so the

global one) vary widely as reaction proceeds. Both intraparticle and interphase effects contribute to the overall diffusion resistance in the experiment.

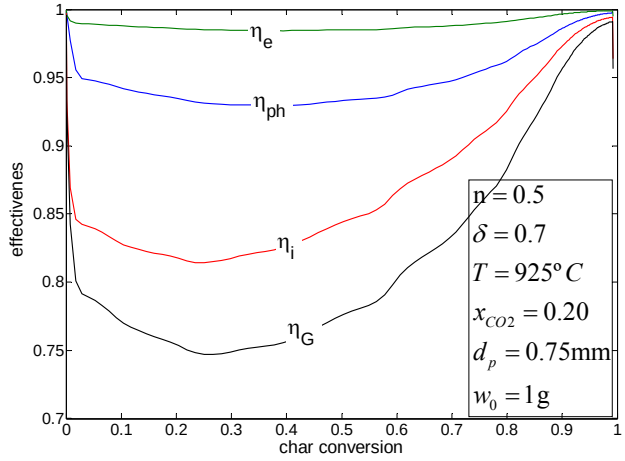

Figure 6.11: Analysis of different effectiveness factors in a typical gasification test

Obviously, the observables depend also on conversion. There is an extreme value in each experiment which leads to a minimum global effectiveness factor, i.e. a maximum resistance to mass transport. In the test referred to, these extremes are: $\omega_{in,\max}$ =0.34, $(X_g/\mathrm{N_a})_{\max}$ =0.14 and $(\mathrm{Da_p}\eta_p)_{\max}$ =0.03. They are reached roughly at x_c ~0.25-0.30 (the same as the minima of the effectiveness factors, as observed in Fig. 6.11). This is just the minimum value, but it could well be taken as representative for the test, since, as shown in Fig. 6.11, the global effectiveness factor is below 0.8 within a wide range of conversion x_c ~0.01-0.6. In spite of the low values of the observables, the computed global effectiveness factor is around 0.8. In fact, initially, this test was thought to be carried out without transport effects. According to the results presented here, however, this cannot be done, and for the evaluation of the char reactivity (intrinsic) a correction factor with a considerable impact should be included to determine the kinetics. Otherwise, to a large extent, these parameters would be falsified by transport effects. Common feature of all gasification tests carried out in this investigation is an external effectiveness factor close to unity.

Figure 6.12 shows the effect of temperature and particle size on different effectiveness factors defined in Chapter 5. More specifically, Fig. 6.12 displays the four effectiveness factors (interphasic, external, external and global) vs. char particle conversion for four of the tests presented in Figs. 6.6-6.8. The tests have been carried out at 20 % CO_2 molar fraction and 900 ºC with 0.75 and 2.1 mm char particles. As seen, the global effectiveness varies with conversion and can be rather low (around 0.55) at 900 ºC for the 2.1 mm char. At higher temperatures, the global effectiveness is practically the same as the intraparticle effectiveness. This clearly shows that the overall process is controlled by the diffusion of CO_2 within the porous char particle. On the other hand, intraparticle and interphasic effects contribute similarly to the overall diffusional resistance in experiments carried out with the small particle size. However, the global resistance is much smaller than that found at larger particle sizes.

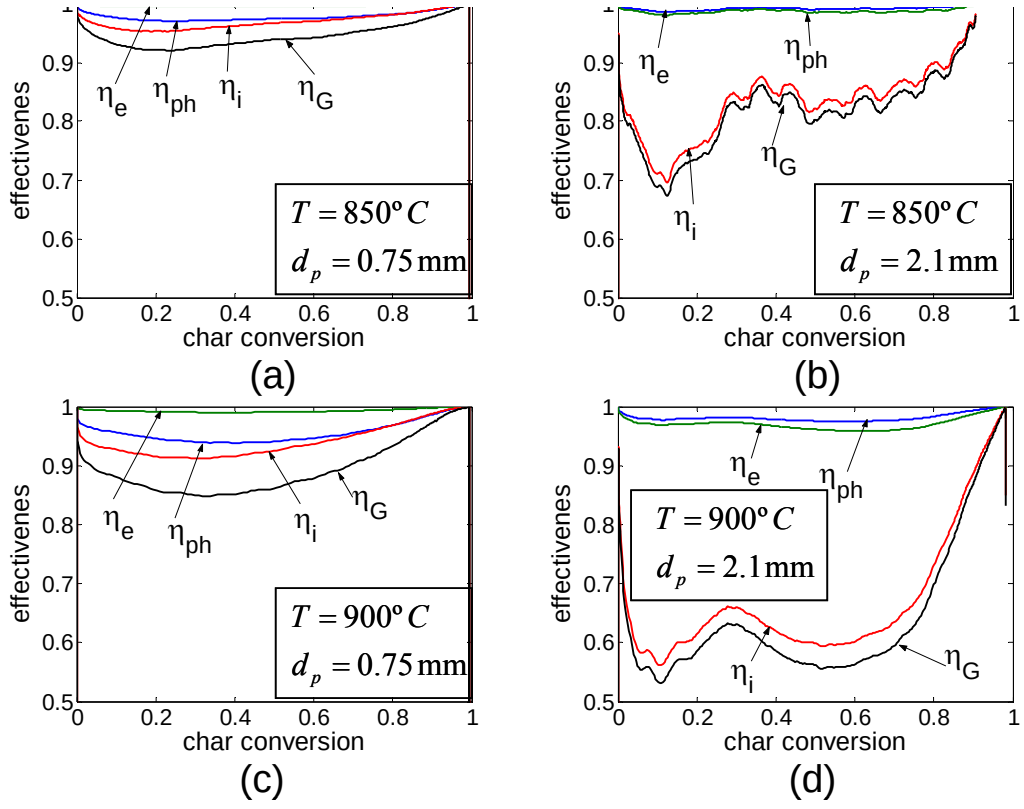

Figure 6.12: Effect of temperature and particle size on different effectiveness factors.

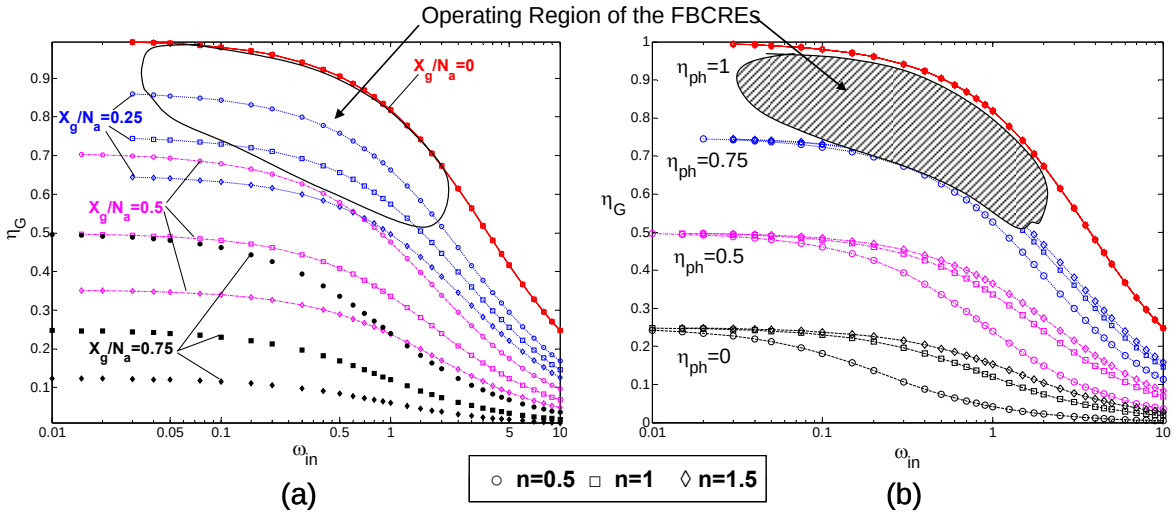

Figure 6.13: Location of the region of operation of the tests carried out on the general charts (a) Chart of observables and (b) Chart of effectiveness factors

Fig. 6.13 presents the regions of the general charts, presented in Chapter 5, in which the FBCREs were carried out. Chart (a) correspond to $Da_p\eta_p$=0 and Chart (b) corresponds to η_e=1. The preceding analysis of the FBCREs test presented here makes it possible to consider these two assumptions valid.

6.9. Correction of apparent kinetics

The char gasification rates were shown to be limited by diffusion effects in most cases. These effects were of minor importance at low temperature (850 ºC), small particle size (0.75 mm) and a batch of 0.5 g and the global effectiveness is near unity. Because the evaluation of the effectiveness factor has a similar uncertainty as a typical measurement, a correction by the effectiveness factor is not actually necessary. However, in most tests carried out here the correction factor is notably below unity, and therefore it should be used to calculate the intrinsic kinetics.

As illustrated in Figs. 6.6 to 6.12, the effectiveness factor varies widely during the course of reaction. Figures 6.11 and 6.12 revealed the existence of a minimum in the η_G–x_c curves located within 0.2-0.4 of char conversion. For most coal chars, the reactivity decreases with increasing conversion, whereas for most biomass chars, it increases. It can also exhibit a maximum or a minimum. So, if a representative reactivity or a unique set of representative kinetics is reported, it should be related to a specific value of conversion. Different conversions, such as 0 % (Scott et al., 2005), 5 % (Bandyopadhyay et al., 1991) and 50 % (Ollero et al., 2003) have been selected. Moreover, other authors use as a representative value of reactivity the average reactivity between two degrees of conversion (Chen et al, 1997; Stoltze et al., 1993; Hansen et al., 1997). In the present study, the range of conversion between 0.2 and 0.8 is taken as the representative. The theoretical basis for the correction was presented in Section 3**.** In principle, the correction procedure can be applied to any char conversion level. In what follows, an average procedure is used just to illustrate the usefulness of the method. By taking the range of conversion between 0.2 and 0.8 as representative, the averaged kinetic constants are

$$k_{\mathrm{ap,av}} = \frac{1}{(0.8-0.2)} \int_{0.2}^{0.8} k_{ap}(x_c)\, dx_c \tag{6.16}$$

$$k_{\mathrm{int,av}} = \frac{1}{(0.8-0.2)} \int_{0.2}^{0.8} k_{\mathrm{ps}}(x_c)\, dx_c = \frac{1}{0.6} \int_{0.2}^{0.8} \frac{k_{ap}(x_c)}{\eta_G(x_c)}\, dx_c \tag{6.17}$$

Also, we define a representative averaged global effectiveness factor as

$$\eta_{\mathrm{G,av}} = \frac{k_{\mathrm{int,av}}}{k_{\mathrm{ap,av}}} \tag{6.18}$$

Table 6.2 shows the results $k_{\mathrm{int,av}}$ $k_{\mathrm{ap,av}}$ and $\eta_{\mathrm{G,av}}$ of some tests carried out in this work. The table included six tests. However, there are only two values of intrinsic kinetics: one for the case *T*=850 ºC and another for *T*=900 ºC. In both tests the CO_2 molar fraction was $x_{CO_2} = 0.20$. The mass of the batch used was 1 g or 2 g and the initial char particle sizes was 0.75 or 2.1 mm. Despite a slight variation, the correction applied seems to be an acceptable approximation, (see for instance: 4.9, 5.5, 5.3 and 6 $(\mathrm{mol \cdot m^{-3}})^{1\text{-}n} \cdot \mathrm{s^{-1}}$ for the case of T=900 ºC). However, the uncertainty of the measures in an FB is high due to the complex processes in it. The differences between 5.5, 5.3 and 6 could be interpreted as an expression of this uncertainty. Therefore, all values

of the kinetic constant determined could be used for a fitting data procedure for the determination of a mean value, for instance by the least squares method.

7. Discussion on assumptions made and parameters used for simulations

Two major assumptions have been made in the calculations above: (1) bubbling regime and (2) isothermal operation. In addition, the use of different values of the parameters (order of reaction, the kinetic parameter, δ given in Eq. (6.11)) can also have relevant effects on the results obtained. These aspects are discussed below.

Table 6.2. Examples of kinetic correction

	d_p=0.75 mm			**d_p=2.1 mm**		
	w_0=1 g T=850 ºC	**w_0=1 g T=900ºC**	**w_0=2 g T=900ºC**	**w_0=1 g T=850 ºC**	**w_0=1 g T=900ºC**	**w_0=2 g T=900ºC**
$k_{int,avg}$	2.42	6.01	5.35	2.08	5.51	4.91
$k_{ap,avg}$	2.21	5.22	4.31	1.42	3.29	2.80
$\eta_{G,avg}$	0.92	0.87	0.81	0.70	0.58	0.57

- x_{CO2}=0.20

7.1. Slug flow

For the calculation of N_a, a bubbling regime of operation was assumed. This condition may be violated in the laboratory scale reactor used, because the narrow internal diameter of the reactor was prompt to operate in slug-flow regime. The correlations used for estimating bed properties and other fluid-dynamic variables (see Table 5.1 in Chapter 5), are strongly affected by this assumption. Stewart and Davidson (1967) presented a simple criterion to test whether slug flow is likely to occur. This criterion establishes an upper limit of the superficial velocity to be used to avoid slugging. According to this criterion, most of the fluidized bed works mentioned in the survey in the beginning of this chapter (Luo et al., 2001a; Scott et al., 2005; Briedis et al., 2002; Spilä, 1986) could have been run in a slugging state. However, according to Baeyens and Geldart (1974) there is a threshold bed-diameter-to-length ratio, over which slugging occurs. According to this ratio the critical height, at which complete slugging sets in, is well above the actual bed height in the experiments. For instance, Luo et al. (2001a) found a critical height of 75 cm according to Baeyens and Geldart's equation, while the actual bed height was 20 cm. Similarly, in our test rig the computed critical value was 70 cm and the actual is 15 cm. Consequently, no slugging should have occurred.

7.2. Isothermicity

Isothermal conditions were assumed throughout this work. This is supported by the relatively low reaction rates of char gasification. However, the larger particle size tested (2.1 mm) and the comparatively high reactivity of WOPS reported in TGA

(Ollero et al., 2003) make us observant about thermal gradients. Different routes have been followed in the literature to determine temperature differences in fluidised beds. Van Aarsen (1985) estimated 3 K maximum decrease in temperature between the emulsion and the particles from a heat balance over the reacting particle. He assumed that the Biot modulus was low and that the heat transfer coefficient was around ~325 W/m^2). Bliek et al. (1985) estimated 4 K as the maximum intraparticle differences in coal-derived char gasification tests. In these calculations, they applied the Prater criterion for strongly diffusion- controlled reactions. In the present work and with the char properties reported by Ollero et al. (2002) and Gómez-Barea et al. (2005a) we have computed intraparticle effects lower than 1 K. In addition, temperature gradients between bubble and emulsion phases are below 0.5 K for heat transfer coefficients such as those reported by Van Aarsen (1985). Therefore, we assume isothermal behaviour along the bed.

7.3. Global kinetic model

The model developed in Chapter 5 adopted a one-parameter (δ) global kinetic model. The calculations made in this work were based on that model and thus, a value of global kinetic parameter δ=0.7 has been assumed. Luo et al. (2001a) assumed char particles of constant diameter (that is δ=1 or uniform model). This assumption should be close to the truth at lower conversion, especially for the experiments carried out at lower temperature and small particle size. At higher conversions, particle size and temperature levels, however, the char particles might shrink considerably from their original diameters. The burn-off behaviour should be in between the uniform and the shrinking-core behaviour (parameter δ between 1 and 0, respectively). Even if the parameter is changed to different values, it still cannot reflect the real change in diameters of char particles. For correct description of the change of char particle diameter during gasification, a more complicated model is needed. However, this would make the model too complex. Therefore, under this uncertainty and in order to cover the whole range of conversion in a proper way an intermediate value of this parameter δ=0.7 was assumed. However, an analysis of the sensitivity of the results to different values (from δ=0.5 to δ=1) showed no major differences, and therefore a δ within the range of 0.5 and 1 does not alter the conclusions presented here.

7.4. Reaction order

The impact of the assumed order of reaction on the computations was checked. Dutta et al. (1977) stated that the rate of C-CO_2 reaction is approximately first order with respect to CO_2 concentration at low pressures (pressure much below atmospheric) for most coals and char-coals. However, it approaches zero order at high pressures (above 15-20 bar). Such dependence may well be explained with the Langmuir-Hinshelwood kinetics, which, as pointed out above, capture the inhibiting effect caused by CO. In general, for near-atmospheric pressure and low partial pressures of CO (differential reactor and small particle char size, for instance) a n^{th}-order reaction correlates rather well experimental results, and the order of reaction is between 0.4 and 0.6 in most cases. Luo et al. (2001a) based on the experiments carried out by Young and Smith (1992) and Hurt et al. (1992) suggested that an order of 0.5 is an adequate approximation for the reaction of carbon. Ollero et al. (2003) surveyed typical kinetic parameters based on a n^{th}-order model kinetics, obtained from CO_2

gasification experiments carried out with different chars derived from biomass. Despite the fact that the activation energy varied widely, the reaction order was found within the range of 0.4 to 0.6 for most chars. Thus, a value of 0.5 was assumed throughout the study.

8. Conclusions

Transport effects have been studied by a set of char reactivity tests carried out in a batch-operated bubbling FB reactor at laboratory-scale. The experimental programme included measurements of the gasification rate of WPOS char of various particle sizes, CO_2 partial pressures, temperatures and initial masses of char batches. The methodology developed in Chapter 5 was applied for the theoretical evaluation of transport effects taking place during the course of FBCRE. The aim was to establish the correct operation of the FB reactor without diffusional or fluid-dynamic effects. For 0.75 mm particle size and the temperature range tested (800-925ºC) the diffusional effects were proven small enough for batch sizes of 0.5 g. Under these conditions global effectiveness was above 0.95. However, coarser particles showed global effectiveness factor well below this value. The batch size was revealed to have an important effect above 0.5 g, whereas the fluid-dynamic resistance under the operating conditions of the rig was negligible. The CO_2 concentration was proven to influence, but its role was secondary compared with temperature and char size. At 925 ºC temperature and 2.1 mm initial char particle size, a global effectiveness factor as low as 0.50 was found for a reasonably small charge of 1 g.

The results of this work have solved the difficulties initially found in the operation of a laboratory FB reactor and have proven useful for selecting optimum (minimum transport effects) conditions for FBCREs. The kinetics obtained after the removal of transport effects is consistent. We have learnt that optimum does not always mean the smallest char size, batch size and superficial velocity. Practical difficulties can make it impossible to have a completely kinetically-controlled regime. To maintain good fluidising condition, a fixed value of superficial velocity of 0.8 m/s was established in our rig. As a result, the feeding of the FB at the top with too small char size was problematic due to severe entrainment. The decision has been to carry out experiments with 1 g of initial char mass and particle size of 0.75 mm with a gas velocity of 0.8 m/s. This decision made it possible to operate the rig with reasonable technical confidence. At 925 ºC this decision leads to the need for correcting the apparent kinetics by a factor of roughly 0.7. In fact, the complete suppression of diffusional effects is not mandatory if the correction for the apparent reactivity can be made with confidence. Often, transport effects in FBCRE cannot be completely eliminated for different reasons and, thus, the procedure developed in this work gives reasonably accurate corrections for the determination of the intrinsic reactivity from the observed gasification rate. This work also would be useful to support the design of new rigs for the determination of char reactivity in order to avoid physical interferences during the determination of intrinsic char gasification reactivity. This kind of analysis is strongly recommended for forthcoming FBCRE works to properly validate the experimental reactivity data with a minor effort.

Chapter 7

Conclusions

1. Aim and significance

The actual reaction rate of a char particle at a given position and instant in an FB gasifier depends on the char particle size, its burn-off history, the concentration of gas species, and the temperature at that position in the reactor.

To evaluate the gasification of char particles in an FB gasifier, we have distinguished three main approaches: a pseudo-empirical approach (PEA), a rigorous approach (RA) and a combined approach (CA). The PEA is widely used because avoids the need to solve a particle model for the char particles. If diffusional effects inside char particles are present, however, this method is questionable. The uncertainty of the FB gasifier models using this approach is high. The RA is accurate and consistent but is computationally complicated. When diffusional effects are likely to be present, it is, in theory, preferable. The CA is a combination of both methods and it is widely used in modelling FB coal and biomass gasifiers. Simple particle models like SCM or UM or GM are used. However, it is rather difficult to assess the validity of the model when using this approach. In most cases kinetic expressions are not adequate and the model chosen to describe the evolution of char particles is not realistic in most cases.

Aiming at consistency, in this work a pseudo-rigorous approach (PRA) is proposed. In it, a simplified, but still rigorous, particle-kinetic model is included. It combines the benefits of the rigorous and pseudo-empirical approaches. In addition, the intrinsic reactivity is an input, which must be determined in the laboratory for the same biomass and the char must be generated under conditions, similar to the real situation in which the FB gasifier model will be used.

The motivation for this thesis is to pave the way towards the PRA for modelling of char particles in an FB gasifier. This task has been presented in two parts:

1. The first part presents a method, which makes it possible to solve any non-catalytic gas-solid reaction involving a single oxidant. This is the case, for instance, of char gasification with CO_2 or with H_2O. The model is applied to the modelling of char gasification with CO_2, and it is validated by comparison with TGA experiments carried out with single char particles.

2. The second part resolves the difficulties caused by transport effects when an FB is used for determination of the kinetics. It presents a simple methodology to evaluate transport effects during the determination of char reactivity in an FB. The method makes it possible to avoid mass-transfer interferences during the experiments. In addition, when transport effects cannot be fully eliminated, it further makes a correction applied to the observed reactivity in order to determine the intrinsic reactivity.

2. List of conclusions

Part I: Modelling and analysis of gasification of a single char particle

Existing char gasification kinetic models

1. Although numerous particle-kinetic studies have confirmed strong diffusional effects under common gasification conditions, these transport effects are usually disregarded when modelling FB coal and biomass gasifiers. A review of the existing literature leads to the conclusion that this simplification, disregarding of tranport effects, is often used for the purpose of obtaining reasonable and tractable models, but it is seldom justified in literature publications.

2. The use of simple particle models, such as UM, SCM or GM, is not generally appropriate under the operating conditions of FB biomass gasifiers.

New method for solving gas-solid reactions

3. Analytical and approximate methods for evaluating gas-solid reactions were extensively reviewed. The conclusion is that most techniques and models available are limited for one (or both) of the following reasons: They are (1) only applicable to first-order kinetics with respect to the gas or solid reactant and/or (2) do not explicitly make allowance for structural changes during the progress of reaction.

4. A new approach, which refines past trials was developed. The simple method of solution makes it possible to incorporate non-linear chemical reaction rate and the changes in porous structure during conversion of a char particle by incorporating different structural profile models and effective properties.

5. The methodology developed in this work is based on the quantize method for decoupling the solid and gas conservation equations and on perturbation and matching techniques for approximating the gas conservation equation. With this strategy, the calculation of gas concentration and solid conversion at any time and position is reduced to the solution of two coupled algebraic equations. This makes it possible to reduce time consumption of computations by three orders of magnitude compared to numerical procedures, like collocation of finite difference methods.

6. The model compares favorably with the exact (numerical) solution for a variety of cases, using non-linear kinetic models like Langmuir-Hinshelwood and complex structural functions to represent the changes in available internal surface with time.

7. The model can be applied to non-catalytic reactions where only one reaction is involved. This is the case of gasification of a char particle, where only a single oxidant is considered (char with CO_2 or char with H_2O).

Application to char gasification

8. An experimental program was carried out in TGA, including measurements of the gasification rates of WPOS at four different particle sizes (0.060, 0.9, 1.2 and 2.1 mm), three CO_2 partial pressures (0.20, 0.35 and 0.50 bar) and four temperatures (800, 850, 900 and 950ºC).

9. The results found experimentally in TGA indicated the presence of considerable diffusional resistances in the gasification of even relatively small single char particles at practical temperatures in real gasification systems.

10. The model developed was applied to TGA experiments. The predictions were in reasonable agreement with the experimental results. In addition, the model made it possible to identify the contribution of the effects that generate physical interaction in tests for determination of char reactivity in gasification.

11. Intraparticle mass limitations were identified as the main factor responsible for the high resistance found under the test conditions in the TGA. External heat and mass transfer were also found to play a relevant role.

Part II: Mass transfer effects during char gasification reactivity tests in lab-scale fluidised bed

Mass transfer effects during determination of gas-solid reaction kinetics in FB

12. Experiments carried out for determination of kinetics in a laboratory-scale FB should avoid the many difficulties caused by the complex flow pattern in FBs. The design of an FB reactor and the choice of its operating conditions, such as the selection of bed material, mass of inventory, surface velocity, etc., should be adjusted to avoid diffusion interferences.

13. A simple methodology was developed for the assessment of mass transport effects during kinetic experiments in FBs (FBKE), where isothermal conditions are assumed and only one reaction takes place.

14. The approach combines a particle-kinetic model with a simple two-phase flow model. The parameters resulting from the model are expressed in terms of three observable quantities, making it possible to evaluate the transport effects in a straightforward way from gas concentration measurements.

15. The analysis facilitates the selection of optimum operating conditions for FB tests to determine gas-solid kinetics. Moreover, it can support dimensioning of new rigs designed for this purpose.

16. The methodology developed can be applied to other isothermal systems to estimate the influence of diffusional effects on the observed reaction rate, i.e., char oxidation and other catalytic or non-catalytic systems.

Application to char gasification reactivity tests in lab-scale fluidised bed

17. Existing FB char reactivity experimental (FBCRE) work shows that transport effects are often present, but a quantitative treatment to determine them is not reported in most cases.

18. Char gasification experiments were carried out in a 26-mm ID bench-scale FB reactor. The char used was wood matter from pressed-oil stone (WPOS), also called *orujillo*. The gasification rates of WPOS were measured at two particle sizes (0.75 and 2.2 mm), two CO_2 partial pressures (0.20 and 0.35) and three temperatures (850, 900 and 925 ºC) using several initial char batches.

19. The model developed in Chapter 5 was applied to this set of FB char reactivity experiments at laboratory scale in order to evaluate mass transport effects.

20. Overall effectiveness factors (a correction to the observed gasification rate for obtaining the intrinsic char reactivity) as low as 0.50 were calculated for the worst scenario (largest Thiele module).

21. When transport effects cannot be completely eliminated, this procedure gives reasonably accurate corrections for the determination of the intrinsic reactivity from the observed gasification rate.

22. This work contributes to making it easier to overcome the difficulties initially found in the operation of the laboratory FB reactor and has proven useful for selecting optimum conditions (minimum transport effects) for FBCREs.

3. Future work

Although the situation in full-scale gasifiers is much more complex than the one in a simple laboratory device, the model developed in Part 1 of this study is a first step toward estimating the char particle gasification rate in an FB gasifier. For the prediction of real gas composition and char-consumption rate, it is necessary to extend the model developed here, in particular, to make it capable of simultaneously considering two heterogeneous char-gasification reactions (with CO_2 and with H_2O in atmospheric gasifiers) and the water-gas shift reaction. This treatment is currently under development by the author.

The methodology for evaluating the mass transport effect in a lab-scale FB is valid for catalytic and non-catalytic gas-solid reactions in isothermal conditions when one reaction occurs. This is the case, for instance, of tests of FB CO_2-char gasification reactivity. For other systems these assumptions need to be assessed prior to application of the method presented here. For example, in FB O_2-char reactivity (char combustion) tests, the isothermal assumption may be violated, depending on the char-to-inert ratio, oxygen concentration, particle size and intrinsic reactivity of the char.

In reactivity tests of H_2O-char gasification kinetics, it is necessary to consider a second (independent), homogeneous reaction, for instance, the water-gas shift reaction. These cases are somewhat more complicated. However, the methodology presented here can be readily extended to cover such cases, although the analytical treatment becomes more complex and an analytical solution can no longer be obtained.

Nomenclature

a	parameter, –
A	Frequency factor
Ar	Archimedes number, defined by $\mathrm{Ar} = d_s^3 \rho_g \left(\rho_s - \rho_g\right) g / \mu^2$,–
b	stoichiometrical coefficient, –
B(X)	conversion-dependant Prater number, –
c	gas or solid concentration, mol·m^{-3}
c_p	gas thermal coefficient, J·K^{-1}·mol^{-1}
C	dimensionless concentration, –
C^*	root of the function $R(C)$, –
d_b	bubble diameter, m
d_c	the instantaneous average diameter of the char particles, m
d_p , d_{c0}	the initial average diameter of the char particles, m
d_s	the average diameter size of ofite, m
d_{or}	diameter of holes on the distributor, m
d_t	diameter of crucible inside the TGA, m
dx_c / dt	carbon conversion rate, s^{-1}
D_e	effective diffusivity, m^2·s^{-1}
D_m , D_g	molecular diffusivity, m^2·s^{-1}
$\mathrm{Da_p}$	particle Damköhler number, –
$\mathrm{Da_R}$	Damköhler number at reactor scale, –
D_t	bed diameter, m
E	activation energy, J·mol^{-1}
f	structural profile, function of local conversion, also a general function, –
F	part of reaction rate which depends on local conversion in Chapters 2-5, –
g	function of conversion, –; also acceleration of gravity, 9.81 m^2·s
G	function of local conversion, also transfer function (in Chapter 6) , –
h	function of dimensionless position, – ; also heat transfer coefficient, W·m^{-2} K
h_{cv}	convective film coefficient, W·m^{-2}K
h_{rd}	radiative film coefficient, W·m^{-2} K
H	height of the pipe containing the FB, m
IR	definite integral of $R(C)$ between 0 and 1, –
j_D	Chilton-Colburn mass j-factor , –

j_h Chilton-Colburn heat j-factor, –

k n^{th}-order kinetic constant, $(mol/m^3)^{1-n}\cdot s^{-1}$

k_a apparent kinetic constant for n^{th}-order kinetics, $(mol/m^3)^{1-n}\cdot s^{-1}$

k_b interchange coefficient for gas reactant (CO_2) between the bubble and emulsion, s^{-1}

k_e effective conductivity, $W\cdot m^{-1}\cdot K^{-1}$

k_G external mass-transfer coefficient, $m\cdot s^{-1}$

k_m molecular conductivity, $W^{-1}m^{-1}K^{-1}$

k_{ps} n^{th}-order pseudo-kinetic constant, $(mol/m^3)^{1-n}\cdot s^{-1}$

k' constant of proportionality, –

K parameter in the Michaelis-Menten kinetic equation, –

K_v apparent pseudo-first order chemical kinetic constant in the bed, s^{-1}

l_{or} spacing between adjacent holes on the distributor, m

L , L_e geometric or equivalent length, m

Le Lewis number, –

L_f bed height, m

L_{mf} bed height at minimum fluidisation conditions, m

m geometric coefficient (m=0 slab, m=1 cylinder and m=2 spherical)

M modified Thiele modulus, –

M_C carbon molecular weight, $g\cdot mol^{-1}$

M^* modified Thiele modulus, –

n order of reaction, –

N number of dimensionless radial points in the computational grid, –

N_a dimensionless number, –

N_t hole density of the distributor, m^{-2}

NTU number of transfer units, –

p pressure, bar; also function of local conversion in Chapter 4, –

q function of local conversion, –

Q_g gas volumetric flowrate under normal conditions, $Nm^3\cdot s^{-1}$

r radial coordinate, m

r_{ch} gasification rate, $kg\cdot s^{-1}$

$r(c_A)$ part of the reaction rate which varies with gas concentration, $mol\cdot m^{-3}\cdot s^{-1}$

$(-r)$ reaction rate, $mol\cdot m^{-3}\cdot s^{-1}$

$r(c,T)$ reaction rate term which varies with gas concentration and temperature, $mol\cdot m^{-3}\cdot s^{-1}$

R reactivity, s^{-1}; also particle radius, m

$R(C)$ dimensionless reaction rate, –

R_g universal constant of gases, J·K·mol^{-1}

$(-R)$ actual or observed reaction rate on volumetric basis, mol/m^3/s

R' derivative of $R(C)$ evaluated at z=1, –

Re_{mf} Reynolds number at minimum fluidisation, $\mathrm{Re}_{mf} = d_s \rho_g u_{mf} / \mu$,–

Re_p Reynolds particle number, $\mathrm{Re}_p = d_s \rho_g u_0 / \mu$,–

Sc Schmidt number, –

Sh Sherwood number,–

t time, s

T temperature, K

T' dimensionless temperature, –

u_b velocity of bubble, m·s^{-1}

u_{br} relative velocity of bubble, m·s^{-1}

u_{mf} minimum fluidised velocity, m·s^{-1}

u_0 superficial velocity, m·s^{-1}

V_p char volume, m^3

w solid sample weight at a given instant, kg

w_s inert (ofite) inventory of the FB, kg

x gas molar fraction, –

X local particle conversion, –

X_p , x_c overall or global particle conversion, –

X_g gas conversion, –

z dimensionless coordinate, –; also axial coordinate in Chapter 5, m

Greek symbols

α kinetic-particle parameter, –

β parameter, –

β_i Prater number or internal dimensionless heat of reaction, –

β_e external dimensionless reaction heat, –

γ Arrhenius number, –

δ kinetic parameter, –

δ_t thermal correction factor of internal effectiveness factor , –

δ_N non-equimolar correction factor of internal effectiveness factor, –

ε local solid porosity, –

ε_b fraction of bubble in bed, (m^3 bubble)·(m^{-3} bed)

ε_c char bed hold-up, (m^3 char)·(m^{-3} bed)

ε_{mf} porosity at minimum fluidisation conditions, –

ε_v volumetric expansion factor, –

ε_c char emissivity, –

η_e external effectiveness factor, –

η_i non-isothermal intraphase effectiveness factor, –

η_i^{iso} isothermal intraphase effectiveness factor, –

η_G overall or global effectiveness factor, –

η_{GOT} Gottifredi's effectiveness factor, –

η_p particle scale effectiveness factor, –

η_{ph} interphase effectiveness factor, –

η_R Ramachandran effectiveness factor, –

η^* critical effectiveness factor, defined, –

$\varsigma(X)$ parameter, function of local conversion, –

ϕ Thiele modulus, –

λ parameter, –

μ gas viscosity, $Pa \cdot s^{-1}$

ν_c volumetric char proportion in the bed inventory, m^3 char m^{-3} particles

ξ ratio of radiative to convective heat film coefficients, –

ξ^{exact} ratio of radiative to convective heat fluxes, –

ρ gas density, $kg \cdot m^{-3}$

ρ_c density of char, $kg \cdot m^{-3}$

ρ_g gas density, $kg \cdot m^{-3}$

ρ_s density of inert, $kg \cdot m^{-3}$

σ Stefan-Boltzmann constant, $W \cdot m^{-2} \cdot K^{-1}$

τ dimensionless time, –

τ_t char tortuosity, –

τ' modified dimensionless time, given by $\tau' = \tau \cdot k'$, –

τ_{ref} reference dimensionless time, –

ω Weisz-Prater module, –

ΔT temperature drop between bulk gas and char surface, ºC

$(-\Delta H_R)$ Enthalpy of reaction, $J \cdot mol^{-1}$

$\Theta(X)$ function of local conversion, –

Subscripts

A reactant A

B	reactant B
av	average (through the bed height L_f) or (through char conversion)
ap	apparent
b	bubble conditions
e	emulsion conditions
i	intrinsic, also dimensionless position index in the computational grid
in	inlet gas conditions
int	intrinsic
j	dimensionless time position in the computational grid
j	dimensionless time position in the computational grid, also any char conversion
m	maximum bubble diameter
out	exit conditions
s	surface conditions
0	at initial time, bulk-gas phase
50	50% char conversion

Superscripts

int	intrinsic
k	k^{th}- test

Symbols and Abbreviations

BFB	Bubbling fluidized bed
CA	Combined approach
CFB	Circulating fluidized bed
EM	Thermodynamic equilibrium model
FB(s)	Fluidised bed(s)
FBCRE	Fluidised bed char reactivity experiments
FBKE	Fluidised bed kinetic experiments
FBG	Fluidised biomass gasifier
GM	Grain model
LH	Langmuir-Hinshelwood.
n.a.	not available.
NAEF	No analytical expression found
PEA	Pseudo-empirical approach
PRA	Pseudo-rigorous approach
RA	Rigorous approach
SCM	Shrinking core model
TE(s)	Transport effect(s)
TGA	Termogravimetric analyser
UCM	Exposed core model
UM	Uniform model

References

Adánez, J., de Diego, L. F., 1993. Reactivity of lignite chars with CO_2: influence of the mineral matter. International Chemical Engineering 33, 656–662.

Adánez, J., Miranda, J. L., Gavilán, J. M., 1985. Kinetics of a lignite-char gasification by CO_2. Fuel 64, 801–804.

Adschiri, T., Shiraha, T., Kojima, T., Furusawa, T., 1986. Prediction of CO_2 Gasification Rate of Char in Fluidized-Bed Gasifier. Fuel 65, 1688–1693.

Agarwal, A.K., Sears, J.T. 1980. The coal char reaction with CO_2–CO gas Mixtures. Industrial & Engineering Chemistry Process Design and Development, 19, 364–371.

Alcantarilla, S., 2002. Determinación de la cinética de gasificación de orujillo con CO_2 mediante análisis de termogravimetría. Estudio de resistencias difusionales y desarrollo del método experimental. Master Thesis. Project no. 2726. 2002-01-21. ESI (University of Seville, Spain).

Arri, L.E., Amundson, N.R., 1978. An analytical study of single particle char gasification. A.I.Ch.E Journal, 24, 72–87.

Ashman, P. J., Mullinger, P. J., 2004. Research issues in combustion and gasification of lignite. Fuel 84, 1195–1205.

Avedesian, M.M., Davidson, J. F., 1973. Combustion of Carbon Particles in a Fluidized-Bed. Transactions of the Institution of Chemical Engineers 51, 121-131.

Aznar, M. P., Garcia-Gorria, F. A., Corella, J., 1989. Minimum and maximum velocities for fluidization for mixtures of agricultural and forest residues with a second fluidized solid. Preliminary data and results with sand-sawdust mixtures. International Chemical Engineering 32, 1, 95–102.

Bacon, D.W., Downie, J., Hsu, J.C., Peteres, 1985. J. Modelling of fluidised bed wood gasifiers. In: R.P. Overend, T.A. Milne and K.L. Mudge, Editors, Fundamentals of thermochemical biomass conversion, Elsevier Applied Science Publishers, London, UK, 717–732.

Baeyens, J., Geldart. D., 1974. An investigation into slugging fluidized beds. Chemical Engineering Science, 29, 255–265.

Ballal, G., Li, C.H., Glowinski, R., Amundson, N. R., 1989. Single particle char combustion and gasification. Computer Methods in Applied Mechanics and Engineering, 75, 467–479.

Bandyopadhyay, D., Chakraborti, N., Ghosh, A., 1988. Re-evaluation of heat transfer effects in carbon gasification reaction. Steel Research 59, 537–541.

Bandyopadhyay, D., Chakraborti, N., Ghosh, A., 1991. Heat and mass transfer limitations in gasification of carbon by carbon dioxide. Steel Research 62, 143–151.

Barrio, M., Hustad, J.E., 2000. CO_2 gasification of birch and the effect of CO

inhibition on the calculation of chemical kinetics. In: Bridgwater A.V, (Ed). Proceedings of the conference: Progress in Thermochemical Biomass Conversion. Tyrol, Austria.

Belleville, P., Capart, R., 1983. A model for predicting outlet gas concentration from a wood gasifier. In: A.V. Bridgwater, Editor, Thermochemical processing of biomass, Butterworks, London, UK, 217–228.

Bhat, A., Bheemarasetti, J. V. R., Rao, T. R., 2001. Kinetics of rice husk char gasification. Energy Conversion and Management 42, 2061–2069.

Bhatia, S.K., Perlmutter, D.D., 1980. A random pore model for fluid-solid reactions: I. Isothermal, kinetic control. A.I.Ch.E. Journal 26, 379–386.

Bhatia, S.K., Perlmutter, D.D., 1981. A random pore model for fluid-solid reactions: II. Diffusion and transport effects. A.I.Ch.E. Journal 27 247–254.

Bhatia, S.K., Gupta, J.S., 1992. Mathematical modelling of gas-solid reactions: Effect of pore structure. Reviews in Chemical Engineering, 8, 177–258.

Bilodeau, J. F., Thérien, N., Proulx, P., Czernik, S., Chornet, E., 1993. A mathematical model of fluidized bed biomass gasification. The Canadian journal of chemical engineering 71,549–577.

Bjerle, I., Eklund, H., Svensson, O., 1980. Gasification of Swedish Black Shale in the Fluidized-Bed - Reactivity in Steam and Carbon-Dioxide Atmosphere. Industrial & Engineering Chemistry Process Design and Development 19, 345-351.

Bliek, A., Lont, J. C., van Swaaij, W. P. M., 1986. Gasification of Coal-Derived Chars in Synthesis Gas-Mixtures under Intraparticle Mass-Transfer-Controlled Conditions. Chemical Engineering Science 41, 1895–1909.

Brem, G., 1990. Mathematical modelling of coal conversion processes. Ph.D. Dissertation. University of Twente.

Brem, G., Brouwers, J.J.H., 1990a. Analytical solutions for non-linear conversion of a porous solid particle in a gas—I. Isothermal conversion. Chemical Engineering Science 45, 1905–1913.

Brem, G., Brouwers, J.J.H., 1990b. Analytical solutions for non-linear conversion of a porous solid particle in a gas—II. Non-isothermal conversion and numerical verification. Chemical Engineering Science 45, 1915–1924.

Bridgwater, AV., 1995. The technical and economic feasibility of biomass. Fuel 74, 631–653.

Briedis, A.J., Ross, D.P., Mullinger, P.J., Ashman, P.J., 2002. Commissioning of a laboratory-Scale, atmospheric-pressure fluidised-bed gasifier. Proceeding of the 9th Annual APCChE congress and CHEMECA, September 2002, Christchurch, NZ, paper 325.

Brunello, S., Flour, I., Maissa, P., Bruyet, B., 1996. Kinetic study of char combustion in a fluidized bed. Fuel 75, 536–544.

Buekens, A.G., Schoeters, J.G., 1985. Modelling of biomass gasification. In: R.P. Overend, T.A. Milne and K.L. Mudge, Editors, Fundamentals of thermochemical biomass conversion, Elsevier Applied Science Publishers, London, UK, 619–689.

Carberry, J. J., Ed. 1976. Chemical and Catalytic Reaction Engineering. McGraw-Hill, New York.

Carberry, J. J., Kulkarni, A. A., 1973. The non-isothermal catalytic effectiveness factor for monolith supported catalysts. Journal of Catalysis 31, 41–50.

Chang, Y.H., 1988. A mathematical model for the gasification of a single char article of coal. International Chemical Engineering, 28, 520–526.

Chejne, F., Hernandez, J.P., 2002. Modelling and simulation of coal gasification process in fluidised bed. Fuel 81, 1687–1702.

Chen, G., Andries, J., Spliethoff, H., 2003. Biomass conversion into fuel gas using circulating fluidised bed technology: the concept improvement and modelling discussion. Renewable Energy 28, 985–994.

Chen, G., Spliethoff, H., Andries, J., Glazer, M. P., Yang, L. B., 2004. Biomass gasification in a circulating fluidized bed–Part I: preliminary experiments and modelling development. Energy Sources 26, 485–498.

Chen, G., Yu, Q., Sjöström, K., 1997. Reactivity of char from pyrolysis of birch wood. Journal of Analytical and Applied Pyrolysis, 491–499.

Chen, J.S., Gunkel, W.W., 1987. Modeling and simulation of co-current moving bed gasification reactors — part I. A non-isothermal particle model. Biomass 14, 51–72.

Chornet, E., Baldoroso, J.M., Tarki, H.T., 1979. Kinetic expressions for coal char-gas reactions. Fuel 58, 395–397.

Ciesielczyk, E., Gawdzik, A., 1993. Non-isothermal fluidized-bed reactor model for char gasification, taking into account bubble growth. Fuel 73, 105–112.

Corella, J., 1980. Kinetics of Non-Catalytic Gas-Solid reactions in semi-continuous integral fluidized-bed reactors - Application to the determination of the kinetics of the fluorination of uranium tetrafluoride. Chemical Engineering Science 35, 25–32.

Corella, J., Sanz, A., 2005, Modeling circulating fluidized bed biomass gasifiers. A pseudo-rigorous model for stationary state. Fuel Processing Technology, 86, 1021–1053.

Czernik, S., Koeberle, P.G., Jollez, P., Bilodeau, J.F., Chornet, E., 1992. Gasification of residual biomass via the Biosyn fluidized bed technology. In: Glasgow: Advances in thermochemical biomass conversion, A.V. Bridgwater, Ed., Elsevier, Amsterdam.

Dasappa, S., Paul, P. J., Mukunda, H. S., Uhrinivas, S., 1994. The gasification of wood-char spheres in CO_2-N_2 mixtures: analysis and experiments. Chemical Engineering Science 49, 223–232.

Davidson J.F., Harrison D., 1963. Fluidised particles. Cambridge University Press. London.

DeGroot, W.F., Shafizadeh, F., 1984. Kinetics of gasification of Douglas Fir and Cottonwood chars by carbon dioxide. Fuel, 63, 210–216.

Del Borghi, M., Dunn, J.C., Bischoff, K.B., 1976. A technique for solution of the equations for fluid—solid reactions with diffusion. Chemical Engineering Science 31, 1065–1069.

Dennis, J.S., Lambert, R.J., Milne, A.J., Scott, S.A., Hayhurst, A.N., 2005. The kinetics of combustion of chars derived from sewage sludge. Fuel 84, 117–126.

Doraiswamy, L.K., Bijawat, H.C., Kunte, M.V., 1959. Chlorination of ilmenite in a fluidized bed. Chemical Engineering Progress, 55, 80.

Doraiswamy, L.K., Sharma, M.M., 1984. Heterogeneous Reactions. Analysis, examples and reactor design, Vol.1. New York, Wiley.

Dudukovik, M.P., Lamba, H.S., 1978. Solution of moving boundary problems for gas-solid noncatalytic reactions by orthogonal collocation. Chemical Engineering Science 33, 303–314.

Dutta, S., Wen, C.Y., Belt, R.J, 1977. Reactivity of Coal and Char. 1. In Carbon Dioxide Atmosphere Industrial Engineering Chemical Process Design and Development 16, 20–30.

Elliot, M.A., 1981.Chemistry of coal utilization (Second supplementary volume), New York. Wiley.

Ergudenler, A., Ghaly, A.E., Hamdullahpur, F., Al-Taweel, A.M., 1997. Mathematical modeling of a fluidized bed gasifier. Part I—model development. Energy Source 19, 1065–1084.

Ergun S., 1956. Kinetics of the reaction of carbon dioxide with carbon. Phys. Chem. 60, 480–485.

Fiaschi, D., Bettagli, N., Desideri, U., 1995. A Biomass Combustion—Gasification model: validation and sensitivity analysis. Journal of Energy Resources Technology, A.S.M.E. Transaction 117, 329–336.

Fiaschi, D., Michelini, M., 2001. A two-phase one-dimensional biomass gasification kinetics model. Biomass & Bioenergy 21, 121–132.

Fogler, H.S., 1992. Elements of Chemical Reaction Engineering. Prentice-Hall, Englewood Cliffs, New Jersey.

Förtsch, D., Schnell, U., Hein, K.R.G., 2001. The effect of boundary layer diffusion on the overall rate of heterogeneous reactions. Chemical Engineering Science 56, 4439–4443.

Frank-Kamenetskii, D.A., 1955. Diffusion and heat exchange in chemical kinetics, Princeton University Press. Princeton.

Froment, G.F., Bischoff, K.B., 1990. Chemical Reactor Analysis and Design, 2nd Ed., New York. Wiley.

Gardner, N.C., Samuels, E., Wilks, K., 1974. Catalysed hydrogasification of coal chars. Advances Chemical Series, 131, 217–236.

Gasash Project, 2005. Improvement of the Economics of Biomass/waste Gasification by Higher Carbon Conversion and Advanced Ash Management. Project N°: ENK5-2001-00635.

Gavalas, G.R., 1980. A random capillary model with application to char gasification at chemically controlled rates. A.I.Ch.E. Journal 26, 577–585.

Gavalas, G.R., 1981. Analysis of char combustion including the effect pore enlargement. Combustion Science Technology 24, 192–197.

Golfier, F., Mermound, F., Salvador, S.J.L., Dirion, van de steene, L., Girand, P., 2004. Modelling of particle gasification at particle scale: How to select the best assumptions in the scope of fixed bed modeling. 2nd World conference on Biomass for Energy and Climate protection.

Gómez-Barea, A., Ollero, P., Arjona, R., 2005a. Reaction-diffusion model of TGA gasification experiments for estimating diffusional effects. Fuel 84, 1695–1704.

Gómez-Barea, A., Arjona, R., Ollero, P., 2005b. Pilot plant gasification of olive stone: a technical assessment. Energy & Fuels, 19, 598–605.

Gómez-Barea, A., Ollero, P., 2006. An approximate method for solving non-catalytic gas-solid non-catalytic reactions. Chemical Engineering Science 61, 3725–3735.

Gómez-Barea, A., Ollero, P., Fernández-Baco, C., Villanueva, A., Salvador, L., 2006a. Evaluation of mass transport effects in a bench-scale BFB gasifier designed for kinetic determination. Proceedings of 19th International Conference of Fluidised Bed Combustion. 20-24 May 2006. Paper 65. (In press)

Gómez-Barea, A., Ollero, P., Leckner, B., 2006b. Transport effects during determination of gas-solid kinetics in fluidised bed. Submitted for publication in Chemical Engineering Science (January 2006).

Gómez-Barea, A., Leckner, B., Ollero, P., Fernández-Baco, C., Salvador, L., 2006c. Mass transfer effects during char gasification reactivity tests in a laboratory-scale fluidised-bed. Submitted for publication in Industrial & Engineering Chemistry Research (April 2006).

Gómez-Barea, A., Ollero, P., Fernández-Baco, C., 2006d. Diffusional effects in CO_2 gasification experiments with single biomass char particles. Part I. Experimental investigation. Energy & Fuels. In press.

Gómez-Barea, A., Ollero, P., Villanueva, A., 2006e. Diffusional effects in CO_2 gasification experiments with single biomass char particles. Part II. Theoretical predictions. Energy & Fuels. In press.

Gómez-Barea, A., Campoy, M., Ollero, P., Fernández-Pereira, C., 2006f. Pilot plant experiences with fluidised bed gasification of orujillo and MBM. Proceedings of 19th International Conference of Fluidised Bed Combustion. 20-24 May 2006. Paper 66. (In press).

Goring, G. E., Curran, G. P., Tarbox, R. P., Gorin, E., 1952. Kinetics of Carbon Gasification by Steam - Effect of High Temperature Pretreatment on Reactivity of Low Temperature Char to Steam and Carbon Dioxide. Industrial & Engineering Chemistry 44, 1051-1057.

Gottifredi, J.C., Gonzo, E.E., Quiroga, O., 1986. Effectiveness factor calculations. In: S. Whitaker and A. Cassano, Editors, Concept and Design of Chemical Reactors, (Chapter 2). Gordon and Breach Publisher, London.

Gottifredi, J.C., Gonzo, E.E., 1996. Approximate expression for predicting concentration and temperature profiles inside a catalyst pellet. Chemical Engineering Science 51, 835–837.

Gottifredi, J.C., Gonzo, E.E., 2005. Approximate expression for the effectiveness factor estimation and a simple numerical method for concentration profile calculation in porous catalyst. Chemical Engineering Journal, 109, 83–87.

Grace, J. R., 1986. Fluid beds as chemical reactors, in Geldart, D. (Ed.), Gas Fluidization Technology, John Wiley & Sons Ltd.

Groeneveld, M., van Swaaij, W., 1980. Gasification of Char Particles with CO_2 and H_2O. Chemical Engineering Science 35, 307–313.

Gururajan, V.S., Agarwal, P.K., Agnew, J.B., 1992. mathematical modelling of fluidized bed coal gasifiers. Trans IChemE, 70, 211–238.

Hamel, S, 2001.Mathematische Modellierung und experimentelle untersuchung der vergasung verschiedener fester brennstoffe in atmosphärischen und druckaufgeladenen staionaären wirbelschichten. Ph.D. Dissertation, Universität Siegen.

Hamel, S., and Krumm, W., 2001. Mathematical modelling and simulation of bubbling fluidised bed gasifiers Powder Technology, 120, 105–112.

Hansen L.K., Rathmann O., Olsen A., Poulsen K., 1997. Steam gasification of wheat straw, barley straw, willow and giganteus. Risø National Laboratory, Optics and Fluid Dynamics Department, Project No. ENS-1323/95-0010.

Hastaoglu, M.A.; Karmann, M.G., 1987. Modelling of catalytic carbon gasification. Chemical Engineering Science 42, 1121–1130.

Hawley, M.C.; Boyd, M.; Anderson C.; DeVera, A., 1983. Gasification of wood char and effects of intraparticle transport Fuel, 62, 213–216

Haynes, H.W., 1981. An improved single particle char gasification model. A.I.Ch.E Journal 28, 517–521.

Heesink, A.B.M., Prins, W., van Swaaij, W.P.M., 1993. A grain size distribution model for non-catalytic gas-solid reactions. Chemical Engineering Journal 53, 25–37.

Hemati, M., Laguerie C., 1988. Détermination de la cinétique de vapogazéification de charbon de bois en thermobalance. Entropie 142, 29–40.

Hindmarsh, A.C., Johnson, S.H., 1988. Dynamic simulation of reversible solid-fluid reactions in nonisothermal porous spheres with Stefan-Maxwell diffusion. Chemical Engineering Science 43, 3235–3258.

Hindmarsh, A.C., Johnson, S.H., 1991. Dynamic simulation of multispecies reaction/diffusion in nonisothermal porous spheres. Chemical Engineering Science 46, 1445–1463.

Howard, J.R., 1989. Fluidized Bed Technology: Principles and Applications. Hardcover, Institute of Physics Publishing.

Hurt, R.H., Mitchell, R.E., Baxter, L.L, Hardesty, D.R., 1992. Proc. of the Ninth Ann. Pittsburgh Coal Conf., Pittsbugh, PA. 634.

Jamshidi, E., Ale-Ebrahim, H., 1996a. An incremental analytical solution for gas-solid reactions, application to the grain model. Chemical Engineering Science 51, 4253–4257.

Jamshidi, E., Ale-Ebrahim, H., 1996b. A new solution technique of moving boundary problems for gas-solid reactions; application to half-order volume reaction model. Chemical Engineering Journal 63, 79–83.

Jamshidi, E., Ale-Ebrahim, H., 1997. A quantized solution for the nucleation model in gas-solid reactions. Chemical Engineering Journal 68, 1–6.

Jamshidi, E., Ale-Ebrahim, H., 1999. A new solution technique for gas–solid reactions with structural changes. Chemical Engineering Science 54, 859–864.

Jennen, T., Hiller, R., Köneke, D., Weinspach, P.-M., 1999. Modeling of Gasification of Wood in a Circulating Fluidized Bed. Chemical Engineering Technology 22, 822–826.

Jensen, G. A., 1975. Kinetics of Gasification of Carbon Contained in Coal Minerals at Atmospheric-Pressure. Industrial & Engineering Chemistry Process Design and Development 14, 308−314.

Jiang, H., Morey, R. V., 1992. A numerical model of a fluidized bed biomass gasifier. Biomass and Bioenergy 3, 431−447.

Johnson, J.L., 1979. Kinetics of Coal Gasification. Wiley, New York.

Jong, W., Ünal, Ö., Andries, J., Hein, K. R. G., Spliethoff, H., 2003. Thermochemical conversion of brown coal and biomass in a pressurised fluidised bed gasifier with hot gas filtration using ceramic channel filters: measurements and gasifier modelling. Applied Energy 74, 425–437.

Kasaoka, S., Sakata, Y., Tong, C., 1985. Kinetic evaluation of the reactivity of various coal chars for gasification with carbon dioxide in comparison with steam. International Chemical Engineering 25, 160−175.

Katta, S., Keairns, D.L.,1981. Study of kinetics of carbon gasification. Industrial & Engineering Chemistry Fundamental, 2, 6 –13.

Khraisha, Y. H., 2005. Batch combustion of oil shale particles in a fluidized bed reactor. Fuel Processing Technology 86, 691−706.

Kinoshita, C. M., Wang, Y., Takahashi, P. K., 1991. Chemical equilibrium computations for gasification of biomass to produce methanol. Energy Sources 13, 361–368.

Knoef, H.A.M., 2003. Pyrolysis and gasification of biomass and waste. In: A.V. Bridgwater, Editor, 315–324. CPL Press, Berks, UK. Also Presentation at the Pyrolysis and Gasification of Biomass and Waste Expert Meeting, 30 Sept.–1 Oct. 2002, Strasbourg, France.

Kojima, T., Assavadakorn, P., and Furusawa, T., 1993. Measurement and Evaluation of gasification Kinetics of Sawdust Char with Steam in an Experimental Fluidized Bed. Fuel Processing Technology 36, 201–207.

Kovacik, G., Oguztöreli, M., Chambers, A., Özum, B., 1990. Equilibrium calculations in coal gasification. International Journal of Hydrogen Energy 15, 125–131.

Kunii, D., Levenspiel, O., 1991. Fluidization Engineering (second ed.), Butterworth-Heinemann, London.

Kurkela, E., Nieminen, M., Simell, P., 2004. Development and commercialisation of biomass and waste gasification technologies from reliable and robust co-firing plants towards synthesis gas production and advanced cycles. 2nd World conference on Biomass for Energy and Climate protection. Rome. Italy. 10–15.

Lee, J. G., Kim, J. H., Lee, H. J., Park, T. J., Kim, S. D., 1996. Characteristics of Entrained Flow Coal Gasification in a Drop Tube Reactor. Fuel, 75, 1035–1042.

Lee, S., Angus, J.C., Edwards R.V., Gardner N.C., 1984. Non catalytic coal char gasification. A.I.Ch.E Journal 30, 583–593

Levenspiel, O., 1972. Chemical Reaction Engineering. Wiley, New York.

Li, X., Grace, J. R., Lim, C. J., Watkinson, A. P., Chen, H. P., Kim, J. R., 2004. Biomass and Bioenergy 26, 171–193.

Li, X., Grace, J. R., Watkinson, A. P., Lim, C. J., Ergüdenler, A., 2001. Equilibrium modelling of gasification: a free energy minimization approach and its application to a circulating fluidized bed coal gasifier. Fuel 80, 195–207.

Liliedahl, T., Sjöström, K., 1997. Modelling of char-gas reaction kinetics. Fuel 76, 29–37.

Liu, G., Niksa, S., 2004. Coal conversion submodels for design applications at elevated pressures. Part II. Char gasification. Progress in Energy and Combustion Science 30, 679–717.

Liu, H., Gibbs, B.M., 2003. Modeling NH_3 and HCN emissions from biomass circulating fluidized biomass gasifiers. Fuel 82, 1591–1604.

Liu, H., Luo, C., Kaneko, M., Kato, S., Kojima T., 2003. Unification of Gasification Kinetics of Char in CO2 at Elevated Temperatures with a Modified Random Pore Model. Energy & Fuels 17, 961–970

Luo, C., Aoki, K., Uemiya, S., Kojima, T., 1998. Numerical Simulation of a Jetting Fluidized Bed Gasifier and the Comparison to the Experimental Data. Fuel Processing Technology 55, 193–218.

Luo, C., Watanabe, T., Nakamura, M., Uemiya, S. and Kojima, T., 2001a. Development of FBR measurement of char reactivity to carbon dioxide at elevated temperatures. Fuel 80, 233–243.

Luo, C., Watanabe, T., Nakamura, M., Uemiya, S., Kojima, T., 2001b. Gasification Kinetics of Coal Chars Carbonized Under Rapid and Slow Heating Conditions at Elevated Temperatures Journal of Energy Resources Technology 123, 21–26.

Maniatis K., 2004. State of the art on Thermochemical conversion tecnologies. 2nd World conference on Biomass for Energy and Climate protection. Rome. Italy. 16–21.

Maniatis, K., 2001. Progress in biomass gasification: an overview. In: A.V. Bridgwater, Editor, Progress in Thermochemical Biomass Conversion vol. 1, Blackwell Science, London, UK, 1–31.

Mansaray, K. G., Al-tawel, A. M., Ghaly, A. E., Hamdullahpur, F., Ugursal, V. I.,

2000a. Mathematical Modeling of a Fluidized Bed Rice Husk Gasifier: Part I–Model Development. Energy Sources 22, 83–98.

Mansaray, K. G., Al-tawel, A. M., Ghaly, A. E., Hamdullahpur, F., Ugursal, V. I., 2000b. Mathematical Modelling of a Fluidized Bed Rice Husk Gasifier: Part II–Model Sensitivity. Energy Sources 22, 167−185.

Mansaray, K. G., Al-tawel, A. M., Ghaly, A. E., Hamdullahpur, F., Ugursal, V. I., 2000c. Mathematical Modeling of a Fluidized Bed Rice Husk Gasifier: Part III–Model Verification. Energy Sources 22, 281–296.

Marcos, G., Tailleur, S., Bagajewicz, M.J., 1991. Analytical approximate solutions of certain nonlinear equations of reaction-diffusion kind. Mathematical and Computer Modelling 15, 77–88.

Mathieu, P., Dubuisson, R., 2002. Performance analysis of a biomass gasifier. Energy conversion and management 43, 1291–1299.

Matsui, I., Kunii, D., Fursuawa, T., 1985. Study of fluidized bed steam gasification of char by thermogravimetrically obtained kinetics, J. Chem. Eng. Jpn. 18 (2) 105–113.

Matsui, I., Kunii, D., Furusawa, T., 1987a. Study of char gasification by carbon dioxide. 1. Kinetic study by thermogravimetric analysis, Industrial Engineering Chemical Research 26, 91–95.

Matsui, I., Kunii, D., Furusawa, T., 1987b. Study of char gasification by carbon dioxide. 2. Continuous gasification in fluidized bed, Industrial Engineering Chemical Research 26, 95–100.

Mermound F., Golfier F., van de Steene L., Salvador S., Girand P., 2004. Factors influencing wood char gasification at macro-particle scale. 2nd World conference on Biomass for Energy and Climate protection.

Mleczko, L., Wurzel, T., 1997. Experimental studies of catalytic partial oxidation of methane to synthesis gas in a bubbling-bed reactor. Chemical Engineering Journal 66, 193-200.

Molina, A., Mondragón, F., 1998. Reactivity of coal gasification with steam and CO2. Fuel 77, 1831−1839.

Morell, J.I., Amundson, N.R. Park, S.K., 1990. Dynamics of a single particle during char gasification. Chemical Engineering Science, 45, 387–401.

Mori, S., Wen, C.Y., 1975. Estimation of bubble diameter in gaseous fluidized beds. A.I.Ch.E Journal 21 (1), 109–115.

Murphy, M.L., 2001. Retrofit of coal-fired power boilers using Fluidized Bed Biomass Gasification Energy Products of Idaho (EPI). SALE-MKT\TECH_DOC\Gasifier Retrofit MLM.wpd.

Nilsson, T, 1990. Modelling of gasification in a fluidised bed. Ph.D. Dissertation, Royal Institute of Technology (KTH), Stockholm, Sweden.

Oka, S. O., 2004. Fluidised Bed Combustion, Marcel Dekker, Inc., New York.

Olivares, E., Silva, E. Sanchez, 1995. Constructive features, operation and sizing of fluidized-bed gasifiers for biomass. Energy for Sustainable Development, II, 52–

57.

Ollero, P., Serrera, A., Arjona, R., Alcantarilla, S., 2002. Diffusional effects in TGA gasification experiments for kinetics determination. Fuel 81, 1989–2002.

Ollero, P., Serrera, A., Arjona, R., Alcantarilla, S., 2003. The CO_2 gasification kinetics of olive waste. Biomass & Bioenergy, 24, 151–161.

Palchonok G., 1998. Heat and mass transfer to a single particle in fluidised bed. Ph.D. Dissertation, Chalmers University of Technology, Gothenburg, Sweden.

Patisson, F., Francois M.G., Ablitzer, D., 1998. A non-isothermal, non-equimolar transient kinetic model for gas-solid reactions. Chemical Engineering Science 53, 697–708.

Petersen, E.E., 1965. Chemical Reactor Analysis, Prentice-Hall, Englewood Cliffs, NJ.

Petersen, I., Werther, J., 2005a. Experimental investigation and modeling of gasification of sewage sludge in the circulating fluidized bed. Chemical Engineering and Processing 44, 717–736.

Petersen, I., Werther, J., 2005b. Three-dimensional modeling of a circulating fluidized bed gasifier for sewage sludge. Chemical Engineering Science, 60, 4469–4484.

Rafsanjani, H., Jamshidi, E., Rostam-Abadi, M., 2002. A new mathematical solution for predicting char activation reactions. Carbon 40, 1167–1171.

Ramachandran, P.A., 1983. Analytical prediction of conversion-time behaviour of gas-solid noncatalytic reaction. Chemical Engineering Science 38, 1385–1390.

Ramachandran, P.A., Doraiswamy, L.K., 1982. Modeling of non-catalytic gas-solid reactions. A.I.Ch.E Journal 28, 881–900.

Raman, P., Walawender, W. P., Fan, L. T., Chang, C. C., 1981. Mathematical model for the fluid-bed gasification of biomass materials. Application to feedlot manure. Industrial & Engineering Chemistry Process Design and Development 20, 686–692.

Ranade, P.V., Harrison, D.P., 1979. The grain model applied to porous solids with varying structural properties. Chemical Engineering Science 34, 427–432.

Ranade, V.V., 2002. Computational Flow Modelling for Chemical Reactor Engineering. Academic Press, New York.

Rapagna, S., Latif, A., 1997. Steam gasification of almond shells in a fluidised bed reactor: The influence of temperature and particle size on product yield and distribution. Biomass & Bioenergy 12, 281–288.

Rathmann, O., Hald, P., Bak, J., Illerup, J.B., Gjernes, E., Fjellerup, J., Olsen A., 1995. Combustion and gasification of coal and straw under pressurized conditions. Riso National Laboratory, Riso-R-819(EN) Denmark.

Rensfelt, E., Blomkvist, G., Ekström, C., Engström, S., Espenäs, B.-G., Liinanki, L., 1978. In D. L. Klass & W. W. Waterman (Eds.), Energy from biomass and wastes III, 465–494. Chicago: Institute of Gas Technology.

Reyes, S., Jensen, K.F., 1986a. Percolation to char gasification in kinetic reactions –

I. Application to char gasification in kinetic regime. Chemical Engineering Science 41, 333–344.

Reyes, S., Jensen, K.F., 1986b. Percolation to char gasification in kinetic reactions – II. Application to char gasification in diffusion regime. Chemical Engineering Science 41, 345–355.

Risnes, H., Sørensen, L.H., Hustad, J.E., 2000. CO_2 reactivity of chars from wheat, spruce and coal. In: Bridgwater A.V, (Ed). Proceedings of the conference: Progress in Thermochemical Biomass Conversion. Tyrol, Austria.

Ross, D.P., Yan, H.M., Zhang, D.K., 2001. An experimental study of propane combustion in a fluidized-bed gasifier. Combustion and flame 124, 156–164.

Ross, D. P., Yan, H.M., Zhang, D.K., 2004. Modelling of a laboratory-scale bubbling fluidised-bed gasifier with feeds of both char and propane. Fuel 83, 1979–1990.

Ross, D.P., Yan, H.M., Zhong, Z., Zhang, D.K., 2005. A non-isothermal model of bubbling fluidised-bed coal gasifier. Fuel 84, 1469–1481.

Sadaka, S. S., Ghaly, A. E., Sabbah, M. A., 2002a. Two phase biomass air-steam gasification model for fluidized bed reactors: Part I–model development. Biomass & Bioenergy 22, 439–462.

Sadaka, S. S., Ghaly, A. E., Sabbah, M. A., 2002b. Two phase biomass air-steam gasification model for fluidized bed reactors: Part II–model sensitivity. Biomass & Bioenergy 22, 463–477.

Sadaka, S. S., Ghaly, A. E., Sabbah, M. A., 2002c. Two phase biomass air-steam gasification model for fluidized bed reactors: Part III–model validation. Biomass & Bioenergy 22, 479–487.

Sahimi, M., Gavalas, G. R., Tsotsis, T. T., 1990. Statistical and continuum models of fluid–solid reactions and transport in porous media. Chemical Engineering Science, 45, 1443–1502.

Satterfield, C.N., 1991. Heterogeneous Catalysis in Industrial Practice, Krieger Pub. Company.

Schmal, M., Monteiro, J. L. F., Castellan, J. L., 1982. Kinetics of Coal-Gasification. Industrial & Engineering Chemistry Process Design and Development 21, 256–266.

Schuster, G., Löffler, G., Weigl, K., Hofbauer, H., 2001. Biomass steam gasification an extensive parametric modeling study. Bioresource Technology 77, 71–79.

Scott, S. A., Davidson, J. F., Dennis, J. S., Fennell, P. S., Hayhurst, A. N., 2005. The rate of gasification by CO_2 of chars from waste. Proceedings of the Combustion Institute 30, 2151–2159.

Scott, S. A., Harris, A. T., Dennis, J. S., Hayhurst, A. N., Davidson, J. F., 2003. Gasification of biomass: the consequences of equilibrium. 17th International fluidized bed combustion conference, Jacksonville, Florida, USA.

Shah, N., Ottino, J. M., 1987. Transport and reaction in evolving, disordered composites — I. Gasification of porous solids. Chemical Engineering Science, 42, 63–72.

Simons, G.A., 1980. The unified coal-char reaction. Fuel 59, 143–144.

Sipilä, K., 1988. Reactivity of biomass chars in fluid-bed steam gasification, Ed. Vol., Elsevier Applied Science, London and New York.

Sørensen, L.H., 1994. Fuel reactivity as a function of temperature, pressure and conversion, Ph. D. thesis, Risø National Laboratory, Denmark.

Souza Santos, M. L., 1989. Comprehensive modelling and simulation of fluidized bed boilers and gasifiers. Fuel 68, 1507−1521.

Souza-Santos, M. L., 2004. Solid Fuels Combustion and Gasification. Marcel Dekker.

Spliethoff, H., 2001. Status of biomass gasification for power production. IFRF Combustion Journal, Article No. 200109.

Srinivas, B., Amundson, N.R., 1980. A single-Particle Char Gasification Model. A.I.Ch.E Journal 26, 487–496.

Standish, N., Tanjung, A.F., 1988. Gasification of single wood charcoal particles in CO_2. Fuel 67, 666–672.

Stevens, D.J., 2001. Hot gas conditioning: recent progress with lager-scale biomass gasification systems. [NREL/SR-510-29952].

Stewart, P. S. B., Davidson, J. F., 1967. Slug flow in fluidised beds. Powder Technology 1, 61–80.

Stoltze, S., Henriksen, U., Lyngbech T., Christensen O., 1993. Gasification of straw in a large sample TGA. In: Nordic Seminar on Solid Fuel Reactivity, Chalmers University of Technology, Gothenburg, Sweden.

Struis, R.P.W.J., von Scala, C., Stucki, S., Prins, R., 2002. Gasification reactivity of charcoal with CO2. Part I: Conversion and structural phenomena. Chemical Engineering Science 57, 3581–3592.

Szekely, J., Evans, J.W., Sohn, H.Y., 1976. Gas-Solid Reactions. Academic Press, New York.

Thunman H., 2001. Principles and models of solid fuel combustion. Ph.D. Dissertation, Chalmers University of Technology, Gothenburg, Sweden.

Thunman H., 2003. Combustion Engineering. Chalmers University of Technology, Gothenburg, Sweden.

Thunman, H., Davidsson, K. Leckner, B., 2004. Separation of drying and devolatilization during conversion of solid fuels. Combustion and Flame 137, 242–250.

Thunman, H., Niklasson, F., Johnsson, F., Leckner, B., 2001. Composition of Volatile Gases and Thermochemical Properties of Wood for Modeling of Fixed or Fluidized Beds. Energy & Fuels15, 1488–1497.

Turkdogan, E.T., Vinters, J.V., 1970. Effect of carbon monoxide on the rate of oxidation of charcoal, graphite and coke in carbon dioxide. Carbon 8, 39–53.

van den Aarsen, F. G., 1985. Fluidised bed wood gasifier. Performance and modelling. Ph.D. Dissertation, Twente University Publication. University of Twente.

van den Enden P.J., Silva, E., 2004 . Design approach for a biomass fed fluidized bed gasifier using the simulation software CSFB. Biomass & Bioenergy 26, 281–287.

Wang, F.Y., Bhatia, S.K., 2001. A generalised dynamic model for char particle gasification with structure evolution and peripheral fragmentation. Chemical Engineering Science, 56, 3683–3697.

Wang, Y. ,Kinoshita, C.M., 1993. Kinetic model of biomass gasification. Solar Energy, 51, 19–25.

Wang, Y., Kinoshita, C. M., 1993. Kinetic model of biomass gasification. Solar energy 51, 1, 19–25.

Watkinson, A. P., Lucas, J. P., Lim, C. J., 1991. A prediction of performance of commercial coal gasifiers. Fuel 70, 519–527.

Wen, C.Y., 1968. Noncatalitic heterogeneous solid fluid reactions. Industrial and Engineering Chemistry 60, 34–54.

Werther, J., 1983. in: D. Kunii, R. Toei (Eds.), Fluidisation IV, Engineering Foundation, New York, 93.

Wurzel, T., Malcus, S., Mleczko, L., 2000. Reaction engineering investigations of CO_2 reforming in a fluidized-bed reactor. Chemical Engineering Science 55, 3955–3966.

Xu, J., Hoffmann, U., 1989. Application of integral transformation and orthogonal collocation in gas-solid non-catalytic reaction with varying diffusivity, temperature and bulk gas concentration. Chemical Engineering Science 44, 1431-1440.

Yan, H.M., Heidenreich, C., Zhang, D.K., 1997. Mathematical modelling of a bubbling fluidiseg-bed coal gasifier and the significance of net flow. Fuel 77, 1067–1079.

Yan, H.M., Heidenreich, C., Zhang, D.K., 1999. Modelling of bubbling fluidised bed coal gasifiers. Fuel 78, 1027–1047.

Yan, H.M., Zhang, D.K., 1999. Modelling of fluidised –bed coal gasifiers: elimination of the combustion product distribution coefficient by considering homogeneous combustion. Chemical Engineering and Processing 39, 229–237.

Yasyerli, N., Dogu, T., Dogu, G., Ar, I., 1996. Deactivation model for textural effects on kinetics of gas–solid noncatalytic reactions—char gasification with CO_2. Chemical Engineering Science 51, 2523–2528.

Yates, J. G., 1983. Fundamentals of fluidized-bed chemical processes. Butterworths. London.

Young, B.C., Smith, I.W., 1981. 18th (International) Symposium on Combustion. Pittsburgh, PA: The Combustion Institute, 1981, 1245.

Zygourakis, K., Arri, L., Amundson, N. R., 1982. Studies on the gasification of a single char particle. Ind. Eng. Chem. Fundam. 21, 1–12.